

Final Report

SustAIIn: Sustainable Autonomous Pandemic Intervention

Group 8

Delft University of Technology



This page is intentionally left blank.

Final Report

SustAIIn: Sustainable Autonomous Pandemic Intervention

by

Group 8

Student Name	Student Number
Lennard de Graaf	4875842
Sophie Keemink	4663926
Pieter Koopdonk	4867866
Bart Kroese	4862279
Nils de Krom	4883349
Max Kukkola	4827104
Lars La Heij	4869982
Moana Lengkeek	4823931
Jasper L'Ortije	4809521
Coen Middelhoek	4672364

Tutor: Clemens Dransfeld
Coaches: Malcom Brown & Salua Hamaza
Institution: Delft University of Technology
Place: Faculty of Aerospace Engineering, Delft

Acknowledgements

This project could not have been completed without the help of our tutor, Clemens Dransfeld, and our coaches, Salua Hamaza and Malcom Brown, and we would like to thank them for all the support and feedback they have given during this DSE. The outcome is most certainly at a higher quality than it would have been otherwise, and we have learnt valuable lessons in the duration of this project.

We would also like to specially thank Chizoba Ogugua for the large amount of support and time she has put in, helping us perform the Life Cycle Assessment, and teaching us about sustainability.

We would further thank the following people who have given their time to provide assistance to this DSE project: Åsa Ek, Calvin Rans, Kunal Masania, Otto Bergsma, Marion Frey, Baris Caglar, Guido Tosello, Tero Nikander, Peter Middelhoek, Sofie Middelhoek, Christian Weimer, Wilbert de Krom and Jan Berbee.

Lastly we would like to thank our family and friends for the support they have given during this busy time. Thanks for putting up with us, and telling us when to take breaks.

Change Log

General

- Added missing citations to previous reports.

Chapter : Summary

- Updated Figure 1.

Chapter 2: Mission Overview

- Expanded the description of project scope to detail the operations division between client and project.

Chapter 3: Final design

- Updated Figure 3.2, Figure 3.6 and Figure 3.7.
- Added results of sensitivity analysis for both trade-offs.
- Reorganised Section 3.3, added Figure 3.8.

Chapter 4: Market Analysis

- Added total tooling cost to Table 4.3.
- Added citation to Table 4.4.
- Updated Figure 4.3.

Chapter 5: Performance

- Added Figure 5.14 in order to detail the change in c.g with ballast.

Chapter 6: Operations

- Updated Figure 6.17.
- Expanded upon use case of returnable electronics.
- Added a discussion about possible methods to attach the glider to the launch vehicle at the launch location.
- Added further recommendations regarding the launch phase for post-DSE.
- Made the crash structure computation and analysis more explicit with an equation, instead of only mentioning it in text.
- Updated Figure 6.18.
- Updated Figure 6.33 such that the text in the diagram is better readable.
- Added Figure 6.24 to add clarity about the active time of each component.

Chapter 7: Structures and Materials

- Updated Figure 7.25.
- Split verification table into Table 7.9, Table 7.10, Table 7.11 and Table 7.10 for clarity.
- In Section 7.8 added a recommendation to perform sensitivity analysis for structural design choices. Also added a recommendation for a redesign of the spar-rib connection.
- Updated Figure 7.66 and Figure 7.67.
- Updated Figure 7.31 (coordinate system)
- Inserted Figure 7.10

Chapter 8: Sustainability

- Removed (previous) Figure 8.6 as it provided the same information as Figure 8.6, and the focus was too much on the Electronics LCA.
- Added Figure 8.5 to provide an overview of how the global warming impacts are distributed over the structure.

- Updated axis title of Figure 8.6.

Chapter 10: Outlook

- Modified Figure 10.1.
- Added description of preliminary and critical design reviews.
- Updated the Gantt chart in Figure 10.3.

Chapter 11: Conclusion

- Updated Figure 11.1.
- Added recommendation for redundancy of electrical systems.

Summary

The largest challenge for every country in the world at present is safeguarding the citizens from a global pandemic; the COVID-19 virus. Left unchecked, the virus would cause widespread devastation, and COVID-19 is not expected to be the last of this sort. The distribution and widespread accepted use of vaccinations aid heavily in the fight against such a virus, but is a challenge, even in the most accessible of locations.

The project

This SustAIIn project addresses the challenge of distributing vaccines by pursuing the need: *"To provide a high-precision, low environmental impact system to deliver low mass cargo to hard-to-reach and potentially hazardous areas"*. The scope of this stage of the project is given by the project objective statement: *"To design an autonomous, bio-degradable, single-use glider, minimising environmental footprint, with a maximum flight mass of 25 kilograms, by ten students in ten weeks"*.

The product

The mission need is attained with the final concept of a tailless glider, made of biodegradable materials and with autonomous communication and navigation system, named GliMed.

In terms of payload, 200 vaccines are carried on board, with sufficient supplies to administer these. Furthermore, GliMed fits within a clearly defined market gap where alternative transport drones are either deficient in range, not biodegradable or carry much larger payload and are therefore much more expensive. GliMed has a market price of €1250, which generates a return of investment of 125% after 15 years of operation.



Figure 1: Render of GliMed final design

Subsystem details

Detailed design is also performed on each of the subsystems of SustAIIn, as well as verification and validation of the requirements.

Performance

GliMed employs two different types of airfoil; a thicker, reflexed airfoil houses the payload, electronics and provides longitudinal stability, while a thinner airfoil is used in the long wings to provide an optimum L/D ratio. Winglets are added to the ends of the wings for additional lateral stability, and elevons provide GliMed with controllability characteristics. The glider has a maximum glide ratio of 29 and is able to glide over 125 [km] in 70% of all wind conditions.

Electrical systems

GliMed also performs autonomous communication and navigation. Long range communication is achieved with the help of spread spectrum modulation of which direct sequence spread spectrum (DSSS) is chosen. Insurance against hostiles in communication has been achieved with adding an additional bit code during the spread spectrum procedure, which is unknown for other parties. Furthermore by adding the code the spectral density of the signal lowers, which allows long range transmission. Besides the spread spectrum modulation the signal will be modulated with quadrature phase shift keying (QPSK). This communication is achieved with the help of an omnidirectional antenna on GliMed, for which there is no pointing required. Furthermore, there is a parabolic antenna on the mobile ground station and a buzzer is used as a beacon when landed, which allows the recipients to find the glider.

In terms of autonomous navigation, three distance sensors and one camera was required. The output of these will be used for map modelling for autonomous flight which is based on Simultaneous Localization and Mapping (SLAM). Furthermore, a path planner was required, and a simple version was built.

These navigation and communication systems, as well as the actuation of the elevons will be powered by a battery system. There are three variants of this system presented, of which the most sustainable and cheapest will be used in 80% of the outgoing missions, the version providing social benefit in 11%, and the remaining option as little as possible.

Launch and Landing

The launch altitude of 5000[m] is achieved by one helicopter UAV, chosen for its low emissions and ease of logistics. The launch vehicle is attached to GliMed with three clamps and it is based on the Camcopter S-100.

The chosen landing method consists of a dive down to just 3[m] above the ground. After this, a quick pitch up will be done by maximum deflection of elevons to ensure quick stall such that the glider will not fall from a significantly large height. As GliMed has no defined landing gear, a crash structure is constructed within the front and lower sections of the glider and around the payload such that it can withstand an impact at the stall speed.

Logistics

The logistics of project SustAIn are also covered, there is one main production location with a large storage area. From here, gliders are transported to the operating countries; Mali, Japan and Norway. Per operating country, there is a centrally located main base that stores the gliders and to which the electronics are returned. A mobile launch truck that can house 16 gliders at a time will drive the glider to within 400[km] of the recipient from where the launch vehicle will be launched with the glider. Within 125[km] of the recipient the glider is then released from the launch vehicle.

Structure and materials

In terms of the structure, a hollow wing box with a paper pulp skin was chosen for the outer wings, which is light weight, fit for mass production, and can degrade relatively fast. A double spar concept with stressed skin was chosen for the payload section as it maximises surface-to-volume ratio, while allowing as much space as possible for the payload to be integrated in a low-thickness fuselage airfoil. The payload will be loaded in from the side of the payload section, after which the wing box of outer wings can be slid into the front spar of the payload section. The payload section and outer wings are attached with screws that go through the skin of the payload section and a thicker rib. The screws can be removed and reused after landing, allowing the payload to be unloaded again. Mass production, utilising batch production of parts, and cellular assembly will ensure that 1000 systems a year are produced. The manufacturing facility will comprise of a CNC saw, CNC router, laser cutter, eight 3D printers, a robotic arm and five workers.

Bio-degradation enhancing mechanisms such as bacteria, fungi and water are employed, ensuring the bio-degradation time stays within 5 years. Furthermore, tear strips to open the wings, will be employed to expose all elements of the structure post landing.

Sustainability

The sustainability of the project was addressed in all three dimensions; environmental, economic, and social, and the environmental sustainability was quantified through the use of a LCA. GliMed was found to be more environmentally sustainable in the category of global warming than a comparative transport drone. A LCA was further used to determine the use cases of the three electric systems used in GliMed. Lastly, the economic and social sustainability of SustAIn has been addressed, but cannot easily be quantified.

Concluding remarks

This report concludes the conceptual design phase and provides a number of recommendations to the engineers taking on the detailed design phase. The most important of these is ensuring the aerodynamic performance is better estimated, either through computational fluid dynamics, or through wind tunnel testing. In addition, flight tests are required to determine the dynamic stability. Furthermore, as GliMed is reiterated for final design, the load factors must be re-analysed as these may shift from from 3 to 3.5. Finally, the market price of GliMed must be re-addressed, in order to be more competitive.

Contents

Acknowledgements	i
Change Log	ii
Summary	iv
Nomenclature	viii
1 Introduction	1
2 Mission Overview	2
2.1 Mission Description	2
2.2 Personas	3
2.3 Payload Description	3
3 Final Design	4
3.1 Configuration Trade-off	4
3.2 Final Design Description	6
3.3 Mass Budget	10
3.4 System Requirements Compliance	11
4 Market Analysis	13
4.1 Stakeholder Analysis	13
4.2 Market Gap and Competition	14
4.3 Cost Breakdown	15
4.4 Recipient and Situational Analysis.	21
5 Performance	22
5.1 Airfoil Selection	22
5.2 Wing Planform Design	23
5.3 Payload Section	26
5.4 Drag Estimation.	27
5.5 Final Geometry Performance	28
5.6 Stability of the Glider	29
5.7 Controllability of the Glider	33
5.8 Flight Conditions	36
5.9 Sensitivity Analysis	39
5.10 Verification and Validation	41
5.11 Compliance	42
5.12 Recommendations	43
6 Operations	44
6.1 Communication System	44
6.2 Navigation System	51
6.3 Electrical Systems	59
6.4 Launch, Landing and Logistics.	64
6.5 End-of-Life Procedures.	75
7 Structures and Materials	79
7.1 Recap Material Trade-Off	79
7.2 Structural Design	80
7.3 Manufacturing Design	91
7.4 Structural Analysis	96
7.5 Bio-degradation Calculations	103
7.6 Verification and Validation	107
7.7 Requirements Compliance Matrix	114
7.8 Recommendations	117

8 Sustainability	119
8.1 Environmental Sustainability	119
8.2 Economical Sustainability	125
8.3 Social Sustainability	125
8.4 Recommendations	125
9 Risk	126
9.1 Influence of Risk on the Design	129
10 Outlook	131
11 Conclusion and Recommendations	134
References	138

Nomenclature

Abbreviations

Abbreviation	Definition	Abbreviation	Definition
ATC	Air Traffic Control	LCC	Life Cycle Cost
AGW	American Wire Gauge	LE	Leading Edge
BWB	Blended Wing Body	MAE	Mean absolute error
CAD	Computer-Aided Design	MGS	Mobile ground station
CFD	Computational Fluid Dynamics	MTOW	Maximum Take-Off Weight
c.g.	Centre of gravity	PFD	Process Flow Diagram
DL	Downlink	PLA	Polylactic acid
DW	Delignified Wood	PVA	Polyvinyl acetate
DWRP	Delignified Wood Reinforced Polymer	QC	Quality Control
EAS	Equivalent Airspeed	ROI	Return of Investment
ECI	Environmental Cost Indicator	SLAM	Simultaneous Localization and Mapping
EOL	End-of-life	S-LCA	Social Life Cycle Assessment
FOV	Field of view	SWOT	Strengths, Weaknesses, Opportunities and Threats
GDP	Gross Domestic Product	TRL	Technology Readiness Level
GNSS	Global navigation satellite system	ToF	Time-of-Flight
ISA	International standard atmosphere	UL	Uplink
IMU	Inertial Measurement Unit	UAV	Unmanned Aerial Vehicle
INS	Inertial navigation system	VTOL	Vertical Take-Off and Landing
LCA	Life Cycle Assessment	WHO	World Health Organisation

Symbols

Symbol	Definition	Unit
A	Aspect ratio	[-]
A_r	Rotor area	$[m^2]$
b	Span	[m]
b_1	distance from thin wing to start of elevon	[m]
b_2	distance from thin wing to end of elevon	[m]
\bar{c}	chord length	[m]
C	electrical capacity	[F]
C_d	2D drag coefficient	[-]
C_{d_0}	Zero-lift drag coefficient	[-]
C_{D_i}	Induced drag coefficient	[-]
C_D	3D drag coefficient	[-]
C_d	Airfoil drag coefficient	[-]
C_{f_c}	Flat plate skin friction coefficient	[-]
C_L	3D lift coefficient	[-]
C_l	Airfoil lift coefficient	[-]
C_{L_α}	Lift curve slope	$[rad^{-1}]$
C_{l_β}	Roll stability due to yaw	[-]

Symbol	Definition	Unit
$C_{m\alpha}$	Moment coefficient slope	[deg ⁻¹]
C_{mtrim}	Trim moment coefficient	[-]
$C_{n\beta}$	Yaw stability due to yaw	[-]
c_r	Root chord	[m]
c_t	Tip chord	[m]
D	Drag	[N]
d_{ant}	Diameter of dish antenna	[m]
e	Oswald efficiency factor	[-]
f	Frequency	[Hz]
FF_c	Component form factor	[-]
G_{coding}	Coding gain	[dB]
G_R	Gain receiver	[dB]
G_T	Gain transmitter	[dB]
h_v	Vertical tail height	[m]
IF_c	Interference factor	[-]
k	Boltzmann constant	[J/K]
L	Lift	[N]
L_{FM}	Fade Margin	[dB]
L_{FS}	Free space loss	[dB]
L_{misc}	Miscellaneous losses	[dB]
l_{npv}	Neutral point of the winglet along the x-axis	[m]
l_{np}	Neutral point of the glider along the x-axis	[m]
L_T	Transmitter losses	[dB]
L_R	Receiver losses	[dB]
P_{RX}	Power received	[dB]
P_{TX}	Power Transmitted	[dB]
R	Data rate	[bits/s]
S	Surface area	[m ²]
S_{ref}	Reference Surface area	[m ²]
S_v	Winglet surface area	[m ²]
S_{wet}	Wetted surface area	[m ²]
SNR	Signal-to-Noise Ratio	[dB]
SNR_{req}	Required Signal-to-Noise Ratio	[dB]
T_{sys}	System noise temperature	[K]
U_{de}	Vertical gust velocity	[m/s]
V	Velocity	[m/s]
V_i	Induced velocity by the helicopter rotor	[m/s]
W	Weight	[N]
x_{ac}	Location of the aerodynamic centre along the x-axis	[m]
x_{cg}	Location of the centre of gravity along the x-axis	[m]
α	Angle of attack	[°]
ρ	Density	[kg/m ³]
λ	Wave length	[m]
λ	Taper ratio	[m]
Γ	Dihedral	[rad]
γ	Flight path angle	[deg]
η	aperture efficiency	[-]
R_{min}	Minimum bend radius	[m]
ϵ_+	Tensile strain to failure	[-]
ϵ_-	Compressive strain to failure	[-]
τ_a	Aileron effectiveness	[-]

1. Introduction

Parachute drops are often used to reach remote areas and locations that are in need of help. This is especially the case when the environment is hazardous or difficult to reach by land. However, parachute drops are not high precision and cannot deliver precious cargo. Another option is single-use gliders. In the second world war, they were used to deliver cargo safely and silently past enemy lines. The advantage of these gliders is that they do not need to be retrieved and that they have a higher precision.

Nowadays, the problem of reaching remote locations is highlighted again, as the world experiences the largest vaccination program in history. However, the process of ending the COVID-19 pandemic is slow and strenuous.¹ The difficulties of reaching remote populations in vaccination programs is unfortunately not a recent development, it has always been a problem. Especially keeping the vaccinations intact and cold enough during transport is challenging. Hence, reconsidering transport gliders as a delivery system is deemed worthwhile.

Originally these gliders were simply left behind at the exact landing spot. However, the influence on the environment is badly explored, and the degradability and how pollutive the gliders are is unknown. Since the effect of pollution and otherwise unsustainable activity is more and more evident in the local and global climate, the influence of the glider on the environment will need to be considered.

This report shows the conceptual design of an autonomous cargo glider that can deliver up to 200 vaccines and the necessary administrations sets. This glider is designed to be as bio-degradable as possible and have a minimised environmental impact in the full cradle-to-grave scenario. The maximum take-off weight is 25[kg] and its minimum range is 125[km]. In previous design phases, the full project planning was made. There, all design options were considered and unfeasible ones were eliminated. This report shows the full concept design of the concept that was deemed most feasible. With this, the concept design phase is concluded.

In Chapter 2, the details of the mission are explained as well as the personas. Then, in Chapter 3 a complete overview of the final concept design is given, as well as a summary and revision of the trade-off. In Chapter 4 the stakeholder analysis and requirements can be found, as well as the business aspects of the concept such as the market gap and the cost breakdown. Then, the report continues with the design chapter, of which the first Chapter 5, where starting with the requirements all performance parameters can be found. Design aspects like the planform, stability, and flight conditions can be found there. Thereafter, Chapter 6 treats the operational aspects of the design, including the communication and navigation systems, electrical system, landing, launch, and logistical aspects. End-of-Life procedures can also be found here. Following, Chapter 7 treats all matters concerning the materials, the structures, and the manufacturing. Chapter 8 describes the sustainability aspects of this project, like the Life Cycle Assessment that is performed. Subjects as economical and social sustainability can also be found there. While that concludes the design chapters of the report, the risks that have been considered and encountered are in Chapter 9. Though this report concludes the concept design phase, the possible future phases and development description can be found in Chapter 10. Finally, Chapter 11 has the conclusion and recommendations.

Each of the design chapters includes the validation and verification of the design methods, and the compliance matrix specific for that chapter.

¹<https://www.unicef.org/immunization> [cited on 21-06-21]

2. Mission Overview

Before designing, it is important to get a view of what the design goal is. This chapter contains the details of the mission and the project's objective. To make the design process easier, personas were created (presented in Section 2.2). Lastly, a detailed description of the payload can be found in Section 2.3.

2.1. Mission Description

In 2005, the WHO estimated that 50% of the vaccines are being wasted worldwide. Most of this waste due to so-called breaking the cold chain, and is most prevalent in poor areas that can usually only be reached by foot. The SustAin project seeks to deliver vaccines and possible other lightweight cargo to these remote areas. This is summarised in the mission need statement: *"Provide a high-precision, low environmental impact system to deliver low mass cargo to hard-to-reach and/or potentially hazardous areas."* This mission need statement is combined with the stakeholder requirements (Chapter 4) to a project objective statement: *"Design an autonomous, bio-degradable, single-use glider, minimising environmental footprint, with a maximum flight mass of 25 kilograms, by ten students in ten weeks."*

In this project, sustainability is considered thoroughly. One of the project objectives is to minimise the life cycle cost and to design for biodegradability. Though a single-use item is not often associated with sustainability, it is a good option in this use case. The fact that the glider will be single-use means there is no contamination risk when sending the glider, operations are easier since it does not need to be retrieved, and the design can be simpler.



Figure 2.1: Locations of Trondheim, Timbuktu, and Fukushima

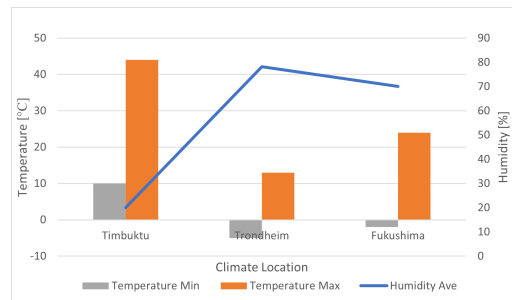


Figure 2.2: The humidity and temperature ranges for each climate zone [36]

The mission is considered in three different areas: Timbuktu in Mali, Trondheim in Norway, and Fukushima in Japan. These locations differ in climate as well as socio-political circumstances, as shown in Figure 2.1 and Figure 2.2. These factors are taken considered in EOL (Section 6.5) and the market analysis (Chapter 4) and wind performance (Section 5.8.2). After starting in these specific areas, the mission can be extended to areas with similar climates without adjustment to the glider. However, as described in Chapter 6, the operational reach will need to be expanded in that case.

Although the ultimate aim of the project is to provide medical aid as widespread as possible, the initial operations will focus on Timbuktu and its surroundings, so a more functional operational plan can be obtained. Around Timbuktu, three regions will be analysed; Timbuktu, Gao, and Kidal.

When the mission is a success, it can be further expanded to other regions as well, see Chapter 10. On top of that, though the payload is based on vaccines for COVID-19, the glider can be used for other purposes as well. First off, other vaccines like the ones for diphtheria, measles, tetanus and hepatitis have the same storing requirements. Moreover, other non-urgent medicine may be sent to small communities that suddenly find themselves unreachable due to for example a natural disaster. Besides, in situations such as a nuclear disaster, it may even be possible to send radiation pills to those in need, if the care is not too urgent. Also in that case, the irretrievability of the glider is advantageous.

Outside the scope of this project is urgent care such as blood, due to the weight, time constraints, and the fact that GlMed is designed specifically to overcome contagion problems. Furthermore, it is assumed the logistics of ordering the payload and contacting the recipients is outside the scope of this project. For now it is assumed the client will provide the payload, landing location, and will handle all contact with the recipient. The organisation of such a task is not the expertise of this project group.

2.2. Personas

To aid the design process, personas are used. Their purpose is to make sure the end-product is useful in different use-cases, and as many aspects as possible are taken into account. For each of the target areas mentioned above, there is a persona.

The first persona is Haruto, a rice farmer in the mountains of Fukushima and chief of his village. When a highly contagious disease starts spreading around Japan, he wants to organise a vaccination program for 200 people living there. This village is surrounded by steep hills and rice fields, and Haruto, as a busy man, would like to dump the glider down the mountain slope instead of partaking in intricate EOL procedures.

The second persona is Jamila, a matriarch of a small village in the area of Timbuktu. Ebola is spreading around, and to keep her town safe contact with outsiders is to be minimised. However, this makes it hard to get medicinal supplies and vaccines. Jamila's village is out in the open, so there are enough landing spots. The village has many children eager to help her investigate the glider once the vaccines are administered. If possible, they would like to reuse components. Because Jamila's communication to the outer world is not very stable, she would like to be able to locate the glider upon landing.

The last persona is Astrid. She is a primary school teacher in a small, secluded village near Trondheim. Approximately 180 children attend her school, and she would like to organise yearly vaccinations. Ideally, she would like to have the vaccines arrive during school time on the school field, so it can double as an educational activity. The children can help retrieve the payload and perform the additional EOL procedures.

These personas are used throughout the design, especially in the market analysis, the EOL procedures, and operations.

2.3. Payload Description

Based on the personas, the payload is everything needed to administer 200 vaccinations. This means there is a cooling box with the vaccine and enough administration equipment. As the dimensions of the payload are driving in the size of the glider and thus its performance, two changes are made compared to the payload description in the Midterm Report[36].

The first change is ordering a custom cooling box, because the one needed is smaller than what is currently on the market. Taking available cooling boxes, the size is extrapolated to one that can still keep its contents between 2-8°C for at least 28 hours. This ensures that the vaccines can stay cool from the moment they are loaded into the glider to when they are administered. During downsizing, it was assumed that only the vaccine storage dimensions are minimised, while the insulation keeps a similar thickness.

The second change is unpacking all contents of the administration set, because they are usually packed in inefficient boxes. All contents are weighed and sized separately. In this case, only the syringes and needles need protection in the form of a crash structure. Summarizing the considered payload, the dimensions and weight can be seen in Table 2.1¹²³. Their integration in the payload section can be seen in more detail in Section 6.4.2.

Table 2.1: Design payload dimensions and mass.

Item	Amount	Weight [kg]	Dimensions [mm ³]
Needles	2	0.170	14x29x11
Syringes	1	1.050	232x149x159
Alcohol wipes	2	0.150	100x55x55
Surgical mask	4	0.016	200x2x100
Vaccination record card	1	0.192	100x20x80
Needle gauge and length chart	1	0.005	297x210x0.1
Cool box, 4 cooling packs, vaccines	1	3.4	133x186x217

¹<https://www.blowkings.co.in/vaccine-carriers.html>[cited 17-06-2021]

²<http://www.ssaapp.com/product/injection-and-venipuncture-1.php>[cited 17-06-2021]

³<https://www.bd.com/en-us/offerings/capabilities/syringes-and-needles/conventional-syringes-and-needles/conventional-syringes/309628>[cited 17-06-2021]

3. Final Design

In this chapter, the final design and the way the subsystems are integrated are shown. This chapter starts with a description of the design trade-off as it was performed, and the changes that were done after the midterm report. Right after the final conceptual design is shown in Section 3.2. There full system drawings can be found along with the functional diagrams. This section shows to full design and how different parts are integrated. Following in Section 3.3, the mass budget is given, also giving an overview of all the parts in the glider. Finally, this chapter ends with the compliance matrix of the system requirements.

3.1. Configuration Trade-off

After the original trade-off, three main stages were reached. In Section 3.1, the original trade-off is explained. Then, in Section 3.1 the first change is explained. This section ends with Section 3.1, where the final trade-off is shown.

Original Configuration Trade-off

In the midterm report [36] three concepts were traded off; a conventional configuration, a flying wing and a blended wing body (BWB). The definitions for each if these is:

- **Conventional configuration:** The aircraft is symmetrical around the $X_b - Z_b$ plane and consists of a tubular fuselage with end caps on either ends and a distinct divide between the fuselage and wing.
- **Flying wing:** The fuselage is lift generating and is integrated with the wing. The aircraft is symmetrical around the $X_b - Z_b$ plane and, with the exception of a single radius of curvature at the nose, has one leading edge sweep angle between $Y_b = 0[m]$ and $Y_b = b/2[m]$.
- **Blended body:** The fuselage is lift generating and is integrated with the wing. The aircraft is symmetrical around the $X_b - Z_b$ plane and has more than one leading edge sweep angle between $Y_b = 0[m]$ and $Y_b = b/2[m]$.

The criteria used in the trade-off are design maturity, weight, manufacturability and performance with weights of $4/5$, $2/5$, $3/5$ and $3/5$, respectively. The first criterion, design maturity, refers to the access to experts, literature, software and general knowledge that the team possessed. This criterion was given the largest weight since it contributed significantly to the feasibility of the design with given time and resources. The second criterion, weight, refers to the structural weight that the glider is estimated to have. This criterion was chosen since the mass of the glider should be under 25 kg. However it wasn't given a high importance as it was estimated that even though it is beneficial to minimise the weight, all configurations would adhere to this mass requirement. The third criterion, manufacturability, refers to the degree to which the configuration would be able to adhere to the necessary production volume of 1000 systems per year. The final criterion, performance, considers the stability and controllability as well as the theoretical aerodynamic performance of each configuration.

Table 3.1: Trade-off summary (system)

Configura-tion	Design maturity	Weight [-]	Manufacturability	Performance
Conven-tional	[Green] Well researched	[Yellow] 0.75-0.875	[Green] Simplest assembly/geometry	[Green] Proven high performance glider
Flying wing	[Blue] Enough material and knowledge available	[Green] 0.25-0.375	[Blue] Moderately difficult assembly/ geometry	[Blue] Good glider performance
Blended wing body	[Red] Large knowledge gap	[Blue] 0.375-0.5	[Blue] Moderately difficult assembly/ geometry	[Blue] Good theoretical performance

Based on the trade-off table, Table 3.1, the conventional configuration was selected. The selection was justified using a sensitivity analysis performed by changing the criteria weights. It showed that the conventional configuration was chosen in 66% of all permutations.

Second Iteration of Configuration Trade-off

In evaluating the midterm [36], new information came to light which made the flying wing the superior concept. Firstly the definitions for flying wing and BWB were reconsidered. An additional condition was set on the change in thickness along the span. The BWB had to have a smooth transition whereas the flying wing was able to have sharp discontinuities as seen in Figure 3.1. The sharp thickness changes meant that the flying wing would be significantly easier to manufacture than previously expected. Additionally, with two distinct and similar wing-like sections (in the flying wing) similar production methods could be employed in their production. The structural weight of the BWB also decreased due to the new definition.

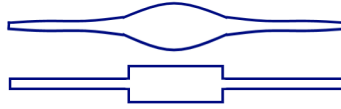


Figure 3.1: New definition. Front view of BWB (top) and flying wing (bottom).

The manufacturing of the conventional configuration was also reevaluated and it was concluded that due to the teardrop shape fuselage requiring many compound curves, it would be difficult to manufacture using the materials considered.

Additionally, more literature was found on the gliding performance of a flying wing. More specifically, a book on the Horten IV sailplane explaining the theoretical and experimental performance of the configuration [41]. The book mentioned many analytical methods that would help estimate the L/D performance. In theory, a L/D of up to 50 is possible for the flying wing. Nonetheless the stability and controllability still remained unchained and difficult.

For the reasons stated above, the manufacturability, weight, and performance criteria for the flying wing and conventional configuration were reevaluated and changed. Table 3.2 table shows the outcome of the new trade-off. The same sensitivity analysis done in the original trade-off was performed for the new trade-off, in light of the new information. It showed that the flying wing was chosen for 82% of permutations.

Table 3.2: Trade-off summary (system)

Configura-tion	Design maturity	Weight [-]	Manufacturability	Performance
Conven-tional	[Green] Well researched	[Yellow] 0.75-0.875	[Yellow] Moderately difficult assembly/ geometry	[Green] Proven high performance glider
Flying wing	[Blue] Enough material and knowledge available	[Blue] 0.375-0.5	[Green] Simplest assembly/geometry	[Green] Good glider performance
Blended wing body	[Red] Large knowledge gap	[Green] 0.25-0.375	[Yellow] Moderately difficult assembly/ geometry	[Blue] Good theoretical performance

Final design decision

Over the course of the design process it became progressively more difficult to work within a limited design space imposed by the definition of a flying wing and BWB. In fact, it became apparent that there is no clear and accepted distinction between a flying wing and BWB in literature. Many papers talking about the design of a particular flying wing configuration could be classified as BWB according to some definitions and vice versa. This issue dates back to the start of the project, in the baseline review [35], where it was decided that the flying wing and BWB were sufficiently different concepts to be traded off against each other. In reality the distinction is ill defined, and the attempt to make an in-house definition only limited the scope and availability of literature to the team.

When considering criteria such as design maturity some errors were made due to the distinction. For example in the design maturity the BWB was given an unfairly low score due to the unavailability of literature. However the BWB as a term is relatively new and it was found that many papers written prior to the 90s discussing “flying wings” could alternatively be classed as BWB.

The current approach is to class the flying wing and BWB as one concept, keeping the design space open enough to work in, but constrained to a lift producing payload carrying section. Furthermore, this enables the final design to possess the best of both initial concepts, in particular when it comes to structural weight.

Furthermore, new materials were introduced after the midterm phase and the manufacturability scores for the BWB changed as a result. In particular the addition of moulded paper pulp, as material for the wing, is said to bring complexity for free as it can be moulded into a shape with many splines without incurring any time or cost penalties. Hence the complex curved shapes in the fuselage-to-wing taper will not make manufacturing more complex, given that it is made out of moulded paper pulp.

3.2. Final Design Description

This section aims to give an overview of the final design and to show the way different subsystems are integrated. Also, it discusses the functions the glider has to perform, such that the design choices in the coming chapters make sense. First of all, bringing all subsystems together, the design was modeled, which can be seen in Figure 3.2. As can be seen, the glider consists mainly of two parts: the thicker middle section that contains the payload, which is henceforth called "the payload section"; and the thin wings. A detailed technical drawing can be found in Figure 3.5. On this drawing, electronics are drawn in (red), as well as the payload (in gray) and their crash structure (in blue), and some of the sensors. In Figure 3.3 and Figure 3.4, a top- and front view of the glider is provided to give an idea on the lay-out.



Figure 3.2: Render of GliMed

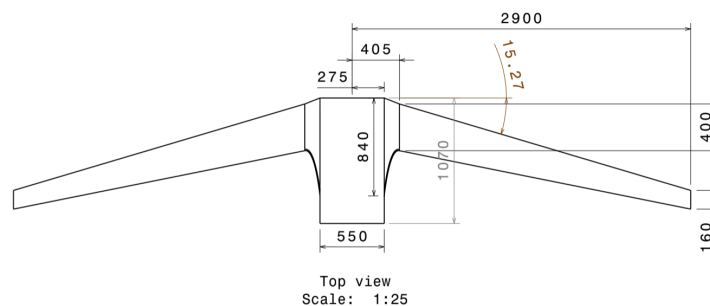


Figure 3.3: Top view of the system with relevant outer dimensions provided in [mm].

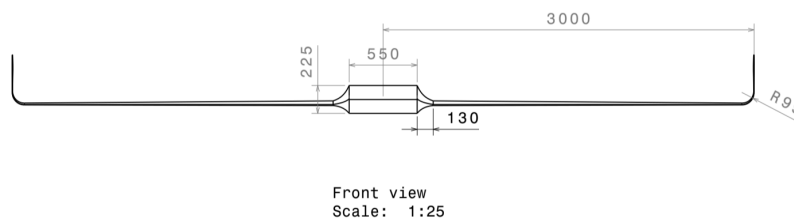


Figure 3.4: Front view of the system with relevant outer dimensions provided in [mm].

The functional breakdown structure and functional flow diagram are given in Figure 3.6 and Figure 3.7. These diagrams provide an overview of the functions GliMed must perform. The global functional flow is visualised in Figure 3.6 and a more detailed break down of those functions is provided in Figure 3.7.

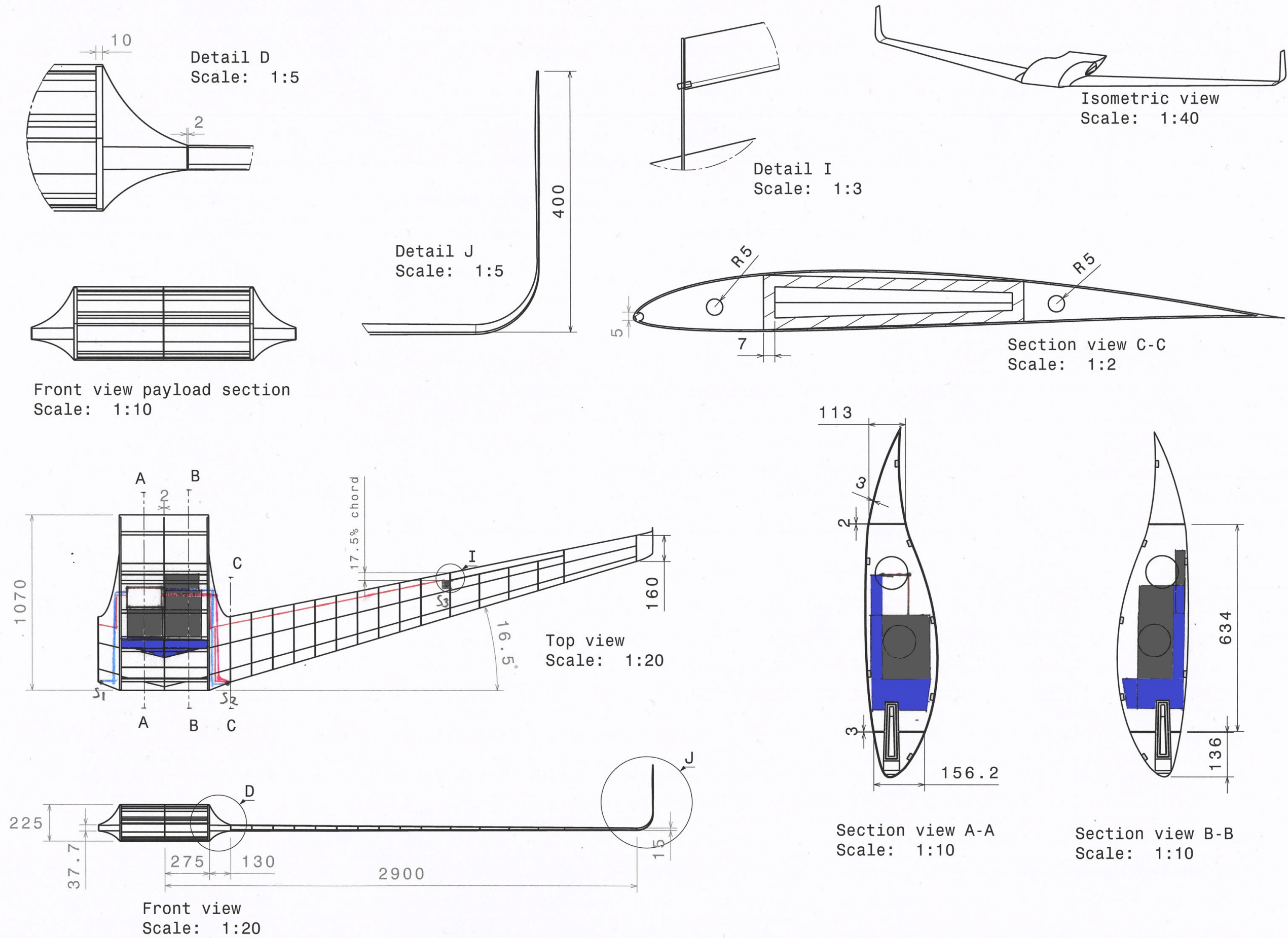


Figure 3.5: Full design drawing with detail drawings

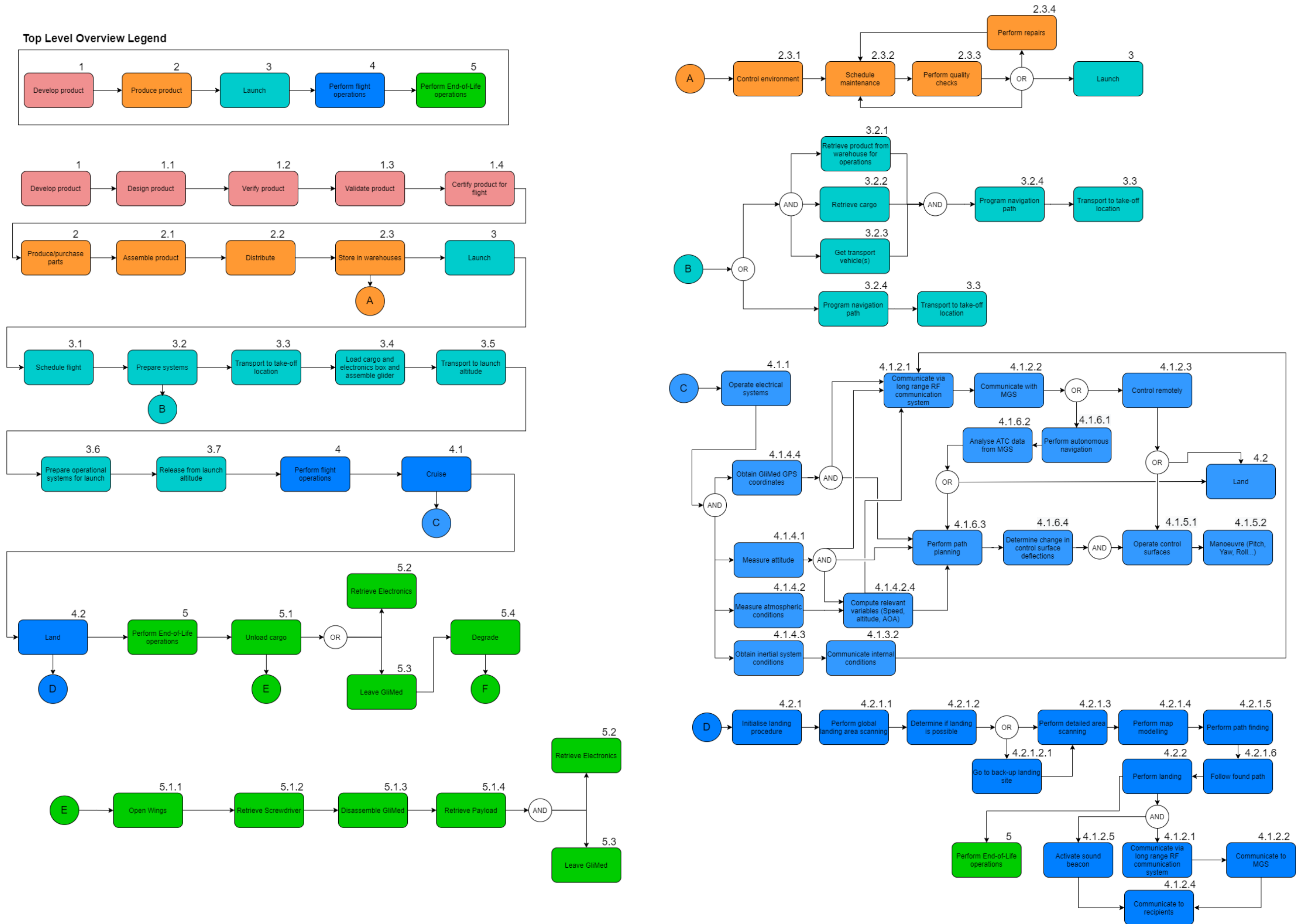


Figure 3.6: Functional flow diagram SustAI.

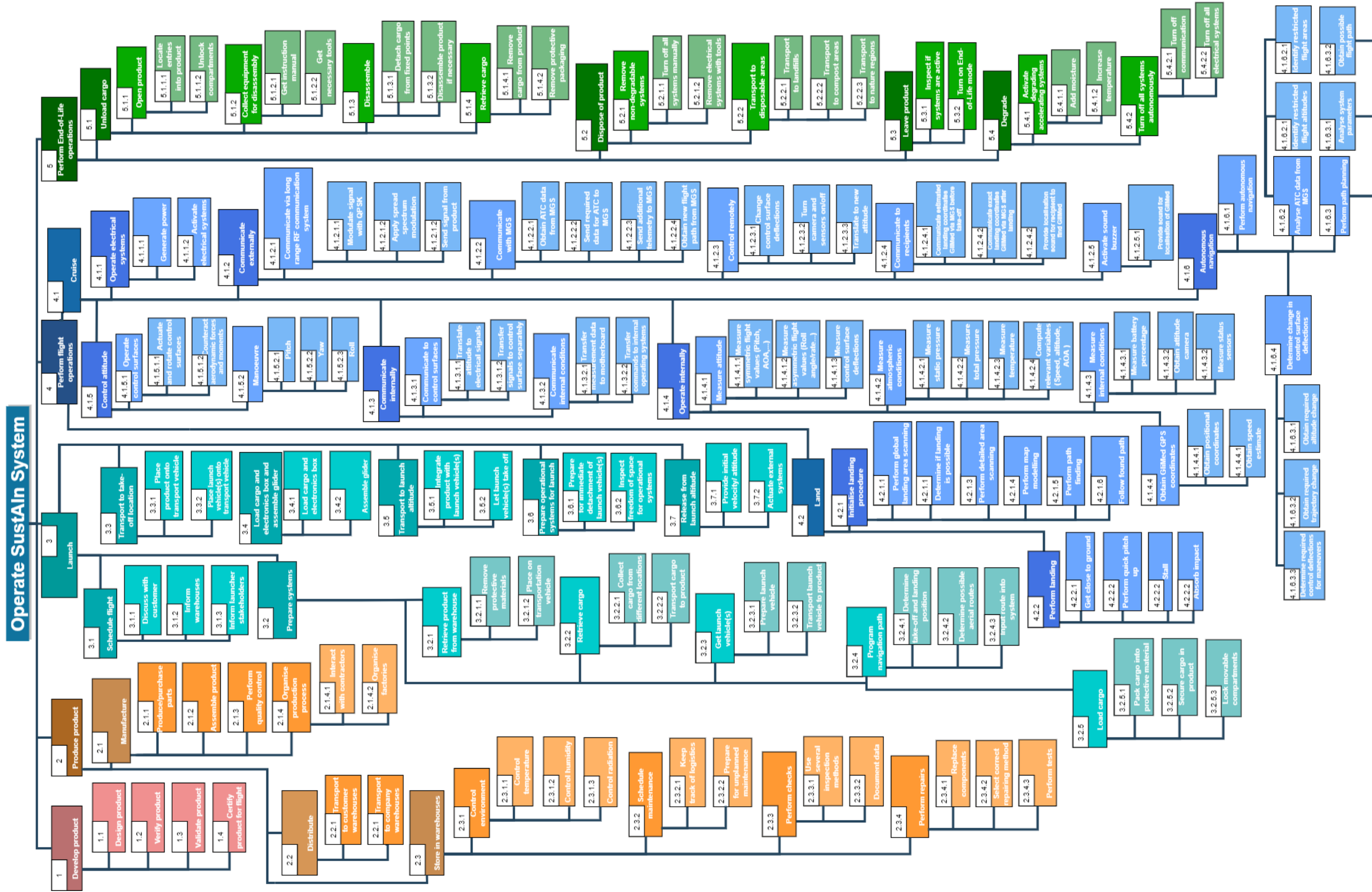


Figure 3.7: Functional breakdown structure SustAIn.

3.3. Mass Budget

While designing, budgets give a good overview of the available design space. In total, the system has four different budgets; the cost-, energy-, power- and mass budgets. The cost breakdown is described in Section 4.3, whereas the energy- and power budgets are described in Section 6.3.9 and Section 6.3.10. Lastly, the mass budget is explained below, starting with a general overview of the complete mass budget. After this, the details are explained of the structural weight, followed by the electronics and ending with the operational items.

Total

In Table 3.3, the complete mass budget can be observed, as well as the operational empty weight. It is visualised in Figure 3.8. In the table, an item called ballast is added. The 4.6 [kg] of ballast (in the form of wet sand) was required near the leading edge of the payload section to make the glider longitudinally statically stable during flight. According to mass percentages, 92.7% of the glider is constructed out of materials from renewable resources.

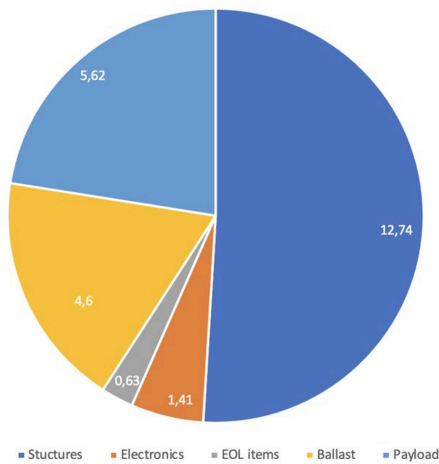


Figure 3.8: Pie chart of the total mass budget, indicating the general contributions of each component.

Table 3.3: Total mass budget of the system.

	Mass [kg]
Structural weight	12.74
Electronics	1.41
EOL items	0.63
<i>Ballast</i>	4.6
Empty weight	19.38
Payload (5% contingency)	5.62
Total	25.0

Structural empty weight

In Table 3.4 and Table 3.5 the weight of all the individual structural components are listed. In Table 3.7 the mass contributions of miscellaneous items are listed. The total weight of the structure comes down to 11.498 [kg]. However, in Section 7.8 it is explained that a large contingency is required because of uncertainties for the load factors the structure is designed for and slight design changes that might be required in future design stages. The mass budget allowed for a contingency of 11%, which causes the structure to weigh a total of 12.74 [kg].

Table 3.4: Structural mass budget of the payload section.

Structural component	Mass [kg]
Stiffeners	0.33
Skin	1.58
Rear spar	0.053
Front spar (with wrap box)	0.65
Centre rib	0.12
Crash structure	0.453
Total	3.186

Table 3.5: Structural mass budget of the outer wings.

Structural component	Mass [kg]
Spar box	4.52
Skin	1.06
All ribs combined	0.138
Elevon	0.086
Winglet	0.204
Two outer ribs	1.18
Total	7.188

Operational items

In Table 3.6, items necessary for end-of-life operations are listed. The total weight comes down to 0.6 [kg]. A contingency of 5% was allowed by the mass budget, which brings the weight to 0.63 [kg].

Table 3.6: Mass contributions of items necessary for end-of-life operations.

	Mass [kg]
Screwdriver	0.120
Liquid solution	0.04
Water	0.4
Bacteria	0.005
Fungi	0.005
Seeds	0.03
Total	0.6

Table 3.7: Mass contribution of miscellaneous structural components.

Structural component	Mass [kg]
Hide glue for all adhesively bonded joints	0.132
Soy glue to bond veneers	0.381
18 screws required to attach ribs of outer wings to payload section and for electrical systems	0.450
PLA film	0.161
Total	1.124

Electronics

In Section 3.3 and Table 3.3, the mass contributions of the electrical systems are listed. Since the glider uses different types of electronics depending on the mission, the worst case scenario is implemented in the tables. The total weight comes down to 1.3283 [kg]. The mass budget allows a contingency margin of 5%, which brings the mass to 1.41 [kg].

Table 3.8: Mass contribution of the electronics box (heaviest option).

	Mass [kg]
Reusable Battery	0.365
Buck converter	0.005
Pi 4	0.046
SD card	0.005
Electronics box	0.372
Servo driver	0.009
GPS	0.007
IMU	0.02
Wiring	0.071
Total	0.9

Table 3.9: Mass contribution of other electrical systems.

	Mass [kg]
Omnidirectional antenna	0.04
Buzzer	0.006
Camera + Tilting mechanism	0.014
Pitot tube	0.0363
3 Sensors	0.036
1 and 2 large Servos	0.133
Electrical wiring	0.163
Total	0.4283

3.4. System Requirements Compliance

In Chapter 4, all the stakeholder requirements are explained. During previous design phases these were converted to system requirements. In the table below, all these requirements can be seen, whether they have been met with the current conceptual design, and what specific section covers meeting it.

This compliance matrix seeks to give a clear overview of what needs to be given attention in the coming design phase, as well as show the progress of the design so far. The subsystem requirements and their compliance matrices can be found in the chapters where they have been treated, as to keep Table 3.10 clear.

The only system requirement that is not addressed in the rest of the report is SAI-SYS-09. At this conceptual design stage, the reliability is very difficult to estimate. In order to comply with the requirement, the following steps have to be undertaken: First, in the detailed design stage, reliability of separate subsystems can be estimated. In the testing phase, the reliability can be tested. This gives an indication for the failure rate of the entire glider during its operational flight. After this, statistical data has to be gathered during the operational phase of GliMed. Gliders are to be sent to several locations. The data can be analysed, providing more certainty on the percentage of gliders that are retrieved by the recipient. The data can be evaluated, referring to effects such as electrical system failure, crashes, recipient not able to find the glider and other effects.

Table 3.10: Compliance matrix for system requirements

Identification	Requirement	Compliance	Discussion
SAI-SYS-01	The system shall be simple enough to allow the manufacturing of a 1000 systems per year.	✓	Section 7.3.6
SAI-SYS-02	The system shall not damage the payload during launch, flight or landing.	✓	Section 7.2, Section 6.4.2

SAI-SYS-03	The system shall allow for unloading of the payload.	✓	Section 7.2.4
SAI-SYS-04	The system shall allow for the loading of the payload.	✓	Section 7.2.4
SAI-SYS-05	The system shall be designed in such a way that it can be found by recipients after landing.	✓	Section 6.1.2
SAI-SYS-06	The system shall not harm the recipient of the payload during payload extraction.	✓	Analysis in detail design
SAI-SYS-07	The life cycle cost of the system shall be minimised for the production of a 1000 systems a year.	✓	Chapter 8
SAI-SYS-08	The system shall be able to operate in three named climate models: Trondheim-NOR, Fukushima-JPN and Timbuktu-MLI.	✓	Section 7.5.2
SAI-SYS-09	The system shall be retrievable by the recipients in <td>% of the launched systems.	TBD	Testing in detailed design
SAI-SYS-10	The system shall have a ground shelf life of at least 10 years.	✓	Section 7.3.7
SAI-SYS-11	The system shall communicate with the user, ATC (Air Traffic Centre) and ground station.	✓	Section 6.1
SAI-SYS-12	The system shall be degraded for at least 90% after five years.	✓	Section 7.5.1
SAI-SYS-13	The system shall have a minimum range of 125 [km] at maximum launch altitude.	✓	Section 5.8.2
SAI-SYS-14	The system shall be able to navigate autonomously from launch up until landing.	✓	Section 6.2
SAI-SYS-15	The cradle-to-grave life cycle of the system shall not have an environmental cost indicator greater than €75,000 regarding the production of a 1000 systems per year.	✓	Figure 8.1.1
SAI-SYS-16	The End-of-Life of the system shall not have a harmful impact on the environment.	✓	Section 6.5
SAI-SYS-17	Materials derived from renewable resources shall be more than 90% of the total materials integrated in the system.	✓	Section 3.3
SAI-SYS-18	The integration of the system with the launch vehicle shall not damage the system and/or launch vehicle under the loads specified by the launch element manufacturer.	TBD	Demonstration in detailed design
SAI-SYS-19	The system shall not damage human-made structures upon landing.	✓	Section 6.2
SAI-SYS-20	The system shall not harm recipients upon landing.	✓	Section 6.2
SAI-SYS-21	The system shall fulfill drone supervision during the mission according to the European Union Aviation Safety Agency (EASA).	TBD	Analysis in detailed design
SAI-SYS-22	The system shall be dispatched in maximum 18 hours after the request for supplies has been made.	✓	Section 6.4.3
SAI-SYS-23	The system shall have a maximum mass, including payload, of 25 [kg].	✓	Section 3.3
SAI-SYS-24	The payload shall have a maximum mass of 10 [kg].	✓	Section 2.3
SAI-SYS-25	The system shall have a maximum power usage of 33.5 [W] during operation.	✓	Section 6.3.10
SAI-SYS-26	The system shall have a maximum energy usage of 208 080 [J] during operation.	✓	Section 6.3.9
SAI-SYS-27	The system shall have a maximum operational lifetime of 24h.	✓	Section 5.8.1
SAI-SYS-28	The system shall have a maximum launch altitude of 5000 [m].	✓	Section 6.4.1
SAI-SYS-29	The payload volume shall be at maximum 0.25 [m ³].	✓	Section 2.3
SAI-SYS-30	The system shall fit inside a 40 [ft] container (12.032 x 2.352 x 2.385 [m])	✓	Section 6.4.3

4. Market Analysis

There are many aspects to the market analysis performed on the SustAln project. The first aspect is related to the origins of SustAln, the stakeholder analysis, and whether the stakeholder requirements have been met. Secondly the business aspect is treated; identification of the market gap and how GliMed competes with similar businesses. The next part is the related to the cost breakdown and when the financial break even point is reached. The last is the situational or recipient analysis; an analysis of the operation scenario in Mali and to what lengths the recipients will go for reusability.

4.1. Stakeholder Analysis

There were a large number of stakeholders identified in the project plan, [37] whose needs determine the parameters within which GliMed was designed. SustAln's These stakeholder needs, translated into stakeholder requirements, must be fulfilled before the design can be accepted, and the project complete.

The stakeholders of SustAln as given in the project plan are:

- Sender of the Payload/User of the Glider
- Recipient of the Payload
- Manufacturers of the glider
- Environmental activist
- Investors and Charities
- Legislative bodies
- Manufacturer of the Payload
- The launcher company

This list has however changed due to mainly operational decisions. The responsibilities of launching the glider, managing the flight mission, and the manufacturing of GliMed all now fall under SustAln.

Therefore there are a few less stakeholders to consider than in the early phases of the project. The largest of these is the sender of the payload. This is a company who, in close collaboration with SustAln, determines the locations the gliders are sent to; organises the communication with the recipient; and organises the payload. This stakeholder is also the largest client of SustAln, and there are a number of possible companies to approach. One of these is MSF, or doctors without borders¹ who already do a large amount of work in supplying international medical aid.

The recipients are an important stakeholder for the design process, and these are discussed further in Section 4.4, as well as described in the personas mentioned in Section 2.2. The remainder of the stakeholders, and their interactions with SustAln is summarised in Figure 4.1.

The mentioned stakeholder requirements are also analysed in order to ensure they are met. Whilst the stakeholders no longer exactly reflect the origins of the requirements, these requirements are still a large part of the design process. To check that they have been accurately taken into account, the reference to the system requirement is given and the compliance is given in Table 4.1.

Table 4.1: Compliance matrix for stakeholder requirements

Identification	Requirement	Compliance	Discussion
SAI-SH-01-GM	The system shall be easy to manufacture.	✓	SAI-SYS-01
SAI-SH-02-PM	The system shall protect the payload.	✓	SAI-SYS-02
SAI-SH-03-PM	The system shall be able to be put the payload into the system before launch.	✓	SAI-SYS-04
SAI-SH-04-PR	The system shall make the payload retrievable to the recipient.	✓	SAI-SYS-03
SAI-SH-05-PR	The system shall be safe to handle.	✓	SAI-SYS-06

¹<https://www.msf.org/> [cited on 15/06/21]

SAI-SH-06-GU	The production volume of the glider shall be a 1000 systems per year.	✓	SAI-SYS-01
SAI-SH-07-GU	The system shall have sufficient reliability.		SAI-SYS-09
SAI-SH-08-GU	The system shall be usable for an extended period of time after production.	✓	SAI-SYS-10
SAI-SH-09-GU	The operator shall know the status of the system at all times.	✓	SAI-SYS-21, SAI-SYS-11
SAI-SH-10-GU	The system shall be used for one single mission.	✓	SAI-SYS-12
SAI-SH-11-GU	The system shall fly far enough.	✓	SAI-SYS-13
SAI-SH-12-GU	The system shall fly itself to hard-to-reach areas.	✓	SAI-SYS-14
SAI-SH-13-EA	The environmental impact of the system in case of a cradle to grave scenario is minimised.	✓	SAI-SYS-07, SAI-SYS-15, SAI-SYS-16, SAI-SYS-17
SAI-SH-14-LC	The system shall not damage the payload during flight or landing.	✓	SAI-SYS-02
SAI-SH-15-LB	The system shall be safe during operation.	✓	SAI-SYS-19, SAI-SYS-20
SAI-SH-16-LB	The system shall be compliant with regulations for drones from the European Union Aviation Safety Agency (EASA) in respect to safety and reliability.	✓	SAI-SYS-21
SAI-SH-17-IC	Those in need shall receive the aid as soon as possible.	✓	SAI-SYS-22, SAI-SYS-27

4.2. Market Gap and Competition

A detailed analysis of the market, and potential competitors was performed in the Baseline report[35]. The most similar competitors identified were Zipline², Logistic Gliders Inc.³, and Silent Arrow⁴; all autonomous drones providing supplies to isolated areas. A comparison of these can be found in Table 4.2, with GliMed included as reference. Note, the costs will be discussed in the following section.

Table 4.2: Table showing the characteristics of the closest competitors of GliMed

	Range [km]	Payload [kg]	Cost [Euro/flight]	Cost [Euro/km/kg]	Single-use	Powered
GliMed	125 + 275	5.35	-	-	Yes	No
Zipline	48	1.8	50	0.579	No	Yes
Logistics Gliders Inc.	130	750	11000	0.113	Yes	No
Silent Arrow	60.5	740	9500	0.212	Yes	No

As well as those competitors mentioned in the table, a number of other transport types were investigated for cost and properties. These include helicopters for air transport, and ground relief transport organisations. Combining this market research, it can be noted that there is no competitor for long range, small mass air transport, and GliMed fits perfectly within this gap.

In further research of the market, a SWOT analysis has also been performed on SustAIn. This can be seen in Figure 4.2. The strongest points of GliMed is that it is fully biodegradable, provides zero contamination risk and considers environmental life cycle cost with great care. These add to the market gap GliMed finds itself in.

²<https://flyzipline.com/> [cited on 15/06/21]

³<https://logisticgliders.com/> [cited on 15/06/21]

⁴<https://silent-arrow.com/> [cited on 15/06/21]

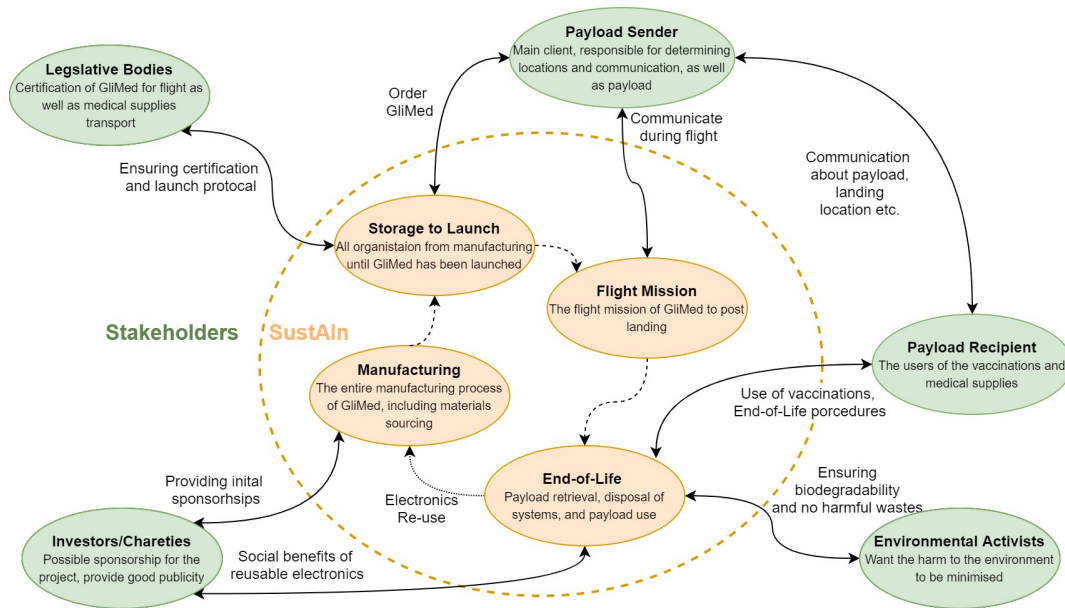


Figure 4.1: The interactions between the stakeholders and SustaIn, as well as the main components within the project itself.

SustaIn SWOT Analysis		Helpful	Harmfull
Internal origin	Strengths	<p>Biodegradability of GliMed Fully biodegradable after EOL procedures</p> <p>Zero Contamination Risk when transferring vaccines for comtagious viruses</p>	<p>Small Payload Size Compared to the single-use gliders among the competitors</p> <p>Detailed EOL Procedures Relying heavily on recipients to realise sustainability</p>
	Weaknesses		
External origin	Opportunities	<p>Growing Industry Large growth of the industry seen in recent years</p> <p>Contract Availability Many contracts for similar products have been made available in recent years</p>	<p>Too Late to Market Many emerging companies seen, which may fill the market gap partiall before SustaIn goes commercial</p> <p>Many Competitors In a similar markets</p>
	Threats		

Figure 4.2: SWOT analysis of the SustaIn project

From comparison with the market price of the competitors mentioned in Table 4.2 and similar modes of transport, the price per kg of payload and km travelled is found to be between 0.30-0.45 Euro/km/kg. With the range of 400km including the launcher, and a payload mass of 5.35 kg, this translate to a optimal market price between 650 and 960 Euros. The actual cost breakdown of GliMed will be presented in the following section.

4.3. Cost Breakdown

The costs of the GliMed company can be divided into three sub-categories; development costs before the system becomes operational, as well as the ongoing costs of production and direct operations per glider. The breakdowns of these costs are shown in Figure 4.3.

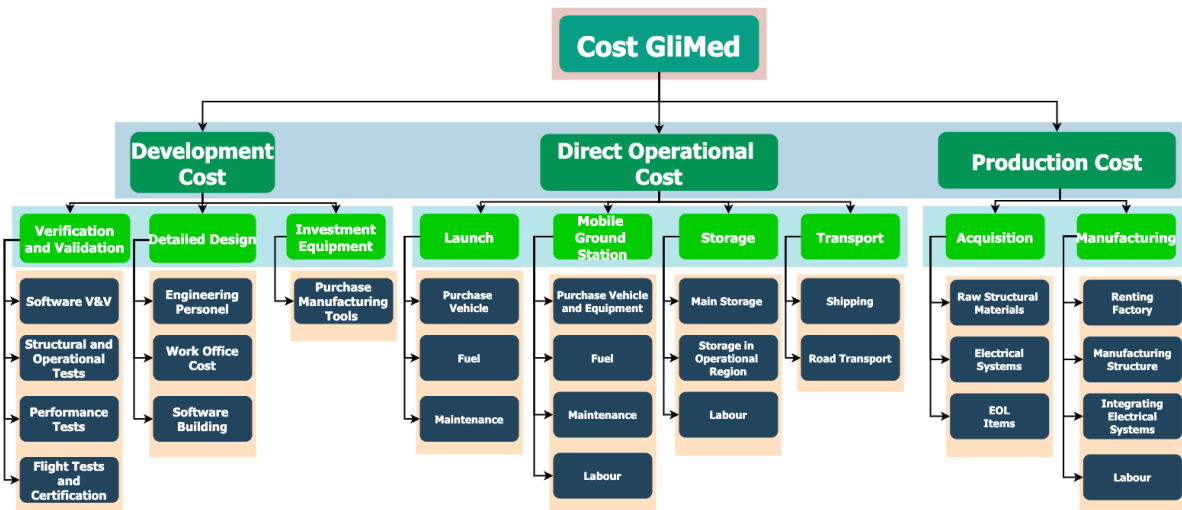


Figure 4.3: The cost breakdown structure of the GliMed company. The general cost sources are displayed in the diagram.

4.3.1. Development cost

The development costs are those associated with getting the system flight ready. Firstly including the detailed design costs, after which verification and validation tests will be performed for certification of the glider. Furthermore, once the final production plan is known, the production of the manufacturing facility will also add to the development costs. The estimation of these costs is based on similar projects, namely Zipline, Otherlab's Everfly and Logistic Gliders Inc. Moreover, development costs for the autopilot are included in this phase.

Detailed Design Costs

For the purpose of this cost breakdown, it is assumed that the detailed design team will still consist of 6 engineers, working 40 hours per week. These six engineers are based on the team Everfly from Otherlab, which has designed a biodegradable glider drone, capable of delivering about 1 [kg] of payload⁵. The average salary of junior startup members ranges from 30,000 to 40,000 euros^{6 7 8}, and the lower value was used for a small start-up. Based on the timelines of Zipline, Otherlab's Everfly and Logistic Gliders Inc., the expected detailed design duration is 2 years.

Verification, Validation and Certification Costs

The estimations of this phase will be based upon Logistic Gliders Inc. and Otherlab's Everfly. Logistics Gliders tested an average of 20 full scale prototypes, and 58 versions of 25% scale prototypes during a period of 5 years. The APSARA drone of Everfly took only 1 year of testing. Since the scale of GliMed glider is in between the APSARA drone and the Logistics Gliders product, testing is expected to take up to 2 years, with the same salaries as in the detailed design stage above. About half of the number of prototypes from Logistics gliders will be used, as this is assumed to be enough for testing the GliMed product. The manufacturing and material costs for these are taken from Section 4.3.3.

Constructing Manufacturing Facility Costs

The machines required for the production of GliMed and prototypes are as mentioned in Section 7.3.6. The costs for these individually are shown in Table 4.3. Finally the total development costs are shown in Table 4.4.

⁵<https://techcrunch.com/2017/02/22/otherlabs-cardboard-drone-can-carry-up-to-2-lbs-then-decompose/>[cited on 19/06/21]

⁶<https://www.computable.nl/artikel/nieuws/computable-next/6239873/250449/startup-scene-groeit-sneller-dan-arbeidsmarkt.html#:~:text='De%20Nederlandse%20startup%2Dmedewerker%20verdiend,hel%20modale%20inkomen%20in%20Nederland>[cited on 16/06/21]

⁷<https://www.payscale.com/research/NL/Location=Delft/Salary>[cited on 16/06/21]

⁸<https://magazine.startus.cc/european-startup-report-2017-uk-dominates-comes-career-prospects/>[cited on 16/06/21]

Table 4.3: Tooling costs for manufacturing facility

Tooling	Cost
Laser cutter ⁹	€2,240
CNC saw ¹⁰	€12,000
CNC router investment ¹¹	€8,875
Robot arm investment ¹²	€18,258
Hand tools	€10,000
Vacuum former (wood) ¹³	€5,000
Veneer mold ¹⁴	€8,000
Moulded paper pulp station ¹⁵	€64,692
3D Printers (x8) ¹⁶	€48,000
Total Tooling	€177,065

Table 4.4: Approximated development cost for GliMed.

Item	Cost
Design Salary	€360,000
Design Office	€206,400
Design Autopilot [52]	€205
V&V Salary	€360,000
V&V Workspace	€516,000
V&V Prototypes	€14,012
Total Tooling	€177,065
Total	€1,633,682
Total with margin (10%)	€1,797,050

4.3.2. Cost electrical systems

This section will focus on the cost of the three electric systems, with the return rates for the reusable electronics factored in. As mentioned in Section 4.4, these are 15% for Mali, and 50% for Norway and Japan. The details on the components of the systems can be found in Chapter 6. Furthermore, it is assumed the electrical system can be used at most 10 times. The limiting factor is the battery lifespan of two-three years. The cost of the return system varies per country due to the difference in cost of shipping and return percentage. These are presented in Table 4.5

Table 4.5: The cost of the three types of electric systems, of which the returnable system is specific to the country

System	Cost
Single-use	€588.00
Reusable for recipients	€615.45
Returnable in Mali	€524.55
Returnable in Japan	€311.50
Returnable in Norway	€316.82

4.3.3. Production cost

The production cost per glider can be broken down into material costs, labor costs, direct other expenses and overhead expenses [57]. The computed values can be seen in Table 4.6. Indirect costs such as labor and overheads were calculated for a year and divided by the 1000 system a year production volume. The material costs are subdivided into individual manufacturing divisions. These costs represent the amount paid to suppliers for raw materials, prefabricates and products used within the glider. In order to minimise the labor costs it would be beneficial to locate the factory in the eastern European region, therefore the labor costs are based on the average Polish hourly labour cost of €11.00 ¹⁷. In Section 7.3.6 it was estimated that 5 full time (8 hour workday) workers were needed. Direct other expenses are based on the electrical consumption of machinery and depreciation of the machinery.

⁹https://www.alibaba.com/product-detail/Wood-Cutter-Laser-Laser-Cutter-Supplier_1600143109743.html?spm=a2700.galleryofferlist.normal_offer.d_title.7f2c7bdcojhHS3&s=p [cited on 16/06/21]

¹⁰https://www.alibaba.com/product-detail/woodworking-CNC-Vertical-wood-cutting-band_60580833484.html [cited on 16/06/21]

¹¹<https://zhongkecnc.en.made-in-china.com/product/mBKEuNkHbIYb/China-12-Cutters-Automatic-Tool-Changer-Woodworking-CNC-Router.html> [cited on 16/06/21]

¹²https://www.alibaba.com/product-detail/5KG-6KG-Payload-6-Axis-Industrial_60608100799.html?spm=a2700.galleryofferlist.normal_offer.d_title.266d11a5TX1vTh [cited on 16/06/21]

¹³https://www.alibaba.com/product-detail/Corian-veneer-3D-silicone-vacuum-membrane_60574496435.html [cited on 16/06/21]

¹⁴<https://3space.com/blog/thermoforming-cost/> [cited on 16/06/21]

¹⁵https://www.alibaba.com/product-detail/Automatic-cups-boxes-plates-containers-pulp_1600245704814.html?spm=a2700.7724857.normal_offer.d_title.14834503rYYqH [cited on 16/06/21]

¹⁶<https://all3dp.com/1/ultimaker-s5-3d-printer-review/> [cited on 16/06/21]

¹⁷https://ec.europa.eu/eurostat/statistics-explained/index.php?title=Hourly_labour_costs [cited on 16-06-21]

Electrical consumption of machinery was estimated based on the technical specification of representative machines and estimated machine hours. Furthermore, 0.07 [€/kWh] was used as a basis for the cost estimation, which is the average industrial cost of electricity in France¹⁸. Depreciation is estimated by the average depreciation for machinery in Italy (5% annually)¹⁹. Overhead expenses consist of the electrical costs and cost of renting a factory. Electrical costs are estimated on the basis of average energy consumption of non refrigerated warehouses (71 [kWh/m²])²⁰. Warehouses are used as a reference since they offer an estimate on the bare minimum energy expenditure the factory may need without any machinery. Finally the rent is based on the average annual industrial rent per square meter in Poland (€43.00)²¹. This value is then further multiplied by the estimated area of the factory (600 [m²]).

Table 4.6: Production cost per glider

Cost item	Cost
Material costs	€29.39 (excl. electronics)
<i>Fuselage structure</i>	€8.61
<i>Wing structure</i>	€4.58
<i>Electronics systems (Energy, Autopilot & Communication)</i>	refer to Table 4.5
<i>End of life systems</i>	€16.20
Labour costs	€115.79
Direct other costs	€13.41
<i>Electrical costs</i>	€5.02
<i>Depreciation</i>	€8.39
Overheads	€65.67
<i>Electrical costs</i>	€39.87
<i>Rent</i>	€25.80

4.3.4. Direct operational cost

The operational costs can be divided into transport costs, labor costs, storage cost, mobile launch truck costs and the costs for the launch vehicle. These latter two also include the fuel and maintenance cost. For more information about the logistics and operations concept, see Section 6.4.3. In Table 4.7, the total cost per glider for each country are presented, while in Figure 4.4, Figure 4.5 and Figure 4.4 the subdivision of the total cost can be found. For costs that are not directly related to the launching of a glider, such as the labor costs²² and the storage costs^{23 24 25 26}, a cost per glider was calculated by dividing the monthly cost by the total number of gliders launched in a month. For the purchasing cost of the mobile launch truck²⁷ and the launch vehicle²⁸, a life time was estimated²⁹ and this was divided by the total number of gliders launched. For the launch vehicle this was 100,000 flight hours, while the mobile launch truck is estimated to last 500,000 [km]³⁰. The average distance that the mobile launch truck will have to travel per launched glider is based on the map of the specific countries. The

¹⁸<https://www.statista.com/statistics/1046605/industry-electricity-prices-european-union-country/> [cited on 16-06-21]

¹⁹https://www.adrioninterreg.eu/wp-content/uploads/2017/06/Adrion_tabel_on_depreciation_updated_2017_09_29-002.pdf [cited on 16-06-21]

²⁰<https://www.eia.gov/consumption/commercial/data/2012/c&e/cfm/pba4.php> [cited on 16-06-21]

²¹<https://www.statista.com/statistics/858110/average-annual-industrial-rent-cost-per-square-meter-by-european-country/> [cited on 16-06-21]

²²<http://www.salaryexplorer.com/salary-survey>[cited on 17-06-21]

²³<https://cityselfstorage.no/self-storage/trondelag/trondheim/>[cited on 17-06-21]

²⁴<https://www.expat.com/en/housing/africa/mali/houses-for-rent.html>[cited on 17-06-21]

²⁵<https://niconicotrunk.com/tokyo/tachikawa-shi>[cited on 17-06-21]

²⁶<https://ecommercenews.eu/warehouse-storage/>[cited on 17-06-21]

²⁷<https://www.bastrucks.com/stock/semi-trailer/closed?page=1>[cited on 17-06-21]

²⁸<https://thefutureofthings.com/5639-camcopter-s-100-uav/>[cited on 17-06-21]

²⁹<https://www.flexport.com/blog/decommissioned-planes-salvage-value/>[cited on 17-06-21]

³⁰<http://www.outdoorsmenforum.ca/archive/index.php/t-132837.html>[cited on 17-06-21]

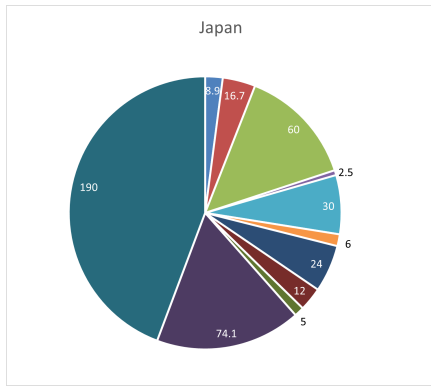


Figure 4.5: Division of operational costs in Japan. All values are in €, and the legend is the same as in Figure 4.4.

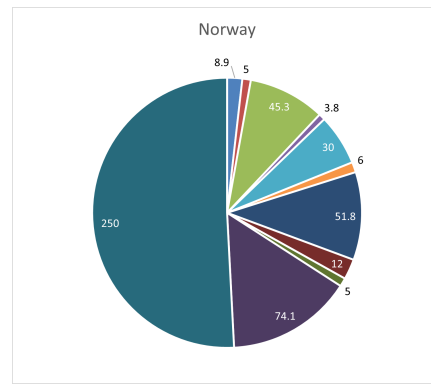


Figure 4.6: Division of operational costs in Norway. All values are in €, and the legend is the same as in Figure 4.4 .

fuel costs ^{31 32 33} is also based on this average distance. For the labor costs, the average monthly salary in each country was taken (except for Mali, where a higher salary was used), again divided by the number of gliders launched per month. Each launch truck is operated by two employees and one employee is manning the base station in each country. For Mali and Japan, 60 gliders can be stored, while in Norway only 16 gliders are stored. The main storage location can store up to 1200 gliders. For the transport costs, both the shipping costs ^{34 35} and the costs of the transport by road [20] are considered.

Table 4.7: The total operational costs per glider in each country

Country	Cost
Mali	€298.20
Japan	€429.20
Norway	€491.90

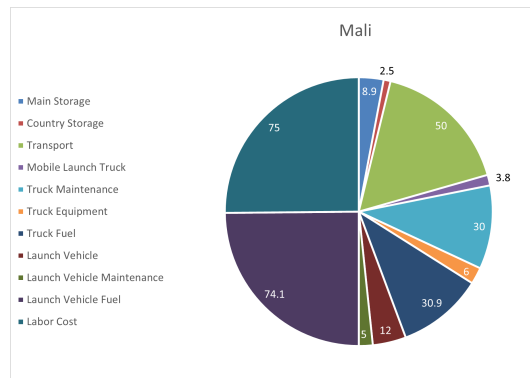


Figure 4.4: Division of operational costs for Mali where all values are in €.

4.3.5. Final glider cost

The final cost per glider sums up both direct operational- and production costs. As three different types of electrical systems will be used for the glider, and these are different in each of the three countries, a

³¹https://www.globalpetrolprices.com/gasoline_prices/#h1126[cited on 17-06-21]

³²https://theicct.org/sites/default/files/publications/EU_HDV_Testing_[cited on 17-06-21]

³³<http://www.airnav.com/fuel/report.html>[cited on 17-06-21]

³⁴<https://www.icontainers.com/ship-container/japan/>[cited on 17-06-21]

³⁵<https://www.icontainers.com/ship-container/africa/>[cited on 17-06-21]

weighted average is used to obtain the final cost. As mentioned in Figure 6.5, Mali will have 80% usage of the returnable system, 11% of the reusable, and 9% single-use. While this has not been calculated for the other countries, it is assumed similar proportions will be used. Furthermore, it is expected the same operational volume will be used in all three countries, once it has been firmly established in Mali.

This gives a final glider cost of €1058.70, and with a 10% contingency this is €1165.00. Unfortunately these values are already larger than the optimal market price of €960.00, and more will be added to cover both profit and developmental costs. Therefore the problem must be approached from a different perspective. Each of the competitors have either a smaller range, or a much larger payload, and are therefore immediately comparable with GliMed. As GliMed lies within its clearly defined market gap, the price does not need to be as comparable to the competitors.

Additionally, to cover a portion of the developmental costs, research grants or funding can be sought. One option for such funding is from the European Research Council, where two grants of over €1.5 million each are available for autonomous vehicles and materials mimicking nature³⁶. Consequently, it can be assumed that at least 75% of the development costs (€1.3 million) can easily be obtained by such grants.

Assuming the remainder of the development costs are spread over the operational years, the profit for each glider cost can be visualised in Figure 4.7. With at least €50 profit per glider (excluding development costs) to overcome uncertainties in the estimation, the market price of the glider can be as low as €1250 if the investment in development costs can be returned over a period of 15 years.

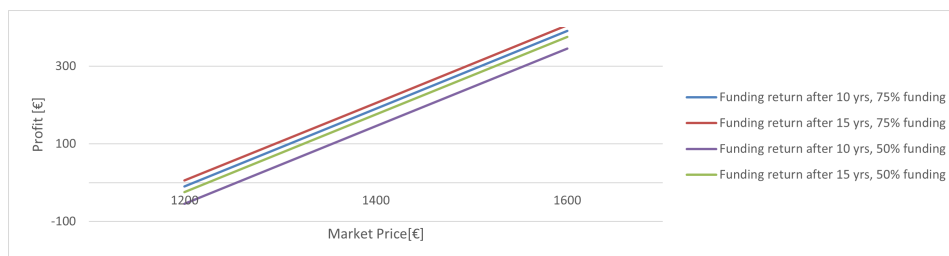


Figure 4.7: Graph showing the profit against market price, for two different periods of investment return, and two different levels of funding.

4.3.6. Breakeven point and return on investment

With the development costs, production costs and market price known, the profit/loss curve is shown in Figure 4.8. From this it can be determined that the break even point occurs during the 12th year of SustAln.

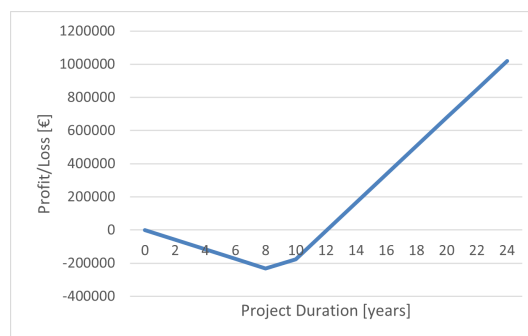


Figure 4.8: Graph showing the profit and loss curve of SustAln, over a 30 year period starting from being of detailed design phase.

The market price of the glider is still larger than that of competitors. Nevertheless, SustAln has a particular niche in the market which cannot be fulfilled by any of the competitors mentioned above. The range of GliMed can only be met by aircraft which are much larger and more expensive, enabling SustAln to establish itself as a more flexible, smaller and cheaper option. Furthermore, the market

³⁶<https://erc.europa.eu/projects-figures/stories/autonomous-flight-inspired-nature> [Sourced on 19/06/21]

price can be decreased slightly when there is less uncertainty about the development and production costs, and if the profit margin is deemed excessive.

In addition to the main service provided by GliMed, SustAln also has a tangible benefit on the social sector. The reusable electronics can be further designed in such a way to markedly enhance the knowledge and financial capabilities of the recipients. Besides this, incentives for the returnable electronics can also be designed in such a way to benefit the society as a whole.

Lastly, these profit and loss values were used to determine the return on investment, according to Equation 4.1. Using this, a return on investment of 125% was calculated for the 24 year period.

$$ROI = \frac{\text{Net Profit/Loss}}{\text{Investment}} \cdot 100\% \quad (4.1)$$

4.4. Recipient and Situational Analysis

While the design of GliMed is a difficult technical challenge, the operations, logistics and end-of-life are heavily influenced by the location of operations and the attitudes of the recipients. It is for this reason that both these points have been thoroughly analysed.

Situational Analysis

As has been mentioned earlier in the report, the operational analysis of the glider will be limited to the surroundings of Timbuktu, as described in Chapter 2. Mali lies in the poorest region of the world, with about 47% of the population lives in extreme poverty³⁷, earning less than \$1.25 per day³⁸. On top of that, the country is politically unstable, with coups occurring in August 2020 and May 2021 in recent years, and according to a medical aid organisation MSF³⁹: *"Access to medical care remains very limited in the north and centre of Mali due to a lack of medical staff and supplies and spiralling violence between armed groups."*

Mali has been a land in crisis for the 6 years, resulting in large amounts of displaced refugees. The three chosen regions are more isolated, and contain a large amount of nomadic communities, which would be ideal for the disposable or reusable glider. 62 of these communities have been aided in the last year by MSF, and a cooperation with this organisation can be to the benefit of all.

Lastly, agriculture is the primary industry in Mali, with 70% of the workforce involved, and generating over 40% of the countries GDP.

Recipient Analysis

Tailoring GliMed to suit the recipients is a large part of making the project attractive to investors and companies as it ensures the use of the project will be optimised. The personas mentioned in Section 2.2 describe a scenario for all three climate zones, but this recipient analysis will focus on the operational scenario in Timbuktu. Furthermore, the glider is deemed unsuitable for providing vaccines for those in cities or towns, as the capacity is not large enough and there is assumed to be another medical supplier available.

This recipient analysis is also a large part of assessing the viability of the three different electronics systems. Research on the return rate of posted surveys shows that response rates of 50-60% can be expected for more affluent regions, while only 15-40% can be expected for lower income regions.[16] Due to the current crisis, political instability and high percentage of extreme poverty, it can be assumed the return rate is at the lower limit. However this return rate can be increased by incentivisation.

There are two types of incentivisation considered; Egoistic and Altruistic. Egoistic incentivisation plays on the inherently selfish nature of the human species. Letting a voice be heard, or giving power to someone can increase the return rate. Altruistic incentivisation focuses on the benefit on the greater society from the cooperation. Here a large emphasis will be placed on the fact that another community will benefit from their additional efforts. Furthermore, monetary incentivisation can be used as a last resort, but further research should be put into making this sustainable and not detrimental. [14]

³⁷<https://www.worldbank.org/en/country/mali/overview> [cited on 08/06/21]

³⁸<https://www.takepart.com/flashcards/what-is-extreme-poverty/index.html> [cited on 08/06/21]

³⁹<https://www.msf.org/mali> [cited on 08/06/21]

5. Performance

The main goal of the aerodynamic design of the GliMed is the ability to perform similarly to a high performance glider, maximising the lift-to-drag ratio and having a formidable glide range. The fact that a flying wing configuration was chosen meant that the wing has to generate the necessary lift as well as provide stability and controllability. This chapter will discuss the design of the outside geometry of the glider required to fulfil the performance requirements. In Section 5.1, the design of the airfoils and wing are discussed, and an overview of the performance of the design is given. In Section 5.6, the control and stability of the configuration and relevant design considerations are discussed. This chapter is concluded with the compliance matrix, showing the requirements that have been fulfilled or that still need to be considered in the post conceptual phase.

5.1. Airfoil Selection

The first choice made during the aerodynamic design process is the choice of airfoils. Due to the configuration change two new airfoils were selected and the trade-off that was performed in the midterm report was revisited [36]. The first airfoil was chosen for the outer wing section of the flying wing glider and the second airfoil would house the payload, both are shown in Figure 5.1 and Figure 5.2. Subsequently, the main functions of lift generation, and stability and control were split between the two airfoils. The exact reasoning behind this choice is explained in Section 5.6.2.

5.1.1. Wing section airfoil

This airfoil, Figure 5.1, was tasked with the generation of the high lift. To ensure that the glide ratio requirement was met while not impacting the control and stability negatively, the airfoil was chosen according to the following criteria. Namely that the airfoil should have:

1. Low drag coefficient at both low and high lift coefficient
2. Gentle stall characteristics
3. Small positive moment coefficient for all angles of attack
4. A high $C_{L_{max}}$
5. A high C_{L_α}

With a thickness over chord of 9.2 % the SA7036-airfoil is a thin airfoil optimised for low-speed conditions and able to easily generate a lift over drag ratio of 80 at the relevant Reynolds numbers. The characteristics of this airfoil are shown in Table 5.1.

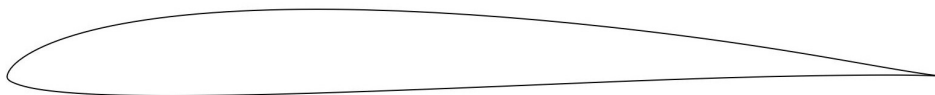


Figure 5.1: SA7036 airfoil (9% t/c)

5.1.2. Payload section airfoil

During the design process the height of the payload section, ≈ 0.22 [m], proved to be a constraint for the flying wing configuration. The minimum allowable height for the cool box was too large for a conventional thin airfoil, thus a custom airfoil was designed. In addition, the main aerodynamic function of this airfoil was chosen to increase the longitudinal stability and controllability of the configuration, since this is not provided by the outer wings. This meant that this airfoil was designed with a reflexed trailing edge, meant to induce a large positive pitching moment, further elaborated on in Section 5.6.2.

Coincidentally, the wing loading of the glider, W/S , constrained the total surface area of the glider used to generate lift. It was preferred that most of the surface was on the thin wing, meaning more wing area to generate lift. Since when analysed the reflexed section proved to have a poorer lift generation performance compared to the thin wing section. To determine the thickness of the airfoil, two airfoil options were traded off: the first with a thickness over chord of 15 % and the second with a thickness

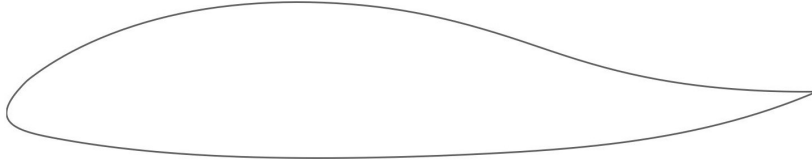


Figure 5.2: Custom reflexed airfoil (21% t/c)

over chord of 21%. Unable to decrease the dimensions of the payload anymore, the thicker airfoil proved to be more efficient. With the thin airfoil the surface area of the payload section was simply too large to fulfill the glide ratio requirement as the total surface area of the glider would become too large. This is explained further in Section 5.2. The airfoil was designed to be able to house the payload as optimally as possible, while maintaining good characteristics. Shown in Figure 5.2, the airfoil was designed to have a thickness over chord of 21% and the trailing edge is reflexed at 70% of the chord. To come to the design of the custom airfoil as shown here, many different reflex trailing edge sections were tested, with the aid of XFLR5 software, a 10° upward reflex deflection of the airfoil was found to be the best compromise between stability and performance. The tests resulted in 12° and 15° reflex airfoils having too much reflex, causing the GliMed custom to stall at low angles of attack, while 8° reflex was not sufficient to increase the C_m at $\alpha = 0$ enough.

5.1.3. Final airfoil Characteristics

An overview of the characteristics of both airfoils is given in Table 5.1. The airfoils have been analysed at the Reynolds numbers that are relevant for their respective flight conditions.

Table 5.1: Airfoil characteristics

Characteristics	SA7036	GliMed custom
C_{l_α} [rad^{-1}]	5.878	5.621
$C_{l_{max}}$ [-]	1.270	0.875
C_{d_0} [-]	0.0069	0.0073
α_{stall} [deg]	10.8	12.3
$(\frac{C_l}{C_d})_{max}$ [-]	84.8	50.4

5.2. Wing Planform Design

To compensate for the lack of propulsion, the weight must counteract the drag and a steady trim condition is only possible in descending, gliding flight (excluding dynamic soaring). When flying at constant airspeed in trimmed flight, the flight path angle γ equals the glide angle. The equations of steady state glide are used to relate the glide ratio to the lift-over-drag ratio. Further, the glide angle can be exchanged by the ratio of the glide range and the altitude. A glider can be optimised for high speed, a minimum rate of descent or an optimal glide speed. GliMed was designed to be optimised for the best glide range, since the best glide speed also grants the best range. This means that the lift-over-drag ratio of the aircraft has to be maximised.

In addition to the lift-over-drag ratio that has to be optimised, the speed polar of a glider, shown in Section 5.8, is heavily influenced by the wing loading W/S . An increase in wing loading will shift the point of minimum glide angle to higher airspeeds and if the wing loading is decreased to much this point will move closer to the stall speed of the aircraft. Since the requirements dictate a maximum glide angle and that additional performance is needed to be able to withstand adverse weather the wing loading may not be decreased below 70 [N/m^2]. Moreover, due to the constraints of the ability of the airfoil to produce lift, their lift coefficients, the surface area may not be decreased below a certain value. The minimum surface area was found to be 1.5, but the airspeed became a problem when the surface area was decreased as the stall speed was approached. This meant that the surface area had to be carefully controlled as too much or too little area would prove detrimental to the performance of the glider. Thus early on in the design process the conclusion was reached that iterations were needed to be able to

converge on the values of S and the glide speed V assuming that the aerodynamic performance would be enough.

The iterations started with the following estimation. Since no statistical data was available on the wing surface area of unmanned, biodegradable gliders, the first steps in the estimation the wing planform came from the wing loading. The total mass of GliMed is constrained to 25 [kg], meaning that the surface area is a function of altitude, the airspeed and the lift coefficient. The air densities were known since GliMed was constrained to fly between sea level and the altitude of 5 [km]. The lift coefficient C_L is dependant on the airfoils and the wing design. Based on the aforementioned airfoil data and other glider aircraft a minimum, middle and maximum achievable lift coefficients were chosen to estimate a wing area, namely 0, 0.6 and 1.2 [-]. The Figure 5.3 was created to show an estimation of the design space.

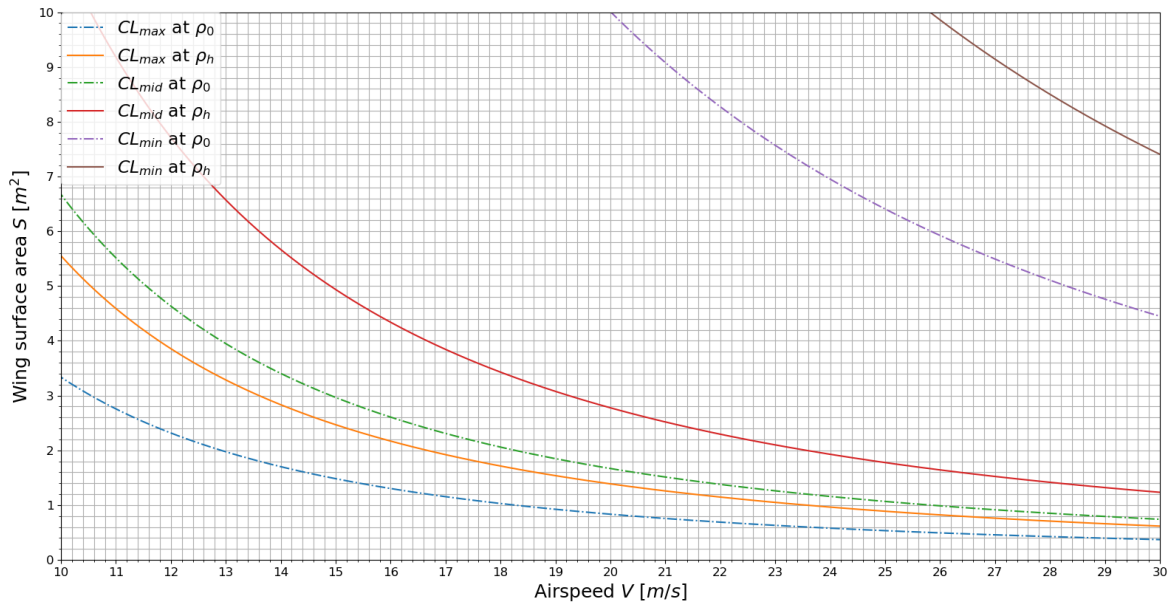


Figure 5.3: Estimation of design space wing surface area

The preliminary estimation of the wing surface area showed that a wing area of between 2 and 3 [m²] was sufficient, in case of lift coefficients of 0.5 and higher at all altitudes. To narrow down the flight speeds range, an estimate was made of the $(L/D)_{max}$ of glider. This was subsequently used to construct a speed polar, a graph relating the ground speed to the sink rate or Rate-of-Descent (RD) of the glider. An iterative procedure was created through the addition of the lift-over-drag plot, the drag estimation, and the effect of wind on the glide range.

This procedure started with the definition of a wing planform, excluding the payload section. The main function of this planform was the lift generation and several parameters were chosen to define the geometry. The root chord c_r , tip chord c_t , half span $b/2$ and leading edge sweep Λ_{LE} were chosen to be the define the wing geometry. Wing twist and dihedral were chosen to set to zero and not investigated. Affirmation of the positive effect of these two design parameter was not able to be achieved in the scope of the design project and through the use of XFLR5¹. The top view of the wing planform is shown in Figure 5.4. The winglet, payload section and tapered fairings connecting the parts are omitted. The elevon is also shown, it is elaborated upon in Section 5.7.2.

The shape of the wing is not constrained by the payload, but is solely dependant on the necessary amount of surface area and its ability to produce lift. An extensive iterative procedure has led to this wing design. The geometry can be summarised by the following values: the root chord $c_r = 0.4$ [m], the tip chord $c_t = 0.16$ [m], half span $b/2 = 2.6$ [m] and leading edge sweep $\Lambda_{LE} = 18.9$ [deg]. The design choices that led to these values are elaborated upon in the coming sections.

¹<http://www.xflr5.tech/xflr5.htm> [cited 10-06-2021]

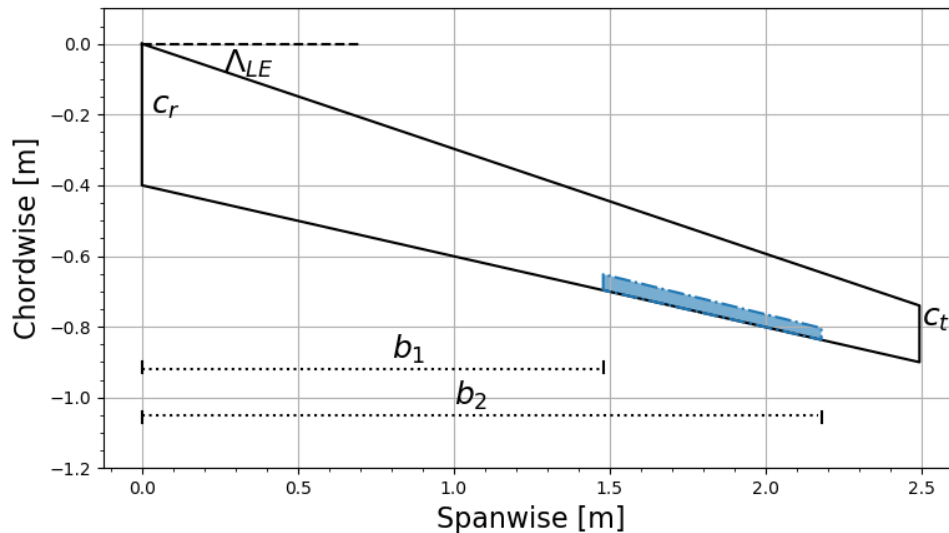


Figure 5.4: Top view of the half wing planform.

5.2.1. Design consideration

The logic that was used to construct the wing geometry is explained in this section. For an accurate design of the wing the effects of taper, sweep and aspect ratio were analysed and researched. All parameters were separately investigated and their combined effect was analysed to come to the final values that are given in text.

Taper

To control the lift distribution along the span and minimise the induced drag of the wings the taper ratio can be varied. To identify what the most optimal taper ratio was for the wing both literature was referenced and an extensive analysis was done using XFLR5 between taper ratios of 0.2 and 1.2 for wings with constant aspect ratio. From literature it was found that there exists an optimum taper ratio range for wings, which is accompanied by a minimum induced drag and a maximised Oswald's efficiency factor. However, decreasing the taper ratio could lead to wing tip stall. The optimum was found to be lie between 0.31 and 0.45 [77].

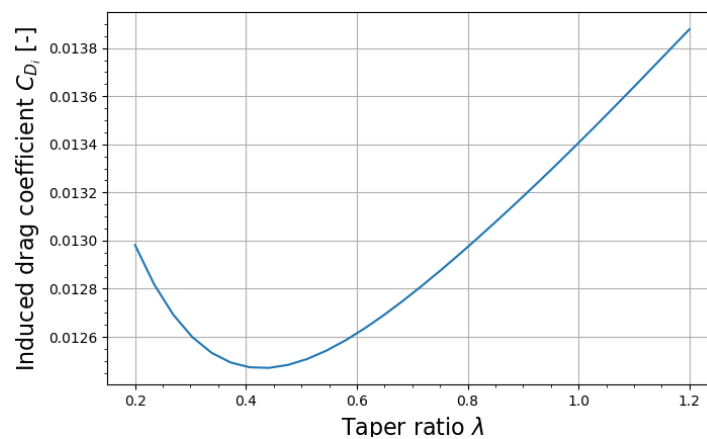


Figure 5.5: Induced drag coefficients against taper ratio

With the XFLR5 analysis of wing models with varied taper ratio and constant aspect ratio the following graph was made, Figure 5.5. For every test the taper ratio was varied and this was repeated for the aspect ratios: 12, 16, 20 and 24. The result that was found by this analysis predicts the same effects as was found in literature. On the basis of this and further intensive design iterations, also taking sweep into account, the taper ratio of the wing planform was chosen to be 0.4, within the optimal range.

Sweep

The addition of sweep to wings is generally used to move the aerodynamic centre of the wing forward or backward. The total wing pitching moment around this point does not change when the angle of attack is changed and it is incredibly important for stability and controllability. As will be explained in Section 5.6.4 the main design choice that led to the leading edge sweep as shown in Figure 5.4 was the need for sweep for stability and control. In the end, a leading edge sweep of 16.5° was chosen.

Aspect ratio

As the aspect ratio of the wing is increased the wing starts to behave more like an airfoil. As a result, the lift curve slope C_{L_α} and the maximum lift coefficient $C_{L_{max}}$ are increased. Coincidentally, the induced drag of the wing is reduced as the aspect ratio is increased. As the drag of an aircraft is made up of parasite drag and induced drag, it is important for a glider to minimise both of these contributions. For this exact reason gliders have high aspect ratio, in the range of 18 – 30. [73] The effect of an increase of the aspect ratio could be visualised by the widening of the drag bucket in the $C_L - C_D$ curve, a slight increase in C_{L_α} and an increase in the maximum L/D . To ensure that GliMed could perform similarly to high performance gliders, an analysis was performed using XFLR5. This analysis found that an optimum maximum aspect ratio existed for a straight, non-tapered wing, when the surface area was kept constant and only the chord and span were allowed to vary. The optimum was found to lie above 30, but due to structural reasons this proved to be difficult to realise. When tested in combination with the taper ratio and structural feasibility, the optimum was found to be between 12 and 27. The final wing geometry, shown in Figure 5.4, was determined to have an aspect ratio of 17.8.

Winglets

Winglets have a positive influence on two things: the effective aspect ratio and the lateral stability. However, the downside is that they add weight and possibly flutter, as well as drag. The lateral stability, which is highlighted in Section 5.6.5, was used to set a requirement on the minimum dimensions of the winglets. As can be read there, the minimum is that winglets exist, though more surface area and higher winglets make the glider more stable. The structural weight was used to set an upper limit on the dimensions, unlike flutter behaviour, which is not taken into account in this conceptual design due to its complexity.

The way winglets have an influence on the glide performance is in form of effective aspect ratio. Simply put, winglets decrease the energy in the wingtip vortices, thus decreasing the induced drag. Especially under low-speed, high-lift conditions [31], the effect of winglets is considerable. The amount with which the winglets decrease the induced drag is quantifiable using a k-factor [77]:

$$k = \frac{A_{eff}}{A} = \frac{C_{D_i}}{C_{D_{i_{eff}}}} = \left(1 + \frac{h_v}{b}\right)^2 \quad (5.1)$$

From this formula it is clear that the height of the winglets is more important than the surface area. However, again for structural simplicity, the root chord of the winglet is chosen to be the same as the tip chord of wing. Because the winglet does not increase the wingspan and thus the velocity, but does increase the glide ratio, their size is maximised. As can be seen in Section 7.2.2, this comes to down to winglet height $h_v = 0.4m$ and surface area $S_v = 0.048$. As can be read there as well, the winglets are in the shape of an airfoil. This is because winglets need to create inward pointing lift to increase their effectiveness [71].

The effect of the winglets on the glide performance has been taken into account by subtracting the induced drag as given by XFLR5 from the total drag, dividing it by k , and adding it again to come to a new total drag.

5.3. Payload Section

As explained in Section 5.2 the total surface area of the glider that is used to generate lift is limited. During the design process several options of housing the payload were therefore considered. Namely the use of a non-lifting payload section versus a lifting payload section. The use of non-lifting surfaces was found to be a difficult design option due to the dimensions of the payload and the choice of configuration. Additionally, the use of a non-lifting payload section was found to experience more drag than the lifting option. This was due to the increase in wetted surface area and the addition of reflexed wing

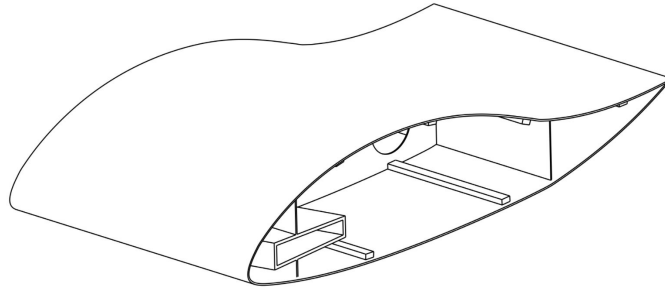


Figure 5.6: Isometric 3D view of the payload section

section that were necessary for the stability and controllability of the glider. The payload section was therefore designed to be a lifting surface, the airfoil shown in Figure 5.2. Since the choice was made to give the payload section the shape of an airfoil the necessary chord and thickness-over-chord had to not negatively impact the performance of the section.

The payload, as discussed in Section 6.4.2, is made up of several packages that all have rectangular shapes. The constraint that the payload had placed on the design of this section were the height, width and depth of the payload bay. The most important package for the height of the payload section was the cool box carrying the vaccines. The cooling box had been designed specifically for use in the GliMed aircraft and its dimensions could not be decreases further. This meant that the minimum height of the payload section had to be ≈ 0.22 [m], and the airfoil and wing section had to be designed around the payload. Simultaneously, the structural parts, such as the front and rear spar, of the section were also taken into account and with the GliMed custom airfoil the payload section was constructed, Figure 5.6.

Based on the height and depth requirements of the payload, the chord of the payload section was determined to be 1.07 [m], and the width of the section was determined to be 0.55 [m]. Due to the thickness-over-chord ratio of the airfoil the height of the payload section is 0.225 [m].

5.4. Drag Estimation

The drag of the glider consists of two parts, the parasite drag C_{D_0} and the lift induced drag coefficient C_{D_i} . To calculate C_{D_0} , Equation 5.2, the component drag build-up method is used.[77] [73]

$$C_{D_0} = \frac{1}{S_{ref}} \sum_c C_{f_c} \cdot FF_c \cdot IF_c \cdot S_{wet_c} + \sum C_{D_{misc}} \quad (5.2)$$

The components that will be taken into account are the payload section and the thin wing planform, their respective wetted surface area are given by their S_{wet_c} . Additionally, C_{f_c} is the flat plate skin friction coefficient, used to estimate the friction coefficients of all components. Depending on the boundary layer and the Reynolds number, this coefficient will vary for the different components. As laminar flow and turbulent flow exist on the wings coincidentally, the total C_{f_c} is a weighted average of the two. Transition analysis and skin roughness coefficients that were found for the materials of the payload section and the wing section [74], determined the percentages of laminar and turbulent flow over the airfoils. The outboard wing section was estimated to have 55 % laminar and 45% turbulent flow and the payload section had 10 % laminar and 90 % turbulent flow. FF_c is the component form factor and several empirical relations where used to determine the form factors of the wing- and payload section.[73] IF_c is the interference factor, it estimates the interaction of two component, e.g. the wing and the winglet, and was based on statistical values [73]. The interference factors for the fairing between the payload section and the wing, and the winglet are 1.4 and 1.04 respectively. Lastly, the miscellaneous drag contribution takes into account excrescence, drag caused by protrusions, control surfaces, etc. This contribution was assumed to add an 15 % to the contributions of the components.

Summing up the contributions of the components gives an estimate of the parasite drag of the glider

in flight. The contributions of the components and the total C_{D_0} is given in Table 5.2. Together with the lift induced drag, a $C_L - C_D$ can be constructed, shown in Section 5.5.

Table 5.2: Parasite drag contribution per component and the total

Component	C_{D_0}	% of total C_{D_0}
Wing	0.00768	55.15
Payload section	0.00443	31.81
Miscellaneous	0.00182	13.04
Total	0.0139	100 %

$$C_{D_i} = \frac{C_L}{\pi A e} \quad (5.3)$$

The other contributions to the drag of the glider is the induced drag, Equation 5.3. It is dependant on the lift coefficient C_L , the aspect ratio A and e is the Oswald efficiency factor. Since the glider is a flying wing with 2 distinct sections, the effective aspect ratio had to be calculated for this configuration. The effective aspect ratio that was used for the calculation of the lift-drag polar was 18.5. [77] The lift-drag curve for the glider is shown in Section 5.5, the values of C_L were found through use of XFLR5.

5.5. Final Geometry Performance

With the wing, payload section and winglets designed, these parts can be connected to form the final aerodynamic design. Connecting the root chord of the wing and the payload section is a fairing that has designed to make the transition between the two sections as optimal as possible while also allowing for structural reinforcements and other subsystems. An overview of how the wing, payload section and fairing fit together has been shown in Figure 3.5. This 3D model has been analysed using XFLR5 at the flight speed of 19 [m/s], which was determined to be the ideal airspeed. The resulting data has been used to generate the following graphs.

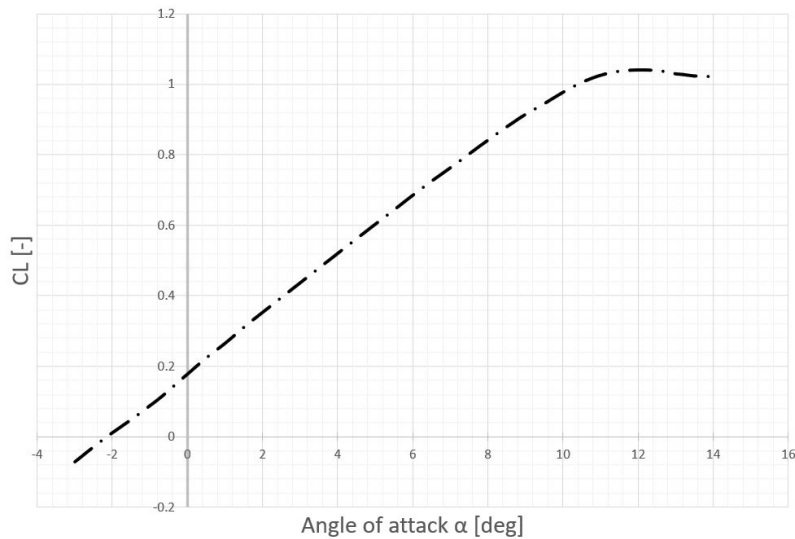


Figure 5.7: C_L versus α curve of the final geometry

The $C_{L_{max}}$ of GliMed equals 1.04 [-] at an angle of 12 [deg].

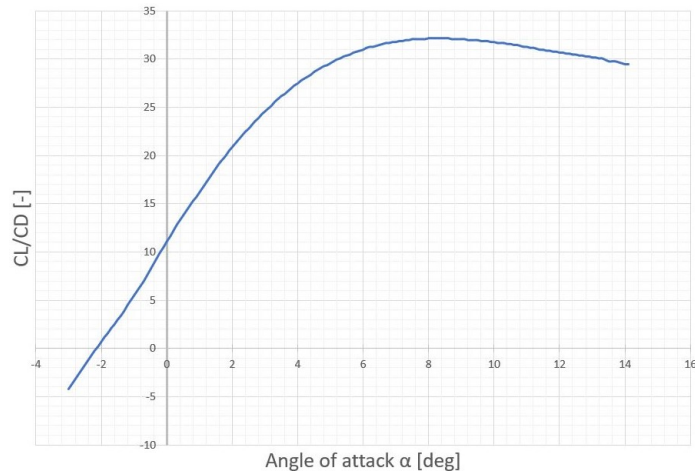


Figure 5.8: C_L/C_D versus α curve of the final geometry

The value for C_{D_0} , found in Section 5.4, has been added to the to the values that were found for the induced drag. When C_L is 0, C_D does not equal C_{D_0} is due to the fact that the induced drag that was found with XFLR5 was scaled by the effective aspect ratio. As a result the minimum drag that is attainable during flight is 0.164 [-].

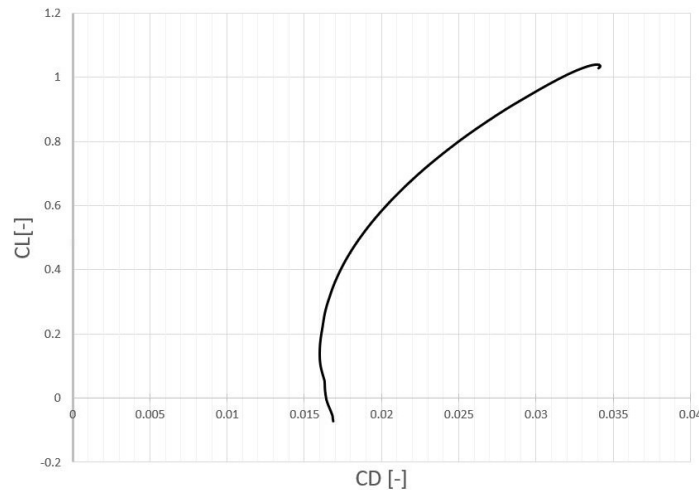


Figure 5.9: C_L versus C_D curve of the final geometry

The maximum attainable lift-over-drag of the configuration of 32 occurs at $\alpha \approx 8$, this occurs at a C_L of 0.84. In trimmed flight, the lift-over-drag ratio is decreased slightly, but GliMed is able to fulfill requirement SAI-SYS-13-PER-07 and achieve a glide ratio of more than 25.

5.6. Stability of the Glider

The first step to making GliMed stable, is ensuring it is statically stable. In order to do so, a sufficiently stable airfoil configuration must be selected. Subsequently, the locations of the centre of gravity the and neutral point need to be established and the influence of different parameters on stability, e.g. sweep and taper, will need to be investigated. Finally, the lateral stability coefficients will be presented.

5.6.1. Stability conditions

A statically stable glider, it is able to return to its equilibrium after a disturbance. To ensure that there is such an equilibrium of moments in flight the aircraft has to be made controllable, discussed in Section 5.7. Assuming that the glider is controllable, the two conditions for static stability are given below:

- $C_{m_{trim}}$ is at an angle of attack with a positive lift

- C_{m_α} is negative

$C_{m_{trim}}$ is the trim point of the aircraft, the point at which longitudinal equilibrium exist. This point should be at an angle of attack of positive lift or else it would be difficult to generate the necessary lift. Preferably, this trim point is located at the angle of attack where the L/D is the highest, as this coincides with the minimised glide angle. The second condition is that C_{m_α} is negative, a pitch up disturbance is countered by a pitch down manoeuvre of the aircraft. The first condition is the most difficult due to the lack of empennage.

5.6.2. Reflexed airfoils

As explained in Section 5.1.1, two airfoils are used for this glider, a thin and optimised airfoil for the long wings of the glider and a thicker airfoil that is used to house the payload. The latter is a custom airfoil that was enlarged in order to have a maximum thickness over chord ratio (t/c) of 21% for the payload integration. However, to be sure that a reflexed airfoil on the payload section was really the best option an analysis was performed between other options. To have an example of a reflexed airfoil the Eppler 339 airfoil was used to compare the performance with the custom airfoil and as a possible option if it proved to be more beneficial. The comparison between the shapes of the Eppler and the custom airfoil are shown in Figure 5.10.



Figure 5.10: Difference between the Eppler 339 and the custom reflexed airfoil

The location of the reflex is important for stability considerations. To investigate what the most optimal placement of the reflexed section on the aircraft three different configurations were considered as seen in Figure 5.11; the yellow, blue and green versions. The first option (yellow), with no reflex, presents GliMed with an Eppler 339 airfoil for the enlarged middle section, to fit the payload, and the SA7036 for the thin wings. The second option (blue) is similar, but the centre airfoil is the custom airfoil with reflex as shown in Figure 5.10. Lastly, the green configuration has a reflexed SA7036 airfoil on half of the thin wings and a normal Eppler 339 airfoil in the enlarged payload section.

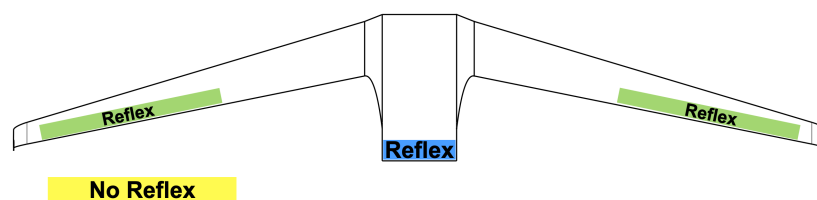


Figure 5.11: Three different airfoil reflex configurations

It must be noted that the use of reflex decreased the maximum L/D . Hence the first configuration has a maximum L/D of 40 and while the third option is 38. These L/D ratios are directly from XFLR5 and are not adjusted with the additional viscous drag estimation, meaning that they are severely overestimated. However, these values are sufficiently precise to be compared for design purposes.

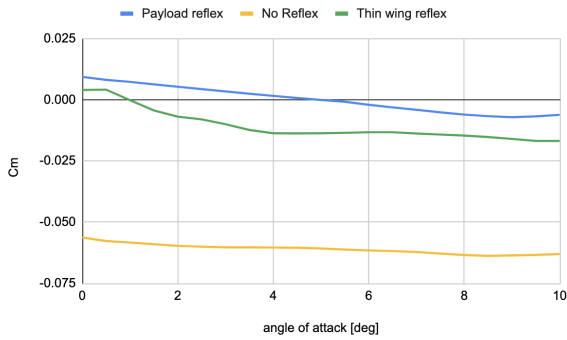


Figure 5.12: Stability of the different airfoil configurations

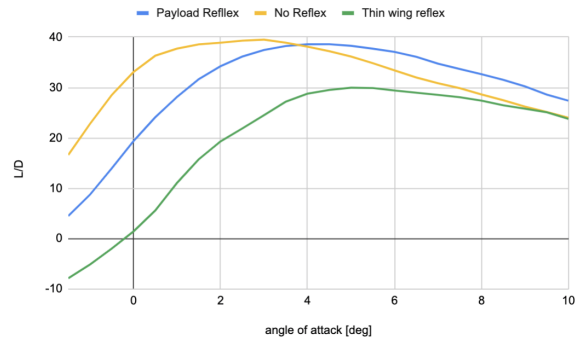


Figure 5.13: Performance of the different airfoil configurations

Placing the reflex on the thin wings is not feasible as the L/D of the glider drops dramatically to 30. This is illustrated by the green line in Figure 5.12 where 10 degree upward reflexed SA7036 airfoils along 50% of the span are used. Furthermore, as can be seen in Figure 5.13, only the green and blue configuration can ensure stability. Therefore, reflex is a necessity, and should be placed on the payload section. As a result, the chosen configuration is the blue one, with the custom reflexed airfoil and a SA7036 airfoil for the thin wings.

5.6.3. Centre of gravity and neutral point location

For the stability of the glider, it is important that the neutral point of GliMed is located behind the centre of gravity (c.g). The centre of gravity is determined based on the following parts of the glider. There are three different weight points used as the ballast, the structure, and the payload each have their own c.g location. The miscellaneous part takes into account the electronics, end-of-lift and other extra subsystems. The masses and x-locations are given in Table 5.3.

Table 5.3: c.g locations of the masses of the glider

	Mass [kg]	X-location [m]
Ballast	4.600	0.075
Structures	12.74	0.350
Payload	5.62	0.430
Miscellaneous	2.05	0.38
Total	25	0.32

The c.g of the structure was determined by means of an weighted average between the outer wings and the payload section, resulting in the 0.35 [m] shown. The c.g. of payload section lies at 0.4 [m] while the c.g. of the outer wings lies at 0.327 [m]. Lastly, the payload location was determined, the method will be explained as the payload and its location will be explored in detail in Section 6.4.2. This has led to a final c.g. location of 0.35 [m] from the leading edge of the payload section. The neutral point is critical to the glider’s stability. This point was calculated by XFLR5 software to be at x=0.380 [m]. Since the c.g is in front of the neutral point the C_{m_α} slope is negative, meaning the second stability condition is met. Additionally, It is interesting to note that without ballast, as seen in Figure 5.14, the aircraft is not stable as the center of gravity is located at 0.410 [m] from the front of the payload section. As mentioned before, by increasing the amount of ballast the c.g is shifted forwards, the aircraft will be stable if the c.g is on front of the neutral point that is located at a distance of 0.380 [m].

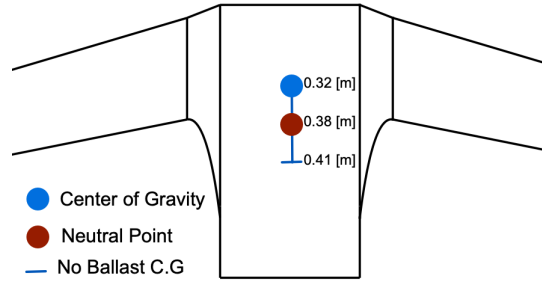


Figure 5.14: Changes in Center of Gravity with different ballasts.

5.6.4. The influence of sweep

Sweep is the most important parameter in making the aircraft stable, a more swept back wing will move back the neutral point, pushing the $C_{m\alpha}$ slope down, but also pushing the c.g. further back. However, it was observed that increasing the sweep had a larger influence on moving the neutral point than the centre of gravity. As explained in Section 5.6, the point of equilibrium should be at an angle of attack of between 4° and 9° at which the L/D is maximum, as visible in Figure 5.8. Via a simple integration, the sweep was increased by small steps with the new centre of gravity location being calculated at each iteration until finding the perfect trim point. The final sweep of the aircraft from the front of the payload section to the front of the tip is 15.23° . The trim point that accompanied this sweep was at an angle of attack of 4.6° . This is before the maximum L/D , and future iterations are needed to assure that the trim point is closer to the optimum. However due to the c.g. of the payload being too far back, this option was chosen.

5.6.5. Lateral stability

In lateral stability, two stability derivatives are considered most important: C_{l_β} and C_{n_β} , the roll stability and the yaw stability due to yaw. These parameters were first calculated without winglets and then the influence of winglets was computed to determine a minimum size of the winglets.

C_{l_β} is influenced by the taper, dihedral, and winglet size. However, dihedral, in turn, is also dependant on the wingtips since there is an effective dihedral effect[77]. This can be computed by:

$$\Gamma_{eff} = 20 \frac{h_v}{b} + \Gamma \quad (5.4)$$

Then, the C_{l_β} can be computed by adding the components of the dihedral and of the winglet.

$$(C_{l_\beta})_\Gamma + (C_{l_\beta})_v = -\frac{C_{L\alpha}\Gamma}{4} \left[\frac{2(1+\lambda)}{3(1+\lambda)} \right] + \frac{S_v}{S} \cdot 0.5 \frac{h}{b} \quad (5.5)$$

This means that, without winglets, there will be no roll stability due to yaw. To achieve stability, this value should be negative and as there is no destabilizing fuselage or other components, the addition of winglets makes C_{l_β} negative. This specific type of stability is achieved, as can be seen in Figure 5.15.

The next stability derivative is C_{n_β} is also dependant on the sweep, as can be see in in the equation below [77]:

$$C_{n_\beta} = C_L^2 \left(\frac{1}{4\pi A} - \left[\frac{\tan(\Lambda)}{\pi A(A + 4 \cos \Lambda)} \right] \cdot \left[\cos \Lambda - \frac{A}{2} - \frac{A^2}{8 \cos \Lambda} \right] \frac{6(\bar{x}_{acw} - \bar{x}_{cg} \sin \Lambda)}{A} \right) + \frac{l_{npv} - l_{np}}{b} \frac{S_v}{S} \quad (5.6)$$

[71] C_{n_β} increases quadratically with C_L . This, along with the positive C_{n_β} can be seen in Figure 5.16, therefore the glider is stable in this respect.

As mentioned above, these stability derivatives were used to determine the minimum size of the winglets. Due to C_{l_β} , winglets are required and by increasing their height, their effectiveness increases. With the dimensions from Section 5.2.1 and a angle of attack of 4.6° , $C_{l_\beta} = -0.0016^\circ$ and $C_{n_\beta} = 0.0058^\circ$.

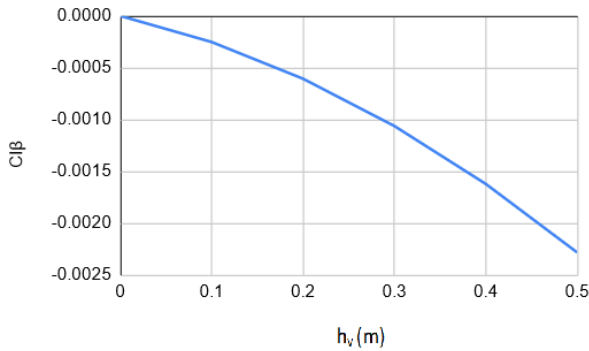


Figure 5.15: C_{l_β} per deg per winglet height

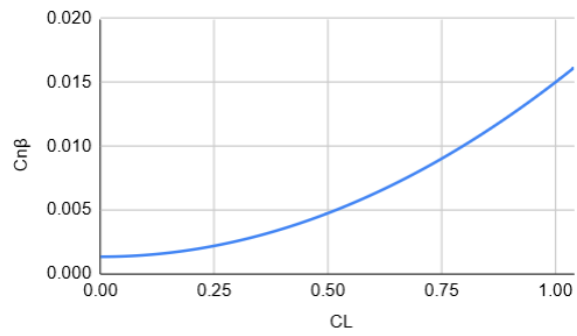


Figure 5.16: C_{n_β} per deg against C_L

5.7. Controllability of the Glider

GliMed must be sufficiently controllable such that the autonomous navigation system can function properly. The glider needs control surfaces for control in all three possible orientations: pitch, yaw and roll. For pitch and roll, active surfaces are used. For yaw a passive surface in the form of a winglet is used. This section shall discuss the design of these control surfaces and the relevant considerations that were needed.

5.7.1. Moment around aerodynamic centre

In order for the aircraft to be controllable, the moment around the aerodynamic centre needs to be studied. Using Equation 5.7 the trim point can be found.

$$C_{m_{ac}} = C_L \left(\frac{x_{ac} - x_{cg}}{\bar{c}} \right) \tag{5.7}$$

For tailless aircraft the aerodynamic centre coincides with the neutral point and since the stability condition dictates that the c.g is in front of the neutral point. The moment coefficient around the aerodynamic centre should be positive for controllability of the glider according to [72].

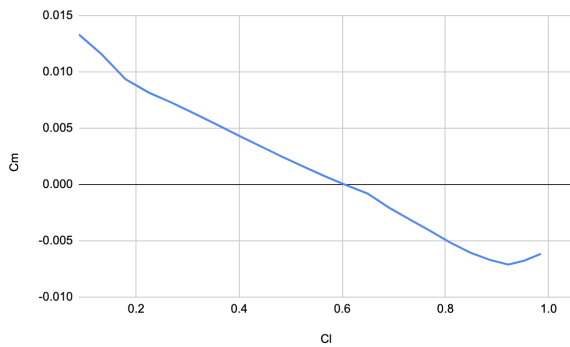


Figure 5.17: The C_m - C_l curve of the glider

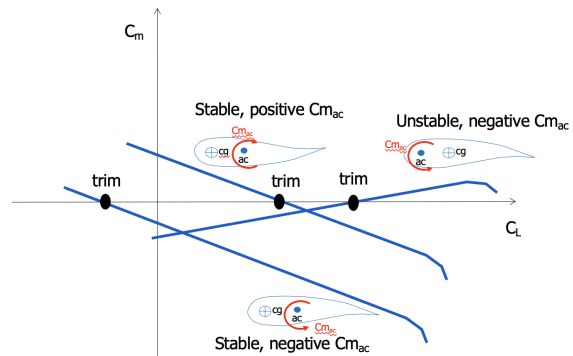


Figure 5.18: The different controllability cases [72]

The trim point of the glider is at a positive moment coefficient, which shows that the glider is controllable at the equilibrium point in addition to being stable. The glider will fly with a lift coefficient of $C_L = 0.6$ at equilibrium.

5.7.2. Active control surfaces

One active surface, the elevon, provides the required deflections needed for pitch and roll manoeuvres. This surface is sized and placed on the wing of the glider. According to [73], the deflection of these control surfaces becomes inefficient at deflections of more than 25° . Therefore, the maximum deflection of the elevon is 25° . Since it is possible to superpose these two control inputs of roll and pitch, the limit for each individual deflection was set to 12.5° so that the glider could roll and pitch in

the same manoeuvre if needed. This choice provides sufficient deflections that meet the requirements SAI-SYS-13-PER-26 and SAI-SYS-13-PER-27 in both rotations.

Roll control

Roll is an important part of the maneuvering of the glider. The glider must meet the roll rate requirement, SAI-SYS-13-PER-26, so the control surface should provide a minimal constant roll rate of 0.2 [rad/s]. This roll rate results in a 30 [deg] bank angle in 2.6 [s]. Using equations Equation 5.8 and Equation 5.9 from [72], the roll control surfaces can be established.

$$C_{L_{\delta_a}} = \frac{2C_{L_\alpha}\tau_a}{S_{ref}b} \int_{b_1}^{b_2} c(y)ydy \quad (5.8)$$

The integration is done from the start of the elevon until the end, C_{L_α} is the lift curve slope of the wing where the elevon is located and b is the wing span of the wing with the elevon. Lastly, τ_a is the aileron effectiveness as seen in Figure 5.19.

$$c(y) = c_r \left(1 + \left(\frac{\lambda - 1}{b/2} \right) y \right) \quad (5.9)$$

The following table contains the values used for the calculation of the roll surfaces:

Table 5.4: Parameters for the sizing of the roll control surfaces

Parameter	Value	Unit
δ_a	12.5	[deg]
Root Chord	0.4	[m]
Taper Ratio	0.4	[-]
Aileron Effectiveness	0.4	[-]
Wing Span (only thin wings)	5.25	[m]
Surface Area (only thin wings)	1.44	[m ²]
Velocity	20	[m/s]
C_{L_α}	6.28	[/rad]
C_{d_0}	0.0134	[-]
b_1 (only thin wing)	1.48	[m]
b_2 (only thin wing)	2.18	[m]

The aileron effectiveness is an important aspect of the sizing of the roll control surfaces. This parameter is found by using the ratio of the control surface chord to the total chord. For GliMed, the control surface to lifting surface ratio was set to 17.5% which results in an aileron effectiveness of 0.4 as seen in Figure 5.19.

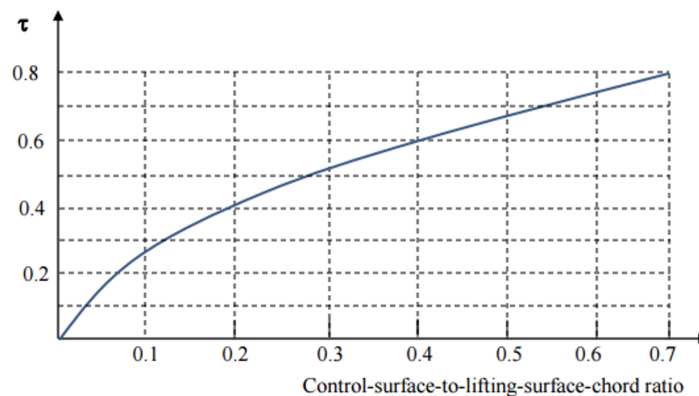


Figure 5.19: Aileron effectiveness [72]

It is also important to note that for the roll sizing, the thicker, payload housing part of the flying wing is ignored as it is deemed to provide low relative lift compared to the thinned outer wings of the glider. As a result, the wing span and surface area only account for the thin part of the wing since that part provides most of the lift. The b_1 and b_2 positions are the distances between the root of the thin wing with the start and end of the control surface. They have been chosen to be close to the tips of the wing to minimise the control surface area. However, while the wing span of the thin wings is 2.5 [m], the control surfaces were placed at a maximum distance of 2.18 [m] from the start of the thin wing in order to not disturb the airflow close to the wingtips which are used for yaw control. Lastly, the precision of the control surface placement coincides with two ribs inside the thin part of the flying wing. The next step is to calculate the roll damping coefficient, the c_{l_α} and c_{d_0} are the airfoil's 2D characteristics.

$$C_{l_P} = -\frac{4(c_{l_\alpha} + c_{d_0})}{S_{ref}b^2} \int_0^{b/2} y^2 c(y) dy \quad (5.10) \quad P = -\frac{C_{l_{\delta a}}}{C_{l_P}} \delta a \left(\frac{2V}{b} \right) \quad (5.11)$$

The steady roll rate can now be calculated in order to make sure that the control surfaces meet the roll requirement. With the current size and placement the control surfaces are able to obtain the roll requirements listed in Table 5.5. The roll angle of 30° is most important since turns will be performed at this bank angle during the mission. This roll time is sufficient to fulfill the SAI-SYS-13-PER-26 requirement.

Table 5.5: Performance of the roll control surfaces

Bank Angle	Time needed
15°	1.09 [s]
30°	2.18 [s]
45°	3.27 [s]

Pitch control

The next step in the control surface sizing is looking at the pitch control. Contrary to conventional aircraft missions, the glider will not take-off from the ground, but be launched from a helicopter. As a result, there is no pitch requirement for that stage of flight. Since the goal of the glider is to fly as efficiently as possible, pitch up and pitch down manoeuvres will only be used as a last resort manoeuvre to avoid an obstacle or disturbances in flight. However, the glider needs to follow a very detailed and precise landing procedure and therefore needs to be able to fly at $C_{L_{max}}$ and stall. Similarly to the roll control surfaces, the maximum deflection for pitch is 12.5 °; leading to a total maximum deflection for the elevon of 25 ° in a turn and climb manoeuvre. As can be seen in Figure 5.20, the pitch up moment is quite high with the elevons deflected upwards at 12.5°. While further investigations will have to be made with experimental testing, the elevons are large enough for pitch control especially considering the fact that in straight flight, the pitch manoeuvre can use up to 25 ° of elevons deflection.

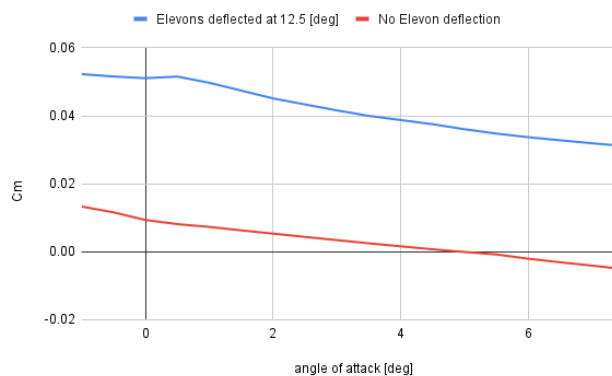


Figure 5.20: C_m - α curve of the glider with elevons deflected upwards at 12.5°

Final Elevon Design

The elevons will start at a distance of 1.885 [m] from the start of the axis of symmetry and will end at a distance of 2.585 [m] from this line. These elevons have a maximum deflection of 25°.

Table 5.6: Parameters for the sizing of the roll control surfaces

Parameter	Value	Unit
b_1	1.48	[m]
b_2	2.18	[m]
start distance from middle of payload section	1.885	[m]
start distance from middle of payload section	2.585	[m]
chord percentage of elevon	17.5	[%]
chord of elevon	4.609	[cm]
surface area of elevon (one side)	322.63	[cm ²]

The final values of the elevon sizing and placement are shown in Table 5.6. The elevons have a control surface to lifting surface chord ratio of 17.5% and can be deflected either upwards and downwards for simultaneous pitch and roll control of the glider.

5.8. Flight Conditions

The sections above mainly describe the aerodynamic parameters and the wing planform. In contrast, this section will show the behaviour of the glider during flight. Starting with the flight speed in Section 5.8.1, the basis is made for the flight profile. Then, the influence of wind on the flight behaviour is treated in Section 5.8.2. Subsequently, the turn performance can be found in Section 5.8.3. This section ends with the loads during flight in Figure 5.25.

5.8.1. Flight speed

The speed of flight during gliding flight is determined by

$$V = \sqrt{\frac{2W}{S\rho C_L} \cos \gamma_d} \quad (5.12)$$

where $\tan \gamma_d = \frac{C_D}{C_L}$. The rate of descent is then $RD = \sin \gamma_d$. Logically, this means that the higher the L/D, the smaller the glide angle is, and thus the bigger the range. From XFLR5, the L/D can be taken. These numbers were then updated with the new form drag and the influence of the winglets. Together with that and using the formulas above, the speed polar is plotted in Figure 5.21. The dots show where the trimmed flight is. It can be seen that the trimmed flight is slightly faster than the optimum glide angle. However, as mentioned in Section 5.8.2, this is actually advantageous for flying with wind.

From this plot, it can also directly be seen what influence a different altitude has. Though the L/D performance stays the same, both the velocity and the RD increase with height. At sealevel, $V = 18.6m/s$, whereas at 5km $V = 23.9m/s$. For 125km, this comes to about 98min of gliding. In turning flight, there is less surface area available to provide the lift, and thus the RD increases. The formulas to compute this are [78]:

$$V = \sqrt{\frac{2W \cos \gamma_d}{S\rho C_L \cos \mu}} \quad (5.13) \quad RD = \sqrt{\frac{2W C_D^2 \cos \gamma_d^3}{S\rho C_L^3 \cos \mu^3}} \quad \tan \gamma_d = \frac{C_D}{C_L} \frac{1}{\cos \mu} \quad (5.14)$$

Using the formulas above the new glide polar can be computed, and this curve is also added to Figure 5.21. This performance is mostly used during landing, and is therefore also computed at sealevel. During turning flight at $\mu = 30^\circ$, $RD = 1.1m/s$. The speed polar for flying with a headwind is also plotted in Figure 5.21, but will be highlighted in the section below.

5.8.2. Wind and range

In ideal conditions, with a L/D, the glider will easily make the 125km range. However, this changes the moment there is a headwind. As per Chapter 2, the wind is analysed at the three locations. The

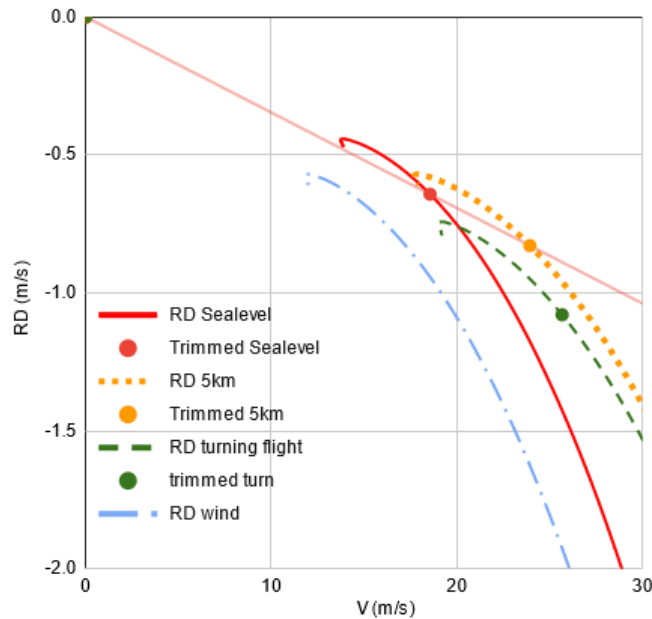


Figure 5.21: Speed polar at sea level, 5km, with headwind, and during turning flight

occurrence of each wind speed can be seen in Figure 5.22. ²

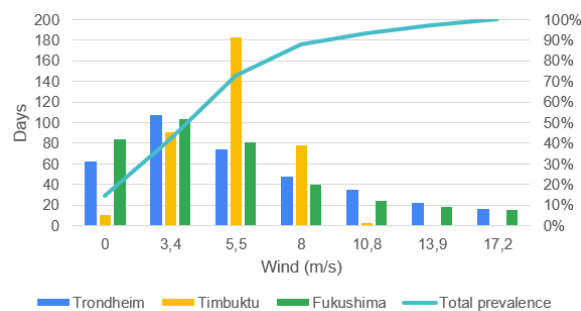


Figure 5.22: Wind speeds in Trondheim, Timbuktu, and Fukushima

Although the wind has no influence on the lift generation of the wings, it does affect the ground speed. Which is now simply the speed it would have without wind, the true air speed, minus the wind speed if it is a straight headwind. This is also plotted in Figure 5.21. The polar of a headwind is down and to the left, simply indicating that the ground speed is lower per *RD*. Because of this, the influence that wind has on the range is bigger the lower the true air speed is. When designing, this was taken into account. From Equation 5.12, the bigger the surface area, the slower the glide speed at a set α , and thus more dependency on wind.

However, the moment the wind is no longer from straight ahead, its influence on the range decreases. This is depicted in Figure 5.23. The influence of the wind can be seen in Figure 5.24. Although the mission is to reach a range of 125km, there may be circumstances that it is possible to be closer to the target. In those cases, it is worthwhile to consider that it is more likely that the weather is favourable and allows the launch of the glider. Naturally, this also works the other way around, and a bigger range is achievable when there is a tailwind.

In total, taking into account the occurrence of different wind speeds from Figure 5.22 and the maximum wind from Figure 5.23, the glider can fly 70% of the days of the year. This was averaged for every location, and assuming that the wind is equally likely to come from every direction.

²www.meteoblue.com[cited 19-06-2021]

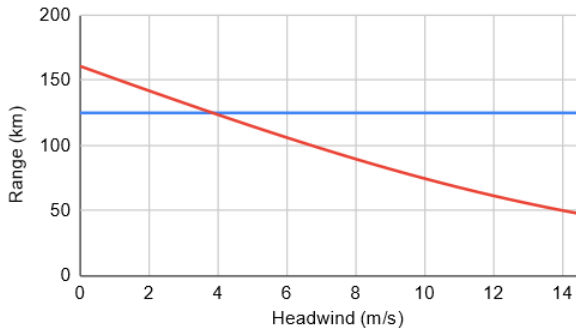


Figure 5.23: Achievable range with straight headwind

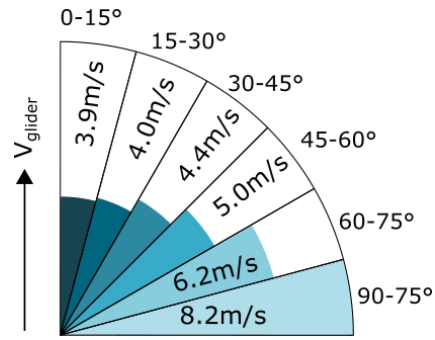


Figure 5.24: Maximum wind per direction to achieve a range of 125km

5.8.3. Turning flight

The time it takes to enter roll has been described in Table 5.5. For turning flight, a roll angle of $\mu = 0^\circ$ is considered. With the V and RD of Section 5.8.1, other parameters such as the radius of a turn can be computed [78]. These values are summarised in Table 5.7.

Parameter	Symbol	Value
Turn radius	R	71.4 [m]
Rate of turn	Ω	0.28 [rad/s]
Turning time for 180°	T_π	11.16 [s]

Table 5.7: Turn parameters

With the roll time of 2.18s, and assuming that no turning is done while rolling, the maximum time it will take from straight steady flight to steady straight flight in the opposite direction is 15.5s.

5.8.4. Flight loading

With the aerodynamic parameters such as $C_{L_{max}}$, C_{L_α} and the surface area, the gust and flight loads are computed, which together form the maneuvering envelope. This was done very roughly at the beginning of the conceptual design, to set up basic parameters to start the structural analysis with. In the midterm report [36], with the help of [78], [10], the maximum loads were estimated at an ultimate positive and negative load of 4.5 and -3. As explained in Section 7.2, a factor of 1.5 was then used to determine the maximum loads that may occur during flight, so 3 and -2.33. With the help of [77], [33] and [2], the gust and flight loads were computed for the final values, and these are summarised in Figure 5.25. The gusts were evaluated at 15[m/s] and 7.5[m/s]. For clarity, the maneuvering envelope is highlighted in orange.

Several conclusions can be made according to these figures. First and foremost, the limiting load factor of 3 appears too low. Notable is the fact that the gust loads are quite high. This makes sense, since the glider is relatively light for its surface area, meaning that if there is a gust the glider will accelerate quickly. Second, the stall loads are below the loads induced by gusts of 15m/s throughout almost the entire flight range.

This may pose a problem depending on a couple of factors. First, the formulas with which the gust loads are approximated may not be accurate because they are based on aircraft with a higher wing loading, and may not reflect the actual loads [77]. Also, with a smaller sized glider the gust may transfer the whole structure, thus reducing loads.[33]

Furthermore, as per Equation 5.12, the cruise speed is 18m/s in EAS. At this speed, the stall speed determines the maximum load that may be induced. Except in exceptional conditions or perhaps during launch, the EAS will exceed 25m/s. Therefore, the gust loads are barely relevant to the glider during cruise. However, what this ultimately means is that when there is a vertical gust of $U_{de} = 15m/s$, the angle of attack will change past the stall angle. This is also illustrated by the fact that V_B , the location where the stall and gust loads cross [2], is beyond the design maneuver speed.

Lastly, the loads all fall within the ultimate loads of -3 to 4.5. This means that although the limiting loads are too low, the glider can withstand these loads.

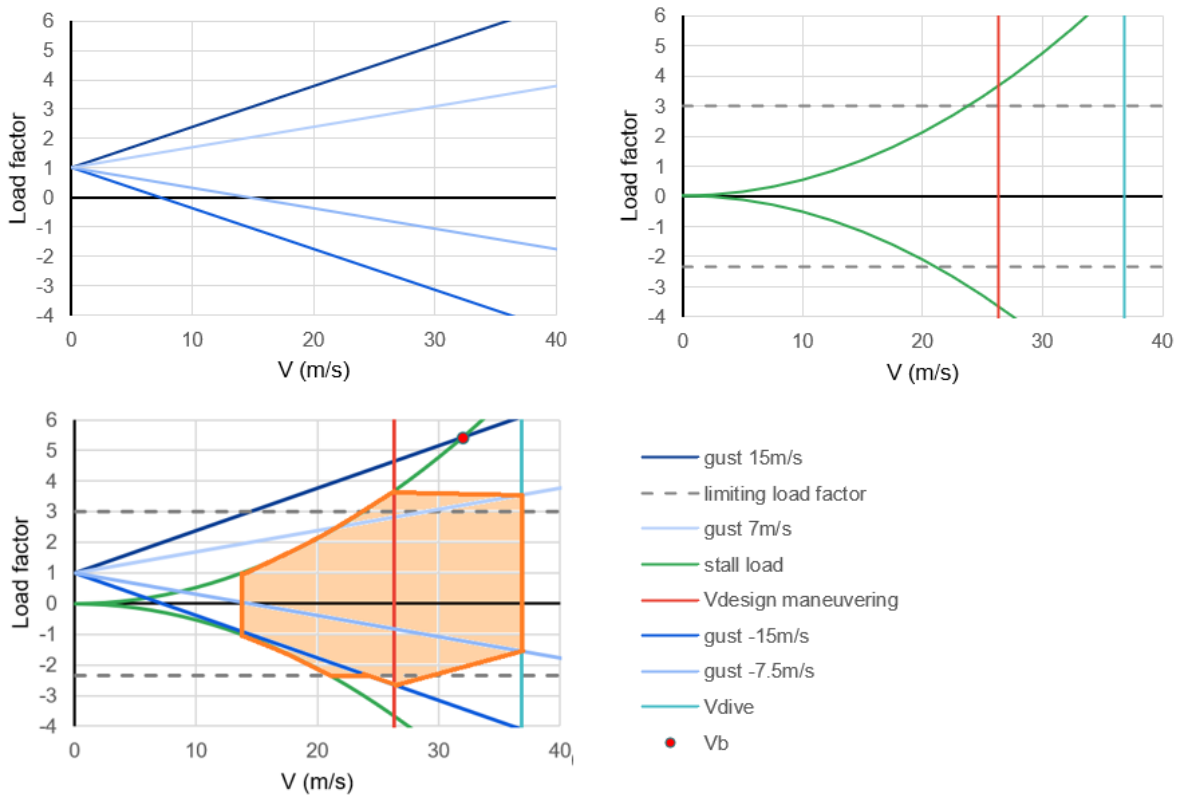


Figure 5.25: Flight loads and flight envelope in flight in EAS

Altogether, what this means is that in the next design phase the actual way a gust induces loads on the structure needs to be tested. Based on that, a design iteration may need to be done to either increase the velocity, increase the stall speed, increase the structural limit loads, decrease the surface area, or a combination of all. This also depends on the gusts that the glider will actually encounter during flight. In the end, this will be further evaluated after wind tunnel testing, and will be taken into account in the recommendations.

Apart from loads encountered during cruise, there is also additional load when turning. This can be computed using $n = \frac{\cos \gamma_d}{\cos \mu}$. When using the glide and roll angle from Section 5.8.1, the turning load $n = 1.15$.

5.9. Sensitivity Analysis

Having come to a final aerodynamic design it is necessary to investigate the sensitivity of the design to a change in certain parameters. Subsequently, the critical parameters can be identified and the feasibility of the design can be tested. In this section sensitivity analyses are performed to investigate the influential parameters of the stability and control of the design, and of the flight conditions.

5.9.1. Stability and Control

For a tailless aircraft stability and control are difficult to manage, as explained in Section 5.7. To investigate what parameters have a larger influence on the control and stability of the tailless GliMed glider the influence of the centre of gravity and the sweep are investigated.

Centre of Gravity Influence

The biggest differences in stability and control are caused by a shift in the centre of gravity location. As a result, the change in ballast amount is examined. The normal ballast amount is 4.6 [kg] located at a 0.075 [m] distance from the leading edge of the payload section. If the ballast mass is reduced by 10%, the stability is affected as the c.g shifts backwards leading to a smaller absolute value of C_{m_α} . Similarly, if the ballast is increased, the c.g shifts forwards leading to a steeper slope as C_{m_α} is larger.

Table 5.8: c.g locations of different ballast masses

	Ballast Mass [kg]	Total c.g X-location [m]
Normal	4.600	0.320
90% Ballast	4.140	0.328
110% Ballast	5.060	0.312

The results of the stability analysis as shown in Figure 5.26 illustrate that this glider is very sensitive to changing the c.g location at the equilibrium point of the aircraft is moved with varying ballast masses.

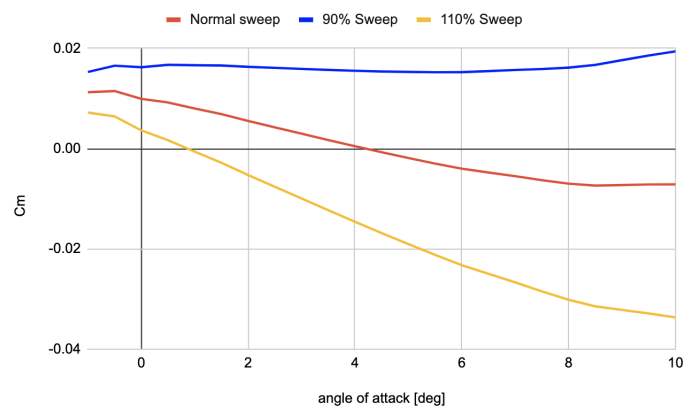
**Figure 5.26:** Comparison of the stability of the different ballast masses

The blue line represents the 90% ballast configuration, it can clearly be seen that the aircraft does not have an equilibrium point as the lines does not cross the horizontal axis. The red line represents the normal configuration with an equilibrium point of 4.6°, close to the optimum L/D. Lastly the yellow line represents the 110% ballast configuration, this glider is stable but the equilibrium point is 3.0° which is not optimal but the glider is stable.

This analysis shows that the c.g has an enormous impact on the stability of the aircraft, and a more forward c.g would require less sweep in order to find the most optimal location of the equilibrium point angle of attack. However, when the c.g is moved backwards, the glider would need more sweep in order to be stable, which in turn affects the centre of gravity location of the structures.

Sweep influence

A sensitivity analysis is done on sweep as it is the main driving element that changes the magnitude of C_{m_α} . Similarly to the c.g analysis, the sweep has been increased by 10% and decreased by 10% in order to investigate the effect of this parameter. Figure 5.27 shows the stability of the three configurations.

**Figure 5.27:** Comparison of the stability of the different sweep configurations

The blue line represents the configuration with 90% sweep, as seen in Figure 5.27, the glider is not stable with only a small change in sweep. The red line represents the normal configuration and the yellow line is the configuration with 110% sweep. This configuration is stable but the equilibrium point is far too low to at 1° which will result in a very low L/D at equilibrium point. Sweep is highly influential as changes will most likely require c.g.-position adjustments to compensate for a potential new design. Trimming the aircraft for the perfect equilibrium point is difficult with varying constantly c.g. and therefore sweep values.

5.9.2. Flight Conditions

To analyse that a small change in external factors does not drastically change the performance of the glider, its sensitivity to factors such as temperature, wind, and drag is compared. These factors are briefly explained below, and Figure 5.28 shows the outcome. Since some changes only had an influence on the performance in wind, the comparison is made with a headwind of $3.9[m/s]$. With this headwind the range without changes is $125[km]$. In the figure, it is shown by how much and to what number the range changes when changing the input to 90% or 110%.

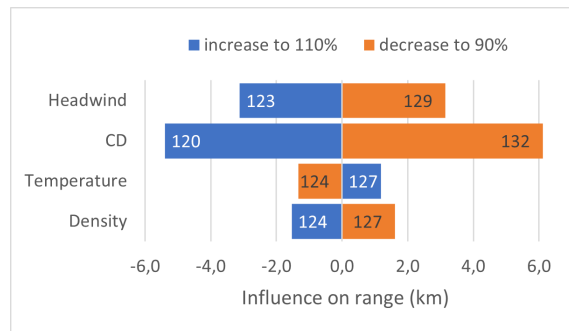


Figure 5.28: Influence of different factors on the range with a headwind of 3.9m/s

- **Headwind:** Changing the headwind has a direct influence on the range. This is discussed more in depth in Section 5.8.2.
- **C_D :** Increasing the drag coefficient changes the L/D, and means a larger glide angle, thus a smaller range. Out of the inputs analysed this has the largest impact. Reasons this may be different than expected are for example damage to the skin or flies on the skin.
- **Temperature:** The performance of the glider was analysed at ISA values. When temperature is increased, the density decreases, which leads to a higher flight speed. Eventually this leads to less influence of the wind. A change of 10% equates $28[K]$ or means the range in the figure is from -13 to $43[^\circ C]$. Translating this to the mission, the maximum average temperature in Timbuktu is $44[^\circ C]$, whereas the minimum average in Trondheim is $-6[^\circ C]$. On average, the glider is more likely to be used at temperatures higher than the ISA standard $15[^\circ C]$. Conveniently, as can be seen in the figure, an increase in temperature leads to better range.
- **Density:** Apart from temperature, other factors such as humidity can have an influence on the air density, which is why it is analysed separately. Again, the density influences the performance in wind.

5.10. Verification and Validation

This section will discuss the verification and validation procedures for the performance of the glider that were performed or are scheduled for future the future. First, the verification procedures are discussed and they are followed by the validation procedures.

5.10.1. Verification

Starting with if the design meets the performance requirements, XFLR5 has been used to test the configuration using a lifting line theory simulation. Together with the drag analysis this provided the plots shown in Section 5.5. With the analysis that was performed using this data and the speed polar,

Section 5.8, the following requirements have been fulfilled through analysis: SAI-SYS-13-PER-07, SAI-SYS-26-PER-08, SAI-SYS-13-PER-09 and SAI-SYS-26-PER-11. To verify that the automated drag estimation code, the control surface design code and the stability analysis code were correct statistics and worked out examples[73] where used. The codes were run multiple times for different examples and in the end the code was able to reproduce the outcomes of the examples. This led to the verification that the requirements: SAI-SYS-13-PER-19, SAI-SYS-13-PER-21, SAI-SYS-13-PER-24, SAI-SYS-13-PER-25 and SAI-SYS-13-PER-19.

Additionally, the flight loads were verified using a paper on the maneuverability diagram of a small UAV [33]. The inputs of the GliMed were changed with the inputs from this paper, and the results compared. After fixing a minor typo, the results were the same. The flight polar was first plotted and then compared to the flight polars given in [78]. For the range plots, unit tests were done, for example using a $C_L = 1$, $C_D = 1$, and $h = 1[m]$ to check if the range was $1[m]$. All intermediate results are verified using hand calculations.

Several requirements were not verifiable during this design phase as certain verification procedure were not able to be performed, such as the use of CFD (Computational Fluid Dynamics), a windtunnel test and a flight test. For example, regarding the control surfaces for pitch and roll, test flights will have to be planned in order to gather data for pitch rotations and especially the landing sequence. The control surfaces need to be tested in real flight conditions or in more advanced softwares since XFLR5 does not provide dynamics stability analysis. All of the requirements can be verified with the inclusions of these procedures, but they are necessary to be able to verify SAI-SYS-13-PER-18, SAI-SYS-13-PER-27, SAI-SYS-24-PER-29 and SAI-SYS-25-PER-31.

5.10.2. Validation

For this project, the software XFLR5 was used to assess the performance of the airfoils, wings and entire configuration. As this software is an external tools that is intended to be used for non-professional use, its accuracy needs to be assessed. As both thin and thick airfoil are used on the designed glider and XFLR5 makes use of thin airfoil theory, it is important to validate its accuracy on both of these airfoil. Therefore, a thick (NACA 2421, 24 % t/c) and a thin (NACA 2412, 12% t/c) airfoil where analysed in XFLR5 and compared with experimental data[5]. Regarding the table, for $C_{m_{c/4}}$ the mean absolute error (MAE) between the experimental and XFLR5 curve is shown. The NACA 2412 airfoil was analysed at Reynolds number $3.1 \cdot 10^6$ and the 2421 airfoil at $2.9 \cdot 10^6$.

Table 5.9: Results of the comparison of XFLR5 and experimental data on the NACA 2412 and 2421 airfoils.

	$C_{L_{\alpha=0}}$ [-]	$C_{l_{max}}$ [-]	$C_{l_{\alpha}}$ [rad^{-1}]	$(L/D)_{max}$ [-]	$C_{d_{min}}$ [-]	$C_{m_{c/4}}$
NACA 2421 Airfoil						
Experimental	0.230	1.677	5.901	104.54	0.0064	-
XFLR5	0.2309	1.596	5.959	107.45	0.0075	-
Difference/MAE	0.39 %	4.83 %	0.98 %	2.78%	17.66%	0.0047333
NACA 2412 Airfoil						
Experimental	0.19	1.24	5.25	83.63	0.0078	-
XFLR5	0.2538	1.5394	6.001	112.65	0.0064	-
Difference/MAE	33.58%	24.15%	14.3%	34.70 %	18.21%	0.0101

For the thin airfoil XFLR5 is able to accurately estimate important airfoil coefficients to within 5 %, with the exception of the drag coefficient C_d . It is however clear that XFLR5 is unable to predict boundary layer behaviour and phenomena such as stall and separation, apparent from the overestimation of $C_{L_{max}}$. For the thick airfoil, XFLR5 is clearly not accurate, the 2D panel method severely overestimates or underestimates the coefficients. In addition, as the moment coefficients of the airfoils are roughly constant around 0.05 for the angle of attack range, the MAE shows that XFLR5 is within 10 % accuracy for the thin airfoil and 20 % for the thick airfoil. These inaccuracies are translated into the 3D wing analysis and thus appear in all analyses shown in this chapter.

5.11. Compliance

In Table 5.10, the compliance matrix summarising this chapter can be seen. Several requirements have been left on to be determined, as they fall outside the scope of this concept design. The section(s) that

discuss the requirement can also be viewed in the matrix.

Table 5.10: Compliance matrix for performance

Requirement ID	Requirement	Compliance	Proof
SAI-SYS-13-PER-07	The system shall have a glide ratio of at least 25 [-].	✓	Section 5.5
SAI-SYS-26-PER-08	The system shall have a rate of descent of maximum 1.0 [m/s].	✓	Section 5.8.1
SAI-SYS-13-PER-09	The system shall have a stall speed of maximum 14.2 [m/s].	✓	Section 5.8.1
SAI-SYS-26-PER-11	The system shall have a maximum cruise speed of 28 [m/s].	✓	Section 5.8.1
SAI-SYS-08-PER-14	The system shall be able to withstand 90 degree cross-winds up to 8.2 [m/s] without losing control of the system	✓	Section 5.8.2
SAI-SYS-13-PER-18	The system shall be dynamically stable during operations.	TBD	Section 5.12
SAI-SYS-13-PER-19	The system shall be longitudinally statically stable during operations.	✓	Section 5.12
SAI-SYS-13-PER-21	The system shall have static lateral stability.	✓	Section 5.6.5
SAI-SYS-13-PER-24	The control surfaces shall be able to deflect with at least 25 [deg].	✓	Section 5.7.2
SAI-SYS-13-PER-25	The system shall be able to perform a turn with a minimal constant turn rate of 0.28 [rad/s].	✓	Section 5.8.3
SAI-SYS-13-PER-26	The system shall be able to perform roll with a minimal constant roll rate of 0.2 [rad/s].	✓	Section 5.7.2
SAI-SYS-13-PER-27	The system shall be able to perform pitch with a minimal constant pitch rate of 0.1 [rad/s].	TBD	Section 5.7.2
SAI-SYS-24-PER-29	The control surfaces of the system shall use no more than 5 [W] to function during operation.	TBD	Section 5.12
SAI-SYS-25-PER-31	The control surfaces of the system shall use no more than 18000 [J] to function during operation.	TBD	Section 5.12

5.12. Recommendations

Several recommendations can be made for the conceptual design phase and the next design phase. Firstly, it proved difficult to design a thick reflexed airfoil (20% t/c) capable of generating high lift with the available tools and within the scope of the project. Also, XFLR5 is unable to accurately predict the performance of this thicker wing section. This has resulted in an overestimation of in particular the $(L/D)_{max}$ and $C_{L_{max}}$ of the glider and caused inaccuracies in the neutral point positioning. Therefore, it is recommended that more high fidelity methods are used to assess the aerodynamic performance of GliMed such as CFD. Also, more refined design iterations are needed to solve the inaccuracies in the centre of gravity that led to great variations in the sweep. The centre of gravity was also moved forwards leading to a last iteration that led too much sweep. This should be revisited in the future to find the trim angle at the maximum L/D point.

Furthermore, for the next design step, the construction of a test/scale model could fill the knowledge gap that currently exists. Coincidentally, due to the lack of real life testing many of the requirements could not be tested. This could aid to investigate the the flight- and structural loads, as well as the performance of the elevons regarding pitch, roll and yaw. To ensure that the aerodynamic design is able to fulfil all performance related requirements, future validation procedures are recommended. In particular, the use of Computational Fluid Dynamics (CFD) and/or wind tunnel tests with a scale model would greatly fill the knowledge gap that currently exist.

6. Operations

The operational life of an aircraft consist out of many different parts, which will be discussed in this chapter. The chapter discusses the communication system of the glider in Section 6.1, the navigation and autonomous system in Section 6.2, the required electrical system in Section 6.3, the launch, landing and logistics of the glider in Section 6.4, and the end-of-life procedures in Section 6.5.

6.1. Communication System

This section will describe the communication system of the complete system. Firstly, the general communication flows will be mentioned and visualised, after which the chosen communication technique will be explained. This is followed by an explanation of the link budget calculation. Next, a sensitivity analysis will be presented and the verification and validation procedures for the communication system will be mentioned. Finally, a requirement compliance matrix for the communication system will be shown.

6.1.1. Overview communication flow

Knowing the communication flows inside the system and with external parties is key in designing a communication system. For that reason, a communication flow diagram has been made for GliMed and it can be found in Figure 6.1. Here, four main parties are visible: the mobile ground station (MGS), air traffic control (ATC), the system, GliMed, itself, and the recipient. These four parties do not all communicate with each other and the links occur at different moments in the systems' operational life. Most communication links will be used during flight, except the links towards the recipients. Instead, the link between the MGS and the recipient occurs before launch and after landing, and the link between the system and the recipient occurs only after landing.

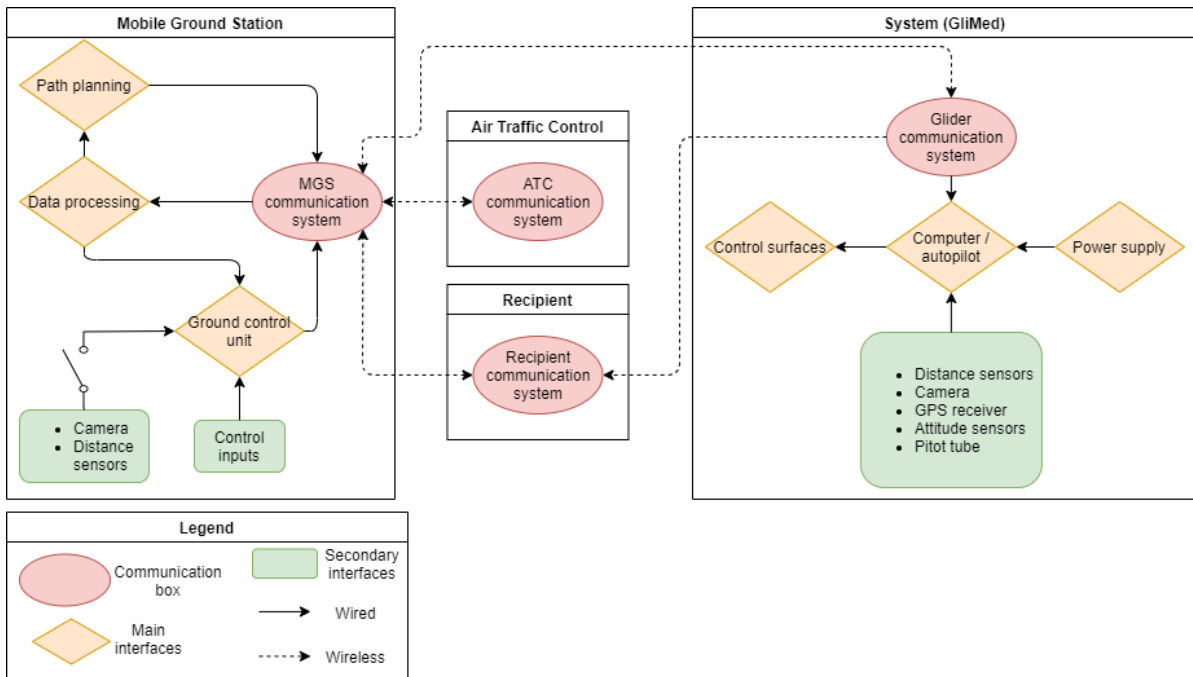


Figure 6.1: Communication flow diagram, representation of the communication streams between different elements during operation.

Figure 6.1 visualises the links between the main parties and the data types that will be processed can be found in Table 6.1. The data names in the table contain the following information: command messages contain change in control surface deflections and reboot messages; ATC messages contain no-fly zone data and positional data about nearby aircraft; additional information for ATC includes data with time estimates for reaching certain areas; and additional telemetry contains control surfaces

deflections, flight velocity, altitude and system health status. In Table 6.1 it can be seen that no visual data link will be send back to the MGS. This has been decided due to the large impact of such a video link on the required data rate of the system. Besides, a pilot would still be able to control the glider based on the attitude and telemetry messages from the glider.

Table 6.1: Overview exchanged data per communication link.

Link	Communicated data
MGS to Glider	Command messages, ATC messages & flight path
Glider to MGS	GPS data, additional information for ATC, attitude data & additional telemetry data
MGS to ATC	Glider GPS data, glider attitude data & additional information for ATC
ATC to MGS	ATC messages
MGS to recipient	Estimated landing area & final glider landing coordinates
Glider to recipient	Location data via sound

The communication inside the system will be regulated by the onboard computer, which for example sends commands to the control surfaces and at the same time obtains information about their states. Furthermore, the onboard computer will obtain measurements from the onboard sensors. A more detailed flow of communication inside the autonomous system of the glider can be found in Figure 6.9. This figure will be explained into more detail in Section 6.2.2.

6.1.2. Communication system technique

With the help of the determined communication flow diagram, Figure 6.1, and the communication distance of 400km, a communication technique can be determined. Where the 400 km communication distance comes from will be described in Section 6.4.

Initially in the midterm [36] it was decided to use satellite communication for the connection between the MGS and the glider, because of the communication distance that had to be covered between the glider and the MGS. However, it was found that this type of communication would be too expensive for the desired application for the system. Therefore, a new approach had to be chosen: the use of radio frequency (RF) communication, combined with spread spectrum modulation. The type of spread spectrum modulation that will be used is code division multiple access (CDMA) which is based on direct sequence spread spectrum (DSSS) modulation. [23][92]

The concept of DSSS is first briefly summarised. The initial data signal is multiplied by a modulation code, also called a Pseudo Random Noise Code (PN code). Due to this the data signal bandwidth will increase with a factor, coding gain (G_{coding}), that equals the code size. While the complete power of the signal remains the same, the spectral density of the power will be lower because the bandwidth increases. Due to the decrease in spectral density the signal will be more noise resistant. Furthermore, the range the signal can travel increases, it is stronger against possible signal jamming, and the applied code establishes protection against hostile users because it will not be known to other users. This means that the reliability of the connection will increase. [23]

On top of that, spread spectrum modulation us applied. This means modulating a signal that is already modulated. Most common modulation techniques in combination with DSSS are binary phase shift keying (BPSK) and quadrature phase shift keying (QPSK). It was chosen to use QPSK because it can send twice the bitrate compared to BPSK at the same bandwidth. [22][92][23] A visualisation of the performed modulation and demodulation can be found in Figure 6.2.

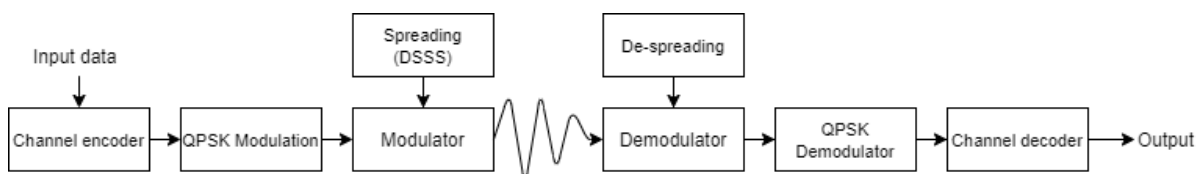


Figure 6.2: Modulation diagram.

With the spread spectrum modulation a frequency band can be obtained. To minimise the cost of the communication system an unlicensed frequency will be used. Possible frequency bands are:

902 – 928[MHz], 2400 – 2483.5[MHz], and 5725 – 5850[MHz]. The 902 – 928[MHz] was because a lower frequency will allow a longer transmission range.[23][24][30][92]

Another important factor for the communication between the MGS and the glider is the equipment. The chosen antenna for the glider is an omnidirectional antenna, since no antenna pointing will be required during flight. Also, a raspberry pi will be used for signal modulation and demodulation, and the MGS will be equipped with a dish antenna. The size of this antenna will be determined in Section 6.1.3. This equipment will be used to establish the link between the MGS and the glider. With the help of this link, important information for ATC will be exchanged, because it was decided to relay the data required for ATC via the MGS to the glider and the other way around to lower the required complexity of the communication system and the power consumption. The MGS has an additional antenna for communication with the ATC. This means that the system can obtain a connection with ATC during operation.

Additionally, the glider will be equipped with a sound buzzer. This will be turned on by the onboard computer after landing. With the help of this buzzer the system can be found by the recipient in case the MGS is unable to send the GPS coordinates of the system to the recipient. Even in the case that the recipients have the GPS of the system after landing the sound buzzer will help them localise the glider quicker. The chosen buzzer can provide acoustic sound for more than three days.,

The chosen equipment for the communication system is shown in Table 6.2. The positioning of the components are as follows: the antenna will be positioned on top of the middle of the payload section at a distance of 60[cm] from the leading edge and the buzzer will be placed inside the right tapered section as seen from the front of the glider at a distance of 35[cm] from the middle, as can also be found in Figure 3.5.

Table 6.2: Used communication equipment.

Component	Product name	Specifications
Omnidirectional antenna	UAV Antenna MP5L900 ¹	Size: 19mmx19mmx223mm, $m = 39.6[g]$, gain: 3[dB], power input: 50[W]
Sound buzzer	HellGate FPV Buzzer DUO ²	Size: 13.2[mm] x 14.8[mm] x 27.4[mm], $m = 6[g]$, Input voltage: 5V, provides acoustic sound for 3 days

6.1.3. Link budget calculation

After deciding on the communication system technique, a link budget calculation was made. Such a link budget calculation is necessary to obtain theoretical confirmation that the intended communication link can be obtained. The link budget is usually calculated in decibels with the help of Equation 6.1 and Equation 6.2. However, if the parameters are initially not represented in decibels they can be converted to decibels with the help of Equation 6.3. Furthermore, Equation 6.1 represents the calculation for the received power by a receiver and Equation 6.2 shows how to calculate the signal-to-noise ratio (SNR) of the system. The SNR represents the actual link budget of the system. [92][23]

$$P_{RX} = P_{TX} + L_T + G_T + G_R + L_R + G_{coding} + L_{FS} + L_{FM} + L_{misc} \quad (6.1)$$

$$SNR = P_R - 10\log(k) - 10\log(R) - 10\log(T_{sys}) \quad (6.2) \quad X[dB] = 10 \cdot \log\left(\frac{X}{X_{ref}}\right) \quad (6.3)$$

Before calculating the link budget for the chosen communication system approach, the minimum required SNR was required. This is determined with the help of the allowed bit error rate (BER) and Figure 6.3. The allowed BER was assumed to be 10^{-6} , based on literature [92] [15]. With the help of the BER value, the chosen modulation technique, QPSK, and Figure 6.3, it can be determined that the required SNR (SNR_{req}) is roughly 11[dB]. This means that if the calculated SNR will be above 11[dB] the link budget will be closed.

¹<https://www.mpantenna.com/product/uav-antenna-mps1900/> [cited 17-06-2021]

²<https://buzzer.hellgatefpv.com/product/hellgate-fpv-buzzer-duo/> [cited 17-06-2021]

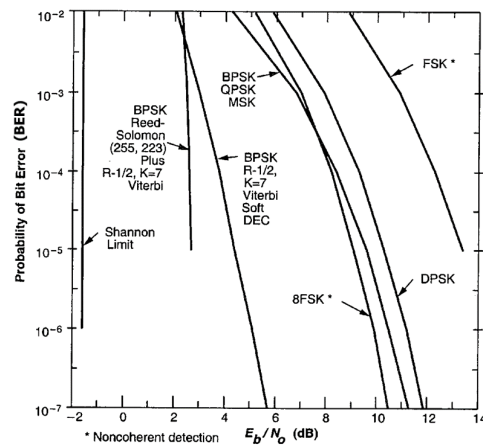


Figure 6.3: Required SNR for modulation techniques based on bit error rate. [56]

The SNR needs to be calculated for both uplink, from MGS to glider, and downlink, glider to MGS. For that reason the bit rates for both links need to be determined, and those can be found in Table 6.3. However, these are the bit rates before the modulation procedure, as described in Section 6.1.2. Therefore, the bit rates still need to be multiplied with the modulation key of the code and the modulation method QPSK. It was chosen to use an 8 bit modulation key, while QPSK has a one on one relation related to bandwidth [23][92]. This leads to the required symbol rate in Table 6.4. With the required bit rate, an initial estimate of the required bandwidth can be made with the help of the Nyquist rate. The Nyquist rate is a measure of the rate a signal must be sent to prevent signal sample overlapping. According to the Nyquist theorem, signal overlapping can be prevented if the sample frequency is at least twice the original sample frequency.[91] Therefore, it was chosen to use a sample frequency 2.5 times higher than the initial frequency, so an additional safety margin is also added. The required bandwidth can be found in Table 6.4.

Table 6.3: Overview bit rate determination uplink and downlink. Data size based on assumptions based on literature.[40][48]

Type of data	Data size [KB]	N/s	Safety margin[%]	Data rate[Bits/s]
Downlink				
GPS data	1	1	20	9830.4
Additional telemetry data	1	1	20	9830.4
Attitude data	1	1	20	9830.4
Additional ATC information	0.88	1	20	8650.8
<i>Total downlink</i>				38142.0
Uplink				
Command messages	0.5	2	20	9830.4
Flight path	1	1	20	9830.4
ATC	1.5	1	20	14745.6
<i>Total uplink</i>				34406.4

Table 6.4: Required symbol rate and bandwidth.

Link	Required symbol rate after modulation	Nyquist bandwidth [MHz]
Downlink	305135.616	0.76
Uplink	275251.200	0.69

With the help of the required bandwidth, roughly $1[MHz]$ for both links, the carrier frequency at which the uplink and downlink signals would be transmitted are found. It was decided to send the uplink at a carrier frequency of $910[MHz]$ and the downlink at a carrier frequency of $920[MHz]$. The gap of $10[MHz]$ includes a guard band, to make sure that the signals will not interfere with each other.

Furthermore, the wavelengths (λ) for both uplink and downlink are determined with the carrier frequencies and Equation 6.6, and can be found in Table 6.5. Besides the wavelengths, all required data for determining the link budgets for both down- and uplink are in Table 6.5.

The transmitting power by the MGS and the glider are both chosen to be $1[W]$ based on spread spectrum modulation regulations in the frequency band $902[MHz] - 928[MHz]$ [92][30]. Furthermore, the characteristics for the glider antenna are based on the chosen antenna, Table 6.2, where the loss factor of the MGS antenna ($L_{T/R_{MGS}}$) is assumed to be 0.8. The free space loss for downlink and uplink are calculated with Equation 6.5 where d_{max} is the maximum distance the signal needs to cover. The coding gain (G_{coding}) was calculated with Equation 6.7, where the bit rate after applying the modulation key is divided by the original bit rate, after which it has to be converted to decibels [23]. The final parameter is the gain of the MGS dish antenna, which is determined with the help of an iterative procedure related to the antenna diameter, d_{MGS} . The gain for this antenna is calculated with Equation 6.4 where η is the aperture efficiency factor. The aperture efficiency factor is usually between 0.55 – 0.65 and therefore it was assumed to be equal to 0.6 [3].

Table 6.5: Required parameters and values for link budget calculation.

Parameter	Value
P_{drone}	1 [W] [92][30]
P_{GS}	1 [W] [92][30]
$L_{T/R_{drone}}$	-0.177 [dB]
$L_{T/R_{MGS}}$	0.8 [-]
G_{drone}	3 [dB]
G_{MGS}	25.42 [dB]
G_{coding}	9.03 [dB]
$L_{FS_{DL}}$	-140.50 [dB]
$L_{FS_{UL}}$	-140.441 [dB]
L_{FM}	20 [dB] [92]
L_{misc}	4 [dB]
f_{up}	910 [MHz]
f_{down}	920 [MHz]
c	299792458 [m/s]
λ_{up}	0.32944 [m]
λ_{down}	0.32586 [m]
d_{MGS}	2.5 [m]
d_{max}	400 [km]
η	0.6 [-]
k	$1.38 \cdot 10^{-23}$ [J/K]
T_{sys}	290 [K] [92]

$$G_{MGS} = \left(\frac{\pi \cdot d_{ant}}{\lambda} \right)^2 \cdot \eta \quad (6.4)$$

$$L_{FS} = \left(\frac{\lambda}{4\pi \cdot d_{max}} \right)^2 \quad (6.5)$$

$$\lambda = \frac{c}{f} \quad (6.6)$$

$$G_{coding} = \frac{B_{RF}}{B} \quad (6.7)$$

$$C = B \cdot \log_2(1 + SNR) \quad (6.8)$$

As can be seen in Table 6.6, the link margins are positive hence the link budgets are closed and a connection to the MGS can be established during its entire operation, and therefore also with the ATC.

Besides the SNR values, the channel capacity (C), which is the maximum theoretical data rate that can be transmitted for both links are also given in Table 6.6. The channel capacity can be calculated with the help of Shannon-Hartley theorem, Equation 6.8, where B is the channel bandwidth in Hertz, in this case the bandwidth after the modulation procedure, and SNR is converted back from decibels. From these theoretical data rates it can be concluded that the required uplink and downlink data rates can be sent every second. This means that the MGS can be updated with the GPS coordinates of the glider every second. Furthermore the theoretical data rates are meeting subsystem requirements SAI-SYS-11-COMM-01 and SAI-SYS-11-COMM-02. Validation procedures on the communication requirements will be discussed in Section 6.1.5.

Table 6.6: Required symbol rate and bandwidth.

Link	SNR [dB]	SNR margin [dB]	Channel capacity [bit/s]
Downlink	17.675	6.675	1799034
Uplink	18.217	7.217	1671667

6.1.4. Link budget sensitivity analysis

It is important to analyse the robustness of the link budget calculations, as small deviations from the aforementioned values should not change the outcome of the link budgets. To analyse if the link budget model is robust enough, ten different parameters will be increased and decreased by ten percent to see the effect on the outcome. The changed parameters are: drone antenna gain, power transmitted drone antenna, power transmitted MGS antenna, maximum signal distance, MGS antenna diameter, system noise temperature, up- and downlink data rates, fade margin and the margin for miscellaneous losses. These parameters were chosen because they have the largest influence on the outcome of the link budget model.

The results of the sensitivity analysis for the downlink budget are visualised in Figure 6.4a and Figure 6.4b. Furthermore, the results for the uplink budget are visualised in Figure 6.5a and Figure 6.5b. When analysing these results it can be seen that a change in the fade margin has the largest effect on the link budgets, namely a $2[dB]$ change, but the effect of changing the other parameters is relatively low. For all these changes in parameters the link budgets are still closed. Therefore it is concluded that the link budget analysis is robust.

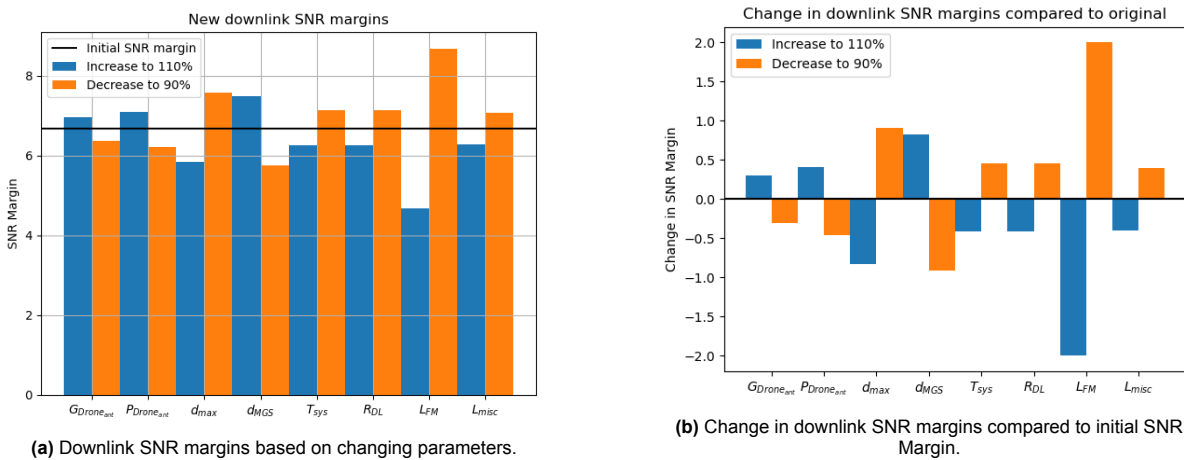


Figure 6.4: Visualisation of the sensitivity analysis of the downlink link budget.

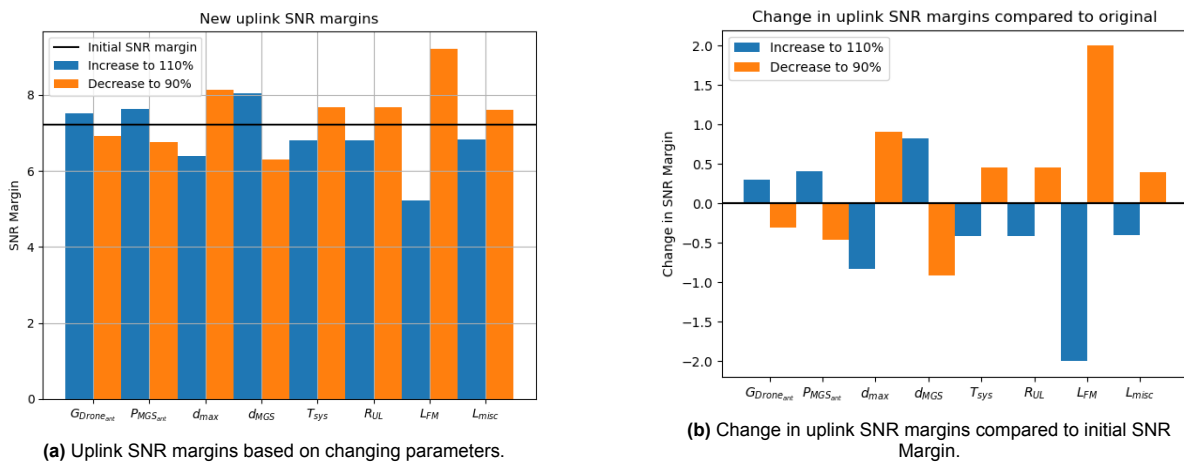


Figure 6.5: Visualisation of the sensitivity analysis of the uplink link budget.

6.1.5. Verification and validation communication system

Besides checking the robustness of the link budget model, verification and validation on the link budget model and the communication system as a whole is also performed. Furthermore, the communication system requirements must be verified.

Firstly, verification on the simple link budget model was performed with the help of the literature to build the model and with the help of hand calculations. For each calculation performed by the model a hand calculation was performed to make sure the same output was obtained. Moreover, the model was verified with examples obtained from literature, by using the same input values and comparing the output of the model with those shown in literature.

Secondly the meeting of the communication system requirements, shown in Section 6.1.6, are verified with the help of performed analysis and documentation.

Lastly, regarding the validation of the communication system, the outlook of the procedure will be hereby described, assuming the use of parts and components listed in Table 6.2.

Validation plan communication system

The first step in the validation procedure is performing a detailed analysis on the parameter values in the link budget model. An analysis will be performed on all the components of the communication system to determine the more detailed values for component loss factors and gain factors of the components. Furthermore, the obtained data rates are validated by constructing example messages to confirm message sizes.

The second step is to recalculate the link budget with the more detailed values to obtain the new SNR. If this budget is not closed, a redesign of the communication system needs to be performed.

The third step is performing tests with a made testing model to get insight on the reliability and robustness of the system. Two types of tests will be implemented. The first validates the maximum range that can be met by the system. A small sized message will be send over multiple distances: *10km, 50km, 100km, 150km, 200km, 300km, 400km* and *450km*. This last distance is a longer range compared to the maximum range, to ensure that communication is still possible at a slightly larger range. The second tests include the size of the messages. For each of the previous mentioned ranges the maximum message size will be send and it will be tested if the communication link is still possible. Both these tests will be performed in the three climate zones.

The fourth step will be implementing the test model in the full-sized glider model to test the reliability and robustness of the communication system during flight. This test will again be performed in the multiple climate zones and for the multiple ranges.

If these steps are successfully completed, the communication system design will be valid. If one of these steps fail an iterative procedure must be started to improve the design and the same validation approach must be repeated.

6.1.6. Requirement compliance check communication system

In this section the compliance of the communication system with its subsystem requirements will be discussed. Compared to the system requirements presented in [35] and [36], requirement SAI-SYS-11-COMM-07 has been removed. This decision was made due to the fact that live video communication to the MGS would have a dramatic effect on the required downlink bit rate which made communication to the ground station not possible. This decision was made in compliance with the client.

In Table 6.7 the remaining communication subsystem requirements are given and a check mark is added if the requirement is met. Requirement SAI-SYS-08-COMM-06 needs to be verified through real world testing, hence at this stage it remains unchecked.

Furthermore, requirement SAI-SYS-21-COMM-16 is based on EASA rules for C3 unmanned aircraft systems [26]. The rules related to command, control and communication are rules 5, 9, 10 and 12. Rule 5 is partly met, because the rule states that when there is communication loss, there should be a predictable method to recover the link or the flight should be terminated in a way that reduces the effect on third parties in the air or on the ground. The current design is that the glider will be following the pre-implemented flight path in case there will be a communication loss. Whether this idea fulfills the requirement, must be confirmed with the help of a more detailed analysis post DSE. Besides, rules 9 and 10 are met in theory with the link budget, but this should be validated with experiments. Rule 12 about protection against unauthorised access is fulfilled by the applied spread spectrum technique. For the reason that rule 5 is certainly met it is stated that at this moment SAI-SYS-21-COMM-16 is not met.

Table 6.7: Compliance matrix for the communication system

Requirement ID	Requirement	Compliance	Proof
SAI-SYS-11-COMM-01	The system shall be able to provide an uplink rate of at least 280000 [bits/s].	✓	Section 6.1.3
SAI-SYS-11-COMM-02	The system shall be able to provide a downlink rate of at least 310000 [bits/s].	✓	Section 6.1.3
SAI-SYS-11-COMM-03	The system shall be able to communicate with the ground station during its entire operation.	✓	Section 6.1.3
SAI-SYS-11-COMM-04	The system shall be able to communicate with the Air Traffic Control centre during its entire operation.	✓	Section 6.1.3
SAI-SYS-11-COMM-05	The system shall be able to communicate with the user when landed.	✓	Section 6.1.1, Section 6.1.2
SAI-SYS-08-COMM-06	The system's communication system shall not fail due to environmental exposure during operation.	TBD	
SAI-SYS-11-COMM-08	The system shall be able to communicate telemetry data.	✓	Section 6.1.1, Section 6.1.2, Section 6.1.3
SAI-SYS-11-COMM-09	The system shall be able to communicate via long range radio frequency communication.	✓	Section 6.1.1
SAI-SYS-11-COMM-10	The system shall be using the 902 - 928 MHz frequency bandwidth.	✓	Section 6.1.1
SAI-SYS-24-COMM-11	The communication system shall not be using more than 55 [W].	✓	Section 6.3.10
SAI-SYS-23-COMM-12	The communication system elements shall have a total mass less than 0.0483 [kg]	✓	Section 3.3
SAI-SYS-11-COMM-13	The system shall be able to store all the data required to complete the mission in the case of temporary connection loss.	✓	Section 6.3.6
SAI-SYS-11-COMM-14	The system shall provide the ground station with its global positional coordinates at least every 5 [s].	✓	Section 6.1.3
SAI-SYS-05-COMM-15	The system shall, after landing, provide the recipient with its global positional coordinates.	✓	Section 6.1.1, Section 6.1.2
SAI-SYS-21-COMM-16	The communication system shall adhere to drone communication regulations stated by the EASA.	TBD	
SAI-SYS-25-COMM-17	The communication system shall not be using more than 41302 [J].	✓	Section 6.3.9

6.2. Navigation System

In this section the designed navigation system will be discussed, starting with the choice of the navigation system components. Then, the autonomous navigation approach followed by the generated path planning software will be discussed. Finally, the verification and validation plan of the system will be shown as well as the compliance matrix of the navigation system.

6.2.1. Choice of navigation components and positioning

This section first describes the navigation related components, followed by the autonomous flight related components. As mentioned in the midterm report [36], it was decided to equip the glider with an inertial navigation system (INS) as well as a global navigation satellite system (GNSS). The main reason for this decision is the importance of redundancy and robustness, and by using the two systems a redundancy factor is built into the system. [50] [28] [75]

To establish an INS three components are vital: an inertial measurement unit, a pitot tube and an onboard computer, because with these components the system attitude, altitude and speed can be obtained without the need for external references. That means that if the connection with the GNSS is lost, the glider will still be able to fly towards its destination [50] [28] [75]. The chosen IMU and

pitot tube for the system can be found in Table 6.8 and the chosen onboard computer is explained in Section 6.3.6. The IMU and onboard computer will be placed in the electronics box of the system, as referred in Section 6.3.3. The pitot tube is positioned in the left tapered section of the glider seen from the front at $32.5[cm]$ from the middle of the glider.

A simple GNSS will be added to the navigation system. To make sure that this system can be used around the globe it was decided to have a GNSS receiver that is able to connect to multiple global satellite navigation networks. The chosen receiver, which can be found in Table 6.8, is able to connect to GLONASS, Galileo, GPS and QZSS. Furthermore, the receiver is stored in the electronics box and is has an accuracy of $2.5[m]$, which helps the system to stick to its flight path without deviating too much.

Similarly, the onboard computer is an important aspect in the autonomous part of the system. As determined in [36] the trajectory of the glider will be partly based on a pre-implemented flight path merged with real-time path planning. To be able to read and save the pre-implemented flight path, the onboard computer must be present.

Besides the previously mentioned components, there are additional instruments that will allow the system to perform real-time onboard path planning, such as a RGB camera and distance sensors. These are needed to obtain the positions of obstacles, which allows the onboard computer to model the systems environment with the help of additional software. Details of the onboard algorithm for mapping and planning will be presented in Section 6.2.2. It was chosen to use one single RGB camera and three time-of-flight (ToF) sensors, which are LIDAR based sensors. The specifications of the camera and the ToF sensors can be found in Table 6.8, and a visualisation of the components can be found in Figure 6.6 and Figure 6.7.



Figure 6.6: Selected RGB camera for obstacle detection. **Figure 6.7:** Selected distance sensor for obstacle detection.

The camera will be attached to a rotating mechanism that will allow two camera orientations, rotated 90 degrees pointing to the ground or pointing to the front of the glider, see Figure 6.8. The mechanism will be made from spruce wood and a small servo. The camera mechanism will be attached to the rib at $27.5[cm]$ from the middle of the glider, see also Figure 3.5. The servo has a width of $23[mm]$ which means that the centre of the camera will be positioned $11.5[mm]$ from the rib.

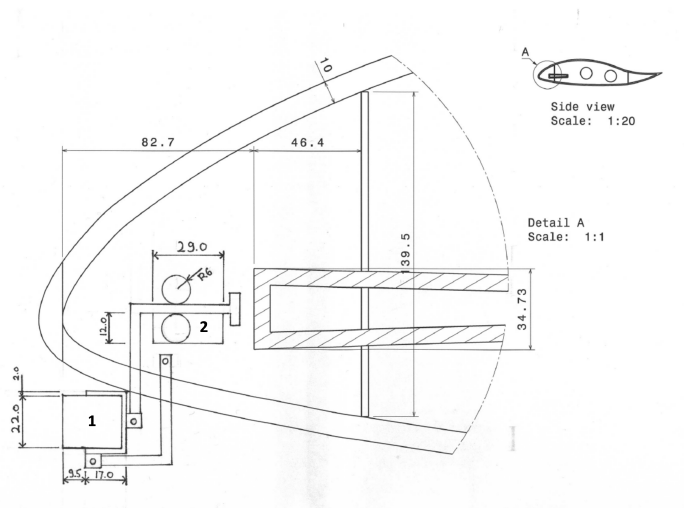


Figure 6.8: Rotating mechanism drawing at the rib attachment, where 1 shows the camera and 2 shows the servo.

Alongside the camera, a ToF sensor will be positioned at $35[cm]$ from the centre. This sensor will be pointing towards the front of the glider and will be tilted 4 degrees away from the centre. The other two ToF sensors will be positioned $30[cm]$ and $35[cm]$ from the centre, at the left tapered part. The

one at 30[cm] will be tilted toward the ground with an angle of 70 degrees while the one at 35[cm] will be titled opposite from the sensor at the camera, also with an angle of 4 degrees. These angles are initial estimates based on the sensors' FOV, further tuning of the angle would be done during validation. These sensors will only be activated as the system enters their operational range, 250m in altitude. The activation will be triggered by the MGS, or autonomously by the onboard computer prior to landing.

Table 6.8: Used navigation components.

Component	Product name	Specifications
Camera	Foxeer toothless camera ³	Power consumption: 170[mA] at DC 5[V], FOV: 125°, size: 24.5[mm]x21.8[mm]x21.8[mm], $m = 9.7[g]$
ToF distance sensors	TeraRanger Evo 60m ⁴	$m = 12[g]$, FOV: 2°, supply voltage: 5[V] DC, supply current: 330[mA], size: 29[mm]x29[mm]x22[mm]
IMU	MPU9250 Inertial Measurement Unit ⁵	$m = 20[g]$, supply voltage: 5[V] DC, size: 20[mm]x20[mm]x2[mm], 3-axis accelerometer, 3-axis gyroscope, 3-axis magnetometer
GNSS receiver	MATEKSYS SAM-M8Q GNSS UQBLOCK ⁶	size: 26[mm]x16[mm]x7.5[mm], $m = 7[g]$, supply current: 40[mA], supply voltage: 5[V] DC, horizontal accuracy: 2.5[m], velocity accuracy: 0.05[m/s], update rate: 10[Hz]
Pitot tube	Pitot Tube Airspeed Sensor ⁷	supply voltage: 3.3[V], supply current: 24[mA], $m = 36.3[g]$ ⁸ , length: 10[cm] ⁹
Servo	Servo	size: 23[mm]x12.2[mm]x29[mm], $m = 9[g]$

6.2.2. Autonomous navigation approach

Whereas the above section described the hardware, this section will describe the software needed for navigation. The tasks of this software during flight are obtaining and processing environmental parameters, to determine attitude, to model the map and plan the path.

The thinking process in the glider for obtaining important parameters and the order in which they occur is visualised in Figure 6.9. From this block diagram the theory of two software actions will be explained in more detail, which are the map modelling and the path planning methodologies. After that, the pathfinder code will be shown and explained. Lastly, some comments are made about trajectory generation software.

Map modelling theory

The map modelling software is based on a methodology called Simultaneous Localization and Mapping (SLAM). SLAM helps to solve the problem of building a spatial map of an unknown environment, while simultaneously determining the location of the system inside of this map. [25][85]

Three main different theoretical approaches used in SLAM include the use of Extended Kalman Filters (EKF), particle filters, and graph-based optimization techniques. The choice for determining the approach mainly depends on the type of SLAM required, either the online SLAM problem, which seeks to obtain only the current robot location, or the full SLAM problem, which involves estimating the entire path of the system together with the map. [25][85] Map modelling is a necessary aspect of autonomous navigation, and it acts as an input to the next component, which is a path planning algorithm.

³<https://www.foxeer.com/foxeer-mini-full-toothless-2-1200tv1-fov-switchable-starlight-fpv-camera-1-2-sensor-super-hdr-g-270> [cited 17-06-2021]

⁴<https://www.terabee.com/shop/lidar-tof-range-finders/teraranger-evo-60m/> [cited 17-06-2021]

⁵<https://makersportal.com/shop/mpu9250-inertial-measurement-unit-imu> [cited 17-06-2021]

⁶<https://droneshop.nl/mateksys-gnss-ublox-sam-m8q> [cited 17-06-2021]

⁷<https://makersportal.com/shop/pitot-tube-air-speed-sensor-for-arduino-and-raspberry-pi?rq=pitot%20tube> [cited 17-06-2021]

⁸<https://www.amazon.com/Dwyer-Stainless-Pocket-Diameter-Insertion/dp/B009PAE7GE> [cited 17-06-2021]

⁹https://dutch.alibaba.com/product-detail/new-original-4-8v-6v-smart-accessories-steering-gear-fixed-180-degree-sg90-9g-micro-servo-motor-servo-sg90-1600101923112.html?spm=a2700.galleryofferlist.normal_offer.d_title.27e8649aXa1NCF [cited 20-06-2021]

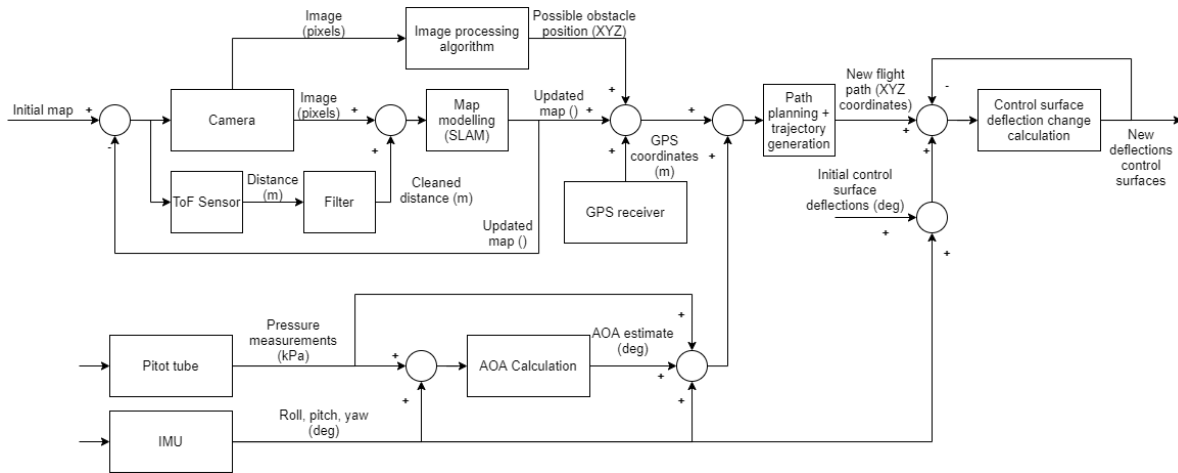


Figure 6.9: Block diagram autonomous thinking process.

Path planning theory

The path planning algorithm of the system will be based on the so called A-star algorithm. This algorithm finds the shortest, lowest cost feasible path for travelling from a start node to an end node. It performs this process with the help of a distance-plus-cost heuristic function Equation 6.9. Here, the path-cost function, $G(x)$, represents the cost to travel from the current node to the next node while the heuristic estimate function, $H(x)$ represents the estimated cost from the next point to the final point. Together they give a cost estimate for the path seen from that point. If an obstacle is in between adjacent nodes, the $G(x)$ is set to infinity. The cost per node determines the order in which the algorithm visits the nodes. [51]

$$F(x) = G(x) + H(x) \tag{6.9}$$

An example of the use Equation 6.9 can be visualised with the help of Figure 6.10. In this figure three different paths from point A to B are visualised. For two of these paths, one and three, the path finder will hit an obstacle, this means that for those paths the final value for $F(x)$ will be infinity, so the path finder will not include these in the determination of the path. Therefore, in this simple example, the best path will be path two as it is the shortest, feasible path..

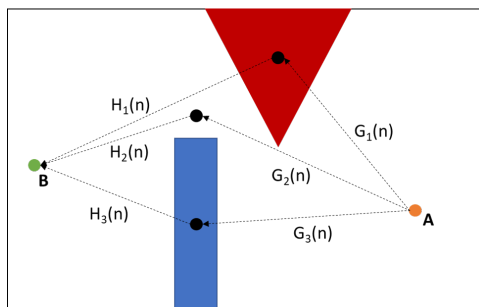


Figure 6.10: A* path finder algorithm visualisation.

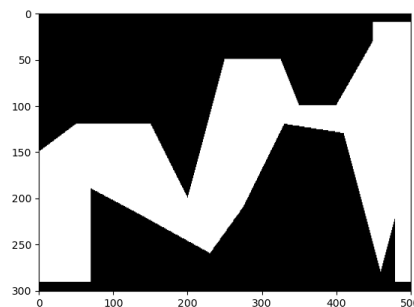


Figure 6.11: Example output 2D map generator.

Design of the A* path planner

An A-star path planner was developed for the GliMed, and tested on several randomly generated maps. The pseudo code and the results of this algorithm will be presented in this section.

Before the actual path planning algorithm was build a 2D map generator was build. This map generator is based on filling up the area within the map boundaries. Each node in the area will be set to a 1 in case of an obstacle, and a 0 for a flyable node. The combination of multiple 'obstacle nodes' creates the effect of no-fly zones within the map, as can be seen in Figure 6.11. The code for this algorithm can be found in algorithm 1.

Algorithm 1: Map generator code

```

Class Mapmaker(max_x, max_y, border_points_up, border_points_down):
    def InitGrid(max_x, max_y):
        Create empty grid with max_y rows and max_x columns ;
        return empty_grid;
    def FillGrid(input_map, side_choice, point_array):
        temp_map = copy(input_map);
        for i in (len(point_array)-1) do
            determine slope between point[i] and point[i+1]
            for j in difference x position point[i] and point[i+1] do
                determine y value for point j between point[i] and point[i+1];
                if side_choice is up then
                    Points from y value till 0 at x value = point[i] + j are 1 in temp_map
                else if side_choice is down then
                    Points from y value till max_y at x value = point[i] + j are 1 in temp_map
            return temp_map;

```

After building the map, the A-star path planning algorithm was made. This algorithm accounts for the glider geometry by adding an additional buffer around the wingspan, to make sure that the glider will not hit map boundaries and obstacles. A visualisation of the coding procedure can be found in algorithm 2. Furthermore, results of the program can be found in Figure 6.12, Figure 6.13 and Figure 6.14. There, it can be seen that a start and end point were set and a path was found between those two points.

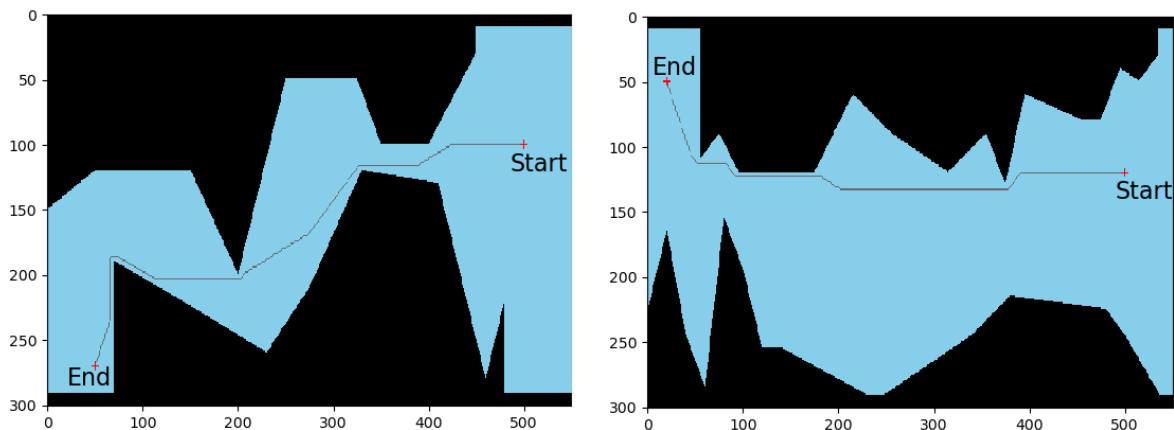


Figure 6.12: A* path finder result 1, travel distance = 574.7 [m]. **Figure 6.13:** A* path finder result 2, travel distance = 539.3 [m].

Algorithm 2: Path planner code

```

Class Node():
    def init(row, col, value):
        | Initialise node parameters
    def get_neighbours(nodegrid):
        | Obtain possible neighbours the node can go to. The 8 surrounding neighbours will be
        | checked. Per neighbour an area of 7 by 7 around it will be checked for an obstacle. If
        | there is no obstacle the neighbour will be added to a list with possible nodes to go.

    def H_path(currentnode, endnode):
        | Obtain estimated distance from the current node to the end node based on Pythagoras
        | theorem.
    def G_path(currentnode, nextnode):
        | Obtain estimated distance from the current node to the next node based on Pythagoras
        | theorem.
    def Final_path(listofpreviousnodes, currentnode, map):
        | Obtain the final path from the current node back through listofpreviousnodes till the start
        | node. Furthermore change value for node coordinates in map.
    def A_star(startnode, endnode, nodegrid, map):
        | Initialise empty Queue;
        | Initialise G list with, length equals to amount of nodes in nodegrid, with values inf;
        | Initialise F list with, length equals to amount of nodes in nodegrid, with values inf;
        while Queue not empty do
            | Get current node from Queue;
            if current node is end node then
                | Obtain final path with Final_path function.;
                | End while.
            for neighbours in neighbours current node do
                | Determine G(x) cost. If G(x) cost is better than current value G(x) neighbour add the
                | neighbour to the Queue.

When Queue is empty and no path is found return False.

```

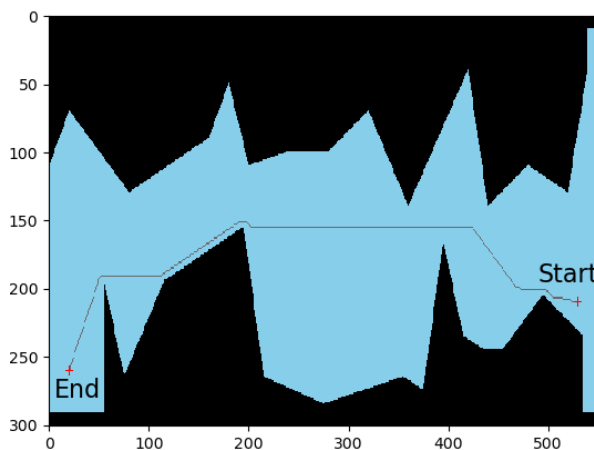


Figure 6.14: A* path finder result 3, travel distance = 602.7 [m].

Trajectory generation software

As can be seen in Figure 6.12, Figure 6.13 and Figure 6.14 the generated paths have sharp corners and do not take the turn rate of the glider properly into account. However, in the future this should be included, else the glider will plan a path that it cannot fly. Trajectory generation software takes the glider flight characteristics and geometry better into account and smoothens any sharp corners and

unfeasible manoeuvres. A simple illustration of this can be seen in Figure 6.15 and Figure 6.16. It is recommended that this step will be performed in the next design phase.

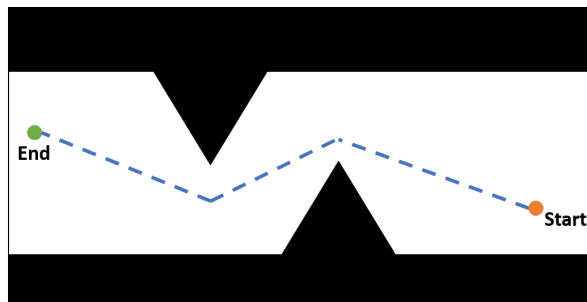


Figure 6.15: Simple visualisation of path before smoothing

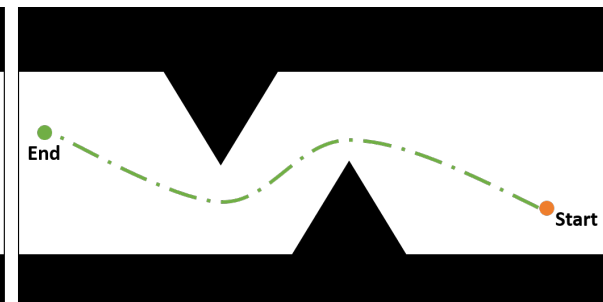


Figure 6.16: Simple visualisation of path after smoothing

6.2.3. Verification and validation navigation system

After designing the conceptual navigation system the system requirements should be verified, and the system as a whole should be verified and validated to make sure it will work as intended.

Verification navigation system

Firstly, navigation system requirements are verified with the help of analysis and documentation. After that, the simple path planner model was verified via inspection by applying the model on multiple maps. By changing the input maps for the model the limits of the model were tested. With the help of Figure 6.12, Figure 6.13 and Figure 6.14 it can be seen that the model indeed works for different maps without obtaining an error, meaning the code of the model is verified.

Validation plan navigation system

The validation of the navigation system will be performed in the detailed design phase, but its plan can be found below. To begin, the chosen equipment should be validated with the help of detailed analyses and testing. In this detailed analysis phase the specifications of the equipment will be validated in different conditions related to the climate zones which the glider will operate in to check their reliability. This is done to make sure that the chosen equipment can operate in all climates. Furthermore, the accuracy of the equipment will be tested to make sure they meet the requirements.

Secondly, the positioning of the camera and ToF sensors will be verified and validated with the help of testing. In this test phase the FOV of the sensors and camera will be tested at the chosen positions to make sure that the surrounding area can be properly scanned.

Thirdly, a simulation will be made to validate the proposed navigation system design. This test will conclude if the chosen set-up can properly perform autonomous navigation.

Fourthly, the navigation system will be applied to a small sized drone to verify that the system will work in a real world scenario. This step will be performed in the different climate conditions.

Finally, the navigation system will be applied to the actual drone design and the system will be tested in multiple flight scenarios and at multiple altitudes. The system will be tested in a forest environment, a mountain area, and an inhabited area. This will be done to verify and validate that the system is safe and reliable enough to be able to fly in those three areas.

6.2.4. Requirement compliance check navigation system

In this section the compliance of the navigation system with its subsystem requirements will be discussed. In Table 6.9 an overview is given with all the subsystem requirements, with a check mark if they are met, and the section in which the proof can be found. As can be seen in this table requirement SAI-SYS-21-NAV-22 is not yet met. This requirement is based on navigation and autonomous system requirements stated by EASA rules for C3 unmanned aircraft systems [26]. The relevant requirements are 3 and 11. Requirement 3 is about the system being safely controllable by a pilot. Although in theory the designed navigation system should be able to provide enough data for the pilot to be able to control the glider, this can not be stated with 100% confidence until testing is performed. Therefore it is stated that this requirement is not met. Rule number 11 states that the system should be able to handle restrictions with respect to limits in access to certain airspace areas. The navigation system is designed

in such a way that the onboard computer will obtain information about restricted airspace areas via the MGS which will then be used for the onboard path planning, so this part of the requirement is met.

Finally, a note about the compliance of the other requirements: the decision that those requirements are met are based on analysis, to be sure that this decision is valid the requirements must also be verified via testing.

Table 6.9: Compliance matrix for the navigation system

Requirement ID	Requirement	Compliance	Proof
SAI-SYS-14-NAV-01	The system shall be able to land in a 40 [m] radius from the designated target.	✓	Section 6.4.2
SAI-SYS-14-NAV-02	The system shall be able to read the pre-implemented flight path.	✓	Section 6.2.1
SAI-SYS-14-NAV-03	The system shall be able to perform real-time path prediction when required.	✓	Section 6.2.1
SAI-SYS-14-NAV-04	The system shall have instruments for analysing flight paths.	✓	Section 6.2.1
SAI-SYS-14-NAV-05	The system shall be able to turn visual instruments on and off when required.	✓	Section 6.2.1
SAI-SYS-14-NAV-06	The system's visual instruments shall have a field of view of 120 degree.	✓	Section 6.2.1
SAI-SYS-14-NAV-07	The system shall have sensors for analysing the system's velocity.	✓	Section 6.2.1
SAI-SYS-14-NAV-08	The system shall have sensors for analysing the system's attitude.	✓	Section 6.2.1
SAI-SYS-14-NAV-09	The system shall have sensors for analysing the system's altitude.	✓	Section 6.2.1
SAI-SYS-14-NAV-11	The system shall be able to follow the pre-implemented flight path when the GPS signal is lost.	✓	Section 6.2.1
SAI-SYS-14-NAV-12	The system shall be able to reboot itself when a software error occurs in flight.	✓	Section 6.3.6
SAI-SYS-14-NAV-13	The system shall be able to be rebooted when in flight by the ground station in case of a software error.	✓	Section 6.3.6
SAI-SYS-14-NAV-14	The system shall support the possibility for updating the pre-implemented flight path when the system is in operation.	✓	Section 6.2.1, Section 6.3.6
SAI-SYS-14-NAV-15	The system shall have a deviation of less then 5 [m] radius from the implemented flight path.	✓	Section 6.2.1
SAI-SYS-24-NAV-17	The navigation system shall not be using more than 6.8 [W].	✓	Section 6.3.10
SAI-SYS-23-NAV-18	The navigation system elements shall not have a total mass of more than 0.119 [kg].	✓	Section 3.3
SAI-SYS-26-NAV-19	The system shall contain a beacon which can provide signal for at least 24 [hours] independant of the environment.	✓	Section 6.1.2
SAI-SYS-20-NAV-20	The system shall not impact the recipient upon landing.	✓	Section 6.2.1
SAI-SYS-14-NAV-21	The navigation system shall be able to detect obstacles to avoid impact.	✓	Section 6.2.1
SAI-SYS-21-NAV-22	The navigation system shall adhere to drone navigation regulations stated by the EASA.	TBD	

SAI-SYS-25-NAV-23	The navigation system shall not be using more than 6385 [J].	✓	Section 6.3.9
-------------------	--	---	---------------

6.3. Electrical Systems

In this chapter the electrical systems will be described. First, an overview of the entire electrical system will be provided, followed by the layout of the system components. After that the different versions of the electrical system will be discussed. After this the raspberry pi will be discussed. Following this the servo placement and wiring will be presented. Next, the energy and power budget will be presented. Furthermore turning the system on and off will be discussed. Finally, the validation and verification procedure together with some recommendation will be described.

6.3.1. Electrical system overview

In Figure 6.17 an overview of the electrical system is provided. As can be seen in the figure many of the components are connected via an i2c bus, which is a common way to communicate between different electrical components. The raspberry pi and the pitot tube sensor communicate via 3.6[V] logic while the other components communicate via a 5[V] logic. Because of this, a converter will be implemented within the i2c bus. To operate the servos a servo driver is used. This device provides power and instructions to the servos. A buck converter converts the 14.4[V] of power provided by the battery to 5[V] so it can be used by the components.

The antenna needs a large amount of power (50[W]) when active, which leads to high currents of 10A. This puts high strain on the system. Thicker cables are needed, otherwise the battery would run the risk of overheating and the buck converter would not be able to handle the current. Since the antenna is only active 0.11[s] with a frequency of 1Hz, the peak load can be smoothed out by placing a capacitor between the antenna and the power supply. This leads to a lower maximum current and thus the aforementioned problems do not occur.

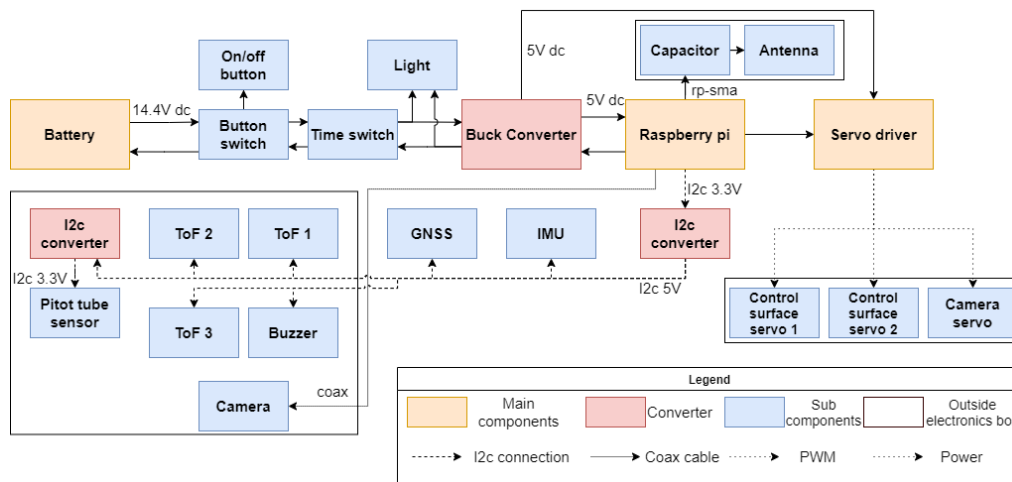


Figure 6.17: Visualisations of the electrical system.

6.3.2. Electronics layout

In Figure 6.18 the layout of the electronics inside the electronics box is visualised. Using this drawing the dimensions of the electronics box can be obtained. The battery is placed as much to the front and to the centre of the glider as possible in order to obtain a c.g. location that is more favourable for stability. Furthermore, the sensors are placed away from the battery to reduce interference.

6.3.3. Electronics box

The electronics are stored in a plywood box in order to protect them during the mission. Plywood has been chosen because it is already used in other parts of the glider. Its good impact resistance and durability are favourable for protecting the electronics. The wall thickness of the box will be 5[mm] and

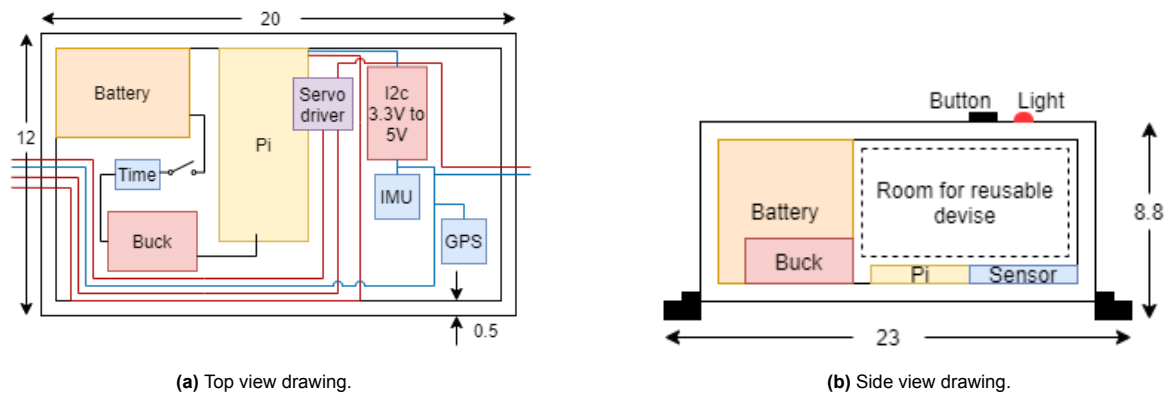


Figure 6.18: Drawing of electronics box and electronics layout, dimensions are in centimeters.

the top panel can be slid out for easy accessibility. The wires will stick out of the box so that they can be easily connected to the wiring in the aircraft. The outer dimensions have been determined to be $230 \times 88 \times 12$ [mm³]. The box itself is not waterproof, however the skin of the glider is, which ensures that water damage will not be a problem.

6.3.4. Three different versions of the electrical systems

GliMed can be outfitted with three different types of electrical systems. The first system is single use and is outfitted with single use Li-SOCL₂ batteries because they are relatively cheap and light. The second system is reusable and uses rechargeable lithium-ion batteries. Although they are heavier and more expensive, this type of battery allows for reuse which leads to cost savings and a better sustainability perspective. The third system allows for partial reusability of the electronics by the recipients. This system will be further discussed in Section 6.3.5. The three systems all have different situations in which they are the best option, therefore the glider can be outfitted with any of the three systems. The sustainability of the different system will be further explained in Figure 6.5 and the cost for the different systems will be explained in Section 4.3.2.

6.3.5. System reusable by recipients

In this section, the design of the reusable system for the recipient will be presented. In this system half of the energy will be supplied by rechargeable batteries and the other half supplied by non-rechargeable batteries. In Figure 6.19 and Figure 6.20 the design of the device that is reusable by recipients is presented. In the reusable system the raspberry pi and rechargeable batteries will be reused and combined with a screen, a solar panel, and a casing to create the device. The casing will be made using a 3d printer. The reusable device has been design with the help of an industrial engineer.

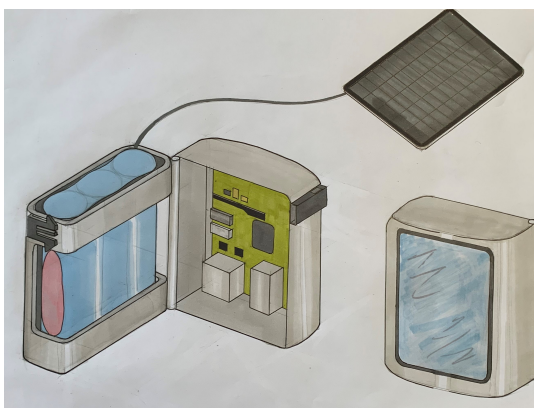


Figure 6.19: Drawing of reusable device.

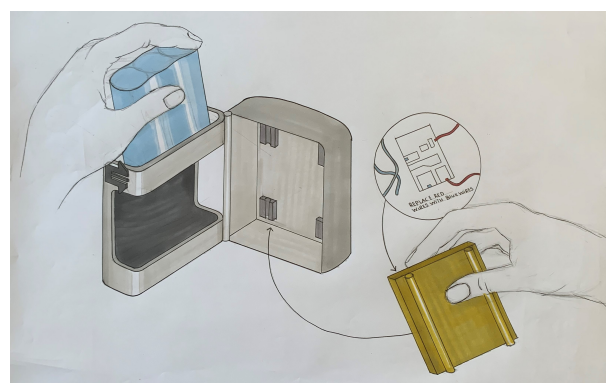


Figure 6.20: Drawing of assembly of reusable device

6.3.6. Raspberry pi

For the computing module a raspberry pi 4 has been chosen. The raspberry pi offers a wide variety of connectors which allows the possibility to connect all electrical components to it. Furthermore, the pi offers a sufficient amount of computing power to run all the software needed for the communication and navigation system. The raspberry pi also has the ability to reboot itself and will be able to shut down the entire electrical system when needed. The raspberry pi will be outfitted with an SD card which can contain necessary software ¹⁰.

6.3.7. Servo placement

The servos that operate the control surfaces do not fit within the regular shape of the wing since the wing is very thin near the wing tips. To make sure the servos could still be placed at the desired locations a droplet shaped dome will be placed around the servo. The placement of the servo and the shape of the dome can be found in Figure 6.21 and Figure 6.22. The dotted shaped line represents the change in the skin shape to create the droplet shaped dome. Since the part of the wing affected by the dome is rather small and far backwards it is assumed that the aerodynamic performance will not be noticeably affected.

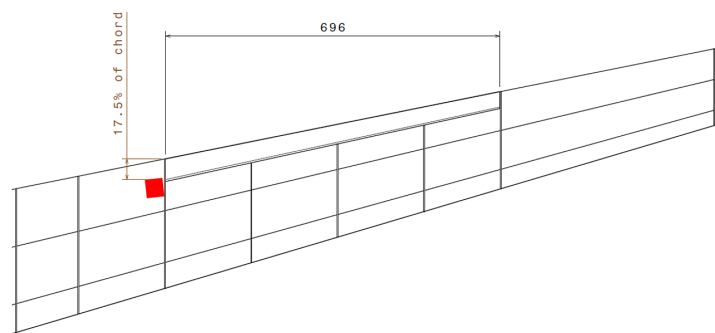


Figure 6.21: Top view of elevon servo placement, shown in red.

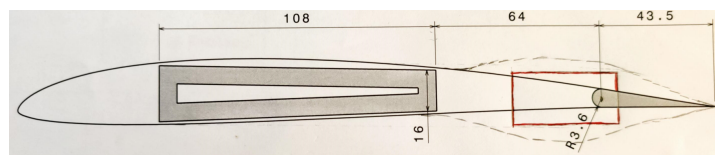


Figure 6.22: Side view of servo and dome placement.

6.3.8. Wiring

The wires used for the electrical circuits will be made out of copper as a the conducting material and PLA as insulation material. PLA is biodegradable so less material will be left in the environment. It offers good properties as an insulator, and manufacturing methods exist to produce PLA insulated electric wiring [69]. In figure Figure 6.23 the layout of the wiring can be found. The blue lines represent the i2c connection and consists of four wires, the red lines represent the servo drive cables (this connection consist of three wires) and the pink line represents the coax cable from the camera to the raspberry pi. From this drawing it has been estimated that a total of $0.079[kg]$ of PLA and $0.084[kg]$ of copper will be needed for the cables. The wires will be $20AGW$, which is enough for most parts of the systems. In some places thicker wires will be applied, for example between the capacitors and the antenna and between the battery and the buck converter. The cables will be put in the glider before the skin is applied. The cables for the different parts will be connected using connectors, the same applies to the cable connection between the electronics box and the rest of the glider. These connectors will be coloured to prevent mistakes being made during assembly and installation of the electronics box. The location of the equipment outside of the electronics box are marked with s1, s2, s3 and s4. At position s1 two distance sensors, the pitot tube and its sensor and an i2c voltage converter can be found. In

¹⁰<https://www.raspberrypi.org/products/raspberry-pi-4-model-b/specifications/>[cited on 22-06-2021]

position s2 one distance sensor, the camera, a servo and the buzzer are located. Furthermore, a big servo is located at position s3. If point s3 is mirrored over the middle spar the position of another big servo can be found, not shown in Figure 6.23. Finally the capacitor and the antenna are located at point s4.

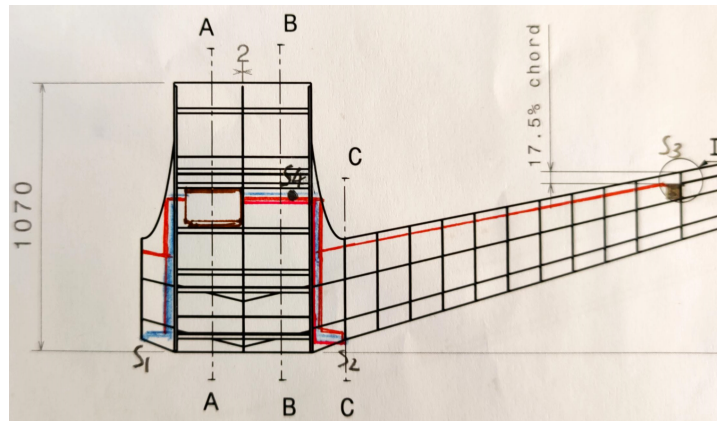


Figure 6.23: Drawing of electronics placement.

6.3.9. Energy budget

The flight time of the glider is $6425[s]$ a margin of 1.1 has been added to this to account for early activation of the electrical systems and landing. This flight time is calculate with a cruise speed of $23.9[m/s]$ and a max range of $125[km]$. The inefficiency in the electrical system is estimated to be 0.85. This value was obtained from discussions with various experts in the field of electrical engineering [66] [83]. The battery capacity is estimated to be 80% of the value provided by the manufacturer. Not all components are active for the entire duration of the flight, as can be seen in Figure 6.24. In table Table 6.11 these components with their respective percentage can be found. After combining all the numbers it was found that the system has an energy need of $57.8[Wh]$. The reusable systems battery has a capacity of $76.96[Wh]$ and the one time use system has been outfitted with $74.88[Wh]$ worth of batteries. The batteries have been over-designed with respect to their energy storage capabilities.

6.3.10. Power budget

To ensure there is always enough power available to supply all the components a power budget will have to be made for the peak cases. This peak situation occurs when the antenna activates at the same time as the control surface servos and the ToF sensors. During this peak condition the system uses about $15.6[A]$. The battery and the buck converter have a maximum current of only $8[A]$. To solve this problem a capacitor has been placed before the antenna. This capacitor will have to deliver $5[v]$ with a current of $10[A]$ over $0.11s$ which equates to a capacity of $0.2[F]$. To be safe a capacitor of $0.6[F]$ has been selected. By doing this the current of the peak case becomes $6.7[A]$ which is within the allowable regime so the power budget is satisfied.

Table 6.10: Average power usage per component.

Component	Power usage
servo 20 kg	2.82 [W]
servo 1.6 kg	0.2325 [W]
pi	10.5 [W]
Antenna	5.5 [W]
gps	0.2 [W]
pitot tube	0.08 [W]
ToF	0.495 [W]
IMU	0.1 [W]
camera	0.085 [W]
total	19.9655 [W]

Table 6.11: Percentage of time the components are active.

Component	Percentage of flight active
2x servo 20 kg	8%
servo 1.6 kg	15%
Antenna	11%
camera	10%
ToF sensors	10%

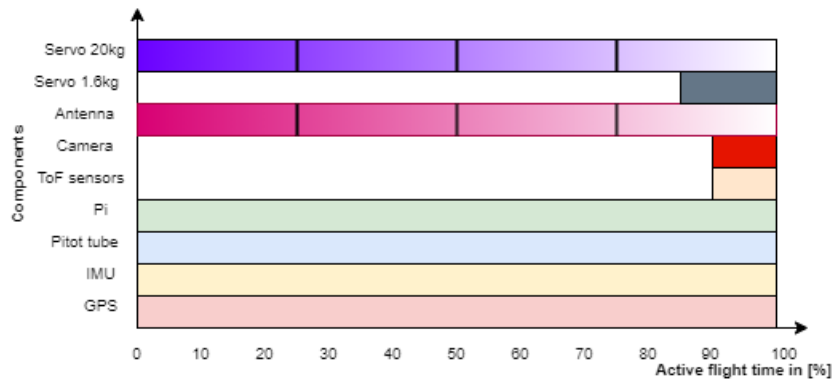


Figure 6.24: Visualised time line, in percentages, when each component is active. The antenna and servos 20kg will be used during the entire flight but will be turned on and off continuously, Table 6.11.

6.3.11. Turning on/off the electrical system

Since the launch phase of the mission can take up to $3.164 [h]$, this number will be discussed in more detail in Section 6.4.1, it is not preferred that the electrical systems are operational for the entire duration of the launch phase. For this reason a timer relay will be added to the system. This device allows the system to turn on after a preset amount of time. The ground crew will set the timer to the right length, depending on the length of the launch phase. Right before launch the timer will be activated by the press of a button on the outside of the aircraft. The electrical system will be given some time to boot up before the glider is launched. When the glider has landed the raspberry pi will shut off the electrical systems. To make sure the recipients will not be in danger of receiving an electric shock due to the raspberry pi not shutting down, the electronics box is outfitted with a red led light. When the light is on the electrical systems are still online and the recipients should not touch them. There will be a manual turn off switch on the outside of the electronics box.

6.3.12. Validation and verification of the electrical system

In the next design phase the electrical system will be tested extensively to make sure everything functions properly. The power consumption of the various components will be tested by subjecting them to flight-like conditions. This will give a better indication of the power consumption of the components. This will especially help with the power consumption of the raspberry pi and the servos since their power consumption heavily depends on mission characteristics and is thus hard to estimate without testing. Furthermore, the temperature of the different components will be measured during operation to see if any additional cooling will be needed. In addition, the components will be tested to see whether the performance claims made by the manufacturers are actually consistent with real world performance. The servos and actuation mechanism will be tested with the help of a test setup to see if the control surfaces can be operated properly and reliably. Finally, the electrical system in its entirety will be subjected to multiple life cycles to test reliability and the re-usability.

6.3.13. Recommendations

It is recommended to investigate the reliability of the system that turns on the electrical system. It is favourable to add redundancy to this system by also making a mechanism that can turn on the electrical system via the launch vehicle. Furthermore redundancy should be added to the wiring that runs from the power supply to the components.

6.3.14. Compliance matrix electrical systems

In this subsection the compliance matrix of the electrical systems will be discussed. All the requirements have been fulfilled except for SAI-SYS-09-ELEC-08. This requirement can only be fulfilled after testing of the system. This will be done in future design phases.

Table 6.12: Compliance matrix for the electrical system

Requirement ID	Requirement	Compliance	Proof
SAI-SYS-06-ELEC-02	The system shall have a method of turning the electrical system on and off.	✓	Section 6.3.11
SAI-SYS-08-ELEC-03	The electrical system shall be protected from water.	✓	Section 6.3.3
SAI-SYS-08-ELEC-04	The electrical system and battery shall not form a fire hazard during normal operations.	✓	Section 6.3.10
SAI-SYS-09-ELEC-08	The electrical systems shall have a reliability of at least 99.5%	TBD	testing in future design phases
SAI-SYS-23-ELEC-09	The electrical system elements shall not have a total mass of more than 1.41 [kg]	✓	Section 3.3
SAI-SYS-24-ELEC-05	The system shall have a least 57.6 [W] as back up power.	✓	Section 6.3.9
SAI-SYS-24-ELEC-06	The system shall have an efficiency of at least 85% when generating power.	✓	Section 6.3.9
SAI-SYS-24-ELEC-07	The system shall be able to generate at least 57.6 [W] during its entire operational life.	✓	Section 6.3.9

6.4. Launch, Landing and Logistics

In this section the launch system, landing procedure, payload integration and the operations and logistics will be presented. The crash structure that protects the payload is also discussed. First the launch vehicle will be discussed and the attachment mechanism to the glider. This is followed by the landing methods and the crash structure design, as well as the payload integration. Finally, the operations and logistics of GliMed are elaborated upon.

6.4.1. Launch

The decision to go with a VTOL-UAV (Vertical Take-Off and Landing) as the launch vehicle was based on it being one of the most sustainable options, on par with a towing UAV launch. What set the VTOL-UAV apart though, are the very easy logistics that come with it. It can be launched at any location and does not need a dedicated runway to take off or land. This is further complemented by the fact that wheels on the glider would be highly unwanted, which would have been necessary in case of a runway launch.

The highest performance VTOL-UAVs are helicopters, especially for higher payloads as is the case with the glider. It was chosen to base the performance estimations on the Camcopter S-100¹¹, since this was the most fuel efficient VTOL-UAV that is capable of carrying the glider. Table 6.13 shows the main parameters of the Camcopter S-100. The Camcopter S-100 works on aviation gasoline (avgas). Unfortunately, since sustainability is such an important aspect of SustAIn, no electrical VTOL-UAV were high performance enough to be able to launch the glider. Either the payload carrying capabilities, the endurance or the surface ceiling were insufficient, or a combination of these. The same was the case for non-electrical helicopters, where the Camcopter S-100 is one of the limited option to be able to fulfill all of these requirements.

As the Camcopter S-100 is built for many different applications, from power line surveillance to naval operations such as coastal patrol, a customised version will be used to decrease the cost and increase the performance even further as it can be specifically designed for carrying the glider. Additionally, the launch attachment to the glider will require a customised mechanism. The concept design for this will be discussed later.

The main question regarding the performance of the Camcopter S-100 is whether it can carry the 25[kg] glider to a launch altitude of 5000[m] as per requirement SAI-SYS-15-LAUNCH-02, and whether it would still have enough fuel to fly back. It is given that it has a surface ceiling of 5500[m], but it is

¹¹<https://schiebel.net/products/camcopter-s-100-system-2/> [cited on 16-06-21]

unknown with how much payload this is. With Equation 6.10, Equation 6.11 and Equation 6.12, where Equation 6.11 is based on an empirical formula as described by McCormick [61], the maximum lift as produced by the helicopter can be estimated. The power used in this formula is only 90 % of the power as given in Table 6.13, since 10 % of the power of the engine goes to the tail rotor to counteract the torque. Furthermore, note that Equation 6.11 only works for SI units. This leads to a total lift of 2511[N] or 256[kg] at sea level, which agrees nicely with the MTOW (Maximum Take-Off Weight) of 200[kg]. With the air at 5000 meters being 0.6 times as dense, this leads to a lift of 1507[N] or 153.6[kg]. This is enough to carry the 25[kg] glider and an additional 18.6[kg] of fuel. With this remaining fuel a distance of just over 275[km] can be covered back to the mobile launch truck, such that the total range of the launch vehicle is 275[km] plus 125[km] of the glider, leading to 400[km] of maximum range from the launch location with the mobile launch truck to the recipient.

The time it will take for the launch vehicle to launch a glider, can easily be calculated. With a cruise speed of 102[km/h], the distance to the destination can be covered in approximately 2.7[h], while the ascent to 5000[m] will take 0.46[h], assuming an average climb rate of 3[m/s]. This is an upper limit estimation of the time it will take (SAI-SYS-22-LAUNCH-12) since the ascent will be done simultaneously. With an additional 2.7[h] for the way back, the total time the launch vehicle is away is approximately 6[h].

Table 6.13: Overview parameters Camcopter S-100

Parameter	Value	Unit
Range	612	[km]
Endurance	6	[h]
Cruise speed	102	[km/h]
MTOW	200	[kg]
Empty Weight	110	[kg]
Payload	50	[kg]
Fuel usage	9.5	[L/h]
Surface ceiling	5500	[m]
Fuel capacity	57	[L]
Engine power	60	[hp]
Rotor diameter	3.4	[m]
Height	1.12	[m]
Width	1.24	[m]
Total length	4	[m]

$$PowerLoading = Power / RotorArea \quad (6.10)$$

$$ThrustLoading = 8.6859 \cdot PowerLoading^{-0.3107} \quad (6.11)$$

$$Lift = ThrustLoading \cdot Power \quad (6.12)$$

Launch attachment mechanism

Concerning the launch vehicle attachment, the main concerns are failure of the attachment mechanism, the loads the glider would endure during the launch phase, and the translation and rotation of the glider during the launch phase. Various options were considered and for the most promising options a concept sketch was made. These are shown in Figure 6.25, Figure 6.26 and Figure 6.27. The first option is to attach a rope to both the under and lower side of the root of the wing, against the tapered section, and connecting those four ropes to the centre section above the glider and attach that to the underside of the launch vehicle. The ropes have a mechanism that allows it to be remotely and electronically detached. This detachment mechanism is located at the bottom of the wing such that the glider can smoothly be detached without obstruction of the ropes.

The second option, shown in Figure 6.26, instead has an the upper part made of a solid rod that can be moved by a mechanism at the top of the launch vehicle. By moving the rod up and down, it will apply pressure to the top of the wing to provide rotational control around the span-axis and ensure that the wing will not tip backwards, for example.

The final option, shown in Figure 6.27, is a small, rigid construction that can clamp the glider around the payload section at both side of the reflexed part and at the leading edge for full control on the gliders' translation and rotation. At the launch altitude, these clamps can be loosened and moved to release the glider.



Figure 6.25: Launch attachment with simple rope.



Figure 6.26: Launch attachment with moving rigid rod.



Figure 6.27: Rigid launch attachment; chosen design.

This last option is chosen for several reasons. This option is the only option to meet requirement SAI-SYS-18-LAUNCH-11, since the rigid attachment ensures that no translational or rotational movement is induced with respect to the launch vehicle. This means the glider is not subjected to unwanted angles and loads, and the glider will remain at the desired attitude. For the other two options, there would be unwanted translation and more importantly rotation with respect to the launch vehicle. Another advantage of this concept is that the launch vehicle can fly at its desired cruise speed for maximum range (102km/h) and not worry about the extensive lift that the glider would create at this velocity. For the first option for example, if the launch vehicle were to fly at this velocity, the glider would start ascending with respect to the launch vehicle. With this rigid attachment, the glider can be launched at its optimal angle of attack. Another advantage is that the clamps are attached to the stronger and stiffer plywood skin, compared to the paper pulp skin for the other two concepts. This eliminates the worry that the paper pulp skin will get damaged during the launch phase (requirement SAI-SYS-18-LAUNCH-04). The fact that three attachment points are necessary for this concept, compared to only two for the other two concepts, is a disadvantage however since it increases the failure chance of the mechanism.

One concern with this concept that was analysed, is the vertical force on the glider from the rotor of the launch vehicle, since the glider is much closer to the rotor with this attachment method compared to the other ones. With Equation 6.13 [60], the induced velocity at the rotor can be calculated. If this velocity vector is added to the velocity vector at cruise, the maximum velocity of the glider (38m/s) is not exceeded. The induced velocity at the glider itself will be even lower than this induced velocity, this therefore ensures that requirements SAI-SYS-18-LAUNCH-05 and SAI-SYS-18-LAUNCH-06 are met.

$$V_i = \sqrt{\frac{L}{A_r} \frac{1}{2\rho}} = 10.6\text{[m/s]} \quad (6.13)$$

It should be noted that in the calculation for the lift at 5000[m] altitude, the reduction of power available due to the lower density has not been accounted for. However, with the chosen rigid attachment method, the glider can be positioned such that it will produce lift equal to its own weight at the cruise speed of the launch vehicle. This way, the launch vehicle will effectively only carry the weight of the attachment mechanism and not the full weight of the glider. This, in combination with the fact that the launch vehicle can make use of autorotation on the way down to save fuel, and that the performance of the launch vehicle will further increase, it can with confidence be said that requirement SAI-SYS-15-LAUNCH-02 is met.

Since the launch vehicle is a helicopter, it can launch the glider at any desired speed. This ensures that requirement SAI-SYS-26-LAUNCH-10 is met as well.

Recommendations for the launch system

One issue that needs to be further investigated in the development phase after the DSE, is how the glider should be attached to the launch vehicle before launch. Since the attachment mechanism is a rigid structure, this could pose problems. One solution would be to hover the launch vehicle slightly above ground, such that the glider can be put into the clamps of the attachment mechanism. This requires additional fuel however, and poses safety concerns as well.

A more feasible solution would be to make the rigid structure strong enough such that it can support the weight of launch vehicle. This way, the glider can simply be attached to the launch vehicle while the launch vehicle is standing on the rigid attachment. How much additional weight would need to be added for this solution must be investigated during the further development.

Finally, another option is to have an assembly jig on which the launch vehicle can be placed at the launch location. The glider can then easily be attached to the launch vehicle. The disadvantage of this option is that the assembly jig would need to be constructed at the launch location, which requires a significant amount of time. Additionally, there needs to be extra space in the mobile launch truck for the assembly jig.

Additional recommendations for the further investigation of the launch phase post-DSE, are to analyse the loads on the structure due to the clamping of the glider by the launch vehicle. This should however not pose a problem as at all three clamping locations the glider can be clamped at the ribs of the payload section to provide the load path into the structure. For the leading edge clamp this can be clamped at the position of the centre rib, while the back two clamps can be clamped at the outer ribs. Furthermore, the exact release mechanism to release the glider at the launch altitude should be further investigated. One way to ensure that the glider can easily and safely fly away is to first loosen the leading edge clamp and move it upwards such that it does not obstruct the glider from flying away. Next, the back two clamps can be loosened and the glider is free to fly away.

Validation of the launch vehicle

The validation of the launch vehicle mainly consists of testing whether the launch vehicle can achieve the 5000[m] altitude with the glider, and achieve the calculated range. This will be done in the detailed design phase with a flight test. The launch attachment and detachment mechanism should also be tested. This can first be done component-wise, to see whether the clamps move as intended. As a next step they can be attached and detached from the glider, while in the end they will have to be tested during a full flight test.

In Table 6.14, the compliance matrix for the launch subsystem is given. As can be seen, only requirements SAI-SYS-18-LAUNCH-04 and SAI-SYS-18-LAUNCH-06 are not met. These latter two can only be validated by demonstration. With the validation procedure described above, it can be tested whether indeed all these requirements are met.

Table 6.14: Compliance matrix for the launch system

Requirement ID	Requirement	Compliance	Proof
SAI-SYS-27-LAUNCH-03	The launch system shall be able to attain an altitude of maximum 5000 [m].	✓	Section 6.4.1
SAI-SYS-18-LAUNCH-04	The launch system shall transport the system to the required launch altitude without damaging the system.	TBD	Section 6.4.1
SAI-SYS-18-LAUNCH-05	The ultimate bearable load of the system shall not be exceeded during transport of the system to the launch altitude.	✓	Section 6.4.1
SAI-SYS-18-LAUNCH-06	The launch system shall not damage the system when releasing the system.	TBD	Section 6.4.1
SAI-SYS-18-LAUNCH-07	The ultimate load of the system shall not be exceeded upon launching the system at the launch altitude.	✓	Section 6.4.1
SAI-SYS-26-LAUNCH-10	The launch system shall provide the system with an initial velocity of a minimum of 23.9 [m/s] after release.	✓	Section 6.4.1

SAI-SYS-18-LAUNCH-11	The system shall be able to be fixed to the launch system, inducing no translational or rotational movement with respect to the launch vehicle.	✓	Section 6.4.1
SAI-SYS-22-LAUNCH-12	The launch system shall transport the system to launch altitude within 11376 [s] from the point that all systems are launch ready.	✓	Section 6.4.1

6.4.2. Landing

The landing phase starts at approximately $100[m]$ altitude above the landing location, where the GliMed will use the camera to scan the pre-determined landing location to check whether it is still feasible. If this is not the case, it will start to scan for other nearby landing locations. Since this scanning process already starts at $100[m]$, there is $97[s]$ before touchdown, such that the glider has enough time to find an alternative landing location. When a suitable landing location is found, the glider will circle down to it to start the final landing phase.

For the final landing phase, several landing manoeuvres are possible. Two possible concepts are discussed and worked out in this section. It should be noted that both of these concepts consider the worst case in terms of available landing area, in the sense that the landing area required is minimised for these landing manoeuvres. If a large open strip of landing area is available, it is best to slowly descent at the stall speed and go into a controlled crash. The crash structure is designed to absorb such an impact and ensure that the payload is intact. Since the L/D at the stall speed is still 19, the approach angle is very shallow, so this will therefore not work if there are obstacles, like trees or buildings, before the landing area.

As mentioned, in case a limited landing area is available there are two options. The best option was found to be using a form of deepstall [86], but for flying wings. The main benefit of deepstall is the low landing area that would be required due to the steep approach angle, allowing for great flexibility when deciding on a landing spot, as close to the recipient as possible. Deepstall for conventional configuration aircraft, with a T-tail, relies on a quick pitch up due to a high upward deflection of the elevator. The main wing will stall and experience very high angles of attacks, while the T-tail is outside the wake of the main wing and not in stall, keeping the aircraft stable. The aircraft will steeply descent with a constant velocity and a (almost) horizontal pitch attitude [17]. Since GliMed is a flying wing, this method does not translate one-to-one. For the stability during the post stall phase, the flying wing is solely dependant on whether it is stable at high angles of attack, since it has no tail to ensure stability. The landing manoeuvre using this method is shown in Figure 6.28.

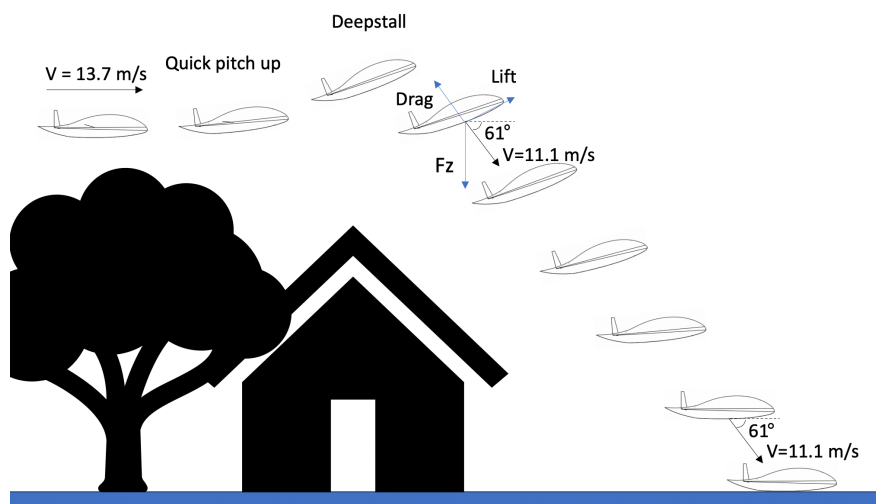


Figure 6.28: Deepstall landing manoeuvre.

To approximate the constant, terminal velocity that the glider will reach and the approach angle at which it will fall, the following method is used. Based on experimental data of the SA7036 airfoil used for the wing section [59] and experimental data of the NACA 4409 airfoil at very high angles of attack

[76], the C_l and C_d at high, post-stall angles of attack were estimated. The lift and drag were calculated, where for the lift it was assumed that only the wing will create lift. From this L/D an approach angle and therefore an angle of attack can be approximated. From this new angle of attack, a new C_l and C_d were taken, leading to a new L/D and a new approach angle and angle of attack again. After iterating several times, an approach angle of $61[deg]$ was gotten, as can be seen in the Figure. This also agrees nicely with approach angles as found from literature [86][17]. From this, by having lift and drag as a function of velocity, it can be calculated at which velocity the lift and drag will counteract the gravity. This velocity is $11.1[m/s]$. Since the crash structure will be designed to withstand an impact of $13.7[m/s]$, which is the stall speed, this would mean that the glider could initiate this deepstall at any height. This is of course beneficial when there would be high obstacles around the designated landing site. With the calculated approach angle, the ratio between height and distance to the landing site at which the deepstall would need to be initiated can easily be determined.

However, an issue with above calculation is that it assumes that the glider is stable at those high angles of attack and will therefore attain a relatively horizontal pitch attitude during the descent. This would ensure that the glider would return to the equilibrium position after the quick pitch up due to the brief elevon deflection. Since XFLR5 can not analyse post-stall, this can not be determined for certain. The next step would be to run extensive CFD simulations to determine this, and finally test this landing method with the actual glider. This is something that would be done in the next design phase.

So, due to the high uncertainty that remains for this landing method, a second option has been considered. This option is visualised in Figure 6.29. When close to the landing area and flying at the stall speed, the glider will dive down to just three meters from the ground. This height is chosen to avoid any small obstacles at the landing area and allow for some error margin for the glider. After this, it will then quickly and briefly deflect the elevons to the maximum ($25[deg]$) upwards deflection to induce quick pitch up and remove the speed and go into heavy stall immediately. This ensures that not much height is gained during this pitch up manoeuvre and the glider will fall from a height that is not much greater than the three meters. As can be seen in the figure, the glider will first hit the ground with the reflexed part of the payload section. This is however not a problem as nothing is in this reflexed part and is even allowed to break off during this impact. The second hit is then on the belly, which will be absorbed by the crash structure.

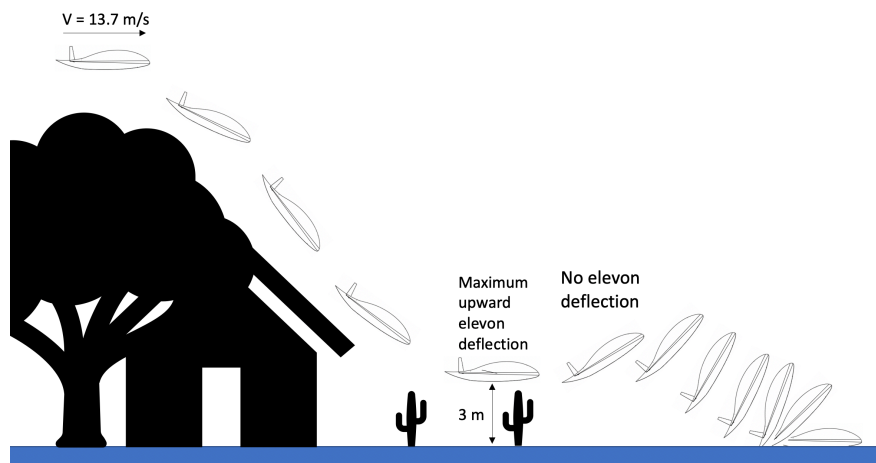


Figure 6.29: Landing manoeuvre of the glider.

To investigate whether this pitch up really happens quickly enough such that the glider will not gain a lot of altitude, the moment that is induced by the maximum elevon deflection has been analysed. The moment coefficient can be found from Figure 5.20. By using Equation 6.14, the angular acceleration can be found.

$$M = I \cdot \alpha \quad (6.14)$$

For the moment ($6.9[Nm]$), only the surface area and average chord of the wing were used. Finally, from the CATIA model and some hand calculations an upper estimate of the mass moment of inertia

was found ($4.2[kgm^2]$). The angular acceleration was then found to be $94[degrees/s^2]$. Since this is a very high angular acceleration, it confirms that the pitch up happens very rapidly.

To determine requirement SAI-SYS-02-LAND-03, a maximum height of $20[m]$ for the obstacles in front of the landing area is assumed, such that an upper estimate for the required landing area can be made. Since the maximum velocity of the glider is $22.8[m/s]$ at $3[m]$ altitude, the maximum required landing area (with a safety factor of 1.5) is $34.2[m] \times 10[m]$, allowing some margin for the width of the glider. This assumes that the pitch up takes 1 second at most, which is reasonable based on the angular acceleration.

For requirement SAI-SYS-07-LAND-04, an additional $5[m]$ is added to this landing area to account for the accuracy in determining the location of the glider, such that the glider will land within $40[m]$ of the pre-determined destination.

Crash structure

As mentioned above, a crash structure will be in place to protect the payload. The crash structure is designed such that it can withstand an impact of $2500J$, which is based on the impact of the glider at the stall speed ($2350[J]$) and dropping the glider from 10 meters altitude, assuming it will fall with the earth's acceleration ($2450[J]$). The crash structure will both be placed at the bottom as well as at the front, such that it can take this full impact energy from both of these sides, and everything in between. This also allows the glider to have more versatility in landing. The crash structure will be made of cellulose foam due to its high biodegradability and high energy absorption capabilities (see Section 7.1). Using Equation 6.15, the needed volume can be calculated to fully absorb the energy. An additional safety factor of 1.5 has been implemented as well, since the impact on the cellulose foam will not be perfect in the sense that the whole volume of cellulose foam will take up all the energy. From this required volume, the thickness of the cellulose foam crash structure on each side can be computed, based on the area of the payload on that side.

$$Volume = \frac{Energy}{Toughness} \quad (6.15)$$

Designing the crash structure this way should ensure that the payload will not break upon impact. This is further confirmed since not only the cellulose foam would take up the energy from the impact, but also the rest of the structure around the cellulose foam. Additionally, some of the impact energy will also dissipate into the environment in which the glider crashes. Requirement SAI-SYS-02-LAND-01 is therefore met. This will further have to be validated as explained in Section 6.4.2.

Payload integration

The most important parameters for the payload integration are that the c.g. of the payload should be as far to the front as possible and that the height of the payload is minimised. As explained in Section 2.3, the volume and specifically the height of the payload needs to be minimised. The cool box for the vaccines is the driving component in terms of the height, with a minimum of $13.8[cm]$, which is the smallest dimension of the vaccine package and the cooling walls combined. Since inside the cooling box there are two boxes of vaccines, it can be chosen to sort them such that the cool box has dimensions of $35.9 \times 13.8 \times 13.8 [cm^3]$ or $13.8 \times 19.1 \times 22.2 [cm^3]$. Since there is a rib in the middle of the centre section, the latter option was chosen to minimise the surface area, as for structural and symmetry reasons any increase in width would have to be done on both sides of the spar. This would have meant that the width of the payload section would be $71.8[cm]$, which does not even include the ribs yet. It should also be noted however that the dimension in the chord direction also cannot be too large, as this would also increase the required height of the centre section. The dimensions ($10.5 \times 28.4 \times 22.2 [cm^3]$) of the box with syringes and needles were then determined based on the height and width of the cool box, such that this would not be the element driving the dimensions of the airfoil but still have the same total volume. The cool box was first placed inside the airfoil to minimise the height and the required chord, and after that the other packages were placed accordingly, to have the c.g. as much to the front as possible. In Figure 6.30, 6.31 and 6.32, the 3D view, side view and top view of the payload section can be seen respectively. As can be seen, some of the front crash structure is cut-off by the spar box to make space for it.

By minimising the height of the boxes, the crash structure can also be lower as the surface area as seen from the bottom is larger. The lower span does mean that a thicker crash structure has to be

present at the front but since this can easily be tapered down, this is not an issue. It can also be seen that despite the fact that the box with the syringes and needles has a larger volume than the cool box, it is not this box that is the limiting factor regarding the design. This is the case since the cool box is limited in the dimensions it can have, while the box with the syringes and needles can be shaped to what is convenient, such that it has a smaller height. Furthermore, the small box with the rest of the items, such as the surgical masks and the alcohol wipes, only contains non-fragile items that do not need a crash structure.

To ensure that the payload does not move inside the payload section during flight and also during impact, they are put into cardboard boxes which are glued to the crash structure with adhesives. The crash structure itself is then also glued to the skin. This way, the recipient can open the cardboard boxes and take out the payload, which would otherwise be prevented by the glue.

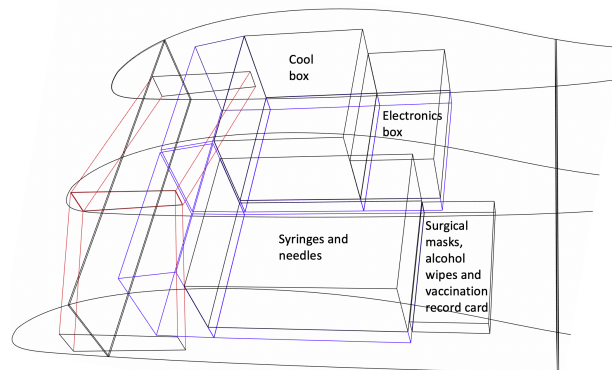


Figure 6.30: 3D-view of the payload section. Blue is crash structure and red is the spar box.

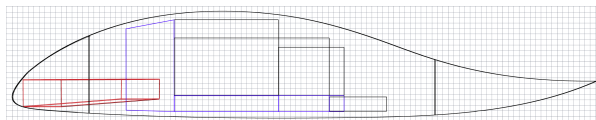


Figure 6.31: Side view of the payload section. The grid is one centimeter.

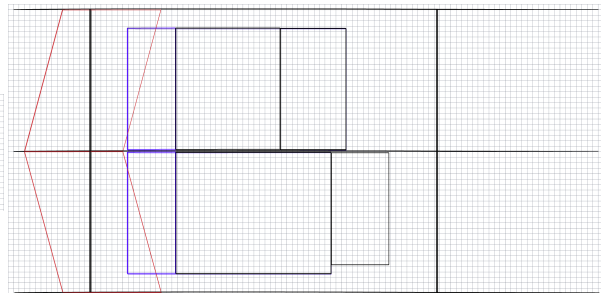


Figure 6.32: Top view of the payload section. The grid is one centimeter.

Validation of the landing system

The validation of the landing system starts with running CFD-simulations at several high angles of attack to see whether the glider is stable at those angles. The next step would be to test a scaled model in a wind tunnel, again to test the gliders behaviour at very high angles of attack. Finally, the characteristics of the glider post-stall are then tested with a scaled model and the full model. The approach angle and the terminal velocity can be tested, as well as the quick pitch up and the impact with the ground.

To test the crash structure, first the toughness of the cellulose foam can be tested, after which multiple crash tests can be done with both scaled models and the final model.

In Table 6.15, the compliance matrix of the landing subsystem is given.

Table 6.15: Compliance matrix for the landing system

Requirement ID	Requirement	Compliance	Proof

SAI-SYS-02-LAND-01	The payload shall not contain visible damage or damage that makes the payload non-functional after landing of the system.	✓	Section 6.4.2
SAI-SYS-19-LAND-02	The system shall not damage any infrastructure upon landing.	✓	Section 6.2.1
SAI-SYS-02-LAND-03	The system shall have a maximum landing distance of 34.2 [m].	✓	Section 6.4.2
SAI-SYS-07-LAND-04	The system shall have a landing accuracy of 40 [m] deviating from the pre-determined destination.	✓	Section 6.4.2

6.4.3. Logistics and Operations

The demand for GliMed is not constant since it is highly depended on whether there is an outbreak of a disease for which there is a vaccine available. Since the glider will have a production of 1000 per year, it will be assumed that this is also the consumption of GliMed. The logistics of SustAI_n will be designed based on there being an outbreak every 5 years, where 2200 gliders will be needed. In the other non-outbreak years, only 700 gliders are needed. Bases on these numbers, the logistics are worked out. The cost of the glider as described in Section 4.3.4 and the numbers given in the coming section, are based on the peak year, with a consumption of approximately 60 gliders per month in each of Mali, Japan and Norway.

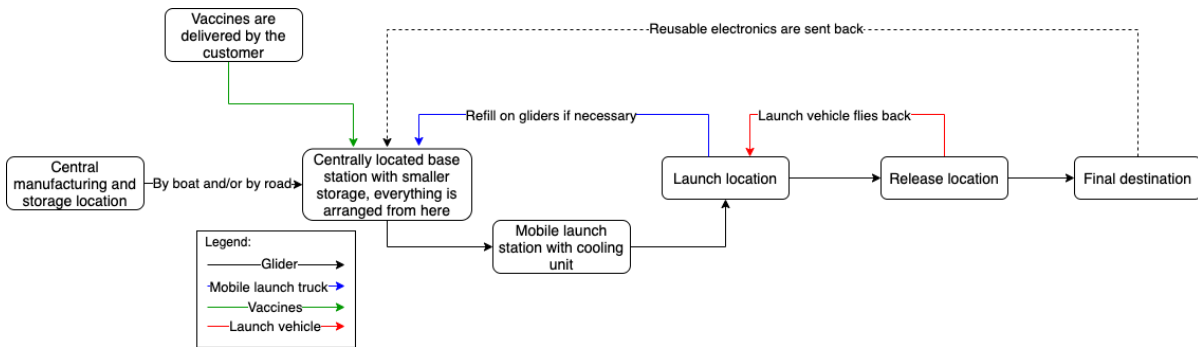


Figure 6.33: Diagram of the logistics flow.

In Figure 6.33, the flow of the logistics are presented. The production location and main storage facility are located in Eastern Europe because of the lower labor costs. From here a batch of gliders are transported, either by boat or over the road, with a regular interval to the different countries that is being operated in. Here the gliders are stored at a centrally located storage facility, and the vaccines are delivered here by the customer. This base will serve as the home base in each country where the trucks will pick up the gliders when they need more and where the recipients will send the electronics. The truck will have a cooling storage for the vaccines, such that the vaccines are loaded into the cool box that will be used in the glider just before launch. When a glider is ordered, the mobile launch truck will drive within 400[km] range of the recipient to send out the launch vehicle with the glider. Note that the launch vehicle has a better fuel efficiency compared to the mobile launch truck. This means that it is always more beneficial to drive just within range of the recipient to launch the glider, instead of driving closer to the recipient such that the launch vehicle would have to cover less distance. For time reasons this is also more beneficial. If multiple gliders need to be send to the same destination, the launch vehicle will first launch the first glider, fly back to the launch location, refuel and launch the next glider. If a mobile launch truck runs out of gliders, it will return to the main base and refill on gliders.

A sketch of the mobile launch truck is presented in Figure 6.34.

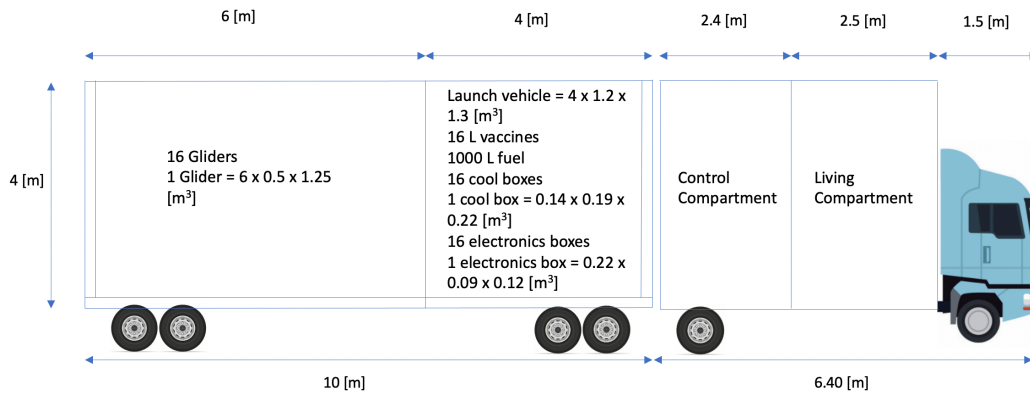


Figure 6.34: Lay-out and dimensions of the mobile launch truck.

It consists of a front truck ($6.40 \times 2.55 \times 4 [m^3]$) with a trailer ($10 \times 2.55 \times 4 [m^3]$) attached to it. The trailer contains a large compartment ($6 \times 2.55 \times 4 [m^3]$) that will be able to fit 16 gliders. A margin is kept here since the gliders will not be stacked directly on top of each other, but they will be placed on a scaffold similar to how rowing boats are transported. This trailer will also contain a compartment ($4.40 \times 2.55 \times 4 [m^3]$) where the launch vehicle ($4 \times 1.3 \times 1.2 [m^3]$), the fuel ($1 \times 1 \times 1 [m^3]$) and the vaccines (16 L) are located. To minimise the time between arriving at the launch location and being ready to send out the launch vehicle with the glider, half of the payload is already in the glider when it is being produced, while the electronics box and the cool box will be put in the glider right before launch. This way only one wing has to be assembled, as the electronics box and the cool box are on the same side in the payload section. This compartment therefore also contains 16 cool boxes and 16 electronics boxes.

In the front truck, there is a compartment ($3 \times 2.55 \times 4 [m^3]$) which contains all the necessary equipment to monitor and control the glider in case of emergency. It also houses a living compartment ($3 \times 2.55 \times 4 [m^3]$) for the two crew members, as the truck can be underway for several days. Additionally, the mobile launch truck can be opened from the side of the back trailer (which contains the glider) such that it can form a roof under which the glider can be assembled in case of rain. This prevents the electronics and the inside of the glider of getting wet. This roof can also be further extended easily similar to how a caravan awning works to get a fully enclosed volume. The concept of this is sketched in Figure 6.35.

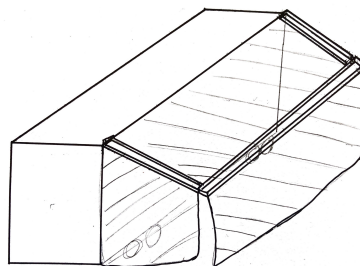


Figure 6.35: Roof mechanism of the mobile launch truck.

After the glider is assembled, it will be tested whether all electronics are working, if data is being sent correctly to and from the mobile launch truck, and whether the control surfaces are functioning. The glider will also be checked for visual damage induced by transport.

Figure 6.36, Figure 6.37 and Figure 6.38 show the maps of the three operating countries with the location of the main base, the transportation of the glider and the vaccines to the main base and the range that the launch vehicle and the glider can reach. Everything outside this range requires the mobile launch truck to drive a certain distance to the recipient. The location of the base station is chosen based on the population density map of the respective country, such that the distance that the mobile launch truck will have to drive is minimised.

For both Mali and Japan, 60 gliders are shipped monthly to the storage location in Seydou and

Tokyo respectively. Since these are more difficult and costly to reach, larger batches are cheaper and more sustainable per glider despite the fact that more storage space is then required in the country itself. Sustainability and cost are also the reasons for shipping the gliders instead of transporting them by plane. For Norway, 16 gliders are transported by road on a weekly basis, such that the required storage space is much smaller. The storage space that is required next to the production location is for 1200 gliders, since this is the maximum surplus after 4 years of no outbreak.

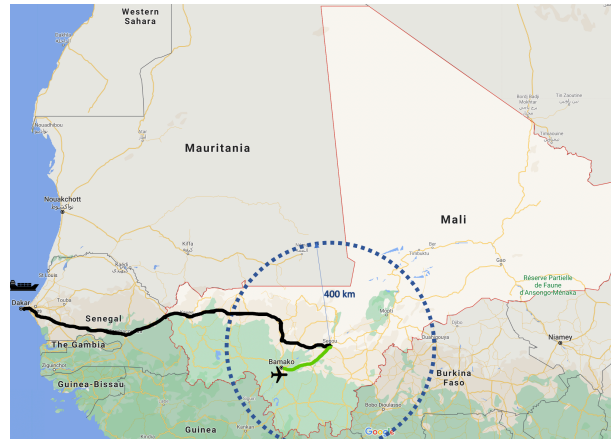


Figure 6.36: Logistics overview for Mali, the black line is the route of the glider to the base station in Segou and the green line is the route of the vaccines to the base station.



Figure 6.37: Logistics overview for Japan, the black line is the route of the glider to the base station in the outskirts of Tokyo and the green line is the route of the vaccines to the base station.

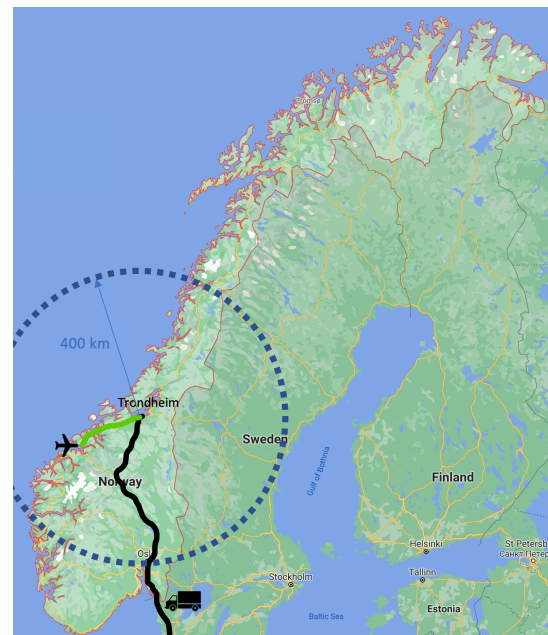


Figure 6.38: Logistics overview for Norway, the black line is the route of the glider to the base station in Trondheim and the green line is the route of the vaccines to the base station.

This concept can easily be extended to other countries as well since the logistics concept remains the same for each country. Only an additional mobile launch truck, launch vehicle and base station needs to be added per country.

The importance of having a VTOL-UAV as the launch vehicle is apparent from this logistics plan. The fact that the launch vehicle can launch at any location is very convenient in combination with the mobile launch truck, allowing for great flexibility in launching the glider. Had this not been the case, then the launch could have only occurred at a dedicated location such as an airport for example, meaning that many more ground stations would have been necessary to achieve the same coverage. This would

have significantly complicated the logistics.

The compliance matrix of the operations and logistics is shown in Table 6.16. Requirement SAI-SYS-13-LOG-06 can only be validated by demonstration. As for requirement SAI-SYS-22-LOG-09, the maximum distance that the mobile launch truck would have to drive is approximately $800[km]$, based on Figure 6.36, Figure 6.37 and Figure 6.38. For Mali, this will take around $13[h]$. After the mobile launch truck has arrived at the launch location, it will take another $1.5 - 2.0[h]$ to load in the payload and electronics box, assemble the glider and get the launch vehicle ready.

Table 6.16: Compliance matrix for the logistics

Requirement ID	Requirement	Compliance	Proof
SAI-SYS-13-LOG-06	The system shall be transported from storage to the launch system without being damaged.	TBD	Section 6.4.3
SAI-SYS-22-LOG-09	The system shall be prepared for launch within 15 [hours] after a request has been made by the user.	✓	Section 6.4.3

6.4.4. Reliability, Availability, Maintainability and Safety

As a balance needs to be struck between having a good reliability and designing for the minimum viable product, the reliability of GliMed is not as high as it can be. As GliMed is a relatively cheap, high product series, a new glider can easily be send to the recipient if the first glider were to fail. Of course, measures are in place to ensure good reliability while still keeping the cost of the glider down. An example of this is the testing of the glider after assembly, as was described previously.

The logistics plan surrounding GliMed has been designed based on sufficient availability of the glider. By having plenty of storage space in the operating country and by transporting new batches of gliders regularly, a glider should always be available to be send if an order comes in.

The maintainability of GliMed is not a high priority function, as it is single use. The glider will be checked for maintenance if it is stored for a long time, as requirement SAI-SYS-09 dictates that it should be able to be stored for 10 years.

Finally, the safety of GliMed is ensured by having well functioning communication and navigation systems, where some redundancy is added as well. With this it should be avoided that the glider damages objects or hits people during the landing phase.

6.5. End-of-Life Procedures

The end-of-life of GliMed is an extensive process design to increase the sustainability of the design by a large amount. However, a balance must be struck between excessive procedures, and cooperation of the recipients; if too much work is demanded, the procedures will not be followed. This section will describe the procedures to be followed by the recipients at end-of-life, and will naturally link closely to the results of the recipient analysis performed in Section 4.4.

These end-of-life procedures start from when the glider has been found by the recipients and there are three main steps to the end-of-life procedures, each of which with varying chances of participants following them. To increase the ease for the recipients, the livery of the Glider will be covered with indications of where items must be retrieved from, as well a detailed, pictographic instruction manual. An example of this can be seen in Figure 6.39. Furthermore, the design of the end-of-life procedures is heavily influenced by the personas mentioned in Section 2.2, as these are representative for the glider recipients.

Retrieving the Payload

The first thing the recipients must do when GliMed has landed is retrieve the payload. This process involves unscrewing the wings from the fuselage section and separating these. Once the wings are removed, the payload can be retrieved through the openings on the sides. This process is highlighted in Figure 6.40.

As there are 4 screws on each side, the process is estimated to take two people approximately 3 min.

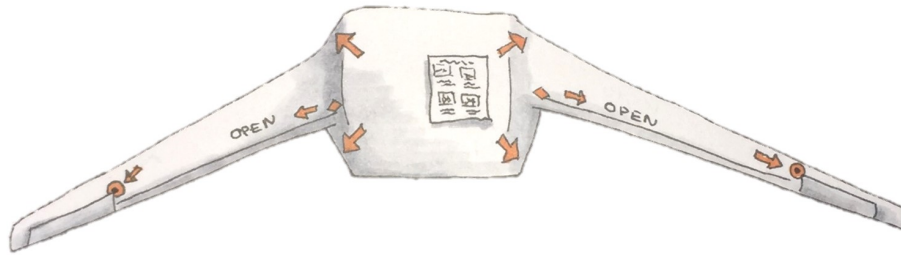


Figure 6.39: Conceptual sketch of a livery for GliMed. The orange arrows indicate where actions must be performed and an instruction sheet is clearly visible on the top surface.

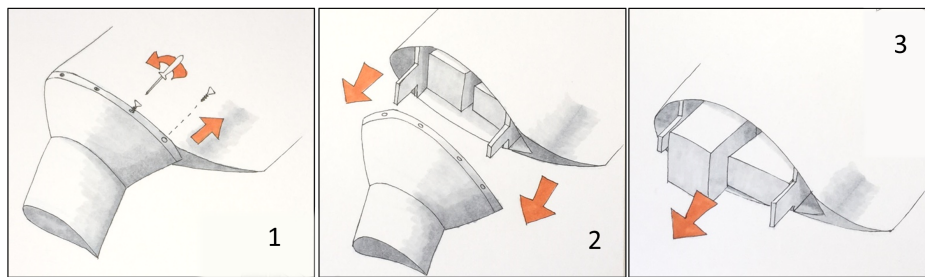


Figure 6.40: Conceptual sketches of payload retrieval instructions

Performing Disassembly Procedures

Besides the retrieval of the payload, there are a number of other motions needed to enhance the biodegradability and sustainability of GliMed. The first of these is opening the glider up further to expose the inside of the wings. The reasoning for this is described in Section 7.5.2, and the instructions for this section are presented in Figure 6.41.

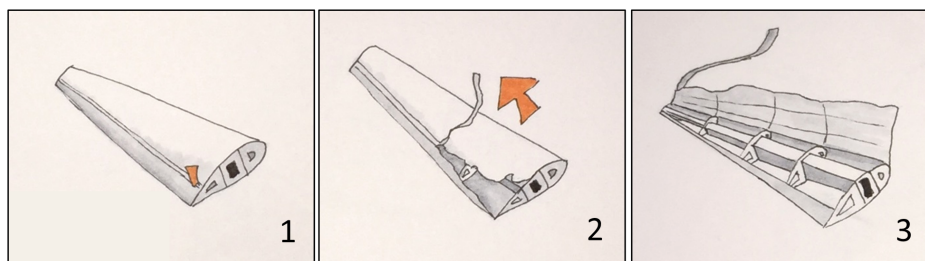


Figure 6.41: Conceptual sketches of wing disassembly procedure instructions

There are two of these strips for disassembly, and it is estimated that with each it will take under a minute to fully expose the wing. The chance of the recipient choosing to perform this movement is smaller than of retrieving the payload, but the novel idea of seeing the structure inside the wing, and the relatively short time required are sufficient incentives to ensure it will be done.

Removing the Electronics

The most complex part of the end-of-life procedures is the removal of the electronics. This is done to prevent hazardous waste and non-biodegradable components from polluting the landing site. Firstly the electronic box must be removed, in a similar fashion to the payload and the attached wires should release easily with connectors. Next the remaining components; the camera, pitot tube, sensors, and servos are located through the aid of arrows and targets on the glider skin. These will have to be dismantled from their location in the glider and taken along with the recipients for one of three purposes. This removal process can be seen in Figure 6.42.

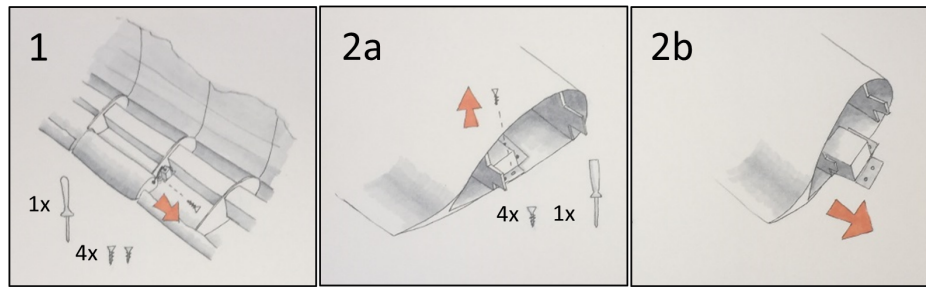


Figure 6.42: Partial conceptual sketches of electronics retrieval instructions. All components will be described in such a manner

After these retrieval procedures, there are three methods to continue the EOL for electronics. The use cases of these depend on the financial, environmental and social impacts of each system.

Electronic Systems Operational Analysis

To determine the optimal electronic system to use in each scenario, each system must be analysed. It must be noted that these electronic system scenarios have been designed for the region around Timbuktu only, and a similar analysis will have to be performed for Fukushima and Trondheim, when SustAln eventually starts operating there.

The first use for electronics at end-of-life is simply incineration for energy recovery. From the LCA performed to compare the electronics systems in Section 8.1.2, this system has the lowest environmental sustainability. This is mainly due to the high impact of incinerating at end-of-life, and the fact that the resources will only be used once. This system is the slightly less expensive than the most expensive system. Furthermore, this option has no additional social benefit for the recipients or anyone else.

The second type of electronics system is for reuse by the participants. As is mentioned in Section 4.4, a large majority of the workforce relies on agriculture, especially in the regions targeted by the glider. Therefore, the reusable electronics system is made in such a way that it transforms into an agricultural knowledge database, as well as a tool and tutorial for managing small business finances. This system is found to be more environmentally sustainable than the previous option, but less than the next. This is because there are additional components included in the system, but the system is also 50% reusable, thereby lowering the impacts. Due to the additional components required, this system is the most expensive of all three. This system is assumed to have a clear social benefit for the recipients of the glider, and can aid development in a third world country.

The third type of electronics system will be packaged up and sent back to the manufacturing facility for refurbishment and reuse. This system will only work in the case there typically is a well travelled route between town and city, and the isolation only holds due to fear of contagion. The assumptions made for return rate of these electrical systems, and the viable range for operation. This last system is the most environmentally sustainable, mainly due to the large amount of reuse the system sees. Furthermore, due to the reuse of components, this system is the cheapest of all three, however the price does vary per country and return rate. This last system is assumed to have some social benefit as the reduced costs of the returned systems can reduce the financial hurdles in sending medical aid with GliMed.

As a result of this analysis on all three systems, it can be seen that the returnable system is the most attractive from both a financial and environmental perspective. However, there is a limit on how often this system can be sent. Therefore, to determine which electronics system can be sent, a limit was set on the distance to be travelled for feasibility of returning. If the recipients are over 150km away from a city or town assumed to have regular transport to Timbuktu, it is deemed infeasible to return the electronics. Using population censuses and google maps, approximately 80% of the communities sent a glider will be in a position to return the electronics. This can be geographically visualised in Figure 6.43.

If the returnable system cannot be sent, it is beneficial from an environmental and social perspective to send the reusable system. However, there is no guarantee that it will be used. Of the remaining 20% of people eligible for the glider, just under 9% are nomadic and will have no use for this agricultural aid. Therefore, 11% will be sent the reusable system, while the remaining 9% receives the single-use

system.

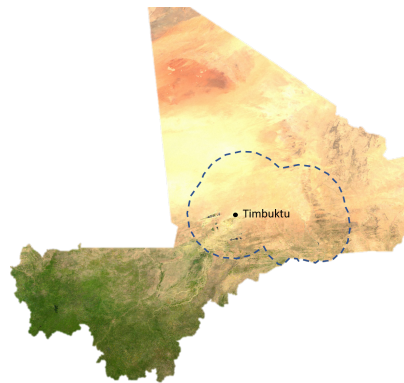


Figure 6.43: Geographical visualisation of the limit where returning locations becomes infeasible

Payload Retrieval Compliance Matrix

A number of EOL requirements pertain to the retrieval of the payload, after mission is completed. These requirements, shown in compliance Table 6.17, are specific to the interaction the recipients will have with GliMed and the payload.

Table 6.17: Compliance matrix for payload retrieval requirements

Identification	Requirement	Compliance	Discussion
SAI-SYS-03-EOL-11	The payload of the system shall be retrievable by the recipient within 10+-30% [minutes] after coming into contact with the system.	✓	Section 6.5
SAI-SYS-03-EOL-12	The system shall provide all necessary means and tools to extract the payload and additional components from the system.	✓	Section 6.5
SAI-SYS-03-EOL-13	The payload extraction shall be doable by people with no manufacturing or technical background.	✓	Section 6.5 and Section 7.2.4
SAI-SYS-03-EOL-14	Any instructions for payload extraction shall be accessible before the payload has to be extracted.	✓	Section 6.5
SAI-SYS-03-EOL-16	The method of turning the system off shall have a location which requires no tools to access.	✓	Section 6.3

7. Structures and Materials

The structure of the airplane forms a protective shell around the payload and ensures that all necessary loads are transferred without failure. It is important to view this section through the trinity concept lens, considering the design, materials and manufacturing together. This chapter will discuss the material trade-off in Section 7.1, the structural design in Section 7.2, the manufacturing design in Section 7.3 and the biodegradation calculations related to end of life in Section 7.5. The chapter will conclude with the verification and validation procedures in Section 7.6 and the compliance matrices for the related departments in Section 7.7.

7.1. Recap Material Trade-Off

The material that the glider will be made out of has a big impact in meeting the requirements. For all the material selections only materials that are non-conductive and non-magnetic were considered, as otherwise they would interfere or disturb the electronics. First of all the structural materials were determined from a trade-off on environmental impact, biodegradability, manufacturability and cost, with the weights 36%, 26%, 26% and 12% respectively. The materials considered for the structural material were flax fibre, jute fibre, hemp fibre, bamboo fibre[21], spruce plywood, balsa plywood, delignified wood[32], delignified wood reinforced plastic[21], cardboard¹²[29] and mycelium³. The delignified wood reinforced plastic and all fibres were assumed to have a PLA matrix. In the end, Balsa plywood came out as the best option from this trade-off and was therefore selected as the main material in the next phase of the structural design (Section 7.2). Spruce plywood was a close second. This material has higher specific properties than balsa wood and was therefore also extensively used during detailed design.

Furthermore, a trade-off was performed for the material of the crash structure, which is covered in more detail in Section 6.4.2. The materials considered in this trade-off were cellulose foam, mycelium foam⁴ and a paperboard honeycomb structure[89], and were traded off based on two criteria: biodegradability and energy absorption. From this trade-off cellulose foam came out as the best crash structure material. Although cellulose foam is not yet on the market, Åsa Ek from Cellutech[27] estimates it to be commercially available within three years. In addition, Ek estimated the mechanical properties of cellulose foam to be comparable to PP and PS foam.

A number of important mechanical properties of the materials that came out from the trade-offs and some materials that will be discussed in the following sections are given in Table 7.1.

Table 7.1: Important material properties of the materials that survived the trade-off in the preliminary phase.

Materials	Density [kg/m^3]	Young's modulus [GPa]	Shear modulus [GPa]
Quasi-isotropic medium density spruce plywood ⁵⁶ [19][46]	425	4.9021	1.157
Quasi-isotropic balsa plywood [87][39][38][53]	180	1.73	0.926
Cellulose foam ⁷ [38]	30	1.25	0.625
Paperboard	1000 [38]	1.129 [38]	-
moulded paper pulp	350	0.13	-
PLA	1240	3.31	1.29
	Tensile strength [MPa]	Compressive strength [MPa]	Shear strength [MPa]

¹<https://www.planetpaper.com/long-cardboard-take-decompose/> [cited on 15-05-2021]

²<https://www.webstaurantstore.com/blog/1138/types-and-sizes-of-corrugated-boxes.html>

³<https://www.grown.bio/contact/> [cited on 17-05-2021]

⁴<https://www.grown.bio/contact/> [cited on 17-05-2021]

⁵<https://www.aircraftspruce.com/menus/wp/plywood.html> [cited on 14-05-2021]

⁶<https://www.thebalancesmb.com/how-long-does-it-take-garbage-to-decompose-2878033> [cited on 17-05-2021]

⁷<http://www.cellutech.se/cellulose-foam.html> [cited on 18-05-2021]

Quasi-isotropic medium density spruce plywood	30.95	20.95	19.4
Quasi-isotropic balsa plywood	11.18	7.25	15.39
Cellulose foam [1][38]	21	21	9
Paperboard	35	35	-
moulded paper pulp	4.43	1.52	-
PLA	50	66	33 [6]

7.2. Structural Design

In the following section, the structural design choices for several components of the system are explained. These design choices are based on the balance between manufacturing, materials and structural feasibility. One thousand systems per year have to be manufactured, which comes down to about three per day. It is key to design a system which can be cheaply and easily manufactured with relatively sustainable methods. The material choices are very important as well. For the materials, environmental impact, biodegradability, manufacturability (how easily complex shapes can be made) and cost were regarded as the most important parameters. However, the design must also be strong and stiff without weighing too much. Based on the mass budget that is explained in Section 3.3, the structure of the system cannot weigh more than $12.74[kg]$. In addition, since the biodegradability is not only influenced by material choice but also by the surface-to-volume ratio, the design aimed to maximise this parameter as well. In Figure 3.3 the dimensions of the system can be seen, which will be often referred to in the following sections.

7.2.1. Structural wing design options

For both the payload section and outermost wings several design options were traded-off. The general outline of these options can be seen in Figure 7.1 along with material options for the several components of the wing.

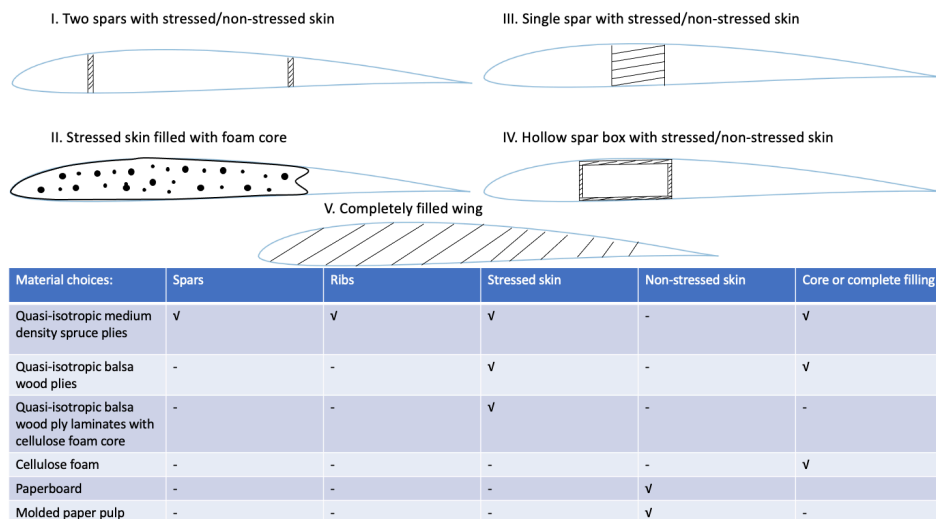


Figure 7.1: General options for the wing structure, cross-sectional view. In the table below are the considered material options for each component of the wing. These are the materials which survived the trade-off described in Section 7.1.

Completely filled wing

V. Completely filled wing



Manufacturing	Degradability	Weight and cost	Integration of systems
Easiest to manufacture	Longest degradation times	Spruce: Too heavy, 10.7 [kg] for outer wings, neglecting ribs	No payload integration
	SAI-SYS-16-EOL-02 cannot be fulfilled	Balsa wood: (4.54 [kg] for outer wings, neglecting ribs) Too expensive, 75\$/[kg]	No integration electrical systems possible

Figure 7.2: Most important points regarding the design of a completely filled wing.

The completely filled wing is a monolithic wing made out of either spruce or balsa wood, which can be seen in Figure 7.2. The option was only viable for the outer wings, as no payload can be housed in this type of wing. The main advantage is that it is the easiest option to manufacture, but the disadvantages outweighed that advantage and thus it is not chosen for the final design.

Stressed skin filled with foam core

II. Stressed skin filled with foam core



Manufacturing	Degradability	Weight and cost	Integration of systems
Lowest TRL level for manufacturing	Fastest degradability due to low density of cellulose foam	Spruce skin and cellulose foam core	No payload integration
		Lightest option due to low density of cellulose foam and thin skin of spruce	Difficult integration electrical systems possible

Figure 7.3: Most important points regarding the design of a wing filled with a foam core.

In Figure 7.3, the main points are summed up for the foam filled wing. The option was only viable for the outer wings, as no payload can be housed in this type of wing. Mainly because of the low TRL of the production of cellulose foam integrated within a wing structure (TRL of five, component validation in relevant environment), along with the other weaknesses, this wing type was discarded as well. With the current manufacturing methods for cellulose foam, too many different steps had to be undertaken to make the wing compared to the other wing types.

Trade-off between design options I, II and IV, materials for the stressed skin

For the first design iteration, a skin of balsa plywood and spars of spruce plywood were considered, as balsa plywood performed very well in the material trade-off. For the thin wings, the problem with balsa plywood is that the skin has to be too thick (namely 8[mm]) in order to ensure sufficient load carrying capabilities. It is too thick for the small airfoil that is chosen, causing the spars to be so small in height that they are almost non-load bearing.

The balsa plywood skin is also not an option for the payload section as the skin together with the stiffeners would have to be over 1.5[cm] thick. As the payload would then not fit anymore in the payload section, the height of the wing has to be increased. However, this is detrimental to the aerodynamic performance. A solution is to use spruce plywood not only for the spars, but also as skin material. This greatly decreases the skin thicknesses, which makes it a feasible option for both the payload section and outer wings.

Trade-off between design options I, II and IV, stressed skin versus non-stressed skin

The minimum bend radius of spruce plywood is $44.24 \cdot t_{skin}[m]$ (Section 7.3.3). Thus the leading edge profile cannot be made by bending the skin. A solid profile will have to be adhesively bonded to the ribs and skin, which can be seen in Figure 7.4. During manufacturing, this creates the risk of misalignment, which is detrimental for aerodynamic performance. Furthermore, because of the aerodynamic performance, the attachment of the outer wings to the fuselage wing will have to be guided by a taper that transitions from the outer wing airfoil to the fuselage wing airfoil, which can be seen in Figure 7.5.

Compound curves are very difficult to make with plywood and requires special equipment. A solution to this is to make a skin of relatively flexible material, but then almost all the loads have to be carried by the spars and ribs. With such a non-stressed skin, shape complexity comes almost for free. In addition, stiffeners are not necessary anymore for the skin. Therefore, the manufacturing capability of a wing with a non-stressed skin is improved compared to the manufacturing of a stressed skin and even necessary for the manufacturing of the taper. The thinner wings will therefore be made with a non-stressed skin.

A disadvantage of a non-stressed skin is that this leads to thicker spars. The spars of the fuselage would be $1.5[cm]$ thick compared to $2[mm]$ thickness if the skin is stressed (spruce plywood skin) with stiffeners. The non-stressed skin is actually 25% lighter than the stressed skin wing and there is enough space for the thick spars and the payload in the payload section. However, these thick spars would have a degradation time that is 61% longer than the $2[mm]$ spars under ideal conditions. The thick spars could not meet the degradation time requirement, as is stated by SAI-SYS-16-EOL-02. Therefore, it was decided to design the payload section with the two spars, stressed skin and stiffeners, all made from spruce plywood with the solid leading edge profile. However, in the end the front spar will be made from PLA. The reason for this is explained in Section 7.2.4.

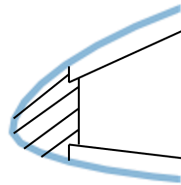


Figure 7.4: Solid leading edge profile made of wood which is required for a wooden skin.

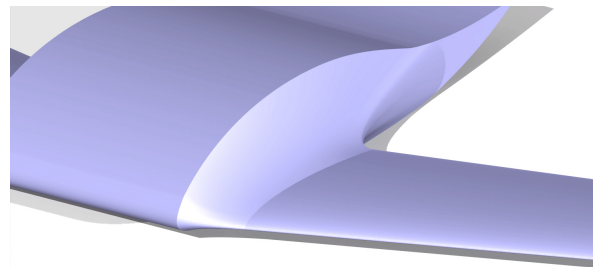


Figure 7.5: Wing taper from the outer wing to the fuselage wing. The airfoil shape smoothly transitions from the outer wing airfoil shape to the airfoil shape of the fuselage wing (without the reflex).

Trade-off between design options I, II and IV, materials for the non-stressed skin

Two types of materials were considered for the non-stressed skin; paperboard and moulded paper pulp. The raw material cost of paperboard and paper pulp is roughly the same, however, paperboard has the advantage that pre-laminated fabricates can be bought and simply pressed into the required shape. For moulded paper pulp, it is required to make your own pulp from paper sheets, vacuum form it and then press it in the desired shape. Afterwards, the pulp has to be dried, thus, a lot more equipment and manufacturing steps are required for paper pulp, causing the cost of the design to increase. However, paperboard is much denser and stiffer than paper pulp which would mean that the weight of the design would increase significantly (skin of the two outer wings would weigh $2.98[kg]$ instead of $1.04[kg]$, which is not allowed by the mass budget), but more importantly, the desired tapering shape from the fuselage wing to the outer wing cannot be achieved with this material. The taper would need to have a much simpler shape, namely a constant airfoil cross-section instead of a smooth transition from one airfoil into the other, which is worse for the aerodynamic characteristics since it has to abruptly change into the payload section's airfoil. This abrupt change is illustrated in Figure 7.11, along with the other options for wing taper. Because of this reason, moulded paper pulp was chosen as the non-stressed skin material type.

Coating choices

Moulded paper pulp is a highly absorbent material, which will therefore, during rainfall, completely lose its aerodynamic shape during flight [38]. Consequently a cover material needs to be used on the skin to protect against moisture, for which a trade-off was performed. In this trade-off, two materials were considered: PLA film and beeswax. These materials were traded-off on the following criteria: manufacturability, biodegradability, weight, hydrophobicity and cost. All relevant material properties for both materials are given in Table 7.2. The weight of the PLA film coating was determined from the required cover surface, estimated thickness of the film and the density, whereas the weight of a beeswax coating was determined from the percentage of absorption of the paper pulp, which would be

infused with the beeswax. From this trade-off the PLA film was chosen to be the coating material of choice.

Table 7.2: Skin cover material trade-off

Material	Manufacturability	Biodegradability	Weight	Hydrophobicity	Cost
	-	Number of months	Grams	-	Euros
Polylactic acid	[Green] Lay in mould	[Green] 1.5 ⁸	[Green] 161 [38][13]	[Green] Excellent	[Green] 0.44 [38]
Beeswax	[Green] Infusible in skin	[Blue] 2.5[42]	[Blue] 278.5 [38]	[Blue] Good	[Blue] 4.16 ⁹

Trade-off between design options I, II and IV, single spar against two spars

In Figure 7.6, the general points are summed for the use of a single spar versus two spars, as well as why a hollow spar box design was chosen above the solid spar design. Because of the ease of manufacturing, the single spar design was chosen, but a hollow box was chosen over a solid spar because otherwise the weight would be too high and the degradation time would be too long. It was determined that the width of the hollow spar box reaches from 20 to 60% of the chord, while the solid spar can be a little thinner, namely from 20 to 55% of the chord. For comparison, at the root of the outer wing the spar caps and webs can be 7[mm] thick, while the solid spar is 3.16[cm] thick. The degradation time of the solid spar is 78% longer than for the solid spar box. In Figure 7.7 the different box designs are shown. The second type is chosen to facilitate manufacturing.

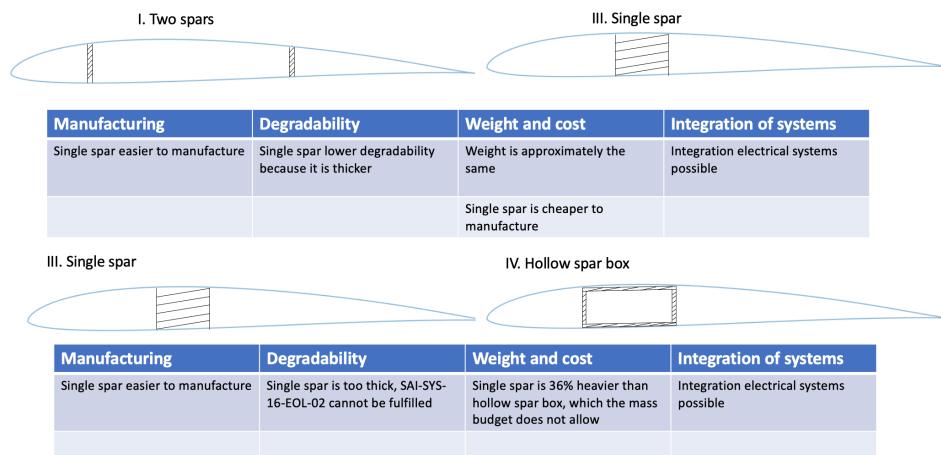


Figure 7.6: General points for the designs choices of two spars versus one and the solid spar versus the spar box.

⁸<https://www.eco-craft.co.uk/pla-biodegradable-spec>

⁹https://imkershop.nl/bijenwas/769-ruwe-bijenwasbrokken-kaarsen-1kg.html?utm_campaign=Product_Listing_Ad&utm_source=Google_Product_Listing_Ad&utm_medium=Product_Listing_Ad&gclid=CjwKCAjwqvyFBhB7EiwAER786X3372H5R6Qq_rz6jxU8vW__osLC13y0KvFoMCNyKFX6bCVtVLSrMxoCUhYQAvD_BwE[cited 20-06-2021]

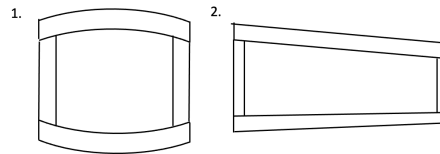


Figure 7.7: Different types of spar box designs. The left design indicates the spar caps conforming exactly to the airfoil shape. The second design fits exactly in the airfoil, but is made with straight veneers. Only the edges have to be shaved off when it is to be adhesively bonded to the skin.

The single spar design would pose a problem for the payload integration in the payload section. This problem is visualised in Figure 7.8. The single spar would have to be 4 [mm] thick. You can see that the payload does not fit in the fuselage anymore, unless the airfoil increases its thickness over chord ratio. An increased height of the airfoil meant that the required lift over drag ratio cannot be achieved, which is why the two spars for the fuselage wing were kept.

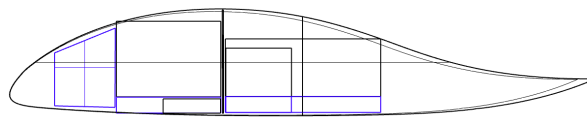


Figure 7.8: Cross-sectional view of the fuselage wing integrated with payload for the single spar design. Blue lines indicate the crash structure, thin lines the payload and the thick line the one spar.

7.2.2. Structural detailed design

In this section the detailed design of the airplane's structure will be presented. This includes all relevant dimensions, parameters and other design choices. In Figure 7.9, the most important dimensions of the structural design are visualised. In Figure 7.10, the inside of the structure is shown.

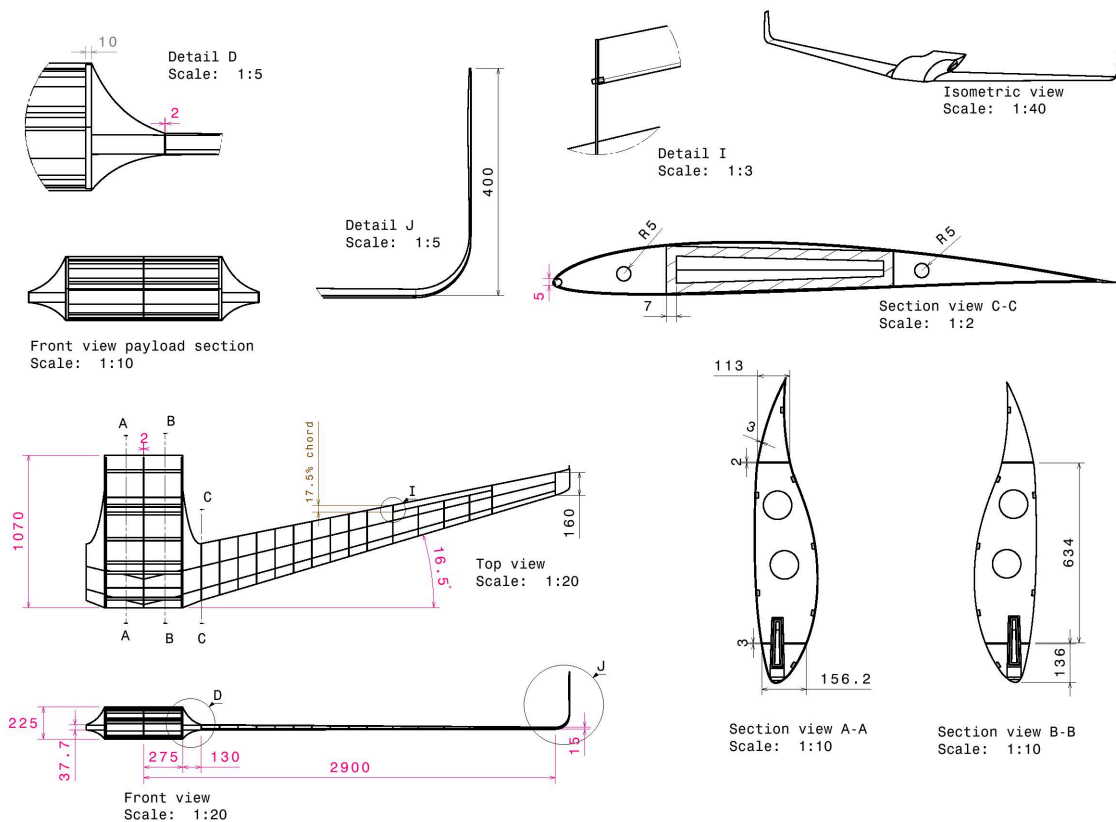


Figure 7.9: Full aircraft technical drawing with dimensions



Figure 7.10: Render of the internal structure of the glider. The white boxes indicate the crash structure, the brown box represents the payload.

Table 7.3: Material selection for the airplane's structure

Component	Materials: Payload section	Materials: Outer wings	
Front spar	PLA	Skin	Moulded paper pulp
Aft spar	Spruce plywood	Spar box	Spruce plywood
Skin	Spruce plywood	Ribs	Spruce plywood
Stiffeners	Spruce plywood	-	
Ribs	Spruce plywood	-	

Taper options

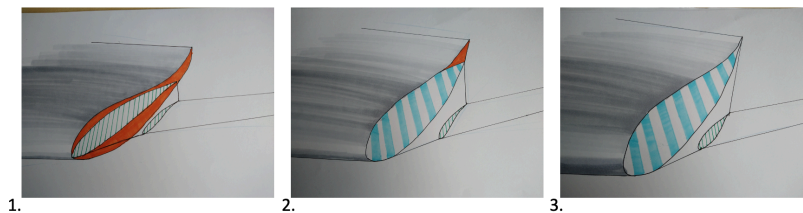


Figure 7.11: The different options for taper. Option 1. displays an abrupt change in airfoil. Option 2. displays a guided taper from the airfoil of the payload section to the airfoil of the outer wing, but the reflex is not tapered. Option 3. displays a full taper, including the reflex.

In Figure 7.11, three different options can be observed for the tapering of the outer wing to the payload section. Option 1. was not chosen, because the abrupt change in airfoil is detrimental to the aerodynamic performance. Option 3. is better than option 2. regarding aerodynamics, but decreases the effect of the reflex. The effect of the reflex had to be maximised, in order to make the glider statically stable in longitudinal direction (otherwise the ballast weight would have to be increased, which was not allowed by the mass budget). Therefore option 2. was chosen as taper shape.

Winglets

In Figure 7.12, an isometric and cross-sectional view of the winglet is provided. The winglet is completely made out of spruce plywood. The winglet has the same airfoil shape as the outer wings, only the maximum thickness over chord ratio is decreased from 9.2% to 3%. The maximum thickness of the winglet at the root is 5[mm] and 2.62[mm] , which made the winglet load bearing enough, while also generating sufficient aerodynamic forces to provide lateral stability. The winglet tapers down from 0.16[m] of chord to 0.8[m] .

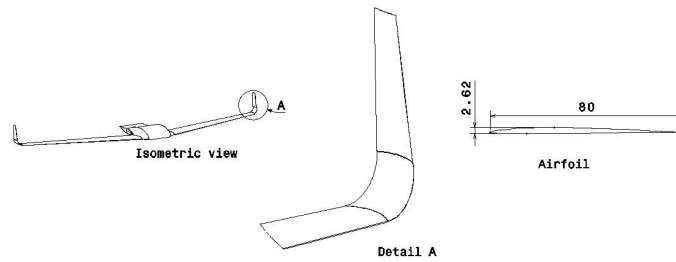


Figure 7.12: Isometric- and cross-sectional view of the winglet.

Elevons

In Figure 7.13, a top view can be seen, which shows the elevon along with relevant ribs. The elevon is made out of solid spruce wood. On both sides of the elevon, a rib is placed on which the elevon is attached with a hinge. The most inboard hinge is connected to a servo (also attached to the rib), which is able to control the rotation of the two hinges and thus the deflection of the elevon. In between the two outer ribs, the ribs are shortened to accommodate to the presence of the elevon. The green line in Figure 7.13 indicates the closing off the wing by the paper pulp, which prevents air flowing into the structure.

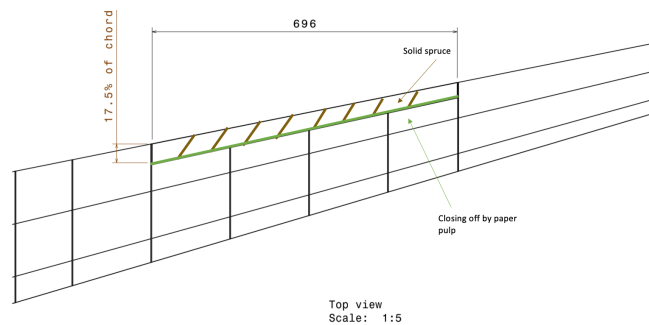


Figure 7.13: Top view of the elevon.

7.2.3. Joining

In this section the subject of joining of structural elements will be covered. This includes the joining of generic structural elements, the rib-spar joint and plywood veneer joining.

Element joining

The glider consists of a number of various parts each of which needs to be joined to one another. Three adhesives were considered for internal structural joints: casein glue, polyvinyl acetate (PVA) and hide glue. The main characteristics of each adhesive can be seen in Table 7.4. Furthermore, mechanical fasteners are no longer viable due to their low biodegradability. Wood welding was also eliminated as a joining technique due to its low TRL.

Table 7.4: Adhesive characteristics.

Characteristic	Casein glue	PVA	Hide glue
Type	Dispersion	Dispersion	Hotmelt
Shear strength	Weaker than spruce [54]	Weaker than spruce [54]	Stronger than spruce [54]
Water resistance	High [80]	Low [81]	Low [80]
Curing time	8 hour [55]	12-24hours ¹⁰	18-24hours ¹¹
Temperature control during application	Used at room temperature [80]	Used at room temperature [80]	Heating required [80]

¹⁰<https://resin-expert.com/en/guide/how-long-does-wood-glue-take-to-dry> [cited on 15-06-21]

¹¹<https://resin-expert.com/en/guide/how-long-does-wood-glue-take-to-dry> [cited on 15-06-21]

<i>Clamping required</i>	Yes	Yes	No [49]
<i>Biodegradability</i>	High ¹²	Low [67]	High [64]

As a result of a trade-off, hide glue was selected as the structural joining adhesive. A number of its properties are advantageous for manufacturing. Firstly, its ability to make rubbed joints removes the need for clamping. Secondly, it is a hotmelt glue, which enables the merging of joining steps with other manufacturing steps that use heat such as the vacuum forming of the skin. Lastly, hide glue is stronger than spruce, meaning fewer overlaps are needed to accommodate joints, making the structure lighter and simpler to manufacture.

However, manufacturing is made more complex due to the heating requirement, but the issue can be overcome by making smaller glue surfaces that can be joined together quickly, or by making the joints within a hot environment. As second negative of hide glue is that it is not water resistant. Joints exposed to the environment cannot be made from this glue. Instead the soy based adhesive chosen for plywood bonding must be used in such cases.

Connection of spars and ribs

In order to make the assembly of the ribs with the spar, cutouts were made in both the spar and the rib (as seen in Figure 7.14). This makes the assembly process fast as ribs simply need to be glued and positioned in place. Two options were considered for the cutout placement, as seen in Figure 7.15, and the second was chosen to ensure the bending load due to lift is transferred through compressive stresses rather than tensile stresses in the adhesive joint.

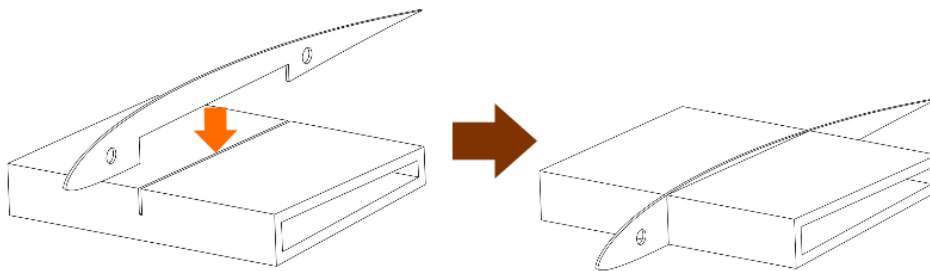


Figure 7.14: Wing assembly

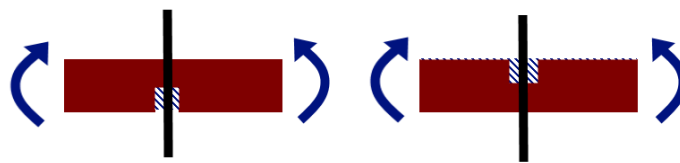


Figure 7.15: Front view of spar with cutout and rib. Option 1 (left) and option 2 (right)

Veneer joining

In order to keep the glider environmentally sustainable, an alternative to the commonly used, toxic urea-formaldehyde glue used to make plywood from veneers had to be found. A number of options were considered: tannin based, lignin based, starch based and soy protein based adhesives. Out of those options only soy protein based adhesives are available on the market and have been noted to be highly susceptible to bio-degradation [43]. Additionally, the production of plywood panels using soy protein adhesives is almost identical to that of urea formaldehyde so many of the established and cost efficient tools and techniques can be utilised during production ¹³.

¹²https://www.intercol.info/en/?page_id=85 [cited on 15-06-2021]

¹³<https://www.solenis.com/en/research-and-development/innovations/soyad-adhesive-technology> [cited on 17-06-21]

7.2.4. Payload loading/unloading

Two different options were considered for loading/unloading the payload, which can be seen in Figure 7.16 and Figure 7.17. In the end, it was decided to design for the attachment/detachment of the outer wings to the payload section because of the points mentioned in Table 7.5. First, the exact assembly principle of the wings is explained in the next section. However, the assembly method is almost the same for the hatch method as for the detachable wings. The only difference is that for detachable wings, the outer wings and payload section have to be connected by screws, which can be removed by the recipients. For the hatch option, the assembly would be done via adhesives. The screws add weight, but the cut-out for the hatch would have to be so large, that a significant amount of reinforcement has to be added. This adds more extra weight than the screws. Secondly, disassembly of the wings is required to expose as much area as possible to the environment. In the figures in Section 6.5, it is explained that for the detachment option, the recipients have to rip open the skin of the outer wings. From the internals of the outer wing, they can collect a screwdriver that allows them to unscrew the attachment of the wings. In this way, the recipients can expose a large internal area of the glider to the outside environment. For the hatch option, the recipients simply open the hatch and retrieve the payload, meaning that a lower internal area can be exposed to the environment. Thirdly, the time span between ordering the glider and delivering the product is not critical. Therefore, making the system launch-ready as fast as possible was determined not to be the most important criterion.

Table 7.5: Payload loading/unloading options

Option	Contribution to mass budget	Time required to make system launch ready	Incentive to disassemble system	Accessibility to system
Hatch	Large cut-out, which requires heavy reinforcements [Yellow]	No assembly required just before launch [Green]	Recipients are not encouraged to disassemble structure [Yellow]	Electronics are not easily accessible [Yellow]
Attachment/detachment of wings	Attachment of thinner wings to payload section has to be held by screws instead of adhesives (0.2 [kg] extra mass). [Blue]	After payload loading, the wings have to be assembled before launch [Yellow]	For unloading payload, recipients are enforced to disassemble the structure [Green]	Before launch, the electronics are more easily accessible [Blue]

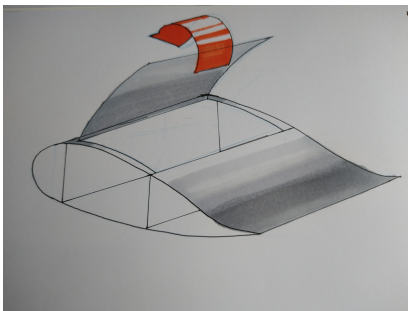


Figure 7.16: Hatch option to load/unload payload and electronics box.

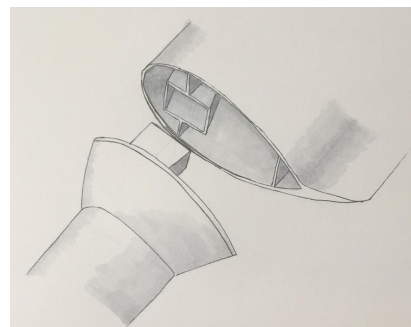


Figure 7.17: Option to attach/detach the outer wings to the payload section by sliding the spar box of the outer wing into the front spar of the payload section, which contains a so-called wrap box. The skin of the payload section will be screwed to the rib of the outer wing. The screws can be unscrewed to detach the wing again.

Load path from outer wings to payload section

In order to guarantee proper load transfer from the outer wings to the payload section, a sound connection is required between the hollow spar box of the outer wing and the front spar of the payload section. The solution found for this load transfer is to extend the hollow spar box into the payload section until the centre rib. Another box of exactly the same shape as the spar box wraps around it. This wrap box is larger in volume than the spar box, allowing a tolerance of $1[mm]$. This tolerance is required in order to slide the spar box out of the wrap box again during payload retrieval. A cross-sectional view of this can be seen in Figure 7.18. A top view can be seen in Figure 7.9 and an isometric view in Figure 7.19. In this top view, it can be seen that the spar- and wrap box, go through the front spar. Therefore, a part of the front spar has to be cut-out. Instead of making a cut in the front spar with a wrap box bonded to it, the front spar and wrap box will be made integral with a 3D printer. This can be seen in Figure 7.17. Spruce plywood cannot be used in additive manufacturing. Therefore, the front spar integral with the wrap box will be made of PLA. The complex design shape that this integral part needs to have can relatively easily be made with additive manufacturing. The idea of the load transfer from the spar box, to the wrap box, and then to the spar can be seen in Figure 7.20. In order to avoid the spar box sliding out of the wrap box, the spar box is adhesively bonded to the outer rib. This outer rib is joined with the payload section by inserting screws through the skin of the payload section and through the ribs.

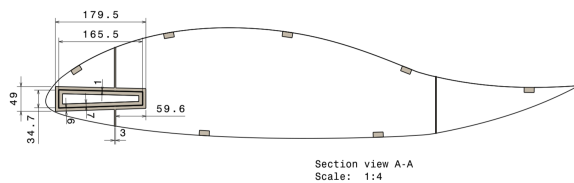


Figure 7.18: A cross-sectional view of the PLA wrap box, covering the spruce spar box of the outer wings. The wrap box is integral with the front spar.

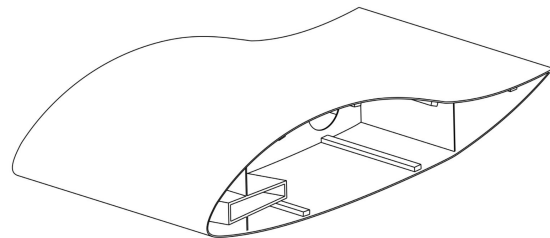


Figure 7.19: Isometric view of the payload section, showing the wrap box and front spar as an integral part.

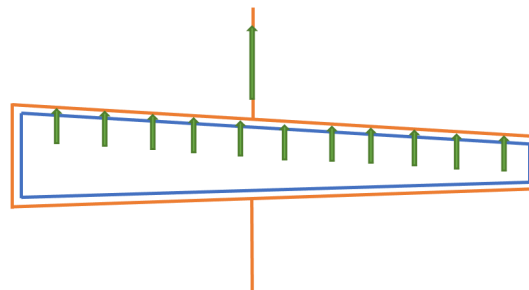


Figure 7.20: Simplified side-view of the payload section, displaying the load transfer. Under normal flight circumstances, the spar box pushes up against the wrap box, which transfers the load to the vertical spar. The spar then transfers the load into the skin.

The downside of PLA is that it is not as biodegradable as spruce wood. It does have much better mechanical properties than spruce plywood, as can be seen in Figure 7.20. In order to enhance the degradation, the PLA component will be made porous with the effect that the surface-to-volume ratio is increased. If the infill percentage of component is 35%, the mechanical properties are approximately the same of spruce plywood. Therefore, during structural analysis the spar was modelled as a solid spruce plywood spar, while in fact the spar is made of PLA. It was computed that the wrap box needs to have a thickness of $6[mm]$, while the vertical spar can have a thickness of $3[mm]$. Actually, $2[mm]$ suffices, but since there are always defects present in a porous component, the $3[mm]$ acts as a safety margin.

Lastly, in Figure 7.9 it can be seen that the hollow spar box becomes increasingly wider from the

tip to the root of the wing. However, the spar box cannot become wider and larger when it extends into the payload section, as one would not be able to slide the spar box into the wrap box. It maintains a constant width and height in this section.

Wing-payload section connection joint trade-off

The wing-fuselage connection serves as the prime loading and unloading section of the glider. It is also a critical load bearing structure as it provides a load path for aerodynamic loads from the wing into the payload section. Therefore the joint had to be made both strong and easily attachable/removable. Five options to connect this joint were considered: Screws, adhesives, belts, snap fit and clearance fit. The joint had to provide a single sided assembly so options such as bolts were not considered.

Screws were the first option considered. More specifically, aluminium screws due to their high specific strength properties. PLA screws would not biodegrade within the necessary time window and had a significantly lower specific strength than aluminum and were therefore not considered. It was found that due to the low number of screws required assembly and, more importantly, the disassembly could be performed very quickly. Screws are also removable albeit only using a tool such as a screwdriver. This is disadvantageous as the tool would need to be provided to the recipient which would increase the weight of the glider. On the other hand, screws require fewer amount of tools and are easier to assemble than adhesive joints. One of the the main drawbacks of aluminium screws is that they would not be biodegradable. This issue however can be overcome by providing a standard sized screw which could then be reused by the recipient, thereby not leaving in the glider.

Adhesives are already the primary joining method within the aircraft and were also considered. However, they cannot be removed once the joint is made. Therefore, if adhesives were used, the recipient would need to damage the glider structure in order to retrieve the payload. However such an action could damage the payload. Additionally more of the protective structure would need to be added on all sides of the payload (as opposed to two sides) which would contribute more to the weight. Furthermore, most adhesives require time to set after they are applied, e.g. hide glue needs 24 hours. This would severely limit the launch window due to the maximum cooling time permitted by the cooling box.

A single belt around the wing was also considered however this option was quickly discarded as it would require a load bearing element with low stiffness. The wing skin (made out of moulded paper pulp) could have been used for this connection however it is designed to be non load bearing and would not be able to sustain the high loads at the root of the wing.

A snap fit joint to connect the wing spar to the fuselage spar was also considered. This would offer a very simple assembly procedure as the wing would simply need to be "clicked" into place before flight. A number of removable snap fit joints exist and the recipient would be able to access such a joint after ripping open the wing skin. However snap fit joints have limited maturity in load bearing applications [84]. For example, it is uncertain how such a joint would perform under cyclic loads.

A clearance fit joint was the final concept considered (as seen in Figure 7.19). A wrap box (hole) would be made within the fuselage at the leading edge spar location. The wing spar (shaft) would then slide into the hole. A clearance fit joint relies on the hole being slightly larger than the shaft in order to ensure sliding during assembly [47]. This concept would be very simple to assemble/disassemble but would require high dimensional tolerances.

At first the option of only having screws was selected. However such a configuration would suffer from a need for excessive structural reinforcement at the ribs since a spar to spar connection could not be made. Therefore it was instead selected to have a clearance fit joint that carried bending loads between spars combined with screws that carried normal forces and provided orientation during assembly.

Determination of screw pitch

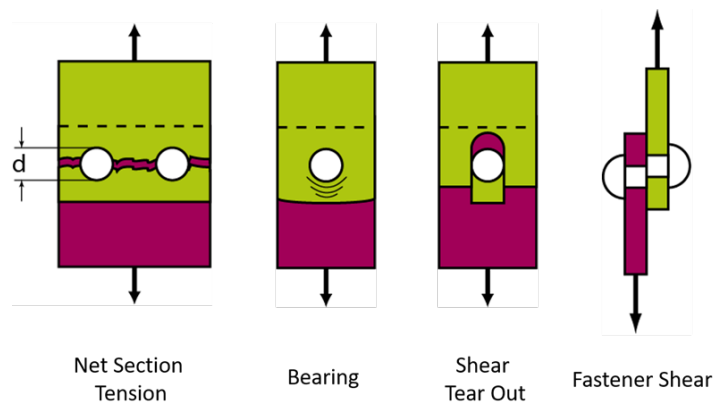


Figure 7.21: Screw failure modes

The pitch and placement of the wing-fuselage screws was evaluated for joint, net section, shear out and bearing failure. The fuselage skin was modeled as a sheet without the contribution of the spars. This was done in order to simplify the problem, making it so that each bolt carries the same load, given a constant screw pitch. This would however, overestimate the loads by 6%. It was assumed that the fuselage skin would be sufficiently flexible so as to insure that the clearance fit joint in the spar carries the entire bending load. Therefore the screws would only carry the normal force in the wing (due to the winglet). From this it was determined that only one guage 2 screw placed 8 [mm] away from the edge of the skin would be required to carry the load. However in order to keep the wing fixed from rotations during transportation and assembly, the number of screws was increased to four per joint.

7.3. Manufacturing Design

This section will highlight the trade-offs made regarding the production and assembly of GliMed. A number of methods will be discussed and traded-off in this section, including separating and machining methods, wing skin attachment, payload section skin attachment. Quality control on each of these mechanisms will also be discussed. Lastly, a production plan presents a high level view on the manufacturing process.

7.3.1. Separating and Machining

Throughout the manufacturing process, separating and machining is utilised to make the various wooden parts. Of these processes, separating is required in the majority of structural parts, including the spars, ribs, stringers, and skin. For these components, three different separating methods were considered for a trade-off; CNC sawing, laser cutting, and water jet cutting.

Table 7.6: Characteristics of separating techniques

	CNC sawing	Laser cutting	Water jet cutting
Speed	0.333 [m/s] [7.7]	0.01 [m/s] [7.7]	0.01 [m/s] [8]
Minimum cut radius	140 [mm] ¹⁴	0.7 ¹⁵ [mm]	0.38 [mm] ¹⁶
Max material thickness	150 [mm] ¹⁷	10 [mm] ¹⁸	50 [mm] ¹⁹

¹⁴<https://www.doityourself.com/stry/band-saw-blade-radius-guide> [cited on 17-06-21]

¹⁵<https://www.stannsheetmetal.co.uk/what-is-laser-cutting.html> [cited on 17-06-21]

¹⁶<https://www.engineersedge.com/manufacturing/water-jet-cutting-hydrodynamic-machining.htm> [cited on 17-06-21]

¹⁷https://www.alibaba.com/product-detail/cnc-woodworking-band-saw-machine-for_60704142506.html [cited on 17-06-21]

¹⁸<https://www.sculpteo.com/en/3d-learning-hub/laser-cutting/laser-cutting-vs-water-jet-cutting/> [cited on 17-06-21]

¹⁹<https://www.sculpteo.com/en/3d-learning-hub/laser-cutting/laser-cutting-vs-water-jet-cutting/> [cited on 17-06-21]

Can start anywhere on sheet	No	Yes	Yes
Delamination	No	No	Yes [82]
Drying after manufacturing	No	No	Yes
Sustainability	Low energy consumption ²⁰	High energy consumption ²¹	High energy and water consumption ²²

The trade-off for separating methods was performed with the information found in Table 7.6. The CNC saw is chosen for parts requiring rectilinear cuts, mainly due to its speed and sustainability advantages. However, this technique is not suitable for parts which require cuts with smaller radii and lightning holes, thus laser cutting is chosen for the ribs. Furthermore, complex 3d shapes such as the leading edge profile are not manufacturable using a separating technique. Hence these parts will be made using a CNC router.

7.3.2. Wing skin

There are three options for adhering the skin to the wing skeleton. The first consists of two individual pieces of top and bottom skin, made to their exact dimensions as seen in Figure 7.22. Although this option would give a near net shape product, it was nonetheless discarded due to the risk of misalignment at both the leading and trailing edges, the former of which would lead to a significant decrease in aerodynamic performance. The second option is a skin structure made in one piece with a hinge as displayed in Figure 7.23. To keep the structure open (a requirement for the thermopressing process) the hinge is required around either the leading or trailing edge. However, placement at the trailing edge increases chance of misalignment, and placement at the leading edge decreases aerodynamic performance due to the protruding hinge. Therefore this option is similarly non-feasible. The third option is similar to the first, but with flanges extruding from the edges as seen in Figure 7.24. These flanges would give a larger area to accurately position the skin. Finally the flanges are cut off, leaving only the thin bonded joint in the leading and trailing edge. This manufacturing option was chosen.

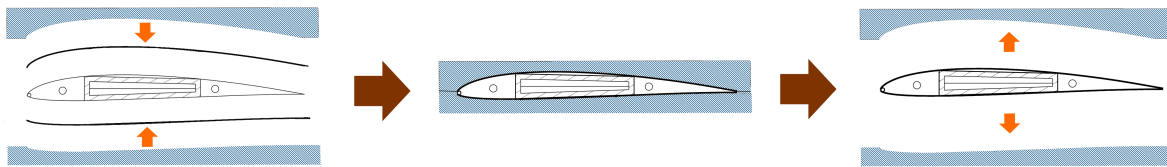


Figure 7.22: Wing skin production option 1

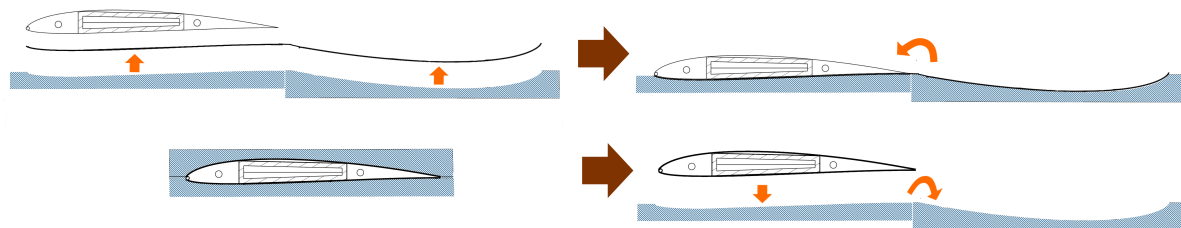


Figure 7.23: Wing skin production option 2

²⁰<https://www.woodguide.org/guide/power-tools/> [cited on 17-06-21]

²¹<https://www.woodguide.org/guide/laser-cutter/> [cited on 17-06-21]

²²<https://www.woodguide.org/guide/waterjet-cutter/> [cited on 17-06-21]

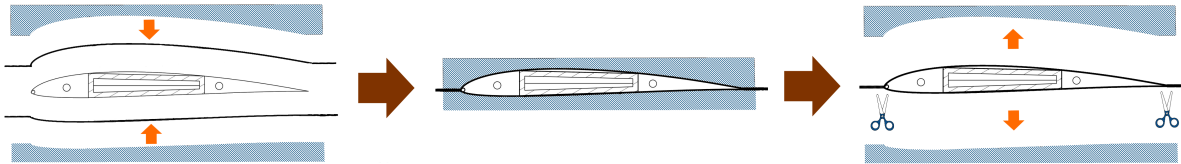


Figure 7.24: Wing skin production option 3

7.3.3. Payload section skin

The payload section skin is formed from stacked spruce veneer. The minimum bend radius (R_{min}) is estimated from the thickness (t) of individual veneers (1 [mm]). It depends on the tensile and compressive strain to failure ϵ_+ and ϵ_- respectively. If $\epsilon_- \approx \epsilon_+$ and $\epsilon_+ \ll 1$, Equation 7.1 can be used to determine the minimum bend radius [79]. The strain perpendicular to the grain is critical and should be used (1.13 [38]).

$$R_{min} = \frac{t}{2\epsilon_+} \quad (7.1)$$

Equation 7.1 yields a minimum bend radius of 44.24 [mm]. This is smaller than the minimum radius of the skin in the payload carrying section. Hence the use of bending enhancements such as kerfing, heating, steaming or chemical treatment is not required, given that the adhesive holding the veneers together can keep the bent shape.

Furthermore, two options were considered for this skin assembly. Firstly, by pressing two skin panels into shape and then attaching them to the skeleton similarly to the first option presented for the wing skin. The second option is to vacuum form two panels around the skeleton as seen in Figure 7.25. The latter option was selected as it enables the skin to attach itself to the skeleton during the forming process, eliminating the need for high dimensional tolerances that would be required if the skin was formed separately. Additionally a vacuum would ensure that pressure is applied along all joint surfaces, which would enable the rubbed joints to "catch".

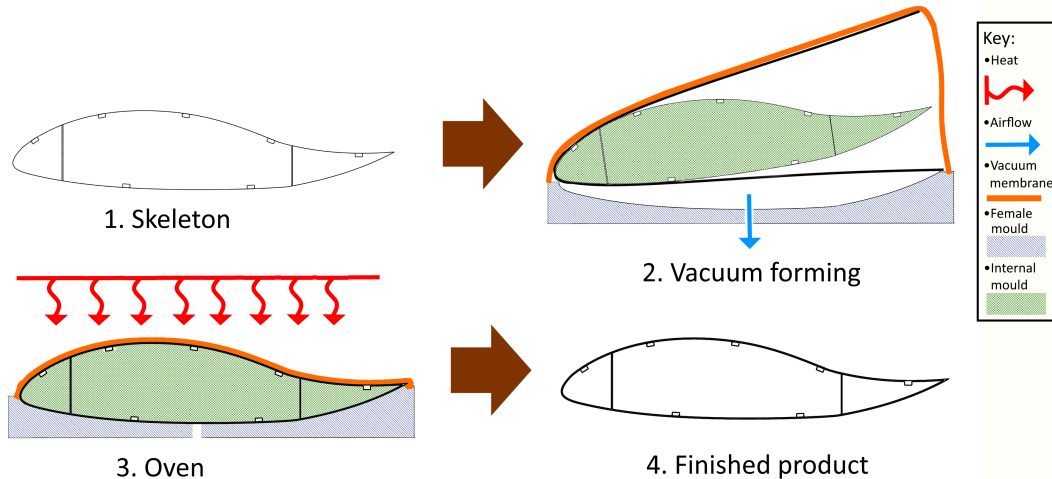


Figure 7.25: Wing skin production option 1

7.3.4. Quality control

Ensuing quality assurance during manufacturing goes a large way in matching the requirements, and meeting reliability standards. For this purpose, two approaches will be taken to assure process quality; dimensional Quality Control (QC) and joint QC. Dimensional QC will be ensured using a laser measurement system. Since laser measuring systems do not rely on contact and they can gather data quickly, they are more suitable for mass production. These types are also more durable due to their lack of moving parts. Furthermore, laser measurement systems are capable of measuring soft materials, such

as the cellulose foam used in the crash structure ²³.

In terms of joint QC, there are a limited number of non destructive tests possible for ensuring adhesive joint integrity [65]. Therefore the more simpler approach is taken of performing destructive tests on comparable specimens. Such an approach is justified in the mass production setting since the cost of production and subsequent loss of one part is relatively low.

7.3.5. Assembly

The assembly principles can be seen in Figure 7.26, where the payload section is shown. The spars and stiffeners will first be adhesively bonded to the rib using a robotic arm, after which skin is attached to the skeleton as described in Section 7.3.3. A similar process is employed in the wing assembly however with more ribs, no stiffeners and a different method to apply the skin.

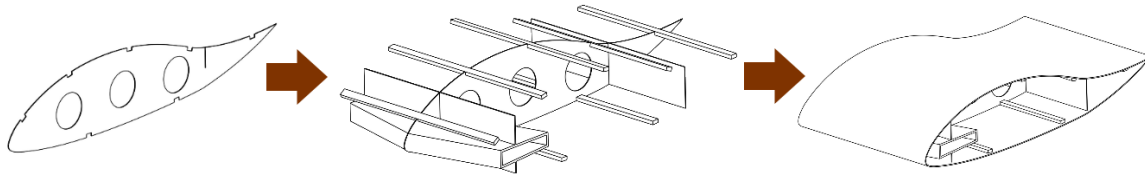


Figure 7.26: Fuselage assembly

7.3.6. Production plan

This section will describe the steps and processes to be followed when manufacturing GliMed. Due to the 1000 systems per year production volume as stipulated by SAI-SYS-01, and the standardised structure, it is beneficial to implement a mass production scheme. This will minimise direct labor costs, improve quality and increase speed of production. Mass production entails that parts are made in batches and later assembled in cells specializing in one particular task. Before constructing the production plan, each production and assembly step is identified. Tasks are then grouped and linked to a machine for parts, or a cell for assembly. In total, GliMed will have 64 structural parts and two manufacturing divisions (the fuselage section and wing section).

Machine Usage

Five primary classes of machines will be used to manufacture parts: a CNC saw, a CNC router, a laser cutter, a moulded pulp station and eight 3D printers. Each class of machine will be operated by one worker. The duration to make one system for the first three machines was estimated using feed rates (Table 7.7) and cutting lengths for each part, as well as the set up time for each machine. The estimated set up times were based on the time to position and clamp a part (30 sec) and programming time for the machine. The CNC router programming time was based on the programming time for a CNC mill. The CNC saw and laser cutter both produce simpler geometries than the CNC router, and it was therefore assumed that the programming time would be less, 1 min 30 sec and 3 min 30 sec, respectively. Furthermore, the duration to make one system for the moulded pulp machine was estimated by splitting the process into pulping, vacuum forming, thermal pressing, and drying. The machine usage can be seen in Figure 7.27. Additionally, although it was excluded from the figure, two 3D printers would need 24 hours to make the wrap box for one glider. This was calculated by loading half of a wrap box into Ultimaker's Cura software with the settings of an Ultimaker S5 3D printer. This gave a print time of 3[days]. For typical prints the Ultimaker S5 has a feed rate of 50[mm/s] ²⁴, however industrial 3D printers are capable of reaching speeds up to 500[mm/s] ²⁵. It was assumed that with an industrial grade 3D printer a feed rate of 150[mm/s] could be attained, as such decreasing the print time to one day. Lastly, the time to glue each component using a robotic arm was found in a similar way to the cutting time, using a feed rate (estimated using a representative video) and a gluing length.

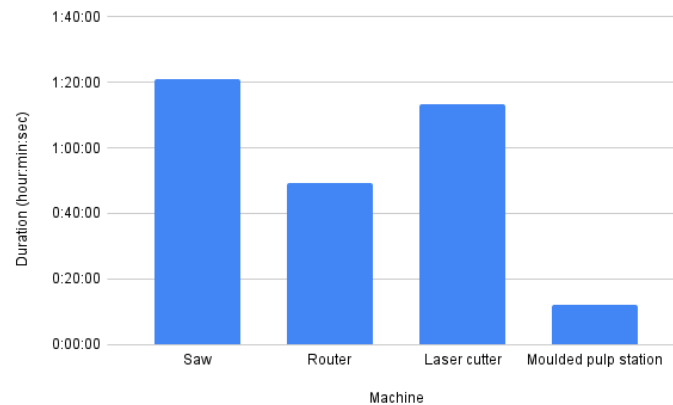
²³<https://www.qualitymag.com/articles/84949-quality-measurement-lasers-pinpoint-measurement> [cited on 17-06-21]

²⁴<https://sites.saic.edu/aoc/wp-content/uploads/sites/68/2018/05/Ultimakerguide.pdf> [cited on 20-06-2021]

²⁵<https://www.3dsourced.com/3d-printers/fastest-3d-printer/> [cited on 20-06-2021]

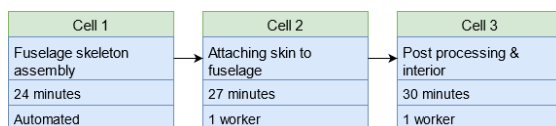
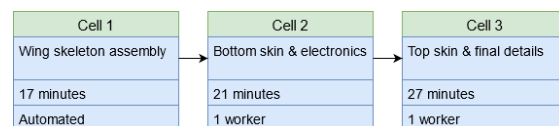
Table 7.7: Estimated feed rates for different tools

Tool	Feed rate (m/s)	Set-up time (min:sec)
<i>CNC saw</i>	0.333 ²⁶	02:30
<i>CNC router</i>	0.076 ²⁷	05:30
<i>Laser cutter</i>	0.01 ²⁸	03:30
<i>Glue dispenser</i>	0.02 ²⁹	05:00

**Figure 7.27:** Machine usage to make one glider

Assembly

The assembly of GliMed was first separated into the manufacturing of the wing and the payload section groups. Both groups require three cells, each of which have work packages of maximally 30 min. Therefore 30 min was selected as the cycle time for cells. A visualisation of the different cells, the estimated cycle time and degree of automation can be seen in Figure 7.28 and Figure 7.29.

**Figure 7.28:** Payload section assembly process flowchart**Figure 7.29:** Wing assembly process flowchart

With the estimated duration for part production and assembly it was estimated that five full time workers would be needed to achieve the 1000 glider per yer volume. Workers would be assigned to both a machine and a manned assembly cell and would rotate in between roles. The fifth worker would be responsible for setting up and controlling the automated machines (such as robotic arms and 3d printers). With the addition of five more workers, and a doubling in 3D printers manufacturing could be scaled to 2000 systems a year if needed.

7.3.7. Storage

A number of factors need to be considered during long term storage of the glider. Firstly, the PLA parts are most susceptible to extreme temperatures and should be kept in a $5 - 25^{\circ}\text{C}$ environment [9]. Secondly, UV light has been shown to increase biodegradation of PLA films by up to 97% [44]. Hence the system will be kept away from direct sunlight as that may damage the coating. Thirdly, both PLA and hide glue are highly hygroscopic meaning that they absorb water from the air. For PLA this leads to a decrease in molecular weight and subsequent decrease in material properties [45]. It is recommended

²⁶<https://www.pegas-gonda.cz/en/product/33/300x300-herkules-x-cnc> [cited on 16-06-21]

²⁷<https://www.cutter-shop.com/information/speed-and-feeds-calculator.html> [cited on 16-06-21]

²⁸https://www.cs.cmu.edu/afs/cs/academic/class/99353-f16/speedsfeeds_RL.pdf [cited on 16-06-2021]

²⁹<https://www.youtube.com/watch?v=3116ukeh6FM> [cited on 16-06-21]

that it be stored at 30 – 70% relative humidity [9]. A similar decrease in material properties is observed in hide glue. According to research done on museum and gallery conservation, which faces similar challenges in keeping joints strong over prolonged periods of time, it is recommended that hide glue be kept in 30 – 60% relative humidity [62]. Additionally hide glue is susceptible to deterioration due to bacteria and other microorganisms [88]. Hence the storage facility will be kept in sanitary conditions. Furthermore, periodic checks will be performed to see if microbial attack has taken place. It has been noted that microbial attacks in hide glue are typically accompanied by an “offensive odor” [88], so quality control can be performed without the need of specialised equipment. In sum, it can be concluded that the glider will need to be stored in a sanitary environment, away from direct sunlight at $5 - 25[^\circ\text{C}]$ and 30 – 60% relative humidity.

7.4. Structural Analysis

In this section, it will be explained how structural analysis was performed in order to determine the final geometry and structural elements of the system. It also addresses the critical failure modes of the design. Certain models are used for this, which will be described here. Verification of these models and a validation plan is presented in Section 7.6.

Loading of the structure

Before the structure could be designed, first the loading case had to be considered. This can be observed in Figure 7.30, which represents a simplified version of the system. In Figure 7.31, a front view of the system is shown which aids the explanation. The loading on the system is approximated in the following way: the total lift force is assumed to be equal to the load factor times the total weight ($25[\text{kg}]$). It is assumed that each half of the structure, as shown in Figure 7.31, carries half of the lift force. This lift force is distributed as an elliptical distribution. The tangential force is assumed to be 5% of the total lift force. This is an overestimation, and thus leads to a slight over-design of the structure. However, the largest portion of the loads is caused by the lift force, so the effect is small. This tangential force is distributed by a uniform distribution, referred to as $T(x)$. The winglet also produces a lift force, which is modelled as a point force $F_{winglet}$. It is assumed that $F_{winglet}$ is equal to 5% of the total lift force, which is again an overestimation, but there was no proper way in this phase of the design to analyse the force exerted by the winglet. The structural weight of the wings are represented by a triangular distribution $w(x)$, since the wing tapers down to the root. This is not a fully correct approximation, but since the weight of the wings are so small compared to the lift forces under the ultimate load factors, the effect of a better weight approximation is small as well. The payload weight is also modelled as a point force $w_{payload}$, which can be seen in Figure 7.31.

The forces are all assumed to act in the centre of pressure. After aerodynamic analysis, it was found that centre of pressure lies between 28% and 50% of the chord. These extreme locations were both used to address the torque in the structure.

In Section 5.8.4, it was explained how the limiting load factors are determined. The structure is designed for these limiting load factors multiplied by 1.5, in order to get the ultimate load factors. These ultimate load factors are considerably high and thus are assumed to provide enough compensation and margin for the approximation made in the loading case.

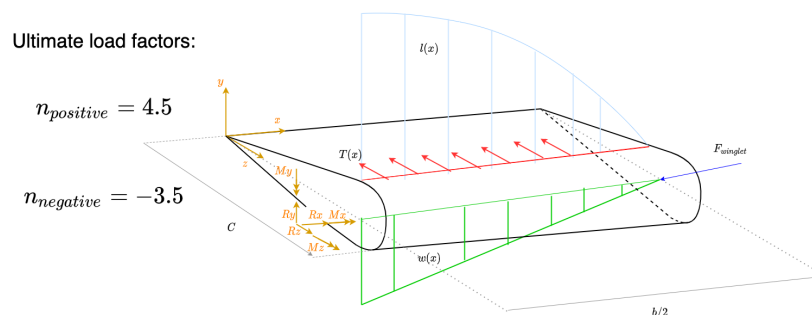


Figure 7.30: Simplified model of the wing with the most important load distributions. All forces are assumed to act in the centre of pressure as two-dimensional forces. $l(x)$ represents the elliptical lift distribution. $w(x)$ represents the triangular weight distribution, $T(x)$ represents the uniform tangential force distribution. $F_{winglet}$ represents the point force caused the winglet. In yellow, the reaction forces and moments are indicated.

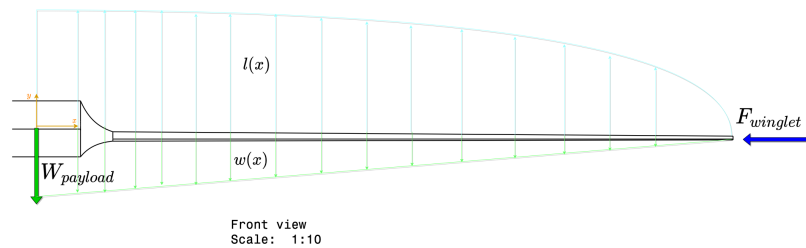


Figure 7.31: External loading on the right half of the structure.

Based on the loading case described here and the dimensions given in Figure 3.3, the internal loading diagrams can be constructed. For the ultimate positive load factor of 4.5, this can be seen in Figure 7.32 and Figure 7.33.

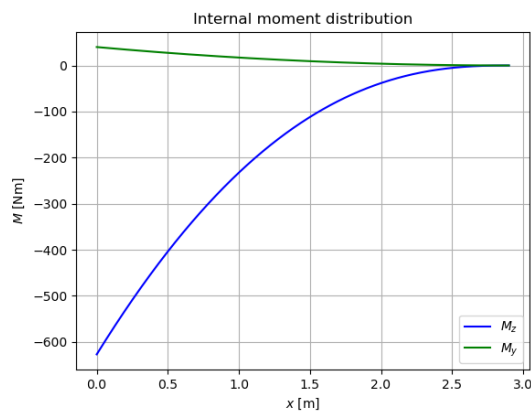


Figure 7.32: Internal moment diagram along the semi-span of the right wing due to a load factor of $n = 4.5$. A clockwise moment is positive for M_z .

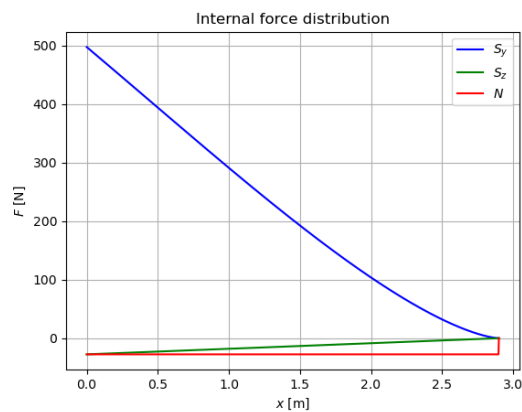


Figure 7.33: Internal force diagram along the semi-span due to a load factor of $n = 4.5$. Positive is upwards for the vertical shear force. Positive is tension for the normal force.

Wing model

During structural design, the following failure modes were considered:

- *Material failure due to tensile, compressive and shear stresses.*
- *Euler buckling, skin buckling and shear buckling.*
- *Failure due to stress concentrations.*
- *Deflection and twist.*

For modeling the structure of the wings, the following assumptions were used:

1. The wing is modelled as an Euler-Bernoulli beam: The bending properties of the wing are calculated using the original geometry, meaning that changes in the cross-sectional shape due to twist and deflection are neglected. This type of beam cannot estimate shear strain. As a result, the deflections will be underestimated. This assumption can be considered valid if the vertical deflection of the wing is very small compared to the span of the wing.

2. Vertical deflection due to twist is neglected: This is because the vertical deflection of the wing due to bending loads is in these ranges of span much larger than the vertical deflection due to twist.

3. The skin and stiffeners are modelled as boom areas: The complex geometry of the skin makes it difficult to approximate analytical expressions for the moments of inertia and shear stresses. Using structural idealisation greatly facilitates this. It underestimates their contribution to the second moment of area and therefore overestimates direct stresses. Because shear stresses are assumed to be constant between two booms, these are underestimated. However, a relatively high number of booms is used when modelling the structure, which minimises these errors.

4. The aerodynamic load is unaffected by twist and deflection: In reality the aerodynamic load changes orientation due to wing twist. To simplify calculations, the aerodynamic load is in this case

always assumed perpendicular to the surface of the wing. The deflections and twist are relatively small, validating the assumption.

5. The materials have isotropic properties: The structural components will mostly be manufactured from quasi-isotropic laminates. It is assumed that this results in isotropic mechanical properties. This assumption is compensated for by the over-estimation in loading case.

6. Sweep is neglected: Sweep introduces a larger torsional moment. However, the sweep angles are relatively small for the structure and the assumption that the forces act at extreme locations for the centre of pressure compensates for this.

Idealisation

The idealisation of the structure starts by discretising the skin into several points, as can be seen in Figure 7.34. The boom areas of two adjacent points i and j can be approximated by Equation 7.2. Note that all points are adjacent to two other points, that only the stiffener area is added at appropriate locations and that this equation does not work near the neutral axis. It was assumed that $\frac{\sigma_j}{\sigma_i}$ is mainly determined by the bending loads. Therefore, this ratio is simply the ratio of perpendicular distances of the booms to the neutral axis. The only problem is that the neutral axis is unknown. As a solution, the neutral axis is assumed to coincide with the horizontal axis. This allows to compute the boom areas for a first iteration, as well as the second moments of inertia and product moment of inertia (contribution of spars may have to be added). After this, the neutral axis is updated using Equation 7.3, which is visualised in Figure 7.35. The boom areas are continuously updated until convergence is achieved.

$$B_i = \frac{t_{sk} \cdot l_{skin}}{6} \cdot \left(2 + \frac{\sigma_j}{\sigma_i}\right) + A_{stringer} \quad (7.2) \quad \tan(\alpha) = -\frac{M_y I_{zz} - M_z I_{zy}}{M_z I_{yy} - M_y I_{zy}} \quad (7.3)$$

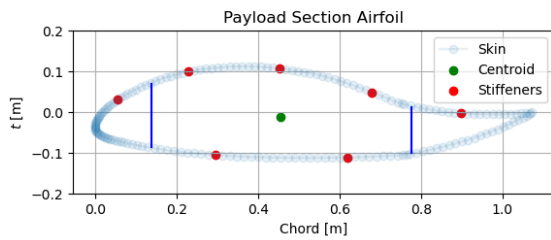


Figure 7.34: Structural idealisation of the payload section airfoil. The dots represent the boom areas.

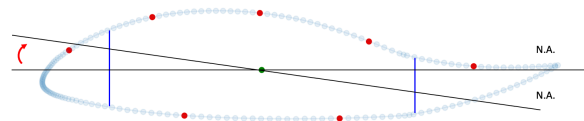


Figure 7.35: Schematic representation as the booms and the neutral axis are updated through several iterations until convergence.

Direct stress analysis of payload section

In Figure 7.9, a cross-sectional view of the payload section can be seen along with the necessary dimensions for the skin thickness and spars to bear the loads. The direct stresses of the payload section were analysed using equation Equation 7.4. This allowed to size the wing to prevent material failure due to tensile and compressive stresses.

$$\sigma_x = \frac{M_z (I_{yy}y - I_{zy}z)}{I_{zz}I_{yy} - I_{zy}^2} + \frac{M_y (I_{zz}z - I_{zy}y)}{I_{zz}I_{yy} - I_{zy}^2} + N_x/A_{cross} \quad (7.4)$$

In Figure 7.36 and Figure 7.37, the direct stress distributions in payload section can be seen.

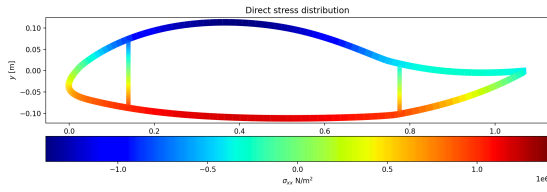


Figure 7.36: Direct stress distribution at the root of the structure for a load factor of $n = 4.5$.

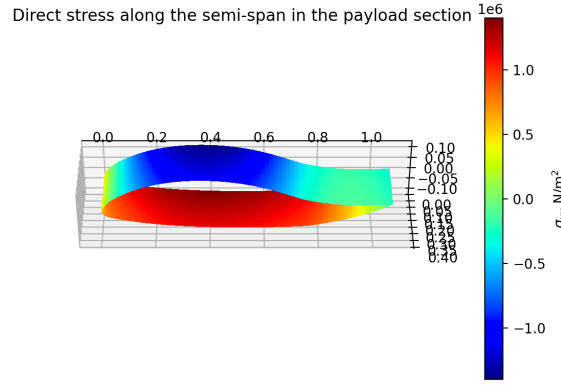


Figure 7.37: Direct stress distribution along the semi-span for load factor $n = 4.5$.

The critical failure mode for the payload section wing is Euler buckling, which is governed by Equation 7.5.

$$\sigma_{cr} \cdot A_{panel} = \frac{\pi^2 E_{sk} I_{zz_{panel}}}{L^2} \quad (7.5)$$

The compression panel was taken to be either the upper or lower side of the skin between the spars, depending on the load factor. σ_{cr} is the largest compressive stress in the panel. For the modelling of buckling, it was assumed that the panel is straight with stiffeners attached to it, as can be seen in Figure 7.38. It was required that L , rib spacing, was $0.275[m]$ to allow the integration of the payload. For this, 7 stiffeners were required in total. 5 almost equidistant stiffeners on the top of the skin and 2 on the bottom panel. Block shapes of spruce plywood veneers were used as these are very easy to manufacture. The dimensions of the stiffeners are $1[cm]$ in height and $2[cm]$ in width. It would be more effective to have a larger height than width, but this was not allowed as otherwise the payload would not fit anymore.

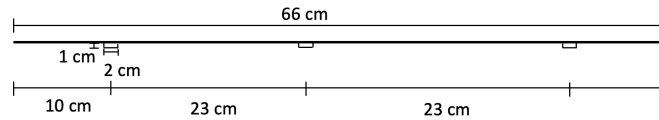


Figure 7.38: Model for the compression panel of the upper skin of the payload section wing between the spars. This model is used for Euler buckling and skin buckling. The skin thickness is $3 [mm]$.

Skin buckling is given by Equation 7.6, where b is taken to be the largest distance between two stiffening elements. The crippling of the stiffeners are given by Equation 7.7. The coefficient C is retrieved from literature [63]. The Poisson ratio of spruce wood is 0.4 [38]. A weighted average (with area) can be used to compute the total buckling stress of the panel. It was found that this failure mode is not critical and occurs at higher stresses than material failure and Euler buckling.

$$\sigma_{cr} = C \frac{\pi^2 E_{sk}}{12(1-\nu^2)} \left(\frac{t_{sk}}{b} \right)^2 \quad (7.6) \quad \sigma_{cc} = \sigma_y \cdot \alpha \left[\frac{C}{\sigma_y} \frac{\pi^2 E_{st}}{12(1-\nu^2)} \left(\frac{h_{st}}{w_{st}} \right)^2 \right]^{1-n} \quad (7.7)$$

Shear analysis of payload section

The booms of the skin and stiffeners were also used for the shear analysis, while for the spars a continuous shear flow distribution was modelled. For the shear flow analysis, only the vertical transverse loads (due to lift and weight) were taken into account, since the shear force due to the tangential force is negligible compared to the vertical loads. The shear flow analysis was used to compute the shear centre. After the shear centre was computed, the contributions due to torsion had to be added. For this, the extreme cases for the centre of pressure (28- and 50%) were considered which result in the largest torque. As can be seen in Figure 7.39, the shear stress is not critical as the material strength is never reached in the cross-section. More critical than material failure due to shear stress is shear

buckling for the thin spars. This was computed according to Equation 7.10, where K_s is a coefficient based on literature (type of clamping) [63]. It was found that this occurs at 4.1 [MPa] and 7.9 [MPa] in the front and rear spar respectively, but these stress levels are not reached.

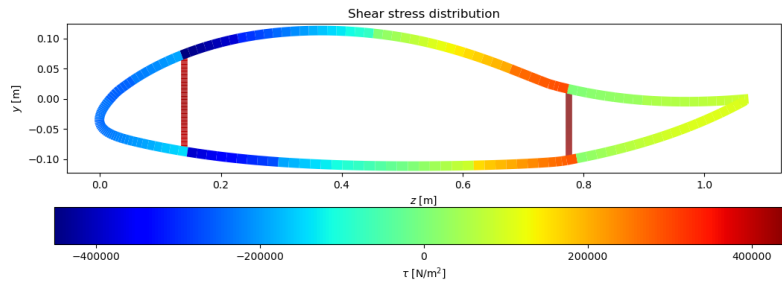


Figure 7.39: Shear stress at the root of payload-section airfoil due to vertical transverse loads and torque (for COP at 28% of the chord).

Sizing of rib holes

In Figure 7.40, you can see the sizing of the holes in the centre rib of the payload section. Since fatigue does not play a critical role for this design, the size of the holes was determined by static loading, namely by the net shear stress according to Equation 7.8 and Equation 7.9, where h is the height of the rib and b the spacing between the holes. h was taken to be the smallest height in between the spars. Figure 7.41 shows the difference for the outer rib. This is because a hole for the spar box had to be made in this rib. The previously mentioned equations do not apply for this hole, but the vertical height of the hole is so small that it will not pose a problem, neither will the width of the hole because of the small horizontal shear force. The rib lay-out of the outer wings can be seen in Figure 7.42. h for the outer wings was taken to be the height where the holes would be placed. It was determined that the diameter of the holes can be no larger than 2.5% of the chord. This diameter is enough for the wires to fit through the holes along the span where it is necessary. That is up until the span reaches 1.755 [m]. Further along the span there are no holes in the ribs anymore as no wires have to be integrated there.

$$\tau_{net_v} = \frac{S_v}{A_{net_v}} = \frac{qh}{t(h - D_{hole})} \quad (7.8) \quad \tau_{net_h} = \frac{S_z}{A_{net_h}} = \frac{qb}{t(b - D_{hole})} \quad (7.9) \quad \tau_{cr} = K_s E_{sp} \left(\frac{t_{sp}}{h_{sp}}\right)^2 \quad (7.10)$$

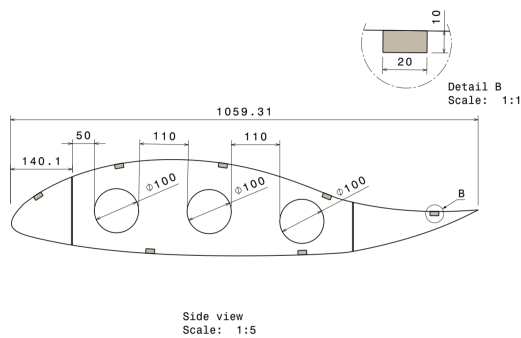


Figure 7.40: Centre rib of the payload section.

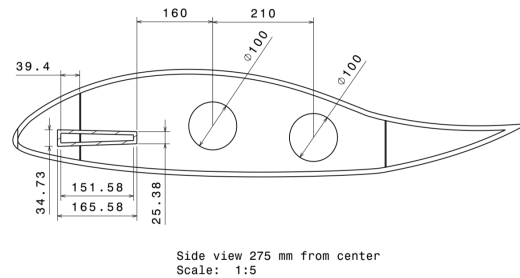


Figure 7.41: Outer rib of the payload section.

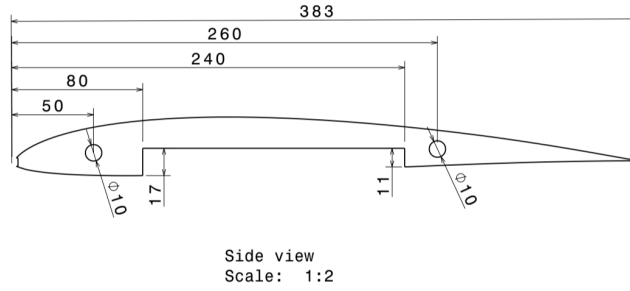


Figure 7.42: Rib of the wing with a chord of 0.40 [m], span is 0.405 [m]. At 12.5% and 65% of the chord, the holes are located. In the middle there is a cut-out through which the spar box connects.

Stress analysis of the wings

In Figure 7.43, a cross-sectional view of the thin wing can be seen. The wing skin is 1 [mm] thick, the spar box extends from 20% to 60% of the chord. The elements are all 7 [mm] thick, until at locations 2.05 [m] and 2.57 [m] of the span the aft- and front spar web disappear respectively, since no space is available for them anymore. After 2.57 [m], the spar becomes fully solid, consisting of only the spar caps, which gradually decrease in thickness to 6 [mm] each at the tip of the wing.

Since this cross-section does not consist of a homogeneous material, Equation 7.4 does not apply. The direct stress distribution is not uniform in the cross section. However, the strain distribution is uniform. The difference between the stress distribution can be seen in Figure 7.44 and Figure 7.45. The flexural stiffness was computed according to Equation 7.11. The same type of equation holds for the cross section. The strain can be computed according to Equation 7.12. Multiplying the strain by the Young’s modulus provides the actual stress in the cross-section. It was checked that the direct stresses do not exceed the material failure stresses of the skin. The product moment of inertia was neglected, but this was found to be an conservative estimation. The compressive stresses are much higher in the outer wings than in the payload section, reaching a maximum value of -19.7 [MPa], just below material failure.

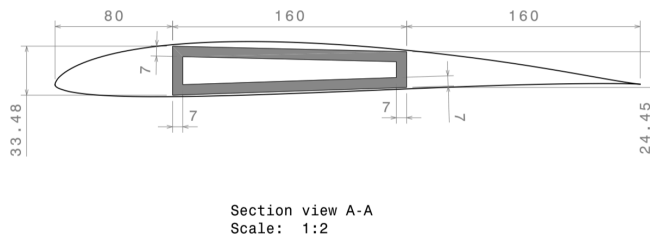


Figure 7.43: Cross-sectional view of the wing with a chord of 0.40 [m], span is 0.405 [m].

$$EI_{(zz/yy)} = E_{sp}I_{(zz/yy)_{sp}} + E_{sk}I_{(zz/yy)_{sk}} \quad (7.11)$$

$$\epsilon_{xx} = \frac{M_z y}{EI_{zz}} + \frac{M_y z}{EI_{yy}} + \frac{N_x}{EA_{cross}} \quad (7.12)$$

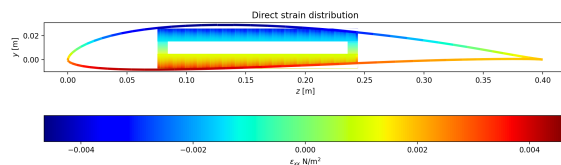
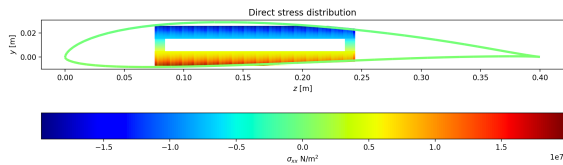


Figure 7.44: Direct stress distribution of the wing at chord is 0.4 [m] (0.405 [m] from the centre). Load factor is 4.5.

Figure 7.45: Direct strain distribution of the wing at chord is 0.4 [m] (0.405 [m] from the centre). Load factor is 4.5.

The Euler buckling analysis estimated the rib pitch, which can be seen in Figure 7.46.

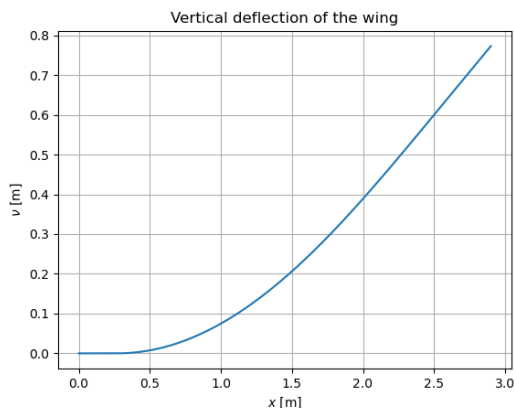


Figure 7.47: Vertical deflection in the wing due to the ultimate load factor of 4.5.

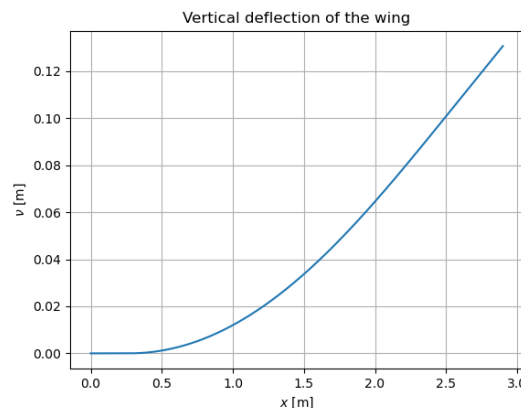


Figure 7.48: Vertical deflection in the wing due to the ultimate load factor of 1.0.

7.5. Bio-degradation Calculations

Ensuring the bio-degradation of the glider occurs at a sufficient rate is a large part in the design for end-of-life of GliMed. To ensure this is accurately calculated, a model for determining the bio-degradation rates of components and/or the glider has been created. The input for this model will be presented in Section 7.5.1 alongside preliminary results, while the design modification to meet the requirements and the results of the analysis will be presented in Section 7.5.2. Lastly a sensitivity analysis will be performed on the results of this model in Section 7.6.2.

7.5.1. Bio-degradation Model

Bio-degradation is defined as the breaking down of materials by bacteria or other living organisms. The activity rate of these organisms depends heavily on both the temperature and local humidity. Furthermore, the thinner or more exposed a material is, the easier it is to decompose. These four factors are the main ones taken into account in the biodegradability model.

There are a number of further assumptions made in the creation of the model. These are:

- **"Ideal" bio-degradation conditions** from research are assumed to be 60% humidity and 30°C
- **Soil pH and Oxygen Availability** also have an effect on the bio-degradation rate, but it is not possible to make an assumption on what these are at the landing location without having visited there prior. Therefore these factors will be excluded from the model
- **The temperature and humidity conditions** are assumed for three climates, Timbuktu, Fukushima and Trondheim. The data for these can be found in the midterm report. [36]

A flow chart of the model can be found in Figure 7.49, and explanations of each of the steps follow.

Temperature

The change in bio-degradation rate due to changes in temperature is assumed to be directly related to the change in the activity rate of micro-organisms. The relationship between these and temperature can be seen in Figure 7.50[70].

Humidity

The degree of bio-degradation of a material can be measured by measuring the degree of polymerisation of the polymers. When this DP decreases, degradation has occurred. A report on the bio-degradation of cellulose under differing humidity levels provided data on the change in DP over time [7]. This relationship is assumed to be representative of bio-degradation, and the change in bio-degradation rate for differing humidity levels can be plotted, as seen in Figure 7.51.

Thickness and Exposure Factor

From a number of studies, the increase in bio-degradation rate is estimated for changing thicknesses [4][58]. The model to determine bio-degradation time applies this factor to any change in thickness

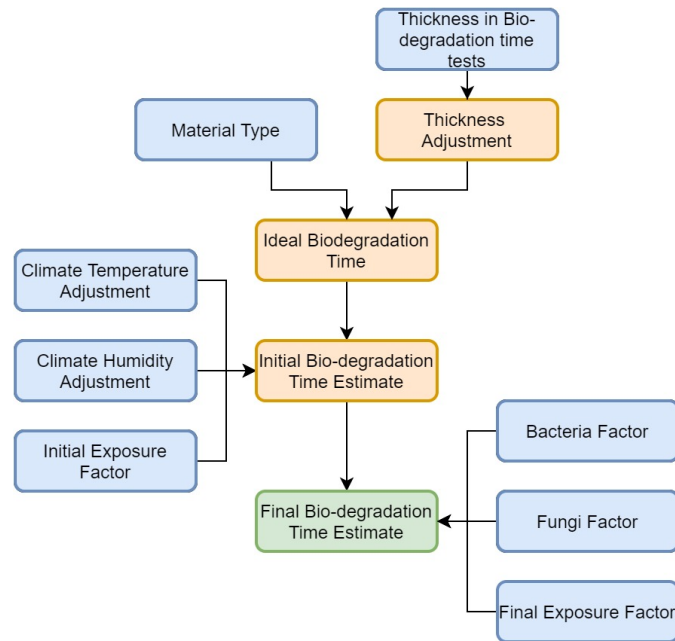


Figure 7.49: Flow chart of the steps taken in calculating the final bio-degradation time of GliMed's components.

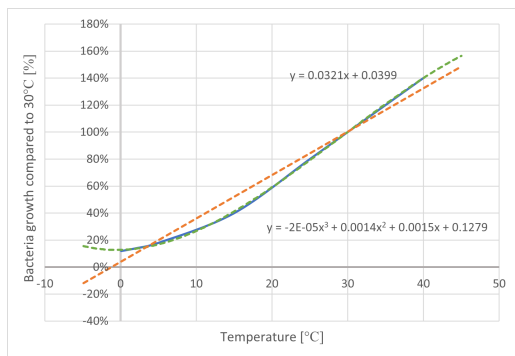


Figure 7.50: Graph showing the change in bacterial activity with temperature, when compared to the base value of 15°C. The data is sourced from *D. B. Nedwell*[70], and the third order polynomial approximation is used in the creation of the model.

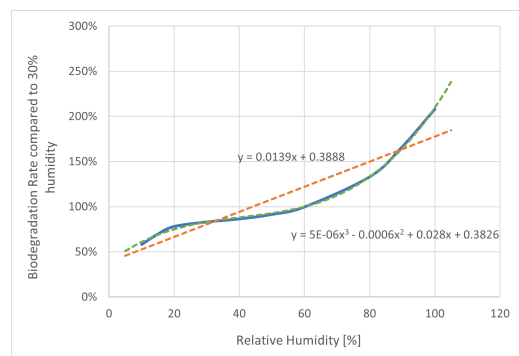


Figure 7.51: Graph showing the change in bio-degradation rate when compared to the base value of 30%. The data is sourced from *A. Barański et al.*[7] and the third order polynomial approximation is used in the model.

from the between the used and reference material samples. Furthermore, a factor is added for the exposure of each part to the environment at the start of end-of-life. The explanation for the exposure factor can be found in Figure 7.52.

Initial Bio-degradation Estimates

At an early stage of the design, estimates were already known for a large number of the structural materials. Using the material properties, reference thicknesses, and climate properties, the bio-degradation times as seen in Figure 7.53 were found. From here, it can be seen that the hollow spar for the thinner wing section is the limiting factor for bio-degradation, and will be used in further calculations. The fuselage ribs are a close second, and will also be monitored throughout the process. Furthermore, in contrast to previous expectations, Trondheim is the limiting climate zone because of the low average temperature.

7.5.2. Design for Bio-degradation

While the initial estimations of the degradation time are within the requirements, the exposure factor is not yet taken into account. With an exposure factor of three (fully enclosed, hollow spar), the bio-

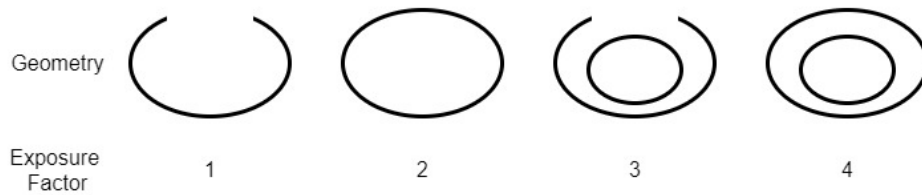


Figure 7.52: Explanation for the exposure factor used in the bio-degradation model. This factor is the amount of surfaces hidden from exposure plus one.

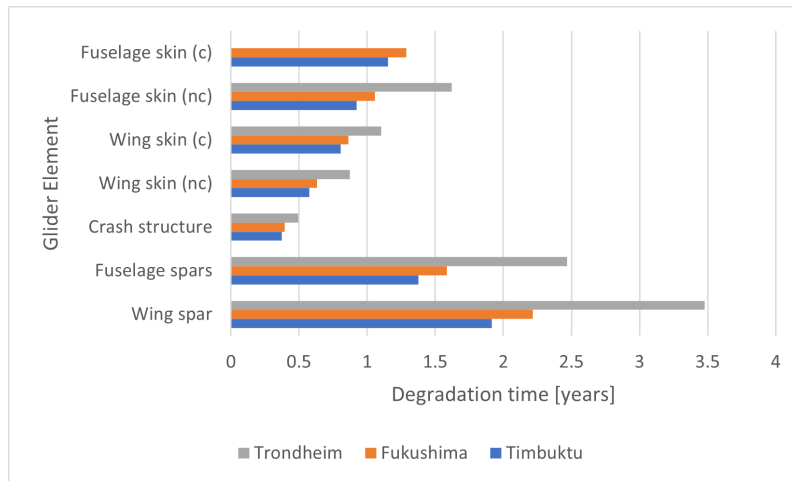


Figure 7.53: The bio-degradation times for different structural components, calculated for each climate zone with an exposure factor of 1. The wing spar is the limiting component, and Trondheim is the limiting climate zone.

degradation time increases to 10.3 years in the Trondheim climate zone. Therefore, actions must be undertaken to ensure the bio-degradation rate is increased drastically.

Design Changes

From the midterm report [36] the options for increasing bio-degradation rate are adding bacteria, fungi, seeds or spores, adding water and breaking the glider in multiple section to increase exposure.

Of these, bacteria, fungi, and increasing exposure will increase the bio-degradation rate by 16% and 13% respectively. [12][34] Initially it was decided that these can be suspended within a nutrient broth and sprayed into the gliders' interior. This can be seen in Figure 7.54. However this brought two challenges. Firstly, it would give additional work during the assembly prior to launch, adding to the complexity and time spent. The suggestion was made to have the nutrient broth ready in the glider throughout the storage period, along with a mechanism to release at EOL. However, the containing structure should biodegrade within minimal time after landing, and there is no material available that is structurally integral and moisture resistant for 10 years in storage, and becomes bio-degradable within 5 years after launch. [38] Secondly, having a liquid loose within the structure poses a large risk to both the function of the electronics as well as the structural integrity of GliMed, as the interior glue is water soluble. Therefore, the concept resulted in having PLA bio-film bags which biodegrade within 6 weeks and will be placed in the hollow wing spar prior to launch³¹, as seen in Figure 7.55.

Adding water will also aid in bio-degradation, however this is only true for Timbuktu. Here, four 100ml PLA bio-film bags can be placed in the glider wings and hollow spar prior to assembly, and will reduce the bio-degradation time by 5%. [7] This will look similar to the concept shown in Figure 7.55 for the nutrient broth.

Adding seeds or spores was not found to have a quantifiable effect on bio-degradation but requires very little additional mass or manufacturing, and will benefit the local ecosystem. Therefore the decision was made to include seed paper strips, containing bee-friendly flower mixes, within the smaller wings

³¹<https://www.eco-craft.co.uk/pla-biodegradable-spec> [Sourced on 07-06-2021]

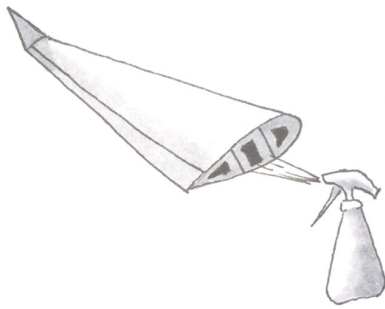


Figure 7.54: Conceptual sketch of spraying the interior of the wing with nutrient broth, bacteria and fungi. This will be done prior to final assembly at the launch site.

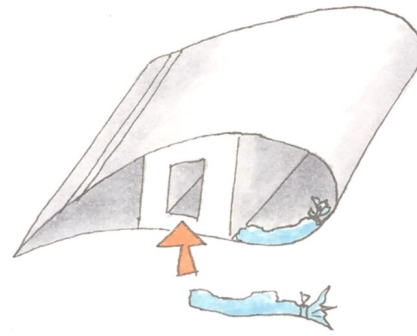


Figure 7.55: Conceptual sketch of the PLA bio-film bags filled with nutrient broth, bacteria and fungi, or water. These can be placed inside the wing cavities, or with the hollow spar before final assembly.

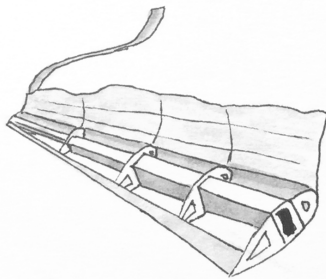


Figure 7.56: Conceptual sketch of the wing-opening mechanism. A strip of tear tape is added to the inside of the wing during manufacture, allowing the compressed paper pulp to be easily torn apart after landing.

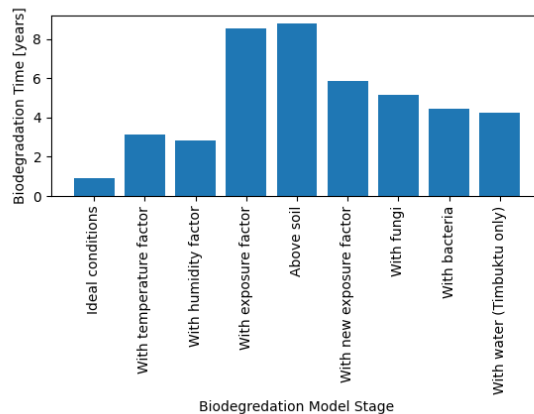


Figure 7.57: The change in bio-degradation times of the hollow wing spar for the Trondheim climate.

for missions to Trondheim or Fukushima climate zones. Timbuktu was not included due to the rarity of such plants in that location, and the risk of introducing invasive species.

Final Bio-degradation Estimate

The model calculates the bio-degradation time in multiple stages. First assuming ideal conditions, then incorporating the temperature and humidity of the chosen climate, as well as the exposure factor before additional design work. It also adds a factor to compensate for the lack of soil coverage at the landing location.

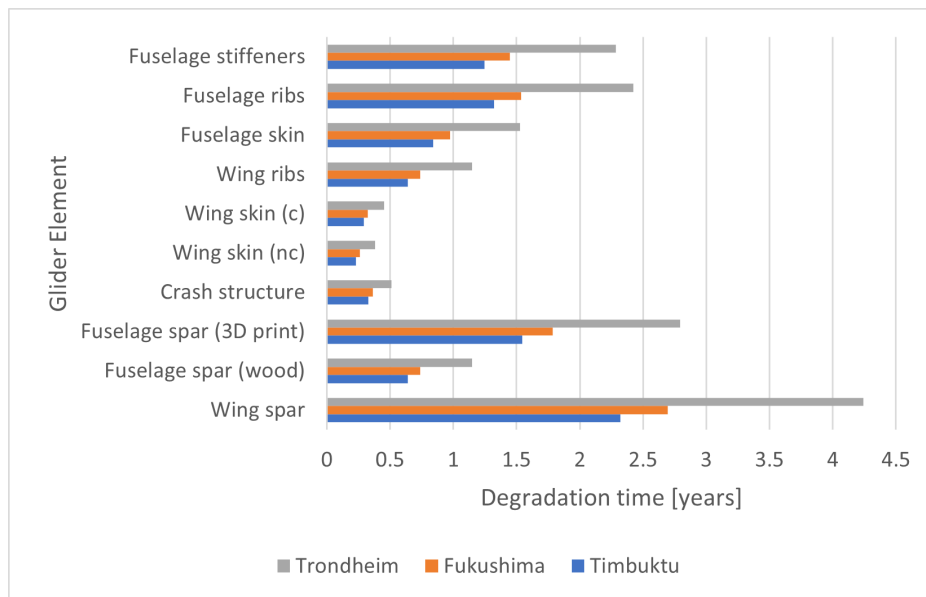
Multiple additional factors were added as a result of design decisions. The limiting factor for bio-degradation is the wing spar. By introducing a mechanism to open the wing skin, as seen in Figure 7.56, the exposure factor can be reduced from three to two. Furthermore, for each of the concepts mentioned above, a factor has been added in the model.

The initial degradation times, thicknesses and exposure factors used in the final bio-degradation time calculation are shown in Table 7.8. As mentioned in Section 7.2, the payload will be retrieved by removing the wings from the glider, thereby also exposing the inner section of the fuselage. The resulting change in bio-degradation time due to the design changes can be seen in Figure 7.57, while Figure 7.58 shows the final bio-degradation time of each component of the glider. The component with the longest bio-degradation time is the central wing spar, with a time of 4.26 years.

It must be noted that a large amount of materials have been excluded from this analysis, mainly the electronics components and mounting screws. This is because there will be removed by the recipients

Table 7.8: Table showing the design parameters used in the calculation of the final degradation times for each component.

Component	Thickness [mm]	Initial Degradation time [weeks]	Exposure Factor [-]
Wing Spar	7	48	2
Fuselage Spar (wood)	2	48	1
Fuselage Spar (3D print)	3	64	2
Crash Structure	88	4	1
Wing Skin (coated)	1	12+64	1
Fuselage Skin	3	48	1
Wing Ribs	2	48	1
Fuselage Ribs	13	48	1
Fuselage stiffeners	10	48	1

**Figure 7.58:** Graph showing the final bio-degradation times of each component, calculated with the design parameters shown in Table 7.8.

after landing, to either be disposed off or reused in a manner. Although there is a possibility that there may be wires and sensors that may still remain behind, these can be counted within the 10% of allowable non-bio-degradable materials as seen in requirement SAI-SYS-16-EOL-02.

As can be seen in Figure 7.58, all components analysed fall within the five year requirement. The remaining components will be removed by recipients, or fall under the allowable 10%. The electronics box will certainly be removed, but if the the remainder of the items not biodegradable within five years are not removed, it comes to 9.4% of the total biodegradable mass, and falls within the requirement.

7.6. Verification and Validation

In this section, verification of the models described in this chapter are explained. In addition, a plan is written down to validate the models (and their assumptions) in future design phases.

7.6.1. Structural analysis models

In Table 7.9, Table 7.10, Table 7.11 and Table 7.12, the verification tests done for the structural models are summarised. The verification tests written in *italic* are further explained in this section.

Verify geometrical effects of structural idealisation

As mentioned before, structural idealisation is used to compute the geometrical properties of the skin of an airfoil, especially relevant for the payload section wing. It had to be verified, how accurate the

structural idealisation is. In Figure 7.59, a simple airfoil shape is shown, for which analytical solutions for the geometrical properties exist. The analytical expressions are compared to the solutions the structural idealisation provided. It was determined that the structural idealisation becomes very accurate if the skin is divided into 100 or more booms. The payload section airfoil skin was divided into 184 booms, while the outer wing airfoil skin was divided into 216 booms.

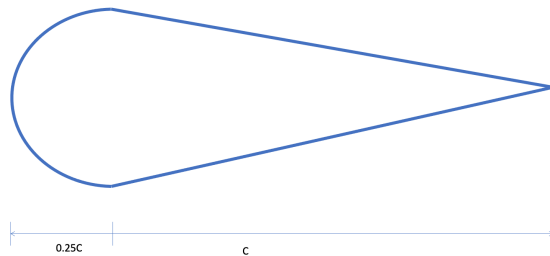


Figure 7.59: The simple airfoil shape for which analytical expressions of the centroid and moments of inertia exist.

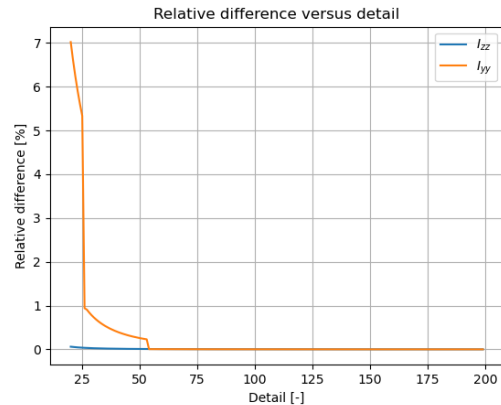


Figure 7.60: Relative difference in moments of inertia between the analytical solution and the structural idealisation versus the number of equidistant booms the skin is divided into.

Sensitivity analysis for the direct stresses

The driving failure mode is Euler buckling due to compressive stresses. It is therefore interesting to see, how the maximum compressive stress in the structure changes as a function of a number of parameters. For this sensitivity analysis, the change in maximum compressive stress at the root of the wing is observed as a function of the span, chord and load factor. In Figure 7.61, Figure 7.62 and Figure 7.63 the results are shown. The relationships are expected, the stress versus semi-span shows a linear relationship, as the internal moment increases linearly with the span. The stress versus the ultimate load factor also shows a linear relationship for the same reason. The stress increases quadratically if the chord decreases because the moments of inertia decrease quadratically. The conclusion can be drawn from this sensitivity analysis that the structure is most sensitive to changes in the chord. An increase in span or load factor is preferred above a decrease in chord in future design phases as this would require less structural reinforcements compared to the situation that the chord has to be decreased. On the other hand, if the structure has to be stronger and stiffer, it is more effective to increase the chord rather than decrease the span/ultimate load factor.

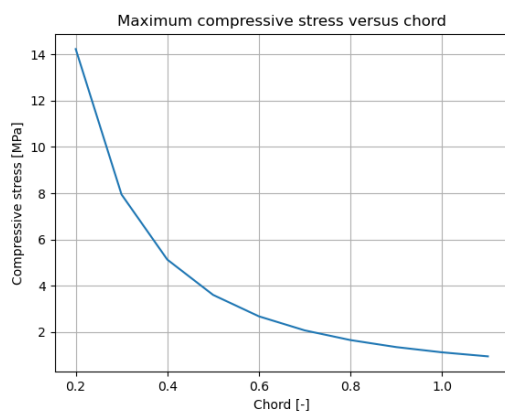


Figure 7.61: Maximum compressive stress in the payload section versus the chord length.

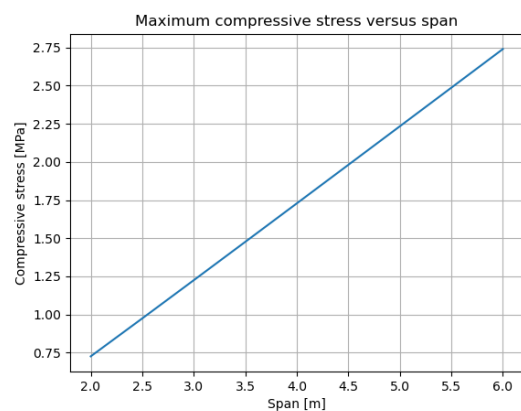


Figure 7.62: Maximum compressive stress in the payload section versus the semi-span length.

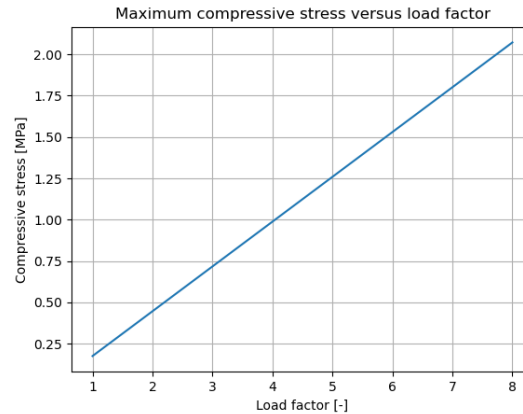


Figure 7.63: Maximum compressive stress in the payload section versus the ultimate load factor.

Order of accuracy test

It was explained that a second order finite difference scheme was used to compute the deflection of the wings. A first order accurate approximation (forward Euler) was used to approximate the slope at the root (which is zero for a clamped beam). This means that the approximation is first order accurate as a whole. An order of accuracy test was performed to check whether this was actually the case. For this, a rectangular beam was modelled with a uniformly distributed load. This deflection can be computed analytically, which serves as a manufactured solution. In Figure 7.64 and Figure 7.65 the results of the order of accuracy test can be seen. It shows that the scheme is indeed first order accurate (the slope of Figure 7.65 is -1).

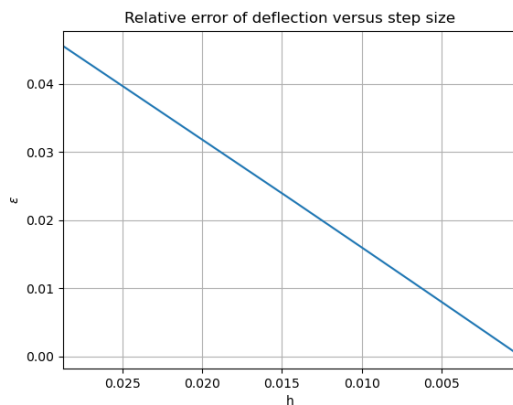


Figure 7.64: Relative error between the analytical- and FDM solution for the vertical deflection versus the step size for h .

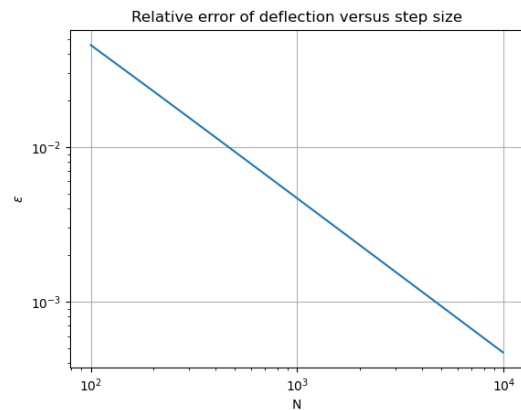


Figure 7.65: Relative error between the analytical- and FDM solution for the vertical deflection versus the number of intervals N .

Compare deflection with analytical expression

For the outer wings, both the internal moments and cross-section vary as a function of the span. In order to check whether the deflection solution computed by the finite difference scheme makes sense, the solution was compared to a beam with a constant cross-section. For a beam with a constant cross-section, the deflection could analytically be computed. The chord linearly decreases from span is 0.275 [m] to 2.9 [m]. As a consequence, the moments of inertia decrease quadratically. It was determined that the relative difference between the deflection of the actual outer wing and a beam with the moment of inertia of the wing at span is 0.5 to 0.6 [m] falls below 5%. If the moments of inertia of the beam are equal to the moments of inertia of the wing at span is 0.275 [m] or 2.9 [m], the relative difference grows quadratically. This makes sense, if the wing had the root chord all along the span, the deflection would be much lower than it actually is. If the wing had the tip chord all along the span, the deflection

would be much higher. Since the moment of inertia decreases quadratically, it makes sense that the deflection of the constant cross-section beam comes closer to the deflection of the actual wing if it has the moment of inertia of the wing at about one third of the semi-span.

Sensibility of shear flows

As a sanity check, it was verified whether the shear stress distribution due to the vertical shear force S_y makes sense. The results of this can be seen in Figure 7.66 and Figure 7.67. It was verified that the shear stresses follow a sensible distribution based on literature.

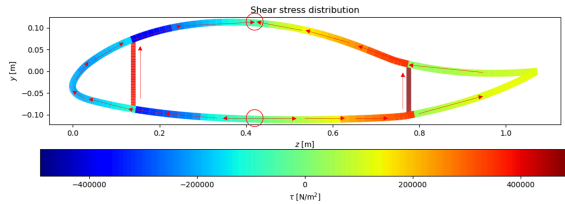


Figure 7.66: Shear stress distribution at the root of the payload section. It can be seen that the shear stress follows an expected pattern. It starts at zero in the bottom of the skin at the horizontal location of the shear centre and ends at zero in the top of the skin at the horizontal location of the shear centre.

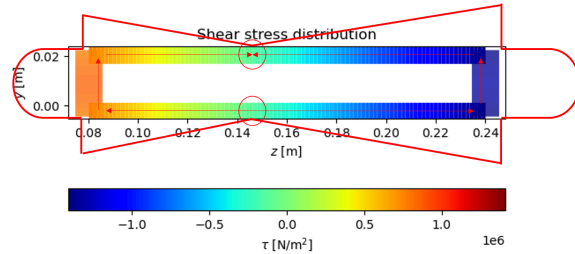


Figure 7.67: Shear stress distribution at the root of the outer wing. It can be seen that the shear stress follows an expected pattern. It starts at zero in the bottom of the spar box at the horizontal location of the shear centre and ends at zero in the top of the spar box at the horizontal location of the shear centre.

Different method used to compute shear in spar box

In order to compute the shear stress distribution in the spar box, it was assumed that the structure is thin walled. Equation 7.14 was used to compute the shear flows in the structure, which is only valid for thin-walled structures. The thin-walled assumption only holds for structures where the length of the component is more than 10 times larger than the thickness. This is true for the spar caps, but not for the spar webs of the hollow spar box. Since the largest shear stresses occur at the neutral axis, the spar webs are critical in shear. Equation 7.15 was used to verify the shear stresses in the spar webs. This equation holds for more thicker walled structures (although still slender). The relative differences were compared at the root of the outer wing and the relative differences increased up to 76%. This means that Equation 7.14 is not accurate at all for the spar webs. Since Equation 7.15 computed the highest shear stresses in the spar webs, this equation was used in further calculations to size the spar webs. However, shear stresses were still not the driving failure mode behind the design.

$$q_s = \left(\frac{S_y I_{zy}}{I_{zz} I_{yy} - I_{zy}^2} \right) \int_0^s t z ds - \left(\frac{S_y I_{yy}}{I_{zz} I_{yy} - I_{zy}^2} \right) \int_0^s t y ds \quad (7.14) \quad \tau = \frac{S_y Q}{I_{zz} t} \quad (7.15)$$

Validation procedures

The most important validation tests that have to be performed are the static loading tests of the structure. It has to be validated that the structure indeed only fails after the ultimate loads are exceeded, while simulating the loading distribution in flight as well as possible. Another purpose of it is to validate and quantify the effects of the assumptions made for the structural models. This requires building full scale prototypes and a test set-up. In addition to analysing the stresses under the ultimate loads, the deflection and twist have to be measured as well. For the twist, the location of the applied loading has to change location along the chord. Fatigue loading does not have to be tested, because the glider is single-use.

The structure may or may not be directly designed for flutter, but the system does have to be subjected to aeroelastic vibrations in order to test that it can sufficiently damp vibrations during flight.

Furthermore, it is important to test that the structure does not fail due to environmental exposure during flight time. In order to test this, the structure has to be exposed to heavy rain and other environmental factors the glider is subjected to during flight. It has to be tested that the structural capabilities are not significantly decreased during the determined flight time. Apart from this, a full scale test has

to be performed, validating that the structure does indeed not degrade during 10 year storage (while controlling the environment).

In addition, operational tests on full- and smaller scale prototypes have to be performed to validate that necessary components are attachable/detachable, that movable parts have enough freedom to rotate and that items can be loaded/unloaded.

Lastly, the structure has to be put on a scale to validate the structural weight. Both the full prototype and separate components can be put on the scale in order to check how much weight each components adds to the overall structure.

Table 7.9: Code verification tests for the structural models (unit tests).

Name:	Method:
Miscellaneous functions:	
Check that distance function correctly computes perpendicular distance line to point	Verified with 10 randomly selected points using hand calculations
Check that moment due to base shear flow is correctly computed	Verified with 10 randomly selected points, compute moment around a point by hand
Loads:	
Integration of distributed load should give the total force represented as point force	Verified by integrating the lift-, weight- and tangential force distribution for various load factors
Visual inspection of load distributions	Verified by checking the correct signs and plausible magnitudes
Internal moment change due to changing span	Linear relationship observed between span and internal moments around the z- and y-axis (expected)
Geometrical properties:	
Check correctness of centroid wing structures	Checked with literature and CATIA, 2% difference for the payload section and 0.1% difference for the outer wings
Increase cross-sectional area skin due to skin thickness increase	Linear relationship observed (expected)
Increase in moments of inertia and enclosed area of wing due to increasing chord	Quadratic relationships observed (expected)
Investigate contribution of spar	Appropriate decrease in moments of inertia if spars are removed
Compare structural idealisation for different airfoils	DU84-132V3 and SA7036 were compared with same chord: The maximum height of the DU is 1.511 times larger than SA7036, thus I_{zz} should be about 2.28 times larger. In reality I_{zz} was 2.15 times larger (expected since airfoil do not have the same shapes). I_{yy} was approximately the same (expected since the chord length is the largest contributor to I_{yy} and that was the same for both airfoils).

Table 7.10: Code verification tests for the structural models (module tests).

Name:	Method:
Stresses and shear flows:	
Magnitudes and signs of direct stresses	Compared the direct stresses to a rectangular box of similar size (sanity check). Verified that the signs of the direct stresses are correct at the correct places (negative where compression should be, positive there should be tension), done by visual inspection

Check neutral axis	Verified that the direct stresses are 0 at the neutral axis
No discontinuous stress distribution	Checked that signs of stresses do not suddenly change instead of first approaching zero [MPa].
Strain distribution is uniform	Verified for outer wings that strain distribution is uniform (stress distribution is discontinuous)
Shear flows must follow Kirchoff's law	Verified that the shear flow going out of a crossing is equal to the sum of the in going flows at that crossing
Shear flow correct loop	Shear flow that starts at cut (zero there), should be zero if it returns to that cut. An absolute difference of order 10^{-7} was found which was determined to be acceptable.
Integrating shear flows due to vertical shear force should result in the magnitude of that vertical shear force	Verified for two different airfoils, relative difference was 2.4-2.6%, which can be explained due to the fact that certain assumptions were made when computing the boom areas near the neutral axis and due to inaccuracies in determining the centroid of the payload section
Movement of shear centre location	Shear centre moves forward if front spar moves more forward and more aft if front spar moves more aft. Same behaviour found if the rear spar changes location (expected behaviour)
<i>Use different method for spar box</i>	<i>Different method used to compute shear stresses and compared</i>
Deflection and twist:	
<i>Order of accuracy test</i>	<i>Check that the finite difference scheme is first order accurate</i>
Signs of deflection and twist	Verified that signs of the deflection and twist are sensible

Table 7.11: Calculation verification tests for the structural models (unit tests).

Name:	Method:
Loads:	
Check force equilibrium if all loads are represented as point forces	Verified for various load factors
Compare centroid of load distributions with analytical expressions	Check by evaluating the analytical expressions for the centroid of an quarter-elliptical distribution and a triangular distribution, differences were negligible
Check internal force and moment equilibria	Internal shear forces, torque and moments are zero at the wingtips
Geometrical properties:	
<i>Verify geometrical effects of structural idealisation</i>	<i>Verify boom method with analytical expressions</i>

Table 7.12: Calculation verification tests for the structural models (module tests).

Name:	Method:
Stresses and shear flows:	

Check shear centre location with literature	Verified that the shear centre location should be approximately half way in between the spars. It was found that the shear centre is located nearer to the front spar than the rear spar, but is indeed approximately half way
<i>Sensibility of shear flows</i>	<i>Verified that the shear flow distribution is sensible</i>
<i>Sensitivity analysis</i>	<i>Verify direct stress changes due to change in chord, load factors and span</i>
Deflection and twist:	
<i>Compare deflection with analytical expression</i>	<i>Compare with spar box of constant cross section</i>

7.6.2. End-Of-Life

The requirements for the EOL subsystem portrayed in Table 7.13 and Table 6.17 have been verified either through analysis if explicitly stated in the corresponding section, or through inspection of the design.

Furthermore, a sensitivity analysis has been performed on the bio-degradation model, as part of the verification. Further verification methods are carried out, but not mentioned in depth in the report. To ensure accurate portrayal of the results, and to further ensure the requirements are met, even if the conditions differ from what has been assumed, a sensitivity analysis has been performed on the bio-degradation model. This was done as part of the verification of the model.

Firstly, the temperature and humidity are changed by $\pm 3^{\circ}\text{C}$ and $\pm 3\%$ respectively, a large change to the average climate, for which the results are given in Figure 7.68. It can be seen that GliMed does not fail the bio-degradation time requirement.

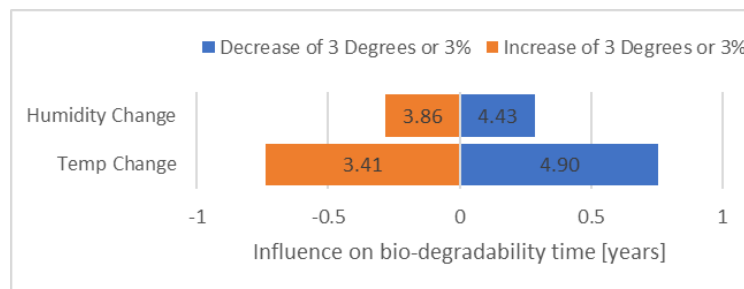


Figure 7.68: Graphs showing the sensitivity analysis performed on the temperature and humidity factors in the bio-degradation model. Climate conditions have been changed by 3°C or $\pm 3\%$ humidity. Displayed along the bottom axis are the changes, m and the labels are given as the final bio-degradation time.

A similar sensitivity analysis was also performed on the effect on thickness, as well as the two factors of bacterial and fungal increase in bio degradation. The results of these can be seen in Figure 7.69. Again, these sensitivity analyses show that the bio-degradation model is robust to small changes in parameters.

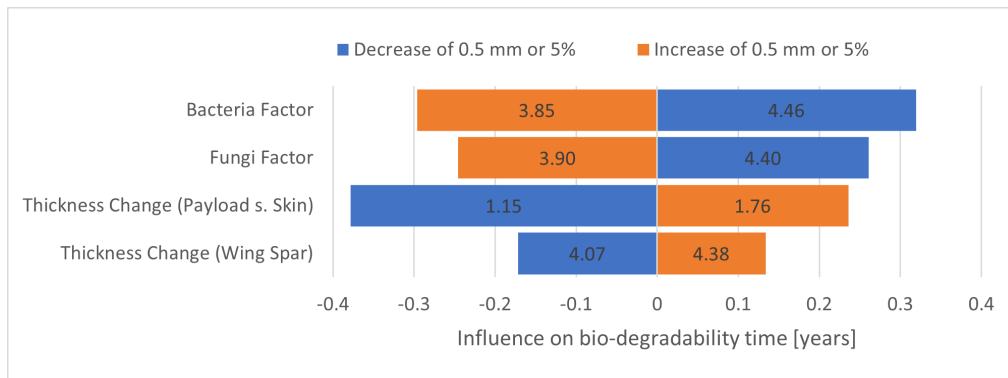


Figure 7.69: Results of sensitivity analysis on the thickness of components and the change in bacterial or fungal factors. Two elements of construction were chosen to be representative for the thickness analysis, and it can be seen that while the thickness does change the bio-degradation rate as intended, it does not exceed the boundaries set by SAI-SYS-16-EOL-02. For the factors, the changes within a range of $\pm 5\%$ from the original value do not cause SAI-SYS-16-EOL-02 to be exceeded.

Further verification tests, such as unit tests have also been performed, and the model was deemed to be verified. Lastly, validation tests will also need to be performed on this model, and will be describe here. However, the tests themselves fall outside the scope of this project, and therefore the model cannot yet be validated.

The main validation tests are to validate the changes made due to temperature, humidity, bacteria, fungi, and thickness variations are accurate, where each time one of the parameters mentioned is varied. For example for testing the effect of temperature, the same size, material, humidity and other conditions will be used, but the experiment can take place at a temperature range from zero to 50 °C. Once this has been validated, the next step would be to determine if the parameters can be combined and do not interfere with each other. A final validation test would be to test the bio-degradation of section of- or the entire glider.

7.7. Requirements Compliance Matrix

Table 7.13: Requirements compliance matrix for the end-of-life

Requirement ID	Requirement	Compliance	Proof
SAI-SYS-16-EOL-01	There shall be no hazardous waste remaining at the disposal site.	✓	Section 6.5
SAI-SYS-16-EOL-02	All components of the system remaining at landing site shall be 90% degraded after 5 years.	✓	Section 7.5.2
SAI-SYS-16-EOL-03	Any non-degradable components shall be removable after mission by the recipient.	✓	Section 6.5
SAI-SYS-12-EOL-07	Degradation of the system shall be possible for temperatures between -5 and 45 degrees Celsius.	✓	Section 7.5.1
SAI-SYS-12-EOL-08	Degradation of the system shall be possible under air humidity levels between 20-86%.	✓	Section 7.5.1
SAI-SYS-16-EOL-10	The disposal of the system shall comply with the EU Waste Framework Directive or similar	TBD	Analysed in detail design

Table 7.14: Compliance matrix for manufacturing

Requirement ID	Requirement	Compliance	Proof
SAI-SYS-01-MAN-01	The system shall have a maximum of 100 structural parts.	✓	Section 7.3

SAI-SYS-01-MAN-02	The system shall have a maximum of three manufacturing divisions	✓	Section 7.3
SAI-SYS-07-MAN-03	The system shall cost a maximum of 300 [euros] to manufacture (excluding material costs).	✓	Section 4.3.3
SAI-SYS-01-MAN-04	The produced system shall comply with all assembly tolerances.	TBD	Analysis in future design stage
SAI-SYS-01-MAN-05	The production process shall adhere to local occupational health and safety regulations.	TBD	Analysis and testing in future design stages
SAI-SYS-01-MAN-06	The loads exerted during assembly shall not exceed the yield loads given in structural requirements.	TBD	Analysis and testing in future design stages
SAI-SYS-01-MAN-07	All production tools used for the manufacturing of the system shall be commercially available.	✓	Table 4.3

A few requirements have been left out of Table 7.15, as these are not applicable to the design concept that was chosen in the end (tailless aircraft), but only to a fuselage concept.

Table 7.15: Compliance matrix for structures

Requirement ID	Requirement	Compliance	Proof
SAI-SYS-13-STRUC-01	The structure of the system shall not fail before 1 loading cycle.	TBD	Section 7.4, re-evaluation load factors necessary
SAI-SYS-13-STRUC-02	The structure of the system shall not fail under the specified ultimate loads during operation.	TBD	Section 7.4, re-evaluation load factors necessary
SAI-SYS-13-STRUC-03	The structure of the system shall not have internal damage before launch.	TBD	Inspection just before launch
SAI-SYS-13-STRUC-04	The wing-tips of the structure shall not deflect more than 0.87 [m] from their initial structural position under the ultimate specified loads during operation.	✓	Section 7.4
SAI-SYS-13-STRUC-05	The wings shall not twist more than 20 [degrees] from their initial structural position under the ultimate specified loads during operation.	✓	Section 7.4
SAI-SYS-13-STRUC-07	The structure of the system shall damp aeroelastic vibrations such that the structure shall not fail during any of the specified loads during operation.	TBD	Testing in future design stages
SAI-SYS-03-STRUC-09	The payload shall be detachable from the structure of the system.	✓	Section 7.2.4

SAI-SYS-13-STRUC-10	The joints of the structure shall not fail due to adhesion failure.	TBD	Analysis and testing in future design stages
SAI-SYS-13-STRUC-11	The joints of the structure shall have a higher ultimate strength than the parent material.	✓	Section 7.2.3
SAI-SYS-10-STRUC-12	The structure of the system shall have detachable parts where necessary.	✓	Section 7.2.4
SAI-SYS-13-STRUC-13	The structure shall allow the control surfaces of the system to deflect as much as necessary during operations.	TBD	Demonstration in future design stage
SAI-SYS-10-STRUC-14	The structure of the system shall allow for as sufficient as necessary inspection during maintenance.	✓	Section 7.2.4
SAI-SYS-10-STRUC-15	The structure of the system shall allow for repairs.	TBD	Inspection in future design stage
SAI-SYS-10-STRUC-16	The structure of the system shall allow for replacement of components.	✓	Section 7.2.2, electrical components can be replaced, full payload section and full outer wing.
SAI-SYS-23-STRUC-17	The structure of the system shall not exceed 12.74 [kg] in mass.	✓	Section 3.3
SAI-SYS-08-STRUC-18	The structure of the system shall not fail due to environmental exposure during operation.	✓	Section 7.5
SAI-SYS-03-STRUC-19	The structure of the system shall not allow translational movement of non-fixed items with more than 1 [cm] before landing impact.	✓	Section 7.2.2
SAI-SYS-02-STRUC-20	The structure of the system shall be able to withstand an impact of at least 2500 [J] without failing.	✓	Section 6.4.2
SAI-SYS-10-STRUC-21	The structure shall not degrade during storage.	✓	Section 7.3.7
SAI-SYS-01-STRUC-22	The structure of the system shall be able to be manufactured with available manufacturing methods.	✓	Section 7.3.6
SAI-SYS-04-STRUC-23	The structure of the system shall allow the loading of the payload without the system losing its original functionality.	✓	Section 7.2.4
SAI-SYS-06-STRUC-24	The structure of the system shall not be harmful to the recipient when disassembling the system.	✓	Section 6.5

SAI-SYS-20-STRUC-25	The structure of the system shall not release any objects that are harmful for the recipient upon landing.	TBD	Inspection during validation and analysis in Section 7.2.2
SAI-SYS-21-STRUC-26	The structure of the system shall adhere to structural drone regulations stated by the EASA.	TBD	Analysis during detailed design
SAI-SYS-28-STRUC-27	The structure of the system shall allow the integration of the payload of volume 0.5 [m ³]	✓	Section 6.4.2

Many of the requirements for materials are left out of Table 7.16. This is because these requirements were not only material dependant, but also structurally dependant. They are incorporated into Table 7.15, Table 7.14 and Table 7.13. Only the requirements that are purely material dependant, are left in Table 7.16. Here it can be seen that requirements SAI-SYS-14-MAT-06 and SAI-SYS-14-MAT-07 still have a TBD value. More research is needed to determine the allowable conductivity and magnetism of the structural materials. The materials chosen are most likely proficient in the current application, but can only be guaranteed after a validation procedure.

Table 7.16: Compliance matrix for materials

Requirement ID	Requirement	Compliance	Proof
SAI-SYS-14-MAT-06	The material used in non-electrical sub-systems shall have a maximum conductivity of <td> Siemens per meter.	TBD	Test during detailed design
SAI-SYS-14-MAT-07	The material used in non-electrical sub-systems shall not be more magnetic than <td> Tesla.	TBD	Test during detailed design
SAI-SYS-16-MAT-09	The material shall not be toxic to the environment it is located in, in its grave phase with respect to the life cycle.	✓	Section 7.2.2

7.8. Recommendations

In this section, recommendations are made for future studies. There are still quite a number of items that have to be investigated or investigated further in order to design a fully functioning product. The most important recommendations are listed here.

Material selection

Many more materials exist on this planet that have not been taken into account in the trade-offs that were performed. For example, the wood species that is used for the plywood has not been researched into great detail, where only a few aspects was focused on. Also the plastic used to waterproof the wings was not researched into much detail and could still be optimised with further research.

Next to this it could happen that after a certain time new materials arise which outperform the current chosen materials. For this reason the material research and trade-off should be revised every year to make sure the materials used are up to date.

Critical points of the structural design

The structural design choices made in this report are based on adding a certain weight to a trade-off criterion. It would be interesting to see how a sensitivity analysis affects the design choices made. The weights of the trade-off criteria can be switched to see whether the structural design choices made are objectively the optimal choices.

The failure mode that drives the design in both the payload section and outer wings is Euler buckling. Once the ultimate loads are reached, the structure will fail in this manner. Very important to note is that the ultimate loads the structure is designed for are too low. As is explained in Section 5.8.4, at a very late stage in the design it was found that the limiting load factors were computed wrongly. Therefore, in future design stages it is required to add structural reinforcements to the structure, which adds weight. The mass budget has tried to take this additional mass increase due to structural reinforcements into account as well as possible via contingencies, but this might not be enough to take into account the full weight increase.

The loads between the outer wings and payload section are transferred via the spar box and wrap box. The wrap box is made out of PLA, which is not nearly as decomposable as spruce. Therefore, the component is made porous with the help of additive manufacturing. This can lead to defects in the component, which should be tested in the detailed design phase. In addition, there is a sharp transition between the wrap box and the rest of the front spar. This can lead to failure due to torsional loads. This has to be analysed and the transition of the wrap box to the front spar possible has to be manufactured more smoothly for a better load transfer. An example of this can be seen in Figure 7.70. Furthermore the screws carrying the normal loads were assumed to not carry any of the bending loads, this needs to be further analysed and verified. Lastly, the connection between the spar box and ribs is designed by making a cut in the spar box. This introduces enormous stress concentrations in the spar box which might be fatal for the structure in flight. Therefore, a design has to be considered with a larger cut in the rib and no cut in the spar box.

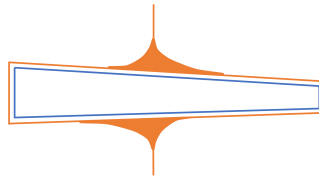


Figure 7.70: A smoother transition between the wrap box and the front spar for better load transfer.

Shear was the least driving failure mode, the structure can handle shear stresses far beyond the ultimate loads. However, many structural elements are adhesively bonded. Despite the adhesive being stronger than the materials, adhesion failure has not been properly investigated. This is something that has to be done (along with validation tests) in the detailed design phase.

It has also not been investigated whether the glider should achieve the necessary L/D performance under the ultimate static loads. If this is the case, the deflection and twist of the wings are too high. It would be required to use either stiffer materials or a different structural design to make the glider stiffer.

Lastly, aeroelastic vibrations have not been analysed. Therefore, it is not known whether the structure will fail due to flutter during flight. This should also be analysed and tested in future design phases.

Manufacturing

First and foremost manufacturing would benefit significantly from a prototype model of the glider. This would identify any assembly steps that cannot be performed due to, for example, obstructions or inaccessible areas. This would however come in a much later design stage, once the entire system is designed.

In the short term, a more detailed analysis of the manufacturing time can be performed. With the CAD model of the glider complete and with machinery suppliers identified, software required to run the machinery could be requested from the suppliers. Using such software more accurate time estimations could be made that take into account all the movements that a tool performs.

8. Sustainability

The definition of sustainability in the scope of this project is to be meeting the needs of the present, without compromising the ecological balance or the needs of the future. Hence, sustainability refers not only to the environment, but has financial and social aspects as well.

8.1. Environmental Sustainability

On the surface, it may appear that the largest aspect of environmental sustainability within the SustAln project is preventing pollution at end-of-life. However, the sustainable design approach taken into account during design is more than just the degrading and polluting of the materials. Other aspects have also been considered, for example where the materials are sourced, the energy that goes into making the materials and the manufacturing process. This has been done with the aid of a Life Cycle Assessment (LCA) to determine the environmental impact on all stages of the cradle to grave life cycle.

During this project, a LCA was performed not only to determine the sustainability of SustAln, but also to determine the sustainability of the different electronic systems presented in Chapter 6. The project LCA will be analysed to determine the processes and components which should be evaluated in further detail to ensure SustAln will have a minimal environmental impact. The electronics LCA will aid in determining which system to use for a particular mission. It must be noted that all requirements pertaining to a value on the sustainability of GliMed have been removed, as there is no viable and absolute method of determining this. The LCA used during this project are mainly comparison devices.

Lastly, the LCA undertaken as part of this project were not as in-depth as they could be, given a broader access to LCA software. Therefore, some decisions were taken under the assumption that the environmental sustainability of GliMed would be increased, however this has not been validated by the LCA. These decisions are listed under Section 8.1.3.

8.1.1. Project LCA

The goal of this LCA is to determine the environmental sustainability of the glider, and evaluate what can be done to further minimise this in coming design stages.

The LCA will be performed in a cradle to grave scenario, with the sourcing and production of components considered wherever possible, as well as the end-of-life of the system. The full processes flow diagram (PFD) for the system is shown in Figure 8.1, however the production of the electronic components has been omitted from this LCA. This is because for these, only the constituent materials will be considered, and not their entire production process. Lastly, the functional unit of this analysis is a single glider.

Methodology

The software used for this LCA is the SimaPro software¹, with the ecoinvent database². The project system is build up from processes as described in the PFD. Each of these are created as a process, with the inputs and outputs as seen in the PFD. These processes are then linked together in another process, creating the system.

Of the three electronics systems, the single-use system as described below was used in this analysis. Therefore it must be noted that the results vary by the amounts determined in Section 8.1.2 if an alternative system is chosen.

The end-of-life of GliMed has not been modeled in the LCA. This mainly because bio-degradation is not covered in the database, and no reliable method was found during literature research. The most similar end-of-life option is land filling bio-degradable waste, but this has a much larger impact on land use than GliMed will have. Furthermore, from looking into this process, it was found there would be no large impacts missing if the end-of-life was neglected in the LCA model used.

¹<https://simapro.com/> [Sourced on 16/06/2021]

²<https://www.ecoinvent.org/> [Sourced on 11/06/2021]

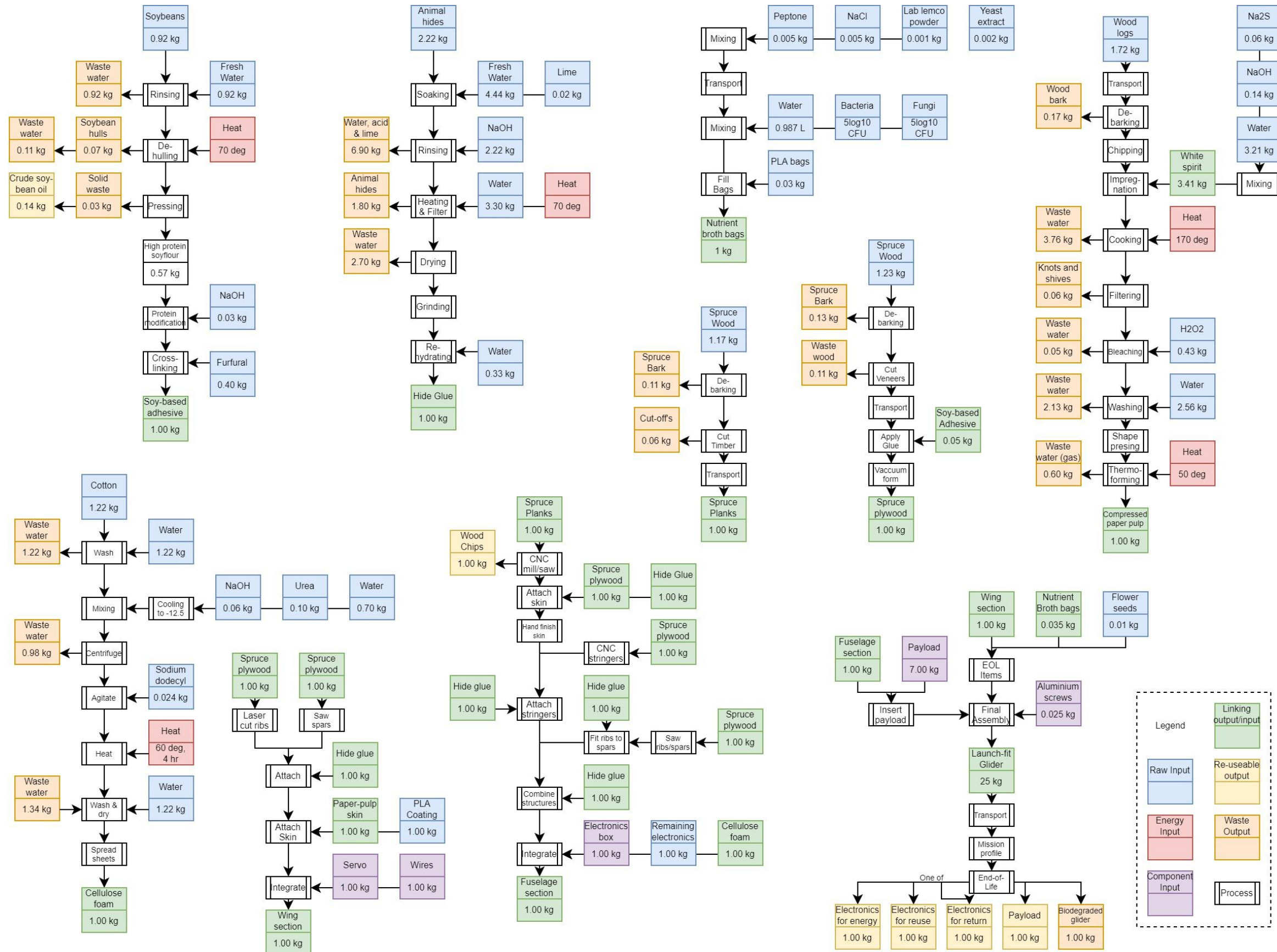


Figure 8.1: The Process Flow Diagram of the Project LCA

There were a number of impact categories chosen to analyse in this LCA in order to present the results in an efficient manner. These are listed below, along with their indicator unit.

- Ozone formation, Human health; [kg NO_x eq]
- Freshwater eutrophication, [kg P eq]
- Land use; [m²a crop eq]
- Water consumption; [m³]
- Global warming; [kg CO₂ eq]
- Freshwater ecotoxicity; [kg 1,4-DCB]
- Human carcinogenic toxicity; [kg 1,4-DCB]
- Mineral resource scarcity; [kg Cu eq]
- Fossil resource scarcity; [kg oil eq]

Furthermore, for all of these but water consumption and land use, and Environmental Cost Indicator (ECI) has been assigned on basis from literature research [11]. This is done to provide an equal unit to compare the impact of each category. Water consumption, land use and both resource scarcities were omitted as the ECI value depends yet unknown parameters. This ECI also helps in determining the full Life Cycle Cost (LCC) which will be described in Section 8.2.

Results

The results of the project LCA can be seen in Figure 8.2. These are separated into two parts, the glider without any electronics, and the single use electronics system as used on the following electronics LCA. The total of this, makes the total impact in each category.

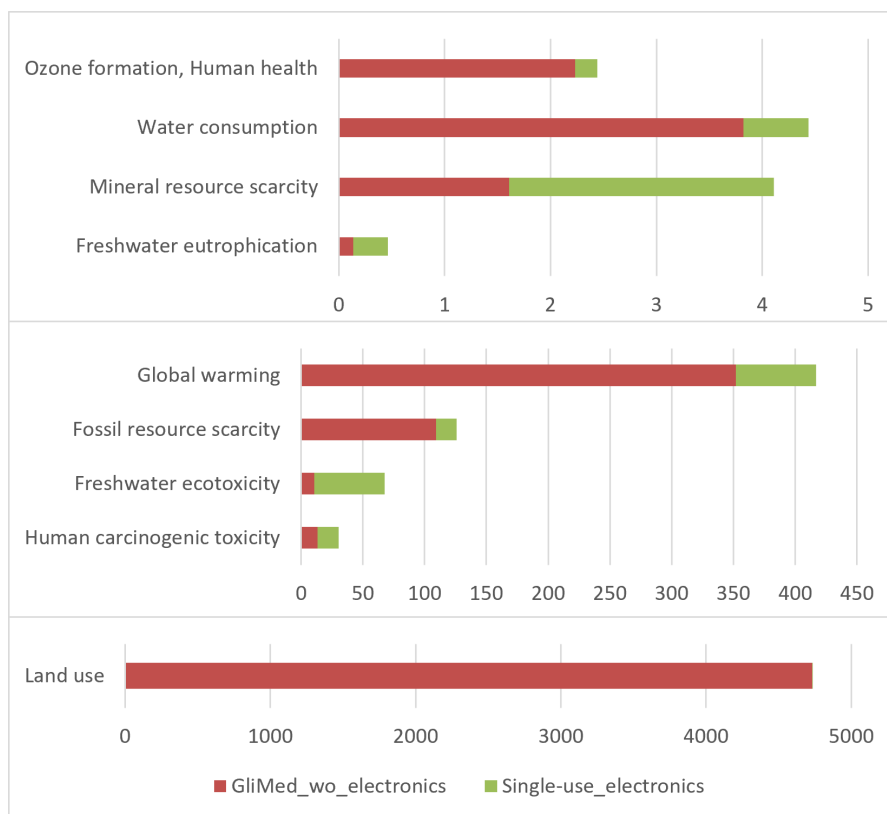


Figure 8.2: Graph showing the results of the project LCA. The units of each impact category are those as stated above.

For the majority of these impact categories, an ECI value has been assigned, and the total comparison can be found in Figure 8.3. Here the category with the largest impact is the Ozone formation at or near sea level and the associated human health risk. This is remarkable as it is the category with the second lowest impact in terms of its own indicator unit. This further highlights that comparing results

in terms of indicator units is only helpful if the unit is the same. When comparing between categories, it is preferable to compare in ECI values. Lastly, the calculated environmental cost indicator of one system is €60, which scales to €60,000 per 1000 systems. Therefore requirements SAI-SYS-15 has been met.

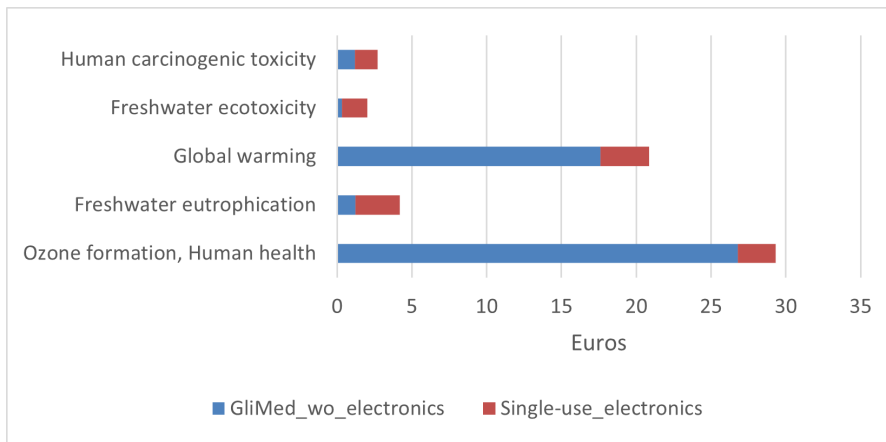


Figure 8.3: Graph showing the results of the project LCA, expressed in converted ECI values.

Furthermore, the system was analysed within the SimaPro software to distinguish which parts of GliMed had the largest impacts. From this, it is apparent that the structure of the glider itself has the largest impacts on the land use category. This is predominantly due to the requirement on biodegradability and the bio-based materials chosen. However the decision to use these types of materials drastically reduces the impact in categories such as freshwater eutrophication and human toxicity.

A comparison between estimated launch impacts and the impacts of the glider in the global warming potential impact category. For this, the process of helicopter transport was used from the Ecoinvent database, and was scaled to more accurately represent the chosen launch system. In addition to this, a comparison has been made between a commercial drone and the launch system plus glider based on a LCA from literature. [90]. The results of this can be found in Figure 8.4.

As can be seen, the comparative drone has a large impact on global warming than GliMed. This could be due to two reasons; firstly that the comparative drone has multiple flights per lifetime, and therefore the use phase has a much larger impact than in the case of GliMed. Furthermore, as can be seen in Figure 8.5, the structure of GliMed has such a large contribution to global warming potential mainly due to the kiln drying of the plywood and wooden planks.

8.1.2. Electronics LCA

There are three different electronic systems proposed in Chapter 6, the single-use system, the reusable system, and the system to be returned by the recipients. However, in order to definitively determine the use cases, the environmental sustainability of each must be analysed. The goal of this LCA is

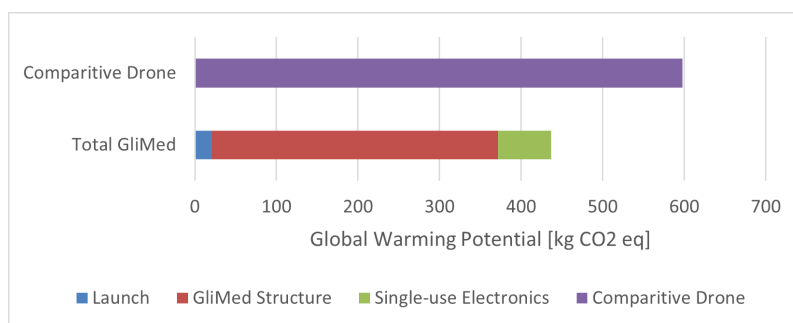


Figure 8.4: Comparison between comparative drone and GliMed, showing the individual contributions of the launch method, structure and electronics.

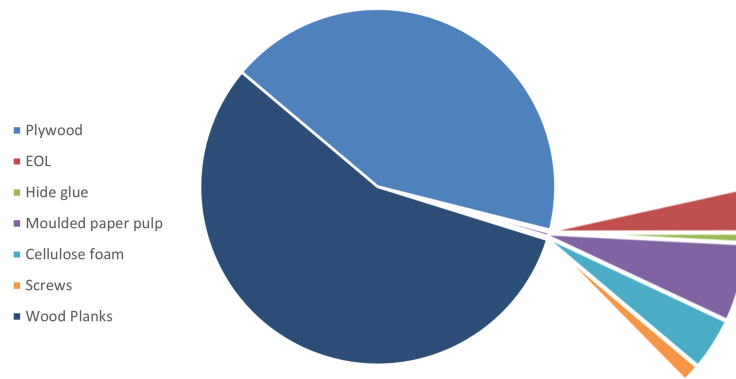


Figure 8.5: The division of the global warming impact category within the structure of GliMed

to compare the environmental sustainability of each of the three electrical systems, and to provide a recommendation on which system to maximise the use of.

The system in this LCA includes only the constituent materials for the electronics, as well as the end-of-life purpose of each system. The production of the electronics is not specifically considered, unless already present in the database. Again, the functional unit is the amount of electronics required per system for a single glider.

Methodology

Similarly to the project LCA, this LCA will be carried out on SimaPro and with the ecoinvent database. Furthermore, the same model for the electronics will be used here as in the project LCA, with slight changes made to compare the three presented systems.

There are a large amount of electronic components that feature in all three electric systems. These were combined into one process, while the varying features (solar panel, screen and batteries) were combines into different processes depending on their configuration. For the single use system, this standard electronics was combined with disposable batteries, and the end-of-life was chosen to be incineration. The returnable system includes reusable batteries, but is credited with 90% of original functionality at end-of-life. Lastly, for the reusable system, reusable batteries, a screen and a solar panel were included. This system is credited with the avoided production of a solar panel, and a touchscreen computer device, but still has multiple components go to incineration at end-of-life.

Similarly to the project LCA a number of impact categories were considered, and an ECI was assigned to compare between these categories.

Results and Discussion

The results of the electronics LCA can be seen in Figure 8.6.

From Figure 8.6 it can be clearly seen that the single-use electronics system has the largest impact on the environment, while the electronics to be returned have the lowest. Therefore, it is recommended to use the return system as much as possible. This furthermore confirms the assumption made in the midterm report that returning the electronics would be the most environmentally sustainable, and it is therefore recommended to use this system as much as possible [36].

Furthermore, it must be noted that direct output of SimaPro, which shows more impact categories than analysed here, shows a negative value for two of these impacts. This can be seen in Figure 8.7. This means that the electronics contribute positively to the environment in terms of fine particulate and terrestrial acidification.

8.1.3. Environmental Sustainability Assumptions

As mentioned above, there were a number of decisions made with an increase to environmental sustainability in mind. However the effect on environmental sustainability has not been quantified with a LCA, and as such it is for now assumed that these decisions have the intended effect. While there were many such decisions made during the course of this project, a limited number are shown here simply to get an indication of the decision making process.

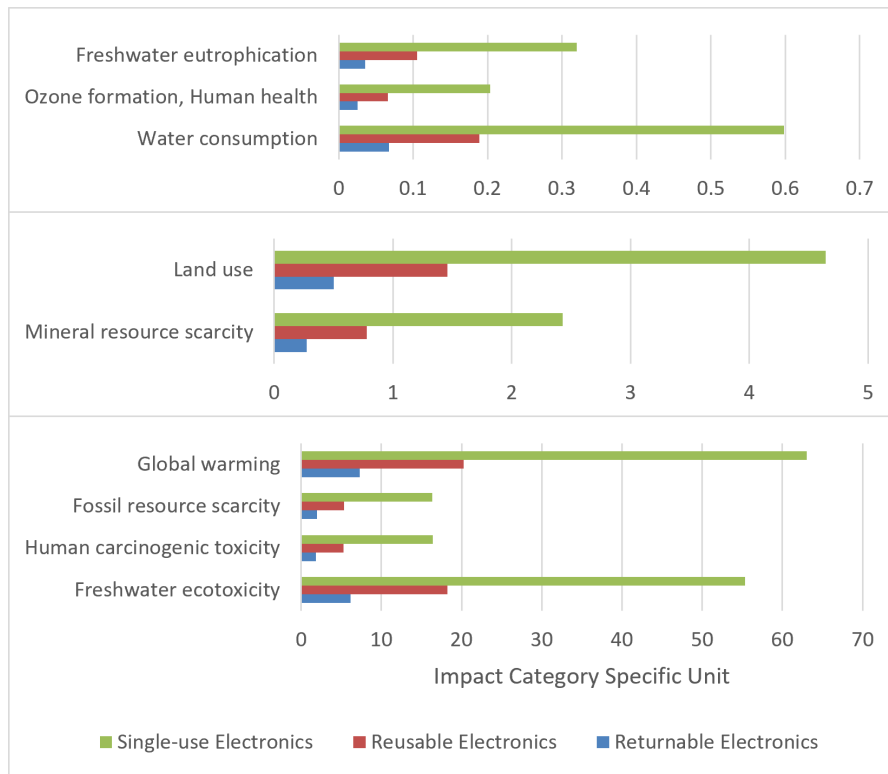


Figure 8.6: Graph showing the results of the electronics LCA, where the units for each impact category are as given above. The larger the value, the lower the environmental sustainability

In terms of operations prior to launch, the mobile launch truck will travel only the minimum distance needed to bring the system within range of the launcher plus glider. This is because it is assumed the fuel consumption of a large truck will be more than that of the small glider and launch system.

Furthermore, the decision to not use balsa wood was made in part because of the difficulties of finding ethically sourced balsa wood. The production and sale of most tropical hardwoods requires either the cutting down of rain forests, or the creation of plantations in already limited tropical areas. It was assumed that most types of wood, including spruce, are more environmentally sustainable than this balsa wood.

Lastly, It was assumed that removing the single-use electronics from the system, and placing these in a landfill or using these for energy recovery is more environmentally sustainable than leaving the harmful wastes in the environment where GliMed landed. However, this decision was also largely influenced by the requirements about hazardous wastes and bio-degradation times.

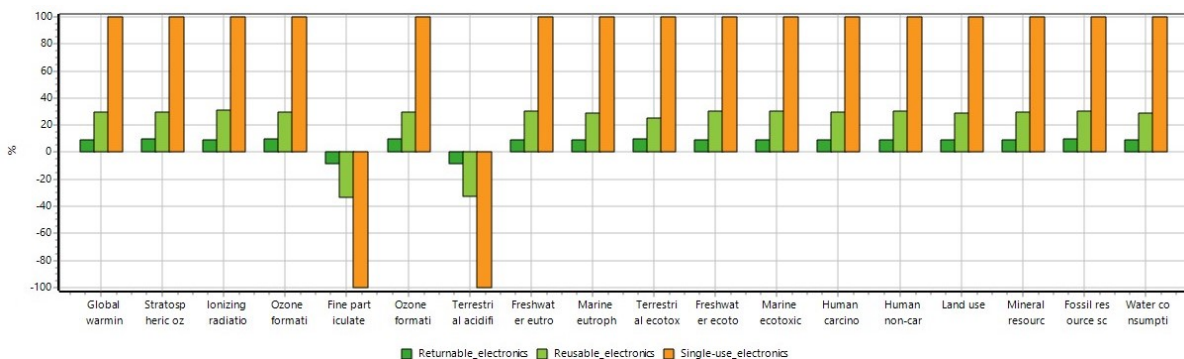


Figure 8.7: Output of SimaPro for the comparison between electronic systems

8.2. Economical Sustainability

Economic sustainability refers to supporting long term investments and growth, without compromising environmental, social or cultural values. Within economic sustainability there are two types of costs; internal and external. These internal costs are what the cost breakdown is based on, the directly visible costs to a business, and in most cases what the product is priced on. External costs are slightly different, these are the costs not directly related to the business, but the socio-environmental costs. Those similar to the ECI values found in the LCA, but there are also methods of getting these for cultural and social values. [18]

Economic sustainability can be achieved by internalising these external costs and including them in the market price. The processes of assessing these costs is Life Cycle Costing (LCC), and will help ensure the economic sustainability of SustAln. From Section 4.3, the production cost per system is €1165, with a market price of €1250. These are the internal costs of the system.

The external costs are much harder to quantify. In the LCA, €60 were quantified to be the external costs among five of the nine impact categories considered. However, these are not the full external costs, and much more research will have to be done by an expert to quantify the remainder of the environmental, social and cultural costs.

Lastly, the economic sustainability is also dependant on the profit and losses of the project, as this determines the long term viability of SustAln. From Section 4.3.6, it is clearly seen that the project has a large expected profit in the long term.

8.3. Social Sustainability

The impact of the glider on social sustainability is difficult to quantify without the use of a social LCA (S-LCA). However, this S-LCA requires much more knowledge about the operations of SustAln, and is infeasible to perform in this stage of project development. Therefore, this section of the sustainable development strategy will be based on assumptions on which items are socially sustainable.

Social sustainability revolves around the impacts on the people involved with the product. This can contain the recipients of GliMed and workers directly involved with operation, but also the work performed during the manufacturing of GliMed, and in the sourcing of components. In many cases this means ensuring workers are paid a living wage, and there is no harm to human health during any of the processes.

Another aspect of social sustainability is discussed with the determination of the electronics system. This type of social sustainability is not to the benefit of workers of SustAln, but aids recipients of GliMed by bringing in knowledge and tutorials of how their work can be improved. Furthermore, developing expenditure and risk management strategies is found to aid heavily in the advancement of agricultural communities[68].

8.4. Recommendations

There are a number of points in the design to take a further look at to increase the sustainability of SustAln. Firstly, the sourcing of the wood and plywood can be investigated further, to determine the reason for the large contribution to the global warming impact category. Once this is known, the cause can be eliminated as much as possible. The same can likewise be done with the components which have a similarly large impact on any category.

Furthermore, a more detailed economic sustainability analysis should be conducted by experts. In addition to this, the social sustainability should be investigated, and more research should be performed on the use case of the reusable electronics.

In terms of the LCA performed on SustAln, this was done with a design outdated by one week, meaning the design change to increase the amount of PLA used is not incorporated in this LCA. Furthermore, without comparisons, it is very hard to justify the environmental sustainability. Therefore, a LCA should be performed on similar products for all impact categories, and this should be compared with that of SustAln.

9. Risk

Risks are an important factor that needs to be taken into account during an entire design process. This chapter will discuss the risk management performed in the SutAIn project. Firstly the updated risk table and risk maps, compared to [36], will be presented. Secondly, it will be discussed how risk management was incorporated into the design process of GliMed and how it influenced the design of GliMed.

In Table 9.1, the definition for the likelihood and impact categories are given, while the updated and added risks are presented in Table 9.2 and Table 9.3. In this latter table, only risks that had their mitigation or contingency plan, or their likelihood or impact category changed compared to the midterm report, are presented. For the unchanged risks, see the midterm report [36]. In Figure 9.1 and Figure 9.2, the risk maps, which contain all of the technical risks, are presented before and after the mitigation and contingency plans.

Two risks from the midterm report, Com-3 and Lau-5, are removed since they are not relevant anymore. For Com-3 this is because the direct glider to ATC communication link is removed and for Lau-5 this is because only one launch vehicle is used, which eliminates the risk of the launch vehicles colliding.

Furthermore, the likelihood of Per-2, Per-3 and Per-4 is increased, due to the change of configuration from the conventional configuration to the flying wing. This made designing for the stability and controllability of the glider more difficult. The mitigation regarding the performance risks have also changed, as it will consists mostly of post-DSE validation and redesigns.

As can be seen in Figure 9.2, risk Com-5 and Per-3 are still in the unacceptable regime. For Per-3 this is because dynamic stability can only be determined after flight tests. For Com-5, environmental effects were not taken into account when determining the link budget, therefore this can also only be determined after validation tests.

Table 9.1: Impact and Likelihood categories

Consequence	Description	Likelihood	Probability
Catastrophic	Mission failure and/or loss of essential equipment	Very High	>60%
Critical	Possible mission failure or subsystem failure	High	30%-60%
Significant	Partial mission failure or possible subsystem failure	Moderate	10%-30%
Marginal	Possible partial subsystem failure	Low	0.5%-10%
Negligible	Minor inconvenience	Very Low	<0.5%

Table 9.2: Overview of the changed and added risks. In the third column, the mitigation and contingency plans are separated by a ','.

Risk code	Risk event	Mitigation/contingency plan	Responsible	Likelihood	Impact	Requirement
Com-1	Full communication loss	Fly predetermined, fully programmed flight path	Com and Nav engineer, risk managers	Low	Critical	SAI-SYS-11-COMM-13
Com-4	Communication signal interference	Modulation technique adds robustness to interference/	Com and Nav engineer, risk managers	Moderate	Critical	
Com-5	Environmental effects (i.e. rain, magnetic field) interference with communication	No mitigation or contingency	Com and Nav engineer, risk managers	Moderate	Critical	
Per-1	Unable to meet aerodynamic performance requirements	Use of CFD, wind tunnel tests, model flight test, verification and validation/redesign	Performance department, risk managers	Moderate	Catastrophic	SAI-SYS-13, SAI-SYS-13-PER-07
Per-2	Statically unstable design	Use of CFD, wind tunnel tests, model flight test, verification and validation/redesign	Performance department, risk managers	Moderate	Catastrophic	SAI-SYS-13-PER-19, SAI-SYS-13-PER-21
Per-3	Dynamically unstable design	Model flight test, verification and validation/redesign	Performance department, risk managers	Very High	Critical	SAI-SYS-13-PER-18
Per-4	Uncontrollable design	Model flight test, verification and validation/redesign	Performance department, risk managers	Moderate	Significant	SAI-SYS-13-PER-22, SAI-SYS-13-PER-24, SAI-SYS-13-PER-25, SAI-SYS-13-PER-26, SAI-SYS-13-PER-27
Per-9	Rain	Waterproof PLA coating	Performance department, risk managers	Moderate	Marginal	
Per-13	Shift of c.g. during flight	Ensure payload and ballast are properly secured/	Performance department, risk managers	Very High	Catastrophic	
Per-14	Control surface failure	Strong enough servos, robust electrical systems, subsystem testing/	Performance department, risk managers	Moderate	Catastrophic	
Lan-1	Payload damaged upon landing	Crash structure and landing manoeuvre/	Operational systems engineer, risk managers	Very High	Catastrophic	SAI-SYS-02-LAND-01

Table 9.3: Overview Risks

Risk code	Risk event	Mitigation/contingency plan	Responsible	Likelihood	Impact	Requirement
Lan-5	Running out of landing area	Choose sufficient landing area with cameras/go into controlled crash, crash structure can take the impact	Operational systems engineer, risk managers	High	Critical	
Lau-6	Launch vehicle runs out of fuel after launch	Proper range and endurance calculation and testing/land with autorotation	Operational systems engineer, risk managers	High	Significant	
EOL-5	Not meeting biodegradation time	Include water bacteria, reduce thickness/	End of life engineer, risk managers	Very High	Marginal	
Struc-6	Excreting electrical system payload, or structural components	Fixing electrical components and payload/	Structural engineer, risk managers	Moderate	Catastrophic	
Struc-7	Payload/electrical system not detachable from structure	Design payload to be detachable using human force/ add screw driver	Structural engineer, risk managers	Moderate	Significant	SAI-SYS-03-STRUC-09, SAI-SYS-06-STRUC-24 SAI-SYS-10-STRUC-12,
Struc-11	Sensors falling off	Use strong adhesives/	Structural engineer, risk managers	Moderate	significant	
Struc-12	Breaking of connection between outer and payload section wing under ultimate load	Testing/ reinforcement, other material	Structural engineer, risk managers	Moderate	Catastrophic	
Mat-5	Cellulose foam not commercially available	Use comparable material (paperboard honeycomb structure)	Materials engineer, risk managers	Moderate	Significant	
Elec-1	Battery fire	Do not overload battery, reducing peak power consumption/	Electrical engineer, risk managers	Moderate	Catastrophic	SAI-SYS-08-ELEC-04



Figure 9.1: Risk map



Figure 9.2: Risk map post mitigation

9.1. Influence of Risk on the Design

In this section the influence of the risk analysis on the design of the different subsystems will be discussed. Design decisions that have been taken with risk analysis in mind are presented per subsystem.

9.1.1. Performance

Risk management was heavily used in designing for the performance requirements of the glider. This is mainly done by overdesigning the glider with respect to the requirements, to minimise the risk of them not being met. The inaccuracy and uncertainty with the use of XFLR5, mainly with regards to it only being able to accurately analyse thin wings, not taking into account sweep for the lift curve and not being able to analyse the tapered section and winglets, requires overdesigning with respect to the results of XFLR5. Another reason to overdesign with respect to the L/D, is to minimise the risk of not being able to make the range due to there being too much head wind. Finally, to minimise the risk of loosing performance due to rain, a waterproof PLA-coating was added to the wing.

9.1.2. Communication and navigation

For the communication, it was decided to remove the glider to ATC communication link because of the possibility of interference if two antennas with different signals would be located very close to each other on the glider. Furthermore, since the glider can still communicate with ATC through the ground station, this was deemed sufficient. This removes the risk of the glider to ATC communication failing.

For the navigation, multiple sensors are placed on the glider to increase redundancy. This lowers the risk of hitting obstacles during the landing phase or loosing the ability to navigate altogether. Finally, the ability of the software to reboot itself has been added, in case of software failure.

9.1.3. Electrical systems

Risk analysis played an important during the design of the electrical system. To make sure the components would not overheat measures have been taken to reduce the peak power required by the system. To make sure the system will be guaranteed to have enough energy available various safety margins have been added. Lastly to reduce interference of the sensors by the battery, the battery has been placed as far away as possible from the sensors.

9.1.4. Launch

For the launch subsystem, risk management was incorporated in the design by choosing to launch the glider with only one helicopter instead of two. This removes the risk of the launch vehicles colliding during the launch phase.

9.1.5. Landing

By having two different landing methods, the risk that the landing will not work at all is minimised. Since there are many uncertainties surrounding the deepstall landing method, this second landing option is added as well.

9.1.6. End of life

Risk analysis also played an important role in the end of life design. To reduce the risk of degradation taking too long a mixture of water, bacteria and fungi will be sprayed over the aircraft after landing to reduce degradation time. Furthermore to ensure the recipients handle the glider and payload extraction in a proper manner, stickers with instruction drawings have been added on the surface of the glider.

9.1.7. Manufacturing

There are various ways the risk management has found its way into the design process for manufacturing. Firstly, various quality control measures have been put into the manufacturing process. Furthermore, measures like adding margins have been taken to reduce the chance of production delays. And last but not least a proper and consistent communication flow has been established between the structures and the manufacturing department. This has been done to guarantee the manufacturability of the glider.

9.1.8. Structures

When designing the structure risk analysis played an important role. Firstly many margins were added to make sure the structure is capable of handling most conceivable situations. Since the skin is made out of paper pulp, a water proof coating has been applied to make sure water will not compromise the skin and the electronics inside. Furthermore, the detachable wings have been designed in such a way that the payload can be easily taken out without being blocked. To reduce the risk of joints failing, strong adhesives have been used and mechanical joints have been over designed by adding additional screws. To reduce the risk of the recipients not being able to access the payload, everything has been designed to be detachable via screw driver and a screw driver has been added. Furthermore, the wings have been made stiff so the aerodynamic performance during normal conditions will not be compromised.

9.1.9. Materials

During the material design risk management has also been taken into account. Firstly, to reduce the risk of compromising the material properties due to degradation during storage the glider will be stored in conditions unfavourable for degradation. Secondly, to reduce the risk of materials being unavailable balsa wood has been excluded as a material option due to its poor availability. Cellulose foam is a material that is not yet on the market but should be in 2-3 years. This would make it available in time to be used in the glider, but if this time frame is not met the crash structure would be without a material. For this reason a comparable back up option has been selected, this is a cart-board honeycomb structure.

10. Outlook

The other chapters in this report show the development of the SustAin project and its glider, and show the current state of the conceptual design phase. After this phase, there are other steps before the project can be implemented into society. This chapter outlines the coming phases. First, a description is given of each of the phases. This description is supported by a project development flow chart, as well as a preliminary planning in the Gantt chart. With this information, the state of the project as of right now and the work to be done in the future is evident.

This project, from start to end, may contain four distinct stages: front-end development, implementation, operation, and possible expansion. Currently, SustAin is halfway through the front-end development stage, which contains all design phases. After that, only the expansions calls in the need of an engineering team. Because of this, the implementation and operation itself are not included in this outlook. The project logic diagram for the following stages can be seen in Figure 10.1. The preliminary and critical design reviews are moments where the design is analysed by external people, and feedback if offered. Here a go/no-go choice is also made, whether the project can advance to the next stage or not.

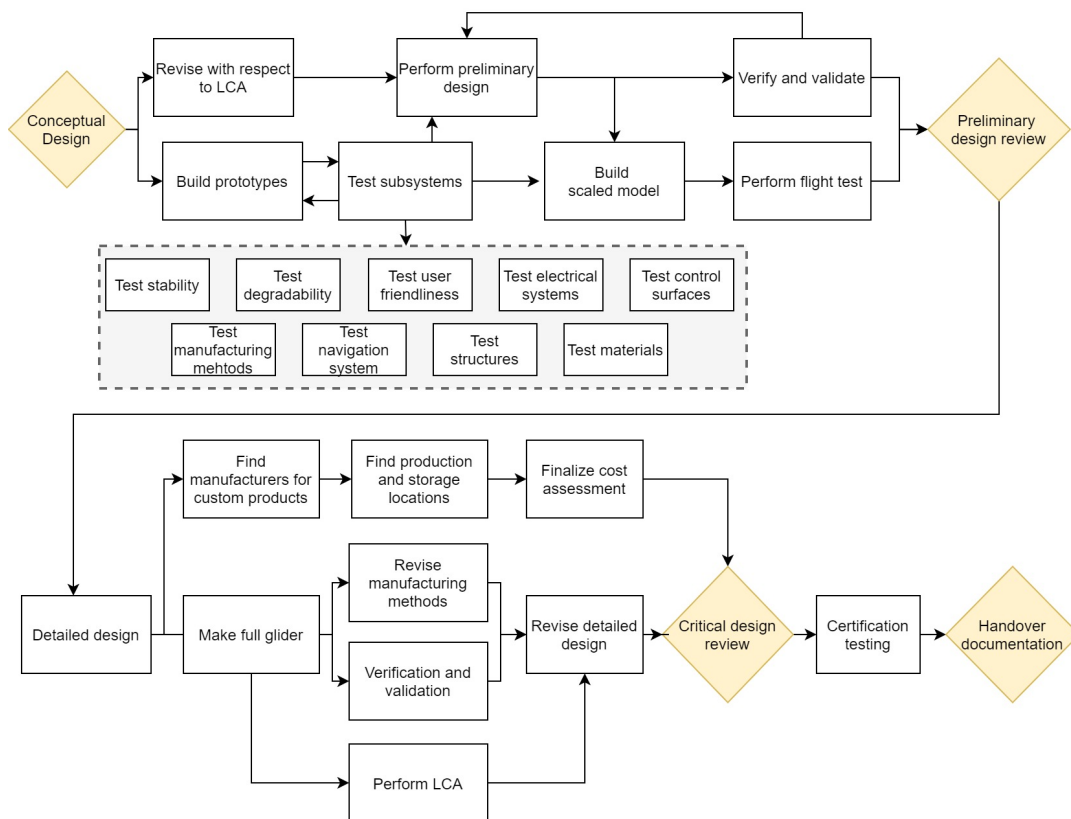


Figure 10.1: Project development flow diagram

The front-end stage can be divided into several design phases:

1. **Conceptual design:** The conceptual design phase is just finished. This phases contained everything up to this report. Most importantly, all design options are explored and traded off, and the first iterations have been made. Verification and validation have been done in limited amounts.
2. **Preliminary design:** This phase will contain subsystem testing, and iterating the conceptual design until all requirements are met. This phase begins with the conceptual design and ends with a preliminary design review. An important aspect of this phase is the subsystem testing. After that, a scaled model can be made for the first flight test.
3. **Detailed design:** This phase finalises the design. Every single part will be designed in as much detail as possible, so it is completely done before implementation. With the help of the LCA and

making a full scale glider, the detailed design can be optimised as much as possible. Again, this phase ends with a critical design review.

4. **Certification:** Before the glider can actually be operated, it must undergo certification testing. Those tests and the certification process are covered by this phase.

As described in Chapter 2, the project may be expanded to a bigger market if it is deemed a success or if there is a demand. In that case, the glider will need to be tested with, and designed for different climates or payload. This can be seen in Figure 10.2.

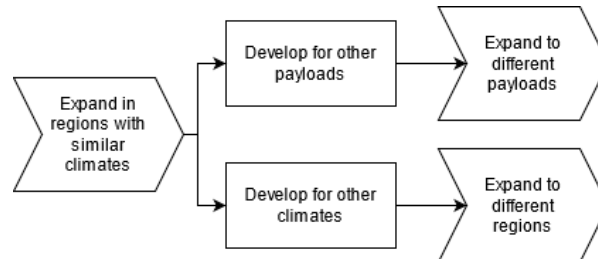


Figure 10.2: Design for future expansion plan

The initial estimated timeline for the SustAIn project is visualised in Figure 10.3. The initial time estimates in this Gantt chart are based on the time estimates derived in Section 4.3.1. The timeline and progress is also dependant on the availability of some other technologies that are being used, such as the cellulose foam.

In the Gantt chart (Figure 10.3) it can be seen that the preliminary design phase would be done around summer 2022, the detailed design start of 2025, and finally the certification summer 2025. The details of the planning will be more clear as the project progresses.

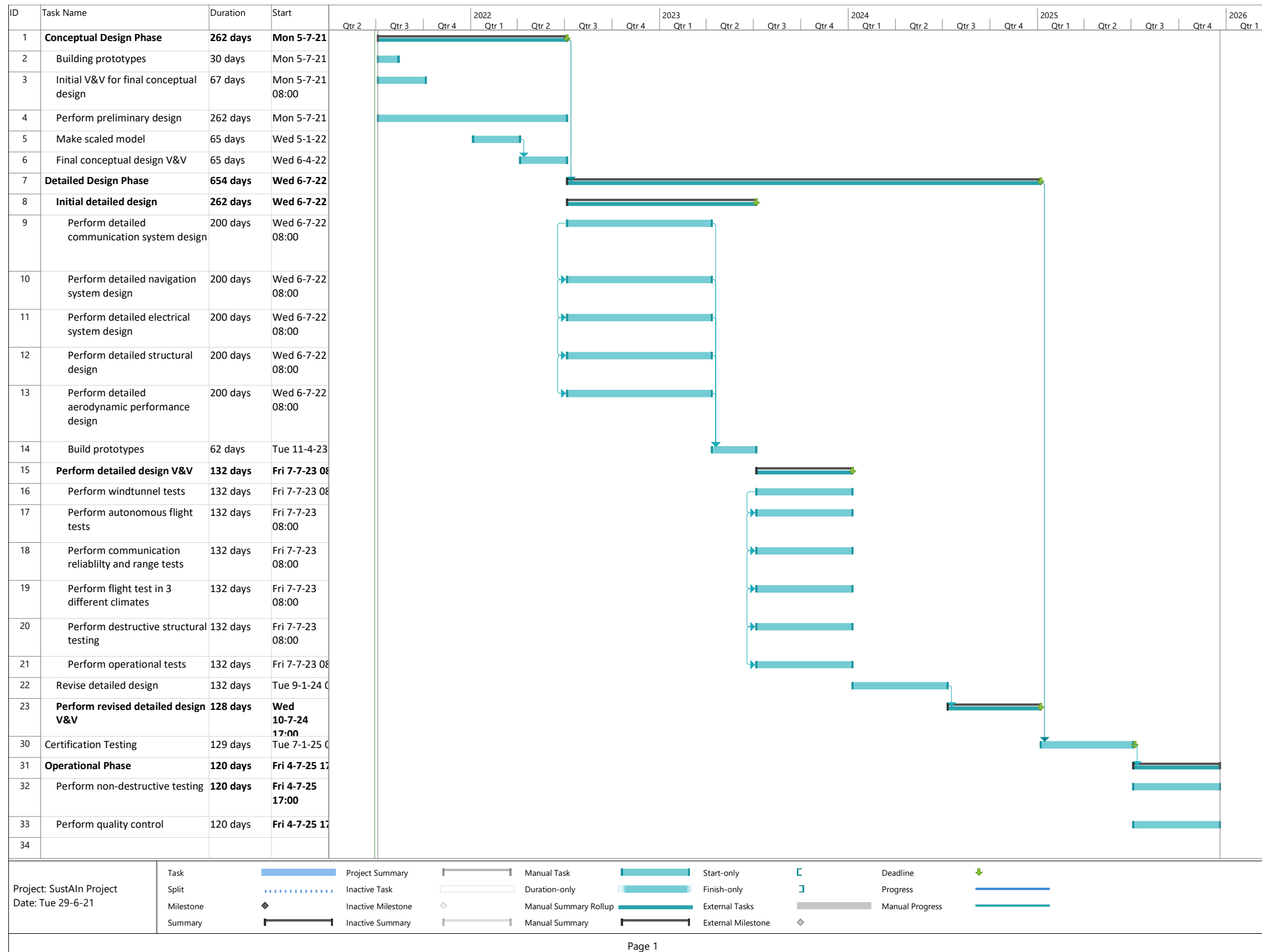


Figure 10.3: Post DSE project Gantt chart. The tasks in the operational phase will continue for 15 years.

11. Conclusion and Recommendations

The aim of this report was to design an autonomous, single-use glider, capable of delivering 200 vaccines to remote and/or hard-to-reach areas. The maximum take-off weight could not be more than 25[kg] and the glide range should be at least 125[km] when released from a launch altitude of 5[km]. These requirements have all been taken into account while minimising the social and environmental life cycle cost in a cradle-to-grave scenario, and making the product competitive on the market.

The configuration chosen to fulfill this purpose and all of the user requirements, is a flying wing made of spruce plywood, moulded paper pulp and PLA. The electrical systems are powered by batteries and can be collected by the recipients to make the product fully degradable and non-toxic to the environment. The payload and main electronics are located in the centre of the product.



Figure 11.1: Render of GliMed.

The main specifications of the glider are:

- Empty weight: 19.38 [kg]
- Glide ratio: 29 [-]
- Market Price: €1250.00
- Production volume: 1000 per year
- Payload weight: 5.62 [kg]
- Wingspan: 6 [m]
- Degradation time: 4.26 [years]
- Storage time: 10 [years]

One of the most important recommendations is to validate the aerodynamic performance of the system. The software used to evaluate the performance introduces a lot of uncertainty when analysing the payload section of the glider (up to 30%). CFD software and wind tunnel tests are required to see whether the glider can actually achieve the found glide ratio. This set-up along with flight tests are also necessary to validate the static stability and investigate the dynamic stability of the glider.

In addition, the landing manoeuvres of the glider heavily depend on the post-stall behaviour of the glider. The flight tests also serve to analyse whether the glider can perform the theoretical landing manoeuvres.

During mission load analysis, gusts introducing load factors of up to 3.5 were found. In future design, this analysis has to be re-evaluated and flight tests have to be performed that validate these results, since these are significantly high loads. If the load factors are indeed this high, the structure has to be redesigned in order to take up ultimate load factors of 5.25 instead of 4.5.

With regards to the structure, tests have to be performed that validate that the loads are properly transferred from the outer wings to the payload section without failure. One critical point is the connection between the outer wings and the payload section. The wing box of the outer wing is slid into a sleeve of the payload section, but not attached to anything. In order to avoid movement of the outer wings, the payload section skin is attached to a rib of the outer wings via screws. These two connection points are most likely to be the breaking points in the design. Tests are required to validate the strength of the connections under the ultimate loads.

Lastly, the market price of the glider is significantly higher than competitors. Despite the fact that the glider lies in a market gap, the product should be made cheaper in order to become more competitive. One of the main contributors to the cost are the electrical systems. Off the shelf equipment was selected for the glider. In later design stages, electrical equipment may have to be designed by the company herself to make the product cheaper. Alternatively, power usage tests can cause battery sizes to shrink, leading to both a reduction in total mass and cost. However, regulations state that all electrical systems require redundancy. In future design, this redundancy has to be added, which increases mass and cost again.

References

- [1] Y.S .Lee, N. Park, and H. Yoon. “Dynamic Mechanical Characteristics of Expanded Polypropylene Foams”. In: *Journal of Cellular Plastics - J CELL PLAST* 46 (Jan. 2010), pp. 43–55.
- [2] European Union Aviation Safety Agency (EASA). *Easy Access Rules for Sailplanes*. European Union, Oct. 2020, pp. 193–194.
- [3] *16 Transmitting and Receiving Antennas*. online. <https://www.ece.rutgers.edu/orfanidi/ewa/ch16.pdf>.
- [4] A.Rezig et al. “Relationship Between Chemical Degradation And Thickness Loss of an Amine-Cured Epoxy Coating Exposed to Different UV Environments”. In: *JCT Research* 3.3 (2004), pp. 173–184.
- [5] I. Abbott, A. Von Doenhoff, and L. Stivers. *Summary of Airfoil Data*. Tech. rep. National Advisory Committee for Aeronautics (NACA), 1945.
- [6] I. Anderson. “Mechanical Properties of Specimens 3D Printed with Virgin and Recycled Polylactic Acid”. en. In: *3D Printing and Additive Manufacturing* 4.2 (June 2017), pp. 110–115. ISSN: 2329-7662, 2329-7670. URL: <http://www.liebertpub.com/doi/10.1089/3dp.2016.0054> (visited on 06/21/2021).
- [7] A. Barański et al. “Effect of Relative Humidity on the Degradation Rate of Cellulose. Methodology Studies”. In: *Restaurator* 25.1 (2004), pp. 68–74.
- [8] Š. Barčík and M. Kvietková. “EFFECT OF THE CHOSEN PARAMETERS ON DEFLECTION ANGLE BETWEEN CUTTING SIDES DURING THE CUTTING OF AGLOMERATED MATERIALS BY WATER JET”. In: *WOOD RESEARCH* 56.4 (2011), pp. 577–588.
- [9] B. Bizubova et al. *FIBROCHEM*, 2018, pp. 30–31.
- [10] M. Brown. *Conversation about flight loads*. en. May 2021.
- [11] S. de Bruyn et. al. *Environmental Prices Handbook*. EU28 version. CE Delft, 2018.
- [12] T. Bupachata, N. Sombatsompob, and B. Prapagdeea. “Isolation and role of polylactic acid-degrading bacteria on degrading enzymes productions and PLA biodegradability at mesophilic conditions”. In: *Polymer Degradation and Stability* 152 (2018), pp. 75–85.
- [13] Y. Byun, Y.T. Kim, and S. Whiteside. “Characterization of an antioxidant polylactic acid (PLA) film prepared with α -tocopherol, BHT and polyethylene glycol using film cast extruder”. In: *Journal of Food Engineering* 100.2 (2010), pp. 239–244. ISSN: 0260-8774. URL: <https://www.sciencedirect.com/science/article/pii/S02608774100186X>.
- [14] L. R. Caporael et al. “Selfishness examined: Cooperation in the absence of egoistic incentives”. In: *BEHAVIORAL AND BRAIN SCIENCES* 12 (1989), pp. 683–739.
- [15] A. Cervone. *Spacecraft Telecommunications, Aerospace Design and Systems Engineering Elements II – AE2111-II*. 2021.
- [16] D.J. Champion and A.M. Sear. “Questionnaire Response Rate: A Methodological Analysis”. In: *Social Forces* 47.3 (1969). <https://www.jstor.org/stable/2575033>, pp. 335–339.
- [17] B. Cheng and Z. Guo. “Study on Small UAVs’ Deep Stall Landing Procedure”. In: *CMAME* 5 (Jan. 2017).
- [18] Y. Chouinard, J. Ellison, and R. Ridgeway. “The Sustainable Economy”. In: *Financial Management* 10 (2011). <https://www.jstor.org/stable/2575033>.
- [19] Army-Navy-Civil Committee. *Design of Wood Aircraft Structures*. en. United States Government Printing Office, June 1944.
- [20] *Cost Figures for Freight Transport - final report*. Zoetermeer, 2020.
- [21] M. Daria, L. Krzysztof, and M. Jakub. “Characteristics of biodegradable textiles used in environmental engineering: A comprehensive review”. In: *Journal of Cleaner Production* 268 (2020), p. 122129. ISSN: 0959-6526. URL: <https://www.sciencedirect.com/science/article/pii/S0959652620321764>.
- [22] A. Das. “Digital Modulation Techniques”. In: *Digital Communication: Principles and System Modelling*. Berlin, Heidelberg: Springer Berlin Heidelberg, 2010, pp. 111–141. ISBN: 978-3-642-12743-4.
- [23] A. Das. “Spread Spectrum Modulation”. In: *Digital Communication: Principles and System Modelling*. Berlin, Heidelberg: Springer Berlin Heidelberg, 2010, pp. 143–167. ISBN: 978-3-642-12743-4.

- [24] D.P. Dickinson. *So Many Wireless Technologies ... Which Is the Right One for My Application?* 2014.
- [25] H. Durrant-Whyte and T. Bailey. "Simultaneous localization and mapping: part I". In: *IEEE Robotics Automation Magazine* 13.2 (2006), pp. 99–110.
- [26] EASA. *Easy Access Rules for Unmanned Aircraft Systems(Regulations (EU) 2019/947 and (EU) 2019/945)*. Tech. rep. European Union Aviation Safety Agency (EASA), 2021.
- [27] Å. Ek. *Interview about Cellulose foam*. en. May 2021.
- [28] G.H. Elkaim, F.A.P. Lie, and D. Gebre-Egziabher. "Principles of Guidance, Navigation, and Control of UAVs". In: *Handbook of Unmanned Aerial Vehicles*. Ed. by Kimon P. Valavanis and George J. Vachtsevanos. Dordrecht: Springer Netherlands, 2015, pp. 347–380. ISBN: 978-90-481-9707-1. DOI: 10.1007/978-90-481-9707-1_56.
- [29] T. Fadji et al. "Investigating the Mechanical Properties of Paperboard Packaging Material for Handling Fresh Produce Under Different Environmental Conditions: Experimental Analysis and Finite Element Modelling". en. In: (Apr. 2017), p. 15. URL: <https://tudelft.on.worldcat.org/oclc/8093196102>.
- [30] Code of Federal Regulations. *Telecommunication: Radio Frequency Devices*. Code of Federal Regulations, 2021.
- [31] J.P. Florance et al. "Contributions of the NASA Langley Research Center to the DARPA/AFRL/NASA/ Northrop Grumman Smart Wing Program". In: 2003.
- [32] M. Frey et al. "Fabrication and Design of Wood-Based High-Performance Composites". In: *Journal of Visualized Experiments* 153 (2019).
- [33] N. Glizde. "Plotting the Flight Envelope of an Unmanned Aircraft System Air Vehicle". In: *Transport and Aerospace Engineering* 4 (2017), pp. 80–87.
- [34] B. Goodell, J. E. Winandy, and J. J. Morrell. "Fungal Degradation of Wood: Emerging Data, New Insights and Changing Perceptions". In: *Coatings* 1210 (2020), pp. 1–19.
- [35] L. de Graaf et al. "Baseline Report: SustAin: Sustainable Autonomous Pandemic Intervention". DSE Reports, Delft University of Technology, Delft. May 2021.
- [36] L. de Graaf et al. "Midterm Report: SustAin: Sustainable Autonomous Pandemic Intervention". DSE Reports, Delft University of Technology, Delft. May 2021.
- [37] L. de Graaf et al. "Project Plan: SustAin: Sustainable Autonomous Pandemic Intervention". DSE Reports, Delft University of Technology, Delft. Apr. 2021.
- [38] Granta Design Limited. *CES EduPack software*. Version 20.1.1. 2020.
- [39] D.W. Green, J.E. Winandy, and D.E. Kretschmann. "Mechanical Properties of Wood". en. In: *Wood handbook - Wood as an engineering material*. 1999, p. 463.
- [40] Scott Gruber et al. "UAV Handbook: Payload Design of Small UAVs". In: *Handbook of Unmanned Aerial Vehicles*. Ed. by Kimon P. Valavanis and George J. Vachtsevanos. Dordrecht: Springer Netherlands, 2015, pp. 143–163. ISBN: 978-90-481-9707-1.
- [41] D. Gyorgyfalvy. *Performance analysis of the horten IV flying wing*. Defense Technical Information Center, 1960.
- [42] A.O. Hanstveit. "Biodegradability of petroleum waxes and beeswax in an adapted CO2 evolution test". In: *Chemosphere* 25.4 (1992), pp. 605–620. ISSN: 0045-6535. URL: <https://www.sciencedirect.com/science/article/pii/004565359290291X>.
- [43] V. Hemmilä et al. "Development of sustainable bio-adhesives for engineered wood panels – A Review". In: *RSC Advances* 7.61 (2017), pp. 38604–38630.
- [44] K. L. Ho and A. L. Pometto III. In: *Journal of Polymers and the Environment* 7.2 (1999), pp. 93–100.
- [45] K. L. Ho, A. L. Pometto III, and P. N. Hinz. "Effects of Temperature and Relative Humidity on Polylactic Acid Plastic Degradation". In: *Journal of Environmental Polymer Degradation* 7.2 (1999), pp. 83–92.
- [46] M. Hughes. "4 - Plywood and other veneer-based products". In: *Wood Composites*. Ed. by M.P. Ansell. Woodhead Publishing, 2015, pp. 69–89. ISBN: 978-1-78242-454-3. URL: <https://www.sciencedirect.com/science/article/pii/B9781782424543000044>.
- [47] *Geometrical product specifications (GPS) — ISO code system for tolerances on linear*

- sizes — *Part 1: Basis of tolerances, deviations and fits*. Standard. Geneva, CH: International Organization for Standardization, 2010.
- [48] ITU-R. *Characteristics of unmanned aircraft systems and spectrum requirements to support their safe operation in non-segregated airspace*. Tech. rep. ITU-R Radiocommunication Sector of ITU, 2009.
- [49] E. Joyce and A. Peters. *The technique of furniture making*. Batsford, 2005.
- [50] M. Khaghani and J. Skaloud. "Autonomous Vehicle Dynamic Model-Based Navigation for Small UAVs". In: *NAVIGATION* 63.3 (2016), pp. 345–358. URL: <https://onlinelibrary.wiley.com/doi/abs/10.1002/navi.140>.
- [51] K. Khantanapoka and K. Chinnasarn. "Pathfinding of 2D 3D game real-time strategy with depth direction A* algorithm for multi-layer". In: *2009 Eighth International Symposium on Natural Language Processing*. 2009, pp. 184–188.
- [52] Robert Klenke and Jose Ortiz. "Low Cost Autopilot System for Unmanned Aerial Vehicles". In: *Infotech@Aerospace 2011* (2011).
- [53] N. Kotlarewski et al. "Mechanical properties of Papua New Guinea balsa wood". In: *European Journal of Wood and Wood Products* 74 (Jan. 2016).
- [54] Forest Products Laboratory. Technical note. No 122, <https://www.fs.usda.gov/treesearch/pubs/32307>. 1920.
- [55] Forest Products Laboratory. U.S. Department of Agriculture, Forest Service, 1980.
- [56] W.J. Larson and J.R. Wertz. "Space Mission Analysis and Design". In: (Jan. 1992). URL: <https://www.osti.gov/biblio/7369177>.
- [57] M. Lembersky. *Realistic cost estimating for manufacturing*. 3rd ed. Society of Manufacturing Engineers, 2016.
- [58] L. Lu, C.A. Garcia, and A.G. Mikos. "In vitro degradation of thin poly(DL-lactic-co-glycolic acid) films". In: *Journal of Biomedical Materials Research* 46.2 (1999), pp. 236–244.
- [59] C.A. Lyon et al. *Summary of low speed airfoil data*. SoarTech Publications, 1997.
- [60] C. Rotaru and M. Todorov. *Flight Physics - Models, Techniques and Technologies*. en. Intechopen, Dec. 2017.
- [61] B.W. McCormick. *Aerodynamics of V/STOL flight*. en. Academic Press Incorporated, June 1967.
- [62] M. Mecklenburg. *Determining the Acceptable Ranges of Relative Humidity and Temperature in Museums and Galleries, Part 1, Structural Response to Relative Humidity*. DSpace Repository. 2007.
- [63] T.H. Megson. *Aircraft Structures for Engineering Students*. Elsevier Science Technology, 2016.
- [64] A. Melià-Angulo, L. Fuster-López, and A. Vicente-Escuder. "Study of the mechanical properties of selected animal glues and their implication when designing conservation strategies". In: *CeROArt HS* (2017).
- [65] M. Michaloudaki. "An approach to quality assurance of structural adhesive joints". PhD thesis. 2005, pp. 1–2.
- [66] P. Middelhoek. *Interview about efficiency of electrical system*. en. May 2021.
- [67] S. Mollasalehi, P. Handley, and G. Robson. "Fungal biodegradation of polyvinyl alcohol in soil and compost environments". PhD thesis. 2013.
- [68] P. Mosley and A. Suleiman. "Aid, Agriculture and Poverty in Developing Countries". In: *Review of Development Electronics* 11 (1 2007), pp. 139–158.
- [69] T. Nakiri et al. "Development of Electric Wire Using Biodegradable Polymer". In: *Industry Applications, IEEE Transactions on* 43 (2007), pp. 1069–1074.
- [70] D.B. Nedwell. "Effect of low temperature on microbial growth: lowered affinity for substrates limits growth at low temperature". In: *FEMS Microbiology Ecology* 30.2 (1999), pp. 101–111.
- [71] K. Nickel, M. Wohlfahrt, and E. Brown. *Tailless aircraft in theory & practice*. 1st ed. Oxford, United Kingdom: Elsevier science & technology, 1994.
- [72] F. Olivero. *Systems Engineering and Aerospace Design - Requirement Analysis and Design principles for A/C stability control - SEAD*. 2020.
- [73] F. Oliviero. *Aircraft Aerodynamic Analysis, Aerospace Design and Systems Engineering Elements II – AE2111-II*. 2021.
- [74] J. Peng and L. Turng Y. Srithep J. Wang. "Comparisons of microcellular polylactic acid parts injection molded with supercritical nitrogen and expandable thermoplastic

- microspheres: Surface roughness, tensile properties, and morphology". In: *Journal of Cellular Plastics* 48.5 (2012), pp. 433–444.
- [75] C. Pippin. "Integrated Hardware/Software Architectures to Enable UAVs for Autonomous Flight". In: *Handbook of Unmanned Aerial Vehicles*. Ed. by Kimon P. Valavanis and George J. Vachtsevanos. Dordrecht: Springer Netherlands, 2015, pp. 1725–1747. ISBN: 978-90-481-9707-1.
- [76] *Post-Stall Wind Tunnel Data for NACA 44XX Series Airfoil Sections*. Colorado, 1985.
- [77] Daniel Raymer. *AIRCRAFT DESIGN: a conceptual approach*. AMER INSTITUTE OF AERONA, 2019.
- [78] G. Ruijgrok. *Elements of airplane performance*. 2nd ed. Delft, Netherlands: VSSD, 2009.
- [79] D. Sandberg and P. Navi. *Introduction to thermo-hydro-mechanical (THM) wood processing*. Swedish Foundation for Strategic Research, 2007.
- [80] Forestry Service and T.R. Truax. *Gluing wood in aircraft manufacture*. U.S. Department of Agriculture, 1930.
- [81] N.R. Short. "Degradation of polymer-cement composites". In: *Durability of Concrete and Cement Composites* (2007), pp. 364–390.
- [82] J. Sinke. "Production of Aerospace Systems Lecture Notes". Readers, Delft University of Technology, Delft. 2021.
- [83] C. Smulders. *Interview about efficiency of electrical system*. en. May 2021.
- [84] R.S. Sodhi, M. Sonnenberg, and S. Das. "Use of snap-fit fasteners in the multi-life-cycle design of products". In: *Proceedings of the 1999 IEEE International Symposium on Electronics and the Environment* (1999).
- [85] C. Stachniss, J.J. Leonard, and S. Thrun. "Simultaneous Localization and Mapping". In: *Springer Handbook of Robotics*. Ed. by B. Siciliano and O. Khatib. Cham: Springer International Publishing, 2016, pp. 1153–1176. ISBN: 978-3-319-32552-1.
- [86] H. Taniguchi. "Analysis of deepstall landing for UAV". In: *ICAS* (Jan. 2008).
- [87] L. TranVan, V. Legrand, and F. Jacquemin. "Thermal decomposition kinetics of balsa wood: Kinetics and degradation mechanisms comparison between dry and moisturized materials". In: *Polymer Degradation and Stability* 110 (2014), pp. 208–215. ISSN: 0141-3910. URL: <https://www.sciencedirect.com/science/article/pii/S0141391014003504>.
- [88] T. R. Truax. *The gluing of wood*. U.S. Department of Agriculture, 1929.
- [89] D.M Wang and Z.W. Wang. "Experimental Investigation into the Cushioning Properties of Honeycomb Paperboard". In: *Packaging Technology and Science* (2008), p. 8.
- [90] K. Yowtak et al. "Comparative life cycle assessment of unmanned aerial vehicles, internal combustion engine vehicles and battery electric vehicles for grocery delivery". In: *Procedia CIRP* 90 (2020), pp. 244–250.
- [91] R.E. Ziemer, W.H. Tranter, and D.R. Fannin. *Signals and Systems: Continuous and Discrete*. fourth. Pearson International Ed., 1983.
- [92] J. Zyren and A. Petrick. "Tutorial on Basic Link Budget Analysis". In: 1998.